Stratification Pattern of Static and Scale-Invariant Dynamic Measures of Heartbeat Fluctuations Across Sleep Stages in Young and Elderly

Daniel T. Schmitt, Phyllis K. Stein, and Plamen Ch. Ivanov*

***Abstract*—Cardiac dynamics exhibit complex variability characterized by scale-invariant and nonlinear temporal organization related to the mechanism of neuroautonomic control, which changes with physiologic states and pathologic conditions. Changes in sleep regulation during sleep stages are also related to fluctuations in autonomic nervous activity. However, the interaction between sleep regulation and cardiac autonomic control remains not well understood. Even less is known how this interaction changes with age, as aspects of both cardiac dynamics and sleep regulation differ in healthy elderly compared to young subjects. We hypothesize that because of the neuroautonomic responsiveness in young subjects, fractal and nonlinear features of cardiac dynamics exhibit a pronounced stratification pattern across sleep stages, while in elderly these features will remain unchanged due to age-related loss of cardiac variability and decline of neuroautonomic responsiveness. We analyze the variability and the temporal fractal organization of heartbeat fluctuations across sleep stages in both young and elderly. We find that independent linear and nonlinear measures of cardiac control consistently exhibit the same ordering in their values across sleep stages, forming a robust stratification pattern. Despite changes in sleep architecture and reduced heart rate variability in elderly subjects, this stratification surprisingly does not break down with advanced age. Moreover, the difference between sleep stages for some linear, fractal, and nonlinear measures exceeds the difference between young and elderly, suggesting that the effect of sleep regulation on cardiac dynamics is significantly stronger than the effect of healthy aging. Quantifying changes in this stratification pattern may provide insights into how alterations in sleep regulation contribute to increased cardiac risk.**

***Index Terms*—Aging, cardiac dynamics, detrended fluctuations, fractal, nonlinear.**

I. Introduction

PHYSIOLOGICAL systems under spatially and temporally integrated neural regulation, such as the cardiac system, display continuous and seemingly erratic fluctuations [1], [2]. However, these "noisy" fluctuations in the intervals between consecutive heartbeats exhibit a temporal organization that is self-similar across a broad range of time scales, and is characterized by long-range power-law correlations [3]–[5] and nonlinear properties [6]–[9], indicating a complex fractal and multifractal structure [10], [11]. These fractal and nonlinear scaling features of cardiac dynamics change under sympathetic and parasympathetic blockade [12]–[14], and break down with pathologic conditions [15], [16]. The scaling exponent associated with these power-law correlations has been shown to be a sensitive marker for predicting mortality [17]. Moreover, the fractal and nonlinear organization of heartbeat fluctuations varies for different physiologic states, such as exercise and rest [18]–[20], wake and sleep [21]–[25], and with the circadian rhythm [26]–[28]. These findings indicate that the scale-invariant temporal organization of heartbeat fluctuations reflects the underlying mechanism of cardiac neuroautonomic regulation that changes with different physiologic states and pathologic conditions.

Recent studies have reported reduced heart rate variability [29] and alterations of the fractal and nonlinear properties of heartbeat fluctuations with healthy aging [30], [31], and these changes in cardiac dynamics have been associated with higher cardiac risk in elderly [26]. Sleep dynamics have also been found to change with advanced age—e.g., elderly subjects typically have more fragmented sleep with frequent arousals and reduced duration of deep sleep [32]. Sympathetic nerve activity measurements as well as spectral analysis of heart rate variability across sleep stages show dominant parasympathetic control during non-REM sleep, and activation of the sympathetic nervous system during REM and wake [33], [34] leading to different morphology in the heartbeat interval time series across sleep stages (Fig. 1). The intricate mechanism of interaction between sleep regulation and cardiac control, and whether this interaction declines with age, however, remains not well understood.

To test how sleep dynamics affect the temporal fractal and nonlinear organization of heartbeat fluctuations across time scales, we compare heartbeat dynamics of healthy young and healthy elderly subjects for different sleep stages. One possible hypothesis is that there will be a well-pronounced stratification pattern in the values of *static* (e.g., mean, standard deviation) and *dynamic* (scaling and nonlinear) measures of heartbeat dynamics across sleep stages, and that this stratification will be present in both healthy young and healthy elderly subjects. An alternative hypothesis is that while there are significant differences in cardiac control with sleep stage transitions for

Manuscript received December 9, 2007. First published February 6, 2009; current version published May 22, 2009. *Asterisk indicates corresponding author.*

D. T. Schmitt is with the Theoretische Physik, Universität Ulm, D-89069 Ulm, Germany. He is also with the Center for Polymer Studies and Department of Physics, Boston University, Boston, MA 02215 USA.

P. K. Stein is with Washington University School of Medicine Heart Rate Variability (HRV) Laboratory, St. Louis, MO 63108 USA.

*P. Ch. Ivanov is with the Department of Physics and Center for Polymer Studies, Boston University, Boston, MA 02215 USA. He is also with the Harvard Medical School, Division of Sleep Medicine, Brigham and Women's Hospital, Boston, MA 02115, USA, and Institute of Solid-State Physics, Bulgarian Academy of Sciences, 1784 Sofia, Bulgaria (e-mail: plamen@buphy.bu.edu).

Color versions of one or more of the figures in this paper are available online at http://ieeexplore.ieee.org.

Digital Object Identifier 10.1109/TBME.2009.2014819

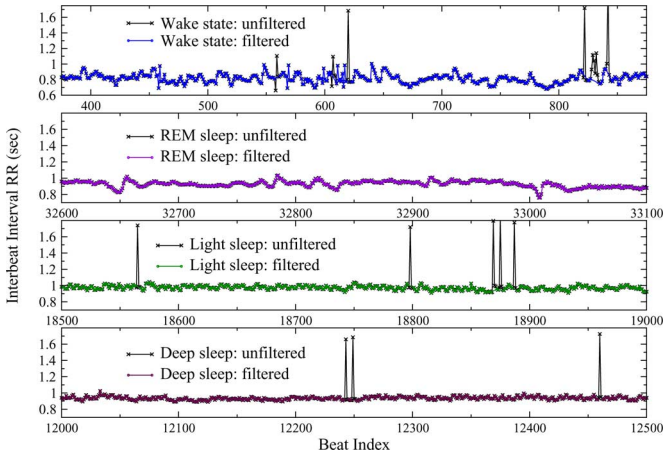

Fig. 1. Representative recordings of segments of 500 RR intervals between consecutive normal heartbeats for a healthy young subject during deep sleep, light sleep, rapid eye movement (REM) sleep, and an intermediate wake state (from bottom to top), part of an 8 h polysomnographic recording. A small percentage of artefacts (e.g., spikes marked with $\times$) have been filtered before the actual analysis (see Section II). Data show (a) gradual decrease of the standard deviation, σ_{RR} (also denoted as SDNN) from wake to REM, to light, to deep sleep (see Fig. 2), and (b) that the heartbeat signal is more homogeneous in deep sleep compared to light sleep, REM sleep, and wake where it exhibits more irregular fluctuations (see Fig. 3).

young subjects, the *static* and *dynamic* features of heartbeat fluctuations in healthy elderly subjects will remain unchanged across sleep stages due to age-related loss of cardiac variability and decline in neuroautonomic responsiveness to changes in sleep regulation. Testing these hypotheses will address the question how sleep regulation influences cardiac dynamics, and whether this influence changes with healthy aging, as sleep disorders have been associated with increased cardiovascular risk [35]–[37]. Probing for changes in the complex temporal organization of heartbeat fluctuations during different sleep stages can help elucidate the mechanisms through which alterations of sleep regulation in elderly may contribute to cardiac risk. This approach is in line with earlier studies where combinations of heart rate variability (HRV) measures as outlined in the HRV task force 1996 [38] were utilized to increase their power in stratifying age- and disease-related cardiac risk [39].

In order to characterize heartbeat fluctuations during different sleep stages, as well as the effect of healthy aging on cardiac regulation, we employ *static* measures, such as the standard deviation σ_{RR} (also denoted as SDNN) of the consecutive RR interbeat intervals and the standard deviation $\sigma_{\Delta\mathrm{RR}}$ of the interbeat increments ΔRR (also denoted as RMSSD). Further, we also analyze *dynamic* measures, such as the scaling exponent α which quantifies the long-term fractal correlations in the RR time series, as well as the scaling exponents α^{mag} and α^{sign} that quantify the long-term nonlinear and linear properties in the magnitude and sign of ΔRR, respectively [40]–[42].

Here, we demonstrate that key fractal, scale-invariant and nonlinear characteristics of heartbeat dynamics do not change and remain stable with advanced age, indicating that fundamental features of cardiac complexity do not break down and are not lost with healthy aging. Moreover, we find that key independent static and dynamic measures of cardiac control change significantly during different sleep stages, and exhibit a previously unknown stratification pattern similar in both young and elderly subjects. This pattern does not break down with aging, despite changes in sleep architecture and reduced heart rate variability in elderly subjects. Further, the difference in these measures between sleep stages far exceeds the difference between young and elderly subjects, suggesting that the effect of sleep regulation on cardiac dynamics may be significantly stronger than the effect of healthy aging.

II. Data and Methods

A. Subjects

We analyze 26 polysomnographic recordings obtained from 13 young subjects (average age 33.3 years; seven males and six females) during two consecutive nights of sleep in controlled laboratory conditions from the SIESTA project [43]. Continuous EEG and ECG signals were recorded during the habitual sleep periods of $\approx$8 h. Sleep stages were annotated in 30 s epocs following standard procedures [44].

We compare the results of the young group from the SIESTA database with healthy elderly subjects from the Sleep Heart Health Study (SHHS) database. Full details of the SHHS study design and cohort are provided in [45] and [46]. Details about obtaining the ECG and polysomnographic recordings are outlined in [47]. Sleep apnea episodes were annotated, and heart rate data during apnea (obstructive and central) were excluded from our analysis . From the SHHS database, we selected a subset of 24 subjects (six males; 18 females) average age of 78.4 years (youngest 72 years; oldest 89 years). These subjects were selected by age, body weight, cardiac conditions, sleep apnea, sleep disorders, and minimum drug intake. Subject with highest age and good health were selected. There is a selection bias towards healthy elderly subject meaning that the selected group is not representative of the average population with the same average age. The purpose of this selection is to separate the effect of healthy aging from the effects of pathologic deviations which become more pronounced with age.

B. Detrended Fluctuation Analysis

The detrended fluctuation analysis (DFA) method [48] has been developed to quantify *dynamic* characteristics of physiologic fluctuations embedded in *nonstationary* physiologic signals. Compared with traditional correlation analyses, such as autocorrelation, power spectrum analysis, and Hurst analysis, the advantage of the DFA method is that it can accurately quantify the correlation property of signals masked by polynomial trends, and is described in detail in [49]–[53]. The DFA method quantifies the detrended fluctuation function $F(n)$ of a signal at different time scales n. A power-law functional form $F(n) \sim n^{\alpha}$ indicates the presence of self-similar fractal organization in the fluctuations. The parameter α, called scaling exponent, quantifies the correlation properties of the heartbeat signal: if $\alpha = 0.5$, there are no correlations (white noise); if $\alpha = 1.5$ the signal is a random walk (Brownian motion); if $0.5 < \alpha < 1.5$ there are

positive correlations, where large heartbeat intervals are more likely to be followed by large intervals (and vice versa for small heartbeat intervals); if $\alpha < 0.5$ the signal is anticorrelated where large heartbeat intervals are likely to be followed by small intervals (with stronger anticorrelations when α is closer to 0).

One advantage of the DFA method is that it can quantify signals with $\alpha > 1$, which cannot be done using the traditional autocorrelation and R/S analyses [54], as well as signals with strong anticorrelations [49]. In contrast to the conventional methods, the DFA method avoids spurious detection of apparent long-range correlations that are an artefact of nonstationary [55]. Thus, the DFA method is able to detect subtle temporal structures in highly heterogeneous physiologic time series.

An inherent limitation of the DFA analysis is the maximum time scale $n_{\max}$ for which the fluctuation function $F(n)$ can be reliably calculated. To ensure sufficient statistics at large scales it was shown that $n_{\max}$ should be chosen $n_{\max} \leq N/6$, where N is the length of the signal [49], [52], [56].

C. Magnitude and Sign Analyses

Since the DFA method quantifies *linear* fractal characteristics related to two-point correlation, we employ the magnitude and sign analyses (MSA) method to probe for long-term *nonlinear* properties in the data. Specifically, it has been shown that signals with identical self-similar temporal organization, quantified by the DFA scaling exponent α, can exhibit very different nonlinear properties captured by the MSA method [40].

The MSA method [40]–[42] consists of the following steps: 1) given a RR_i series we obtain the increment series $\Delta RR_i = RR_{i+1} - RR_i$; 2) we decompose the increment series into a magnitude series $|\Delta RR|$ and a sign series $\mathrm{sign}(\Delta RR)$; 3) because of limitations in the accuracy of the DFA method for estimating the scaling exponents of anticorrelated signals ($\alpha < 0.5$), we integrate the magnitude and sign series; 4) we perform the DFA scaling analysis; 5) to obtain the scaling exponents for the magnitude and sign series, we measure the slope of $F(n)/n$ on a log–log plot, where $F(n)$ is the fluctuation function and n is the time scale.

This approach is sensitive to nonlinear features in signals encoded in the Fourier phases [57]. We find that positive correlations in the magnitude series ($\alpha^{\mathrm{mag}} > 0.5$) are a reliable marker of long-term nonlinear properties, which are represented by the scaling behavior over a range of time scales of moments other than the second moment and relate to the width of the multifractal spectrum [42]. Thus, the MSA is a complementary method to the DFA, because it can distinguish physiologic signals with *identical* long-range fractal correlations, as quantified by the DFA method, but *different* nonlinear properties and different temporal organization for the $\mathrm{sign}\ (\Delta RR)$ series.

D. Data Processing

From the annotated ECG recordings, only the intervals RR between consecutive normal beats are considered. Intervals containing nonnormal beats are disregarded. The RR time series are then segmented corresponding to sleep stages. Within each data segment, corresponding to a given sleep stage, outliers due to missed beat detection in the ECG (which would give rise to erroneously large intervals) are marked as gaps of size G and taken out. Heartbeat RR intervals are identified as outliers when outside the interval [0.5 s; 1.55 s] or when an interbeat increment $\Delta RR > 0.35$ s (illustrated in Fig. 1). This results in removing on average 1.2% and no more than 5% of the data points for each record. Segments of RR intervals were concatenated when separated by gaps smaller than $G = 70, 35,$ and 10 heartbeats for the analysis of the time series of RR, $|\Delta RR|$, and sign (ΔRR), respectively. Segments separated by gaps larger than G were analyzed separately without concatenation.

We note that cutting out gaps in positively correlated fractal signals, such as the RR time series, does not effect the DFA and MSA scaling behavior at intermediate and large time scales [51]. For large values of G, in general, more segments of data are concatenated, which allows to explore larger time scales n in the DFA and MSA scaling analyses. We choose different values of G for the RR, $|\Delta RR|$, and sign (ΔRR) time series as we estimate α, α^{mag}, and α^{sign} at large ($n \in [50, 250]$), intermediate ($n \in [10, 150]$), and short ($n \in [7, 13]$) time scales, respectively (where n is in beat numbers). For larger values of G larger time scales n in the DFA and MSA scaling analyses are affected by the concatenation of adjacent data segments. The values for G are chosen conservatively small—our tests show that choosing larger values of G does not affect the scaling results for the fitting ranges mentioned earlier.

Because sleep stages were annotated in epocs of 30 s such coarse-graining leads to inaccuracy in determining the actual positions of sleep stage transitions. To assure that this inaccuracy does not affect our analysis, we disregard 40 heartbeats on each side of every sleep stage transition in the polysomnographic recordings. To avoid masking effects of occasional periodic breathing and sleep apnea episodes, which strongly affect cardiac dynamics [58]–[60], we disregard sections of heart rate data corresponding to central and obstructive apnea episodes, including additional 60 heartbeats before the beginning and after the end of each apnea episode to eliminate transient apnea effects.

Data segments separated by gaps due to sleep stage or apnea events transitions are never concatenated, and are always analyzed separately. For example, segments of heartbeat data during separate REM sleep stages throughout the night are treated separately in our analysis. Thus, when calculating the standard deviation σ_{RR} and $\sigma_{\Delta \mathrm{RR}}$ for these separate segments (each of which may have a different mean value), we subtract the global average for all segments (Fig. 2 and Table I). We note that subtracting the average in each segment separately leads to qualitatively the same results with the same relative difference in σ_{RR} and $\sigma_{\Delta \mathrm{RR}}$ between young and elderly and to the same stratification patterns across sleep stages as shown in Fig. 2.

E. Statistical Tests

We apply the Student's *t*-test to test the statistical significance of differences between individual pairs of conditions (age or sleep stage). Further, we use the multiple analysis of variance (MANOVA) with 2×4 design for the two groups of young and elderly and for four physiologic states, wake, REM, light, and

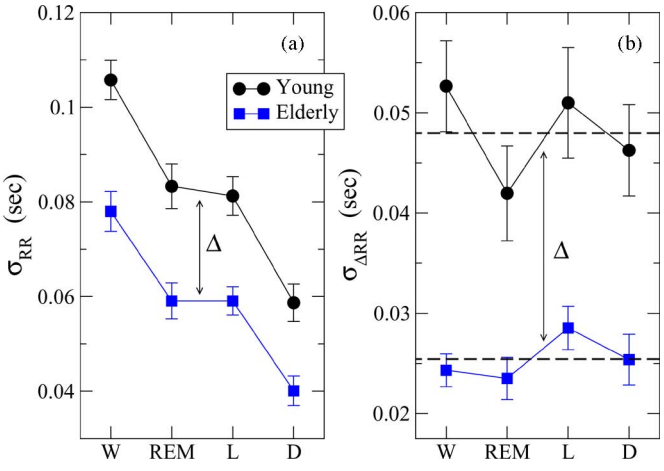

Fig. 2. Static measures of heart rate variability across sleep stages for young and elderly. (a) Group average standard deviation of the interbeat RR intervals σ_{RR} (SDNN) exhibits a statistically significant stratification across sleep stages for both young and elderly (for young: p-value $= 2.4 \times 10^{-8}$ between wake and deep sleep, and p-value $= 2.4 \times 10^{-3}$ between REM and deep sleep). (b) Group average standard deviation $\sigma_{\Delta \mathrm{RR}}$ (RMSSD) of the interbeat increments ΔRR does not show a statistically significant dependence of sleep stages for both young and elderly. Average values across all stages are indicated by dashed lines for each group. For elderly both σ_{RR} and $\sigma_{\Delta \mathrm{RR}}$ exhibit a statistically significant (see Table I) vertical shift of $\Delta \approx 0.02$ s across all sleep stages. Error bars represent the standard error.

TABLE I
STATIC AND SCALE-INVARIANT DYNAMIC CHARACTERISTICS OF HEARTBEAT FLUCTUATIONS FOR ALL SLEEP STAGES IN YOUNG AND ELDERLY

	static		*dynamic*		
	σ_{RR}	$\sigma_{\Delta \mathrm{RR}}$	α	α^{mag}	α^{sign}
Wake					
Young	.11±.03	.05±.02	.97±.14	.65±.08	.29±.22
Elderly	.08±.03	.02±.01	1.03±.13	.60±.18	.09±.17
p-value	$\mathbf{1{\times}10^{-4}}$	$\mathbf{1{\times}10^{-9}}$	.075	0.20	$\mathbf{1.6{\times}10^{-4}}$
REM					
Young	.08±.03	.04±.02	.89±.13	.69±.06	.27±.16
Elderly	.06±.02	.02±.01	1.02±.18	.62±.09	.06±.18
p -value	$\mathbf{8.9{\times}10^{-4}}$	$\mathbf{2.8{\times}10^{-4}}$	.015	.003	$\mathbf{1.6{\times}10^{-5}}$
Light					
Young	.08±.03	.05±.03	.74±.17	.61±.06	.09±.18
Elderly	.06±.02	.03±.01	.63±.15	.59±.08	.09±.16
p-value	$\mathbf{2{\times}10^{-4}}$	$\mathbf{7.4{\times}10^{-5}}$	.011	0.22	0.97
Deep					
Young	.06±.03	.05±.02	.61±.21	.58±.11	-.04±.19
Elderly	.04±.02	.03±.02	.57±.17	.55±.12	-.03±.16
p-value	**.002**	$\mathbf{8.1{\times}10^{-5}}$	.465	0.36	0.77

Subjects for which the DFA maximum scale $n_{\max} < 220$, 110, and 12 were not included in the calculation of the group average α, α^{mag}, and α^{sign}, respetively. ($n_{\max} \equiv N/6$, where N is the signal length)

deep sleep with subjects as nested random effects (JMP version 5.1.2 software analysis package, SAS Institute, Cary, NC).

III. RESULTS

A. Variability in Heartbeat Intervals and their Increments

To test whether heart rate variability changes according to sleep stage transitions (Fig. 1), and whether this variability is reduced in healthy elderly subjects for certain sleep stages, we first estimate for each subject and for each sleep stage the standard deviation of the RR interbeat intervals σ_{RR} (SDNN) and the standard deviation of the increments in the consecutive interbeat intervals $\sigma_{\Delta \mathrm{RR}}$ (RMSSD). For the group of healthy young subjects, we find that the group average σ_{RR} is highest for wake with $\langle \sigma_{\mathrm{RR}}^{\mathrm{W}} \rangle \pm \sigma = 0.11 \pm 0.03$, lower for REM and light sleep with $\langle \sigma_{\mathrm{RR}}^{\mathrm{REM}} \rangle \approx \langle \sigma_{\mathrm{RR}}^{\mathrm{L}} \rangle \approx 0.08 \pm 0.03$, and lowest for deep sleep with $\langle \sigma_{\mathrm{RR}}^{\mathrm{D}} \rangle \pm \sigma = 0.06 \pm 0.03$ [Fig. 2(a)]. A Student's t-test shows a significant difference between $\langle \sigma_{\mathrm{RR}}^{\mathrm{W}} \rangle$ and $\langle \sigma_{\mathrm{RR}}^{\mathrm{D}} \rangle$ for the young group, with a p-value $= 2.4 \times 10^{-8}$. A statistically significant difference, with a p-value $= 2.4 \times 10^{-3}$, we find also when comparing $\langle \sigma_{\mathrm{RR}}^{\mathrm{REM}} \rangle$ and $\langle \sigma_{\mathrm{RR}}^{\mathrm{L}} \rangle$ with $\langle \sigma_{\mathrm{RR}}^{\mathrm{D}} \rangle$.

Compared to the young subjects, for the group of healthy elderly subjects, we observe a very similar stratification of the values of σ_{RR} for the different sleep stages. Specifically, we find that for the elderly subjects $\langle \sigma_{\mathrm{RR}}^{\mathrm{W}} \rangle \pm \sigma = 0.08 \pm 0.03$ is significantly different from $\langle \sigma_{\mathrm{RR}}^{\mathrm{REM}} \rangle \pm \sigma = 0.06 \pm 0.02$ with p-value $= 2 \times 10^{-3}$—very similar to the statistical significance with p-value $= 6 \times 10^{-3}$ of the difference between $\langle \sigma_{\mathrm{RR}}^{\mathrm{W}} \rangle$ and $\langle \sigma_{\mathrm{RR}}^{\mathrm{REM}} \rangle$ for the young group [see Fig. 2(a)]. Further, we find that for the elderly subjects $\langle \sigma_{\mathrm{RR}}^{\mathrm{L}} \rangle \approx 0.06 \pm 0.02$ is statistically different from $\langle \sigma_{\mathrm{RR}}^{\mathrm{D}} \rangle \approx 0.04 \pm 0.02$ with p-value $= 6.4 \times 10^{-5}$. These observations demonstrate that the variability in cardiac dynamics in elderly subjects exhibits a remarkably similar stratification pattern across sleep stages as the one observed for young subjects [Fig. 2(a)].

We note that the elderly group average values for σ_{RR} are significantly lower (with a shift of $\Delta \approx 0.02$ s) for all sleep stages compared to the young group. The observed identical shift in σ_{RR} for all sleep stages [Fig. 2(a)], indicates significantly reduced heart rate variability in elderly subjects, in agreement with earlier studies [35], [59], [61], [62]. However, the response of cardiac dynamics to sleep stage transitions in healthy elderly subjects remains the same as in young subjects, as evident from the similar stratification patterns in σ_{RR} for both groups. A MANOVA-test shows that σ_{RR} changes significantly (p-value < 0.0001) with age and also with sleep stage (p-value < 0.0001).

We next consider $\sigma_{\Delta \mathrm{RR}}$, another standard static measure which quantifies the variability in consecutive beat-to-beat increments. In contrast to σ_{RR}, we do not find a stratification in the values of $\sigma_{\Delta \mathrm{RR}}$ for different sleep stages in both young and elderly subjects [Fig. 2(b)]. However, we again observe a significant reduction in the values of $\sigma_{\Delta \mathrm{RR}}$ with a shift of $\Delta \approx 0.02$ s for elderly subjects compared to the young group, consistent with earlier reports of lower heart rate variability in elderly [31]. This is also confirmed by a MANOVA-test which shows that $\sigma_{\Delta \mathrm{RR}}$ changes significantly (p-value < 0.0001) with age and but not with sleep stage (p-value $= 0.23$).

B. Fractal Temporal Correlations

We next test whether the temporal organization of heartbeat fluctuations responds to sleep stage transitions, and whether it changes with advanced age. Previous studies have shown that heartbeat fluctuations exhibit self-similar fractal organization characterized by power-law correlations over a broad range of time scales from seconds to many hours [3]–[5]. The scaling exponent α quantifying these power-law correlations has been found to change significantly with transitions from sleep to wake state [21] and with the circadian rhythm [26], [27], indicating a complete reorganization of the fractal temporal structure in cardiac dynamics across all scales.

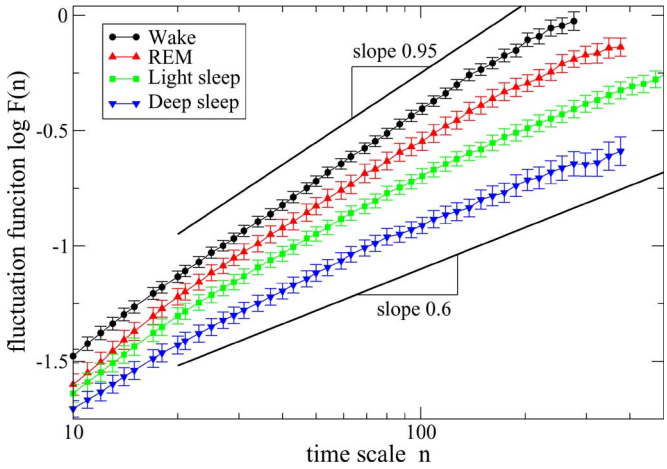

Fig. 3. Log–log plots of the group average fluctuation functions $F(n)$ versus time scale n (measured in beats) for group of young subjects using DFA-2 analysis of the heartbeat intervals RR during different sleep stages. Scaling curves $F(n)$ for all sleep stages indicate presence of long-range power-law correlations characterized by scaling exponent α over a broad range of time scales. The exponent varies from $\alpha \approx 1$ for wake (indicating strong correlations) to $\alpha \approx 0.6$ for deep sleep (week correlations) suggesting different fractal temporal organization in heartbeat fluctuations during different sleep stages. Error bars represent the standard error. The scaling curves $F(n)$ are vertically offset for clarity. As the durations of different stages vary among subjects and thus the maximum time scale $n_{\max}$ of the DFA analysis may be different for different subjects, only $F(n)$ data points averaged over at least 14 recordings are presented for each stage.

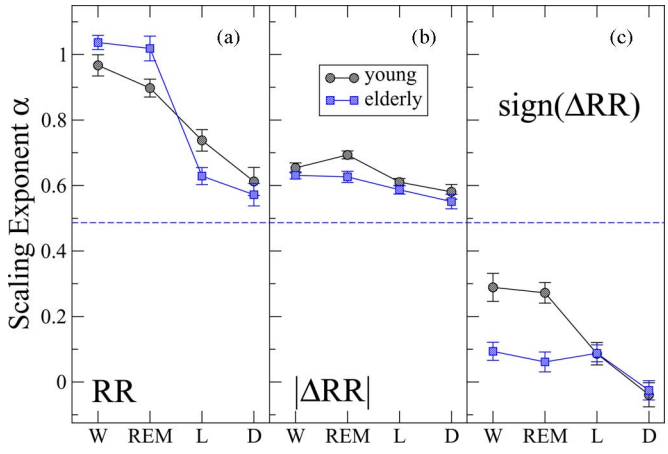

Fig. 4. Scale-invariant dynamic measures of heart rate variability across sleep stages for young and elderly. (a) Group average scaling exponent α for the time series of heartbeat intervals RR exhibits a pronounced and statistically significant stratification across sleep stages for both young and elderly. High degree of fractal correlations is observed during wake an REM with $\alpha \approx 1$ and much weaker correlations during light and deep sleep with $\alpha \approx 0.6$. Uncorrelated (white noise) behavior with $\alpha = 0.5$ is indicated by a dashed line. (b) Group average scaling exponent α^{mag} for the time series of $|\Delta RR|$. Both young and elderly exhibit long-term nonlinear behavior with $\alpha^{\mathrm{mag}} > 0.5$ and with a very similar stratification pattern across all stages: higher α^{mag}-values and higher degree of nonlinearity during wake and REM; lower α^{mag}-values and closer to linear behavior during light and deep sleep. (c) Group average scaling exponent α^{sign} for the time series of $\mathrm{sign}(\Delta RR)$. A statistically significant stratification pattern with decreasing values of α^{sign} across all stages is observed for the young group. Elderly subjects exhibit a different pattern with significantly lower values of α^{sign} during wake and REM (see Table I). Data are obtained after fitting the DFA scaling curves $F(n)$ for each individual recording in the range of time scales: $n \in [50, 250]$ beats for α; $n \in [10, 150]$ for α^{mag}; and $n \in [7, 13]$ for α^{sign}. Error bars represent the standard error.

To probe how the scale-invariant organization in the interbeat intervals RR changes across sleep stages for both young and elderly subjects, we apply the DFA scaling analysis. We find a very pronounced difference in the scaling behavior of the fluctuation function $F(n)$ for the different sleep stages (Fig. 3) with significantly different values for the DFA scaling exponent α [Fig. 4(a)]. Specifically, we find a clear stratification in the group average scaling exponent α, with highest value for the wake state, followed by a lower value for REM sleep and even lower values for light and deep sleep (Fig. 4(a) and Table I). Employing a Student's *t*-test for both young and elderly subjects we find a statistically significant difference between the group average exponent α^{W} for wake and α^{D} for deep sleep with p-value $= 2 \times 10^{-7}$ and p-value $= 10^{-17}$, respectively (see Table I). We also find a statistically significant difference between α^{REM} for REM sleep and α^{L} for light sleep with p-value $= 9 \times 10^{-4}$ and p-value $= 6.5 \times 10^{-12}$, respectively for the young and elderly groups. Performing a MANOVA-test we find a significant change in α_{RR} across sleep stages (p-value < 0.0001) but an insignificant change with age (p-value $= 0.93$).

Our findings indicate 1) a significant change in the fractal temporal organization of heartbeat fluctuations in response to transitions across sleep stages, in agreement with [22] and [24], and surprisingly 2) that fractal correlations within each sleep stage remain robust and do not significantly change with healthy aging.

C. Magnitude and Sign Correlation

Scale-invariant fractal processes with identical long-range power-law correlation may exhibit very different dynamics for the magnitude and sign of their fluctuations [40]. It has been found that the information contained in the temporal organization of the magnitude and the sign time series is independent and complementary to the correlation properties of the original time series [41], [42]. For cardiac dynamics of healthy subjects during routine daily activity, it was shown that heartbeat intervals exhibit power-law correlations at intermediate and large time scales characterized by a scaling exponent $\alpha \approx 1$ [15], while at the same time scales the magnitude series of the increments ΔRR in the consecutive heartbeat intervals is characterized by $\alpha^{\mathrm{mag}} \approx 0.75$ [40]. Further, while the correlations in RR reflect the linear properties of cardiac dynamics, the temporal structure in the magnitude of heartbeat increments ΔRR relates to the nonlinear properties encoded in the Fourier phases [42], [57]. For certain pathologic conditions, such as congestive heart failure, which are associated with loss of nonlinearity in cardiac dynamics [6], [9], [11], previous studies have reported breakdown of the nonlinear multifractal spectrum [10] and reduced scaling exponent α^{mag} [40] related to loss of Fourier-phase correlations.

To probe how the long-term nonlinear properties of heartbeat fluctuations change across sleep stages, we investigate the correlations in the magnitude of the interbeat interval increments ΔRR. For both groups of young and elderly subjects we find that for all sleep stages, the scaling exponent α^{mag} is significantly higher than 0.5, indicating nonlinear dynamics during

sleep [Fig. 4(b)]. We also find that both young and elderly subjects exhibit a clear stratification in the group average values of α^{mag} across all sleep stages (although not so pronounced as in α). In particular, we find highest values for α^{mag} during wake, followed by lower values during REM and light sleep, and lowest α^{mag}-values during deep sleep (Fig. 4(b) and Table I), in agreement with [23].

Our results indicate a nonlinear behavior, consistent for both young and elderly subjects, where cardiac dynamics exhibit higher degree of nonlinearity during wake and REM sleep, and closer to linear behavior during light and deep sleep [Fig. 4(b)]. Furthermore, based on a paired Student's *t*-test, for the elderly subjects, we find a slight but not statistically significant shift to lower α^{mag}-values for all sleep stages compared to the young group (Table I). Applying a MANOVA-test, we find a p-value $= 0.005$ with age and a significant change in α^{mag} across sleep stages (p-value $= 0.0002$).

For the sign of the interbeat increment ΔRR time series in young subjects we again find a clear and significant stratification in the values of the scaling exponent α^{sign} (Fig. 4(c) and Table I). In particular, we find highest α^{sign}-values during wake, followed by REM and light sleep, and lowest α^{sign}-values during deep sleep—a stratification pattern very similar to the one we observe for σ_{RR}, α, and α^{mag}. This indicates stronger anticorrelations in the sign (ΔRR) time series during light and deep sleep, and weaker anticorrelations during REM and wake. This stratification pattern is in contrast to the behavior we find for the elderly subjects, where there is no significant difference between wake, REM, and light sleep [Fig. 4(c)]. The values of α^{sign} during light and deep sleep are almost the same for both young and elderly. In addition, we observe a significant difference between young and elderly subjects during wake (with a p-value $= 1.6 \times 10^{-4}$) and during REM (with a p-value $= 1.6 \times 10^{-5}$), with elderly subjects characterized by lower values for the exponent α^{sign} [Fig. 4(c)]. The result of a MANOVA-test indicates a statistical significant difference between the two age groups (p-value $= 0.0001$) and a significant difference across sleep stages (p-value $= 0.0001$). These results suggests that the difference between young and elderly subjects is most pronounced in the sign (ΔRR) time series during wake and REM with stronger anticorrelations for elderly.

IV. Discussion

Our results show that key static and dynamic measures of heart rate variability exhibit a pronounced and statistically significant stratification pattern across sleep stages. We find a remarkably similar stratification pattern for both static and dynamic measures, with consistently higher values during wake, lower values during REM and light sleep, and lowest during deep sleep. This stratification of static and dynamic measures is surprisingly robust, as we observe very similar patterns for both young and elderly subjects, despite significantly reduced heart rate variability with age (Table I) [31], [35]. These results indicate that the influence of sleep regulation on the autonomic cardiac activity does not break down with progressive healthy aging.

A. Static Measures

We find that the standard deviation σ_{RR} of the heartbeat intervals, a static measure of cardiac dynamics, decreases significantly when comparing wake, REM, light, and deep sleep (Fig. 2). This indicates a strong responsiveness of cardiac dynamics to changes in sleep regulation across different sleep stages. The coupling between sleep and cardiac control appears to be robust, as we find the same stratification pattern in σ_{RR} for both healthy young and elderly subjects (Fig. 2). While the stratification patterns in σ_{RR} are the same for the young and the elderly groups, there is a significant vertical shift of size $\Delta \approx 0.02\,\mathrm{s}$ to lower values of σ_{RR} in elderly subjects, consistently across all sleep stages [Fig. 2(a)]. These findings are in agreement with earlier reports of reduced heart rate variability with healthy aging during REM and non-REM sleep [59], [62]. However, the existence of a specific stratification pattern in the values of σ_{RR}, which remains unchanged with advanced age, has not been previously reported. We note, that for both young and elderly groups the difference in the group average standard deviation between wake and deep sleep $\langle \sigma_{\mathrm{RR}}^{\mathrm{W}} \rangle - \langle \sigma_{\mathrm{RR}}^{\mathrm{D}} \rangle \approx 0.04$ s is approximately twice larger than the vertical shift Δ we find between young and elderly. These results indicate that the effect of sleep regulation on heart rate variability, as measured by $\langle \sigma_{\mathrm{RR}} \rangle$, is stronger than the effect of aging (average age difference of 45 years between the young and elderly groups).

The pronounced stratification pattern we find in σ_{RR} across sleep stages relates to reduction in sympathetic tone during light and deep sleep compared to wake and REM [33], [34]. As the sympathetic activity is represented by the low-frequency range in the heart rate power spectrum [34], [63], bursts of sympathetic tone and parasympathetic withdrawal lead to increased nonstationarity of the interbeat interval time series characterized by higher values of σ_{RR} during wake and REM. With gradual decrease of sympathetic tone during light and deep sleep the degree of nonstationarity also decreases, and therefore, σ_{RR} is reduced. This is also observed for the group of healthy elderly subjects, however, with lower values of σ_{RR} for all sleep stages due to reduced parasympathetic tone in elderly.

In contrast to σ_{RR}, for the standard deviation $\sigma_{\Delta \mathrm{RR}}$ of the increments in the consecutive heartbeat intervals ΔRR, another static measure, we do not find a significant change across sleep stages for both young and elderly subjects. This measure is insensitive to nonstationarity in the interbeat time series as it filters out low-frequency trends associated with sympathetic activity. Thus, $\sigma_{\Delta \mathrm{RR}}$ does not capture the different degree of nonstationarity related to changes in the level of sympathetic activity during different sleep stages. However, $\sigma_{\Delta \mathrm{RR}}$ reflects the high-frequency variability in the interbeat time series related to parasympathetic activity. For the elderly subjects, we find a significant reduction of $\Delta \approx 0.025$ s in the values of $\sigma_{\Delta \mathrm{RR}}$ for all sleep stages, indicating a reduction in parasympathetic tone with aging (Fig. 2(b) and Table I).

There is a strong positive correlation between σ_{RR} and low-frequency heart rate variability, as well as between $\sigma_{\Delta \mathrm{RR}}$ and high-frequency variability [64]. As $\sigma_{\Delta \mathrm{RR}}$ represents high-frequency parasympathetic inputs and filters out low-frequency

sympathetic inputs, the fact that we do not observe a significant reduction in $\sigma_{\Delta \mathrm{RR}}$ between REM and deep sleep suggests that parasympathetic tone does not significantly change. This, in turn, suggests that the statistically significant drop we find in σ_{RR} between REM and deep sleep in both healthy young and elderly subjects is due to a significant reduction of sympathetic activity. On the other hand, a similar drop of $\Delta \approx 0.02$ s between σ_{RR} for the young and σ_{RR} for the elderly subjects during REM must be caused by suppression of parasympathetic tone in elderly, as we also find a similar drop of $\Delta \approx 0.02$ s in $\sigma_{\Delta \mathrm{RR}}$, which is a measure sensitive only to parasympathetic tone. Thus, while both σ_{RR} and $\sigma_{\Delta \mathrm{RR}}$ are static measures, they reflect fundamentally different aspects of cardiac control: while σ_{RR} captures both sympathetic and parasympathetic activity, and thus changes across sleep stages as well as with advanced age, the complementary measure $\sigma_{\Delta \mathrm{RR}}$ is only sensitive to changes in the parasympathetic activity, and thus changes only with age.

B. Dynamic Measures

Our results demonstrate that dynamic measures, such as α, α^{mag}, and α^{sign}, which probe the temporal fractal and nonlinear organization in heartbeat fluctuations, also change with transitions across sleep stages. Moreover, this change is very similar for both young and elderly subjects indicating a robust influence of sleep regulation on the temporal fractal correlations of heartbeat fluctuations. Specifically, we find significantly stronger correlations during wake and REM compared to light and deep sleep [Fig. 4(a)].

The scaling exponent α is determined over a range of long and intermediate time scales corresponding to low and intermediate frequencies in the power spectrum (Fig. 4). Thus, α mainly quantifies the contribution of the sympathetic component of neuroautonomic control to the fractal temporal organization of heartbeat fluctuations, as sympathetic tone affects low and intermediate frequencies [65]—i.e., higher values of α during wake and REM reflect significantly higher sympathetic activity compared to lower values of α during light and deep sleep. We note that although traditional heart rate variability measures, such as high and low frequency power [38], have been found to change significantly between healthy young and elderly subjects [59], [62], a consistent stratification pattern across sleep stages has not been previously found.

Our observation that two independent measures—the static measure σ_{RR} and the dynamic measure α that quantify different aspects of cardiac dynamics—change consistently across sleep stages and exhibit a very similar stratification pattern for both young and elderly subjects confirm our hypothesis of strong coupling between sleep and cardiac regulation. These results clearly indicate that heart rate variability changes significantly with transitions from one sleep stage to another in response to changes in sleep regulation during different sleep stages, where the values of σ_{RR} and α follow a particular order. In other words, our findings of a similar stratification pattern for both σ_{RR} and α indicates that the underlying regulatory mechanism affects two independent[1] measures in a similar way. As the reflexive-responsiveness of cardiac dynamics in healthy young subjects is intact, the observed stratification pattern in the values of σ_{RR} and α—highest for wake, lower for REM and light sleep, and lowest for deep sleep—can only be attributed to the influence of different modes of sleep regulation during different sleep stages. As described in the Section III, the variability σ_{RR} is almost the same in REM and light sleep with significant differences to the wake and deep sleep states. In contrast, the α-values show most pronounced changes, specifically in elderly, between REM and light sleep.

We note that, compared to the young group, elderly subjects are characterized by higher values of the scaling exponent α during wake and REM, and slightly lower values for light and deep sleep. In contrast to σ_{RR} and $\sigma_{\Delta \mathrm{RR}}$ we do not find a significant shift to lower values for the scaling exponent α in elderly. The higher values of α for elderly subjects during wake and REM indicate higher degree of correlations in heartbeat fluctuations, and reflect lower parasympathetic tone in elderly compared to young subjects.

A similar, however, less pronounced stratification pattern we observe also for the scaling exponent α^{mag}, which quantifies the long-term nonlinear properties of heartbeat dynamics encoded in the Fourier phases [42], [57]. This finding indicates higher degree of nonlinearity in cardiac dynamics during wake and REM, and closer to linear behavior during light and deep sleep. We find this tendency to hold for both young and elderly subjects [Fig. 4(b)]. We note that while there is a slightly lower degree of nonlinearity in elderly (lower α^{mag}-values) for all sleep stages, the difference in α^{mag} between wake/REM and light/deep sleep is larger compared to the difference between the young and elderly groups. This indicates that the influence of sleep regulation on the nonlinearity, as measured by α^{mag}, is stronger than the effect of aging in healthy subjects.

Finally, for the scaling exponent α^{sign} that quantifies the short-term correlations in the directionality of heart beat increments, we again find a pronounced stratification pattern with statistically significant differences between the values α^{sign} for different sleep stages. As for σ_{RR}, α, and α^{mag}, the values of α^{sign} for young subjects are highest during wake, lower during REM and light sleep, and lowest during deep sleep [Fig. 4(c)]. In contrast to α and α^{mag}, the values of α^{sign} during wake and REM sleep are very different (much lower values) for elderly subjects (Table I).

Our findings have implications for comparative studies (healthy versus disease, young versus elderly, etc.) when ECG data during sleep are analyzed without prior knowledge of the sleep stages. The observation that certain measures of cardiac dynamics significantly change across sleep stages forming specific stratification patterns, may facilitate the development of

[1]Note that σ is a static measure of the standard deviation of a signal, while α measures the temporal correlations of signal. In fact, signals with identical σ can exhibit completely different temporal correlations. Inversely, e.g., dividing all data point values in a correlated time series by a factor of 2 would reduce the σ by a factor of 2 but will leave the scaling exponent α, representing the temporal correlations unchanged.

automated detection of sleep stages based only on ECG recordings.

In summary, our results show that key static and dynamic measures of cardiac control change significantly in response to sleep stage transitions and exhibit a pronounced stratification pattern across sleep stages. For both static and dynamics measures this stratification pattern is characterized by highest values during wake, and decreasing values for REM, light and deep sleep. Our results indicate that not only the heart rate variability but also the fractal and nonlinear organization of heartbeat fluctuations follow the same stratification pattern, suggesting a fundamentally different cardiac dynamics during different sleep stages. This stratification pattern appears remarkably robust as we observe it both in young and elderly subjects. Moreover, for all sleep stages the elderly subjects exhibit very similar values for the linear and nonlinear scaling measures of cardiac dynamics compared to the young subjects, indicating that the fractal temporal organization of cardiac dynamics does not break down with healthy aging.

Further, our observations indicate that under healthy conditions the coupling between the mechanism of sleep regulation and the neuroautonomic cardiac control does not break down with progressive aging, despite significant reduction in heart rate variability and alterations of sleep architecture in elderly. Moreover, we find that the differences between the values of key static and dynamic measures of heart rate variability for different sleep stages exceed the differences between young and elderly subjects, suggesting that the effect of sleep regulation on cardiac dynamics is significantly stronger compared to the effect of healthy aging. Finally, these findings suggest a significant revision of the current theory of complexity loss with aging compared to disease, and provide new understanding of how sleep regulation affects cardiac dynamics in young and elderly. Quantifying changes in the stratification pattern, we uncover, across sleep stages can provide insights into how alterations in sleep regulation contribute to increased cardiac risk.

ACKNOWLEDGMENT

This paper represents the work of the authors and not the SHHS. This study was supported by National Institutes of Health (NIH) Grant 2 RO1 HL071972 and the Volkswagen Foundation.

REFERENCES

[1] J. Bassingthwaighte, L. Liebovitch, and B. West, *Fractal Physiol*. London, U.K.: Oxford Univ. Press, 1994.

[2] M. Malik and A. J. Camm, *Heart Rate Variability*. Armonk, NY: Futura, 1995.

[3] M. Kobayashi and T. Musha, "$1/f$ fluctuation of heartbeat period," *IEEE Trans. Biomed. Eng.*, vol. BME-29, no. 6, pp. 456–457, Jun. 1982.

[4] J. Saul, P. Albrecht, R. Berger, and R. Cohen, "Analysis of long term heart rate variability: methods, $1/f$ scaling and implications.," *Comput. Cardiol.*, vol. 14, pp. 419–422, 1988.

[5] C.-K. Peng, J. Mietus, J. M. Hausdorff, S. Havlin, H. E. Stanley, and A. L. Goldberger, "Long-range anticorrelations and non-Gaussian behavior of the heartbeat," *Phys. Rev. Lett.*, vol. 70, no. 9, pp. 1343–1346, 1993.

[6] J. H. Lefebvre, D. A. Goodings, M. V. Kamath, and E. L. Fallen, "Predictability of normal heart rhythms and deterministic chaos," *Chaos*, vol. 3, no. 2, pp. 267–276, 1993.

[7] J. Kurths, A. Voss, P. Saparin, A. Witt, H. J. Kleiner, and N. Wessel, "Quantitative analysis of heart rate variability," *Chaos*, vol. 5, no. 1, pp. 88–94, 1995.

[8] G. Sugihara, W. Allan, D. Sobel, and K. Allan, "Nonlinear control of heart rate variability in human infants," *Proc. Nat. Acad. Sci. USA*, vol. 93, pp. 2608–2613, 1996.

[9] C.-S. Poon and C. K. Merrill, "Decrease of cardiac chaos in congestive heart failure," *Nature*, vol. 389, pp. 492–495, 1997.

[10] P. Ch. Ivanov, M. G. Rosenblum, L. A. N. Amaral, Z. R. Struzik, S. Havlin, A. L. Goldberger, and H. E. Stanley, "Multifractality in human heartbeat dynamics," *Nature*, vol. 399, pp. 461–465, 1999.

[11] P. Ch. Ivanov, L. A. N. Amaral, A. L. Goldberger, S. Havlin, M. G. Rosenblum, H. E. Stanley, and Z. Struzik, "From $1/f$ noise to multifractal cascades in heartbeat dynamics," *Chaos*, vol. 11, pp. 641–652, 2001.

[12] Y. Yamamoto and R. L. Hughson, "On the fractal nature of heart rate variability in humans: Effects of data length and beta-adrenergic blockade," *Amer. J. Physiol.*, vol. 266, no. 1, Pt 2, pp. R40–R49, 1994.

[13] Y. Yamamoto, Y. Nakamura, H. Sato, M. Yamamoto, K. Kato, and R. Hughson, "On the fractal nature of heart rate variability in humans: Effects of vagal blockade," *Amer. J. Physiol. Regul. Integr. Comp. Physiol.*, vol. 269, pp. R830–R837, 1995.

[14] L. A. N. Amaral, P. Ch. Ivanov, N. Aoyagi, I. Hidaka, S. Tomono, A. L. Goldberger, H. E. Stanley, and Y. Yamamoto, "Behavioral-independent features of complex heartbeat dynamics," *Phys. Rev. Lett.*, vol. 86, no. 26, pp. 6026–6029, 2001.

[15] C.-K. Peng, S. Havlin, H. E. Stanley, and A. L. Goldberger, "Quantification of scaling exponents and crossover phenomena in nonstationary heartbeat time series," *Chaos*, vol. 5, no. 1, pp. 82–87, 1995.

[16] K. K. L. Ho, G. B. Moody, C.-K. Peng, J. E. Mietus, M. G. Larson, D. Levy, and A. L. Goldberger, "Predicting survival in heart failure cases and controls using fully automated methods for deriving nonlinear and conventional indices of heart rate dynamics," *Circulation*, vol. 96, pp. 842–848, 1997.

[17] H. V. Huikuri, T. H. Mäkikallio, C.-K. Peng, A. L. Goldberger, U. Hintze, and M. Moller, "Fractal correlation properties of R–R interval dynamics and mortality in patients with depressed left ventricular function after an acute myocardial infarction," *Circulation*, vol. 101, pp. 47–53, 2000.

[18] R. Karasik, N. Sapir, Y. Ashkenazy, P. Ch. Ivanov, I. Dvir, P. Lavie, and S. Havlin, "Correlation differences in heartbeat fluctuations during rest and exercise," *Phys. Rev. E*, vol. 66, no. 6, 062902, 2002.

[19] M. Martinis, A. Knezevic, G. Krstacic, and E. Vargovic, "Changes in the Hurst exponent of heartbeat intervals during physical activity," *Phys. Rev. E*, vol. 70, no. 1, pp. 012903-1–012903-9, 2004.

[20] J. C. Echeverria, S. D. Aguilar, M. R. Ortiz, J. Alvarez-Ramirez, and R. González Camarena, "Comparison of RR-interval scaling exponents derived from long and short segments at different wake periods," *Physiol. Meas.*, vol. 27, no. 4, pp. N19–N25, 2006.

[21] P. Ch. Ivanov, A. Bunde, L. Amaral, S. Havlin, J. Fritsch Yelle, R. Baevsky, H. E. Stanley, and A. Goldberger, "Sleep–wake differences in scaling behavior of the human heartbeat: Analysis of terrestrial and long-term space flight data," *Europhys. Lett.*, vol. 48, no. 5, pp. 594–600, 1999.

[22] A. Bunde, S. Havlin, J. W. Kantelhardt, T. Penzel, J.-H. Peter, and K. Voigt, "Correlated and uncorrelated regions in heart-rate fluctuations during sleep," *Phys. Rev. Lett.*, vol. 85, no. 17, pp. 3736–3739, 2000.

[23] J. W. Kantelhardt, Y. Ashkenazy, P. Ch. Ivanov, A. Bunde, S. Havlin, T. Penzel, J.-H. Peter, and H. E. Stanley, "Characterization of sleep stages by correlations in the magnitude and sign of heartbeat increments," *Phys. Rev. E*, vol. 65, no. 5, 051908, 2002.

[24] I. Dvir, Y. Adler, D. Freimark, and P. Lavie, "Evidence for fractal correlation properties in variations of peripheral arterial tone during REM sleep," *Amer. J. Physiol. Heart Circ. Physiol.*, vol. 283, no. 1, pp. H434–H436, 2002.

[25] T. Penzel, N. Wessel, M. Riedl, J. W. Kantelhardt, S. Rostig, M. Glos, A. Suhrbier, H. Malberg, and I. Fietze, "Cardiovascular and respiratory dynamics during normal and pathological sleep," *Chaos*, vol. 17, no. 1, 015116, 2007.

[26] H. Moelgaard, K. E. Soerensen, and P. Bjerregaard, "Circadian variation and influence of risk factors on heart rate variability in healthy subjects," *Amer. J. Cardiol.*, vol. 68, pp. 777–784, 1991.

[27] K. Hu, P. Ch. Ivanov, M. F. Hilton, Z. Chen, R. T. Ayers, H. E. Stanley, and S. A. Shea, "Endogenous circadian rhythm in an index of cardiac vulnerability independent of changes in behavior," *PNAS*, vol. 101, no. 52, pp. 18223–18227, 2004.

[28] P. Ch. Ivanov, K. Hu, M. F. Hilton, S. A. Shea, and H. E. Stanley, "Endogenous circadian rhythm in human motor activity uncoupled from circadian

influences on cardiac dynamics," *Proc. Nat. Acad. Sci. USA*, vol. 104, no. 52, pp. 20 702–20 707, Dec. 2007.
[29] V. D. A. Corino, M. Matteuccib, L. Cravelloc, E. Ferraric, A. A. Ferrarid, and L. T. Mainardi, "Long-term heart rate variability as a predictor of patient age," *Comp. Methods Prog. Biomed.*, vol. 82, no. 3, pp. 248–257, 2006.
[30] L. A. Lipsitz and A. L. Goldberger, "Loss of 'complexity' and aging. Potential applications of fractals and chaos theory to senescence," *JAMA*, vol. 267, no. 13, pp. 1806–1809, 1992.
[31] K. Umetani, D. H. Singer, R. McCraty, and M. Atkinson, "Twenty-four hour time domain heart rate variability and heart rate: Relations to age and gender over nine decades," *J. Amer. College Cardiol.*, vol. 31, no. 3, pp. 593–601, 1998.
[32] D. L. Bliwise, "Sleep in normal aging and dementia," *Sleep*, vol. 16, no. 1, pp. 40–81, 1993.
[33] V. K. Somers, M. E. Dyken, A. L. Mark, and F. M. Abboud, "Sympathetic-nerve activity during sleep in normal subjects," *N. Engl. J. Med.*, vol. 328, no. 5, pp. 303–307, 1993.
[34] A. Baharav, S. Kotagal, V. Gibbons, B. K. Rubin, G. Pratt, J. Karin, and S. Akselrod, "Fluctuations in autonomic nervous activity during sleep displayed by power spectrum analysis of heart rate variability," *Neurology*, vol. 45, no. 6, pp. 1183–1187, 1995.
[35] H. Tsuji, F. J. Venditti, E. S. Manders, J. C. Evans, M. G. Larson, C. L. Feldman, and D. Levy, "Reduced heart rate variability and mortality risk in an elderly cohort. The framingham heart study," *Circulation*, vol. 90, pp. 878–883, 1994.
[36] L. Grote, T. Ploch, J. Heitmann, L. Knaack, T. Penzel, and J. H. Peter, "Sleep-related breathing disorder is an independent risk factor for systemic hypertension," *Amer. J. Respir. Crit. Care Med.*, vol. 160, no. 6, pp. 1875–1882, 1999.
[37] V. Mohsenin, "Sleep-related breathing disorders and risk of stroke," *Stroke*, vol. 32, no. 6, pp. 1271–1278, 2001.
[38] Electrophysiology, Task Force of the European Society of Cardiology the North American Society of Pacing, "Heart rate variability: Standards of measurement, physiological interpretation, and clinical use," *Circulation*, vol. 93, no. 5, pp. 1043–1065, 1996.
[39] A. P. Hallstrom, P. K. Stein, R. Schneider, M. Hodges, G. Schmidt, and K. Ulm, "Structural relationships between measures based on heart beat intervals: Potential for improved risk assessment," *IEEE Trans. Biomed. Eng.*, vol. 51, no. 8, pp. 1414–1420, Aug. 2004.
[40] Y. Ashkenazy, P. Ch. Ivanov, S. Havlin, C.-K. Peng, A. L. Goldberger, and H. E. Stanley, "Magnitude and sign correlations in heartbeat fluctuations," *Phys. Rev. Lett.*, vol. 86, no. 9, pp. 1900–1903, 2001.
[41] Y. Ashkenazy, P. Ch. Ivanov, S. Havlin, C.-K. Peng, Y. Yamamoto, A. L. Goldberger, and H. E. Stanley, "Decomposition of heartbeat time series: Scaling analysis of the sign sequence," *Comput. Cardiol.*, vol. 27, pp. 139–142, 2000.
[42] Y. Ashkenazy, S. Havlin, P. Ch. Ivanov, C.-K. Peng, V. Schulte-Frohlinde, and H. E. Stanley, "Magnitude and sign scaling in power-law correlated time series," *Physica A*, vol. 323, pp. 19–41, 2003.
[43] G. Klösch, B. Kemp, T. Penzel, A. Schlögl, P. Rappelsberger, E. Trenker, G. Gruber, J. Zeitlhofer, B. Saletu, W. M. Herrmann, S. L. Himanen, D. Kunz, M. J. Barbanoj, J. Röschke, A. Värri, and G. Dorffner, "The siesta project polygraphic and clinical database," *IEEE Eng. Med. Biol. Mag.*, vol. 20, no. 3, pp. 51–57, May/Jun. 2001.
[44] A. Rechtschaffen and A. Kales, *A Manual of Standardized Terminology, Techniques and Scoring System for Sleep Stages of Human Subjects*. Bethesda, MD: U.S. Dept. of Health, Education, and Welfare, 1968.
[45] S. Quan, B. Howard, C. Iber, J. Kiley, F. Nieto, G. O'Connor, D. Rapoport, S. Redline, J. Robbins, J. Samet, and P. Wahl, "The Sleep Heart Health Study: Design, rationale, and methods," *Sleep*, vol. 20, no. 12, pp. 1077–1085, 1997.
[46] B. K. Lind, J. L. Goodwin, J. G. Hill, T. Ali, S. Redline, and S. F. Quan, "Recruitment of healthy adults into a study of overnight sleep monitoring in the home: Experience of the Sleep Heart Health Study," *Sleep Breath*, vol. 7, no. 1, pp. 13–24, 2003.
[47] S. Redline, M. H. Sanders, B. K. Lind, S. F. Quan, C. Iber, D. J. Gottlieb, W. H. Bonekat, D. M. Rapoport, P. L. Smith, and J. P. Kiley, "Methods for obtaining and analyzing unattended polysomnography data for a multicenter study. Sleep Heart Health Research Group," *Sleep*, vol. 21, no. 7, pp. 759–767, 1998.
[48] C.-K. Peng, S. V. Buldyrev, S. Havlin, M. Simons, H. E. Stanley, and A. L. Goldberger, "Mosaic organization of DNA nucleotides," *Phys. Rev. E*, vol. 49, no. 2, pp. 1685–1689, 1994.
[49] K. Hu, P. Ch. Ivanov, Z. Chen, P. Carpena, and H. E. Stanley, "Effect of trends on detrended fluctuation analysis," *Phys. Rev. E*, vol. 64, no. 1, 011114, 2001.
[50] J. W. Kantelhardt, E. Koscielny-Bunde, H. H. Rego, S. Havlin, and A. Bunde, "Detecting long-range correlations with detrended fluctuation analysis," *Physica A*, vol. 295, no. 3–4, pp. 441–454, 2001.
[51] Z. Chen, P. Ch. Ivanov, K. Hu, and H. E. Stanley, "Effect of nonstationarities on detrended fluctuation analysis," *Phys. Rev. E*, vol. 65, no. 4, 041107, 2002.
[52] L. Xu, P. Ch. Ivanov, K. Hu, Z. Chen, A. Carbone, and H. E. Stanley, "Quantifying signals with power-law correlations: A comparative study of detrended fluctuation analysis and detrended moving average techniques," *Phys. Rev. E*, vol. 71, no. 5, 051101, 2005.
[53] Z. Chen, K. Hu, P. Carpena, P. Bernaola Galvan, H. E. Stanley, and P. Ch. Ivanov, "Effect of nonlinear filters on detrended fluctuation analysis," *Phys. Rev. E*, vol. 71, no. 1, 011104, 2005.
[54] J. Feder, *Fractals*. New York: Plenum, 1988.
[55] M. Taqqu, V. Teverovsky, and W. Willinger, "Estimators for long-range dependence: An empirical study," *Fractals*, vol. 3, no. 4, pp. 785–788, 1995.
[56] A. V. Coronado and P. Carpena, "Size effects on correlation measures," *J. Biol. Phys.*, vol. 31, no. 1, pp. 121–133, 2005.
[57] J. Theiler, S. Eubank, A. Longtin, B. Galdrikian, and D. J. Garmer, "Testing for nonlinearity in time series: The method of surrogate data," *Physica D*, vol. 58, pp. 77–94, 1992.
[58] T. Penzel, J. Kantelhardt, C. Lo, K. Voigt, and C. Vogelmeier, "Dynamics of heart rate and sleep stages in normals and patients with sleep apnea," *Neuropsychopharmacology*, vol. 28, pp. S48–S53, 2003.
[59] G. Brandenberger, A. U. Viola, J. Ehrhart, A. Charloux, B. Geny, F. Piquard, and C. Simon, "Age-related changes in cardiac autonomic control during sleep," *J. Sleep Res.*, vol. 12, no. 3, pp. 173–180, 2003.
[60] D. T. Schmitt and P. Ch. Ivanov, "Fractal scale-invariant and nonlinear properties of cardiac dynamics remain stable with advanced age: a new mechanistic picture of cardiac control in healthy elderly," *Amer. J. Physiol. Regul. Integr. Comp. Physiol.*, vol. 293, no. 5, pp. R1923–1937, 2007.
[61] N. Iyengar, C.-K. Peng, R. Morin, A. L. Goldberger, and L. A. Lipsitz, "Age-related alterations in the fractal scaling of cardiac interbeat interval dynamics," *Amer. J. Physiol. Regul. Integr. Comp. Physiol.*, vol. 271, no. 4, pp. 1078–1084, 1996.
[62] V. Crasset, S. Mezzetti, M. Antoine, P. Linkowski, J. P. Degaute, and P. van de Borne, "Effects of aging and cardiac denervation on heart rate variability during sleep," *Circulation*, vol. 103, no. 1, pp. 84–88, 2001.
[63] M. H. Bonnet and D. L. Arand, "Heart rate variability: Sleep stage, time of night, and arousal influences," *Electroencephalogr. Clin. Neurophysiol.*, vol. 102, no. 5, pp. 390–396, 1997.
[64] H. Otzenberger, C. Gronfier, C. Simon, A. Charloux, J. Ehrhart, F. Piquard, and G. Brandenberger, "Dynamic heart rate variability: A tool for exploring sympathovagal balance continuously during sleep in men," *Amer. J. Physiol. Heart Circ. Physiol.*, vol. 275, no. 3, pp. H946–950, 1998.
[65] S. Akselrod, D. Gordon, F. A. Ubel, D. C. Shannon, A. C. Berger, and R. J. Cohen, "Power spectrum analysis of heart rate fluctuation: A quantitative probe of beat-to-beat cardiovascular control," *Science*, vol. 213, no. 4504, pp. 220–222, 1981.

Daniel T. Schmitt received the M.S. degree in theoretical physics from the University of Massachusetts at Dartmouth, North Dartmouth, in 2003, and the Ph.D. degree in statistical physics and biophysics from the University of Ulm, Ulm, Germany, in 2007.

He received a two-year research grant from the Volkswagen Foundation, which enabled him to work on physiological time series analysis at Boston University and Harvard Medical School.

Phyllis K. Stein received the Ph.D. degree in health promotion from the University of Virginia, Charlottesville, VA, in 1990.

She is currently a Research Associate Professor of Medicine in the Division of Cardiology, Washington University School of Medicine, and where she is the Director of the Heart Rate Variability (HRV) Laboratory. Her current research interest includes the integration of heart-rate-based markers, including HRV, and information from polysomnography as markers of cardiovascular autonomic and central nervous system function, and as predictors of functional status and survival in the elderly.

Plamen Ch. Ivanov received the M.S. degree in theoretical physics/condensed matter physics from Sofia University, Sofia, Bulgaria, in 1988, the Ph.D. degree in biophysics from Boston University, Boston, MA, in 1998, and the D.Sc. degree from the Bulgarian Academy of Sciences, Sofia, in 2007.

He is currently a Research Associate Professor at the Physics Department, Boston University, a Lecturer at Harvard Medical School, Brigham and Women's Hospital, Boston, and a Professor at the Institute of Solid State Physics, Bulgarian Academy of Sciences. His current research interests include methods of analysis and modeling of integrated biological and physiological systems and networks; multiscale dynamical properties emerging from cellular level interactions; neural regulation; stochastic processes and phase transitions. He has served as an editor of Fluctuation and Noise Letters (FNL) in the period 2000–2002, and he is currently on the Editorial Board of the Journal of Biological Physics (JOBP) and Europhysics Letters (EPL).

Stratification Pattern of Static and Scale-Invariant Dynamic Measures of Heartbeat Fluctuations Across Sleep Stages in Young and Elderly

By: Schmitt, DT (Schmitt, Daniel T.)[1,2,3]; Stein, PK (Stein, Phyllis K.)[4]; Ivanov, PC (Ivanov, Plamen Ch.)[1,2,5,6]

View ResearcherID and ORCID

IEEE TRANSACTIONS ON BIOMEDICAL ENGINEERING
Volume: 56 **Issue:** 5 **Pages:** 1564-1573
DOI: 10.1109/TBME.2009.2014819
Published: MAY 2009
Document Type: Article
View Journal Impact

Abstract

Cardiac dynamics exhibit complex variability characterized by scale-invariant and nonlinear temporal organization related to the mechanism of neuroautonomic control, which changes with physiologic states and pathologic conditions. Changes in sleep regulation during sleep stages are also related to fluctuations in autonomic nervous activity. However, the interaction between sleep regulation and cardiac autonomic control remains not well understood. Even less is known how this interaction changes with age, as aspects of both cardiac dynamics and sleep regulation differ in healthy elderly compared to young subjects. We hypothesize that because of the neuroautonomic responsiveness in young subjects, fractal and nonlinear features of cardiac dynamics exhibit a pronounced stratification pattern across sleep stages, while in elderly these features will remain unchanged due to age-related loss of cardiac variability and decline of neuroautonomic responsiveness. We analyze the variability and the temporal fractal organization of heartbeat fluctuations across sleep stages in both young and elderly. We find that independent linear and nonlinear measures of cardiac control consistently exhibit the same ordering in their values across sleep stages, forming a robust stratification pattern. Despite changes in sleep architecture and reduced heart rate variability in elderly subjects, this stratification surprisingly does not break down with advanced age. Moreover, the difference between sleep stages for some linear, fractal, and nonlinear measures exceeds the difference between young and elderly, suggesting that the effect of sleep regulation on cardiac dynamics is significantly stronger than the effect of healthy aging. Quantifying changes in this stratification pattern may provide insights into how alterations in sleep regulation contribute to increased cardiac risk.

Keywords

Author Keywords: Aging; cardiac dynamics; detrended fluctuations; fractal; nonlinear

KeyWords Plus: FRACTAL CORRELATION-PROPERTIES; ENDOGENOUS CIRCADIAN-RHYTHM; POWER SPECTRUM ANALYSIS; RATE-VARIABILITY; TIME-SERIES; CARDIAC DYNAMICS; LONG; RISK; AGE; BEHAVIOR

Author Information

Reprint Address: Ivanov, PC (reprint author)

+ Boston Univ, Dept Phys, Boston, MA 02215 USA.

Addresses:

+ [1] Boston Univ, Dept Phys, Boston, MA 02215 USA

[2] Boston Univ, Ctr Polymer Studies, Boston, MA 02215 USA

[3] Univ Ulm, D-89069 Ulm, Germany

[4] Washington Univ, Sch Med, Heart Rate Variabil HRV Lab, St Louis, MO 63108 USA

[5] Harvard Univ, Sch Med & Dent, Div Sleep Med, Brigham & Womens Hosp, Boston, MA 02115 USA

[6] Bulgarian Acad Sci, Inst Solid State Phys, BU-1784 Sofia, Bulgaria

E-mail Addresses: plamen@buphy.bu.edu

Suggest a correction

If you would like to improve the quality of the data in this record, please suggest a correction.

Funding

Funding Agency	Grant Number
NHLBI NIH HHS	R01 HL062181 2 RO1 HL071972 R01 HL062181-07 R01 HL071972

Publisher

IEEE-INST ELECTRICAL ELECTRONICS ENGINEERS INC, 445 HOES LANE, PISCATAWAY, NJ 08855-4141 USA

Journal Information

Impact Factor: Journal Citation Reports

Categories / Classification

Research Areas: Engineering

Web of Science Categories: Engineering, Biomedical

See more data fields

Cited References: 65

Showing 30 of 65 **View All in Cited References page** *(from Web of Science Core Collection)*

1. **POWER SPECTRUM ANALYSIS OF HEART-RATE FLUCTUATION - A QUANTITATIVE PROBE OF BEAT-TO-BEAT CARDIOVASCULAR CONTROL** **Times Cited: 3,445**
By: AKSELROD, S; GORDON, D; UBEL, FA; et al.
SCIENCE Volume: 213 Issue: 4504 Pages: 220-222 Published: 1981

2. **Behavioral-independence features of complex heartbeat dynamics** **Times Cited: 186**
By: Amaral, LAN; Ivanov, PC; Aoyagi, N; et al.
PHYSICAL REVIEW LETTERS Volume: 86 Issue: 26 Pages: 6026-6029 Published: JUN 25 2001

3. **Decomposition of heartbeat time series: Scaling analysis of the sign sequence** **Times Cited: 27**
By: Ashkenazy, Y; Ivanov, PC; Havlin, S; et al.
COMPUTERS IN CARDIOLOGY 2000, VOL 27 Book Series: COMPUTERS IN CARDIOLOGY Volume: 27 Pages: 139-142 Published: 2000

4. **Magnitude and sign scaling in power-law correlated time series** **Times Cited: 108**
By: Ashkenazy, Y; Havlin, S; Ivanov, PC; et al.
PHYSICA A-STATISTICAL MECHANICS AND ITS APPLICATIONS Volume: 323 Pages: 19-41 Published: MAY 15 2003

Levels of complexity in scale-invariant neural signals

Plamen Ch. Ivanov,[1,2,3,*] Qianli D. Y. Ma,[2,4] Ronny P. Bartsch,[2] Jeffrey M. Hausdorff,[5,6] Luís A. Nunes Amaral,[7] Verena Schulte-Frohlinde,[1] H. Eugene Stanley,[1] and Mitsuru Yoneyama[8]

[1]*Department of Physics and Center for Polymer Studies, Boston University, Boston, Massachusetts 02215, USA*

[2]*Harvard Medical School and Division of Sleep Medicine, Brigham and Women's Hospital, Boston, Massachusetts 02115, USA*

[3]*Institute of Solid State Physics, Bulgarian Academy of Sciences, Sofia 1784, Bulgaria*

[4]*Nanjing University of Posts and Telecommunications, Nanjing 210003, China*

[5]*Tel-Aviv Sourasky Medical Center and Tel-Aviv University, Tel-Aviv 69978, Israel*

[6]*Harvard Medical School, Boston, Massachusetts 02115, USA*

[7]*Department of Chemical Engineering, Northwestern University, Evanson, Illinois 60208, USA*

[8]*Mitsubishi Chemical Group, Science and Technology Center Inc., Yokohama 227-8502, Japan*

(Received 5 May 2004; revised manuscript received 3 January 2009; published 21 April 2009)

Many physical and physiological signals exhibit complex scale-invariant features characterized by $1/f$ scaling and long-range power-law correlations, indicating a possibly common control mechanism. Specifically, it has been suggested that dynamical processes, influenced by inputs and feedback on multiple time scales, may be sufficient to give rise to $1/f$ scaling and scale invariance. Two examples of physiologic signals that are the output of hierarchical multiscale physiologic systems under neural control are the human heartbeat and human gait. Here we show that while both cardiac interbeat interval and gait interstride interval time series under healthy conditions have comparable $1/f$ scaling, they still may belong to different complexity classes. Our analysis of the multifractal scaling exponents of the fluctuations in these two signals demonstrates that in contrast to the multifractal behavior found in healthy heartbeat dynamics, gait time series exhibit less complex, close to monofractal behavior. Further, we find strong anticorrelations in the sign and close to random behavior for the magnitude of gait fluctuations at short and intermediate time scales, in contrast to weak anticorrelations in the sign and strong positive correlation for the magnitude of heartbeat interval fluctuations—suggesting that the neural mechanisms of cardiac and gait control exhibit different linear and nonlinear features. These findings are of interest because they underscore the limitations of traditional two-point correlation methods in fully characterizing physiological and physical dynamics. In addition, these results suggest that different mechanisms of control may be responsible for varying levels of complexity observed in physiological systems under neural regulation and in physical systems that possess similar $1/f$ scaling.

DOI: 10.1103/PhysRevE.79.041920 PACS number(s): 87.10.−e, 87.19.Hh, 05.45.Tp, 05.40.−a

I. INTRODUCTION

Many dynamic systems generate outputs with fluctuations characterized by $1/f$-like scaling of the power spectra, $S(f)$, where f is the frequency. These fluctuations are often associated with nonequilibrium dynamic systems possessing multiple degrees of freedom [1,2], rather than being the output of a classic "homeostatic" process [3–5]. It is generally assumed that the presence of many components interacting over a wide range of time or space scales could be the reason for the $1/f$ spectrum in the fluctuations [6,7]. Fluctuations exhibiting $1/f$-like behavior are often termed "complex," since they obey a scaling law indicating a hierarchical fractal organization of their frequency (time scale) components rather than being dominated by a single frequency. $1/f$ behavior is common in a variety of physical, biological, and social systems [7–15]. The ubiquity of the $1/f$ scale-invariant phenomenon has triggered in recent years the development of generic mechanisms describing complex systems, independent of their particular context, in order to understand the "unifying" features of these systems [16–19].

To evaluate whether fluctuations in signals generated by integrated physiological systems exhibit the same level of complexity, we analyze and compare the time series generated by two physiologic control systems under multiple-component integrated neural control—the human gait and the human heartbeat. We chose these two particular examples because human gait and heartbeat control share certain fundamental properties, e.g., both originate in oscillatory centers. In the case of the heart, the pacemaker is located in the sinus node in the right atrium [20]. For gait, pacemakers called central pattern generators are thought to be located in the spinal cord [21].

However, these two systems are distinct suggesting possible dynamical differences in their output. For example, heartbeat fluctuations are primarily controlled by the involuntary (autonomic) nervous system. In contrast, while the spontaneous walking rhythm is an automaticlike process, voluntary inputs play a major role. Further, gait control resides in the basal ganglia and related motor areas of the central nervous system, while the heartbeat is controlled by the sympathetic and parasympathetic branches of the autonomic nervous system [20,22].

Previous studies show comparable two-point linear correlations and $1/f$ power spectra in heart rate [23–27] and human gait [28–31] suggesting that differences in physiologic control may not be manifested in beat-to-beat and interstride interval fluctuations. Recent studies focusing on higher order correlations and nonlinear properties show that the human

*Corresponding author; plamen@buphy.bu.edu

heartbeat exhibits not only $1/f$ fractal but also multifractal properties [32]. Since multifractal signals require many scaling indices to fully characterize their scaling properties, they may be considered to be more complex than those characterized by a single fractal dimension such as classical $1/f$ noise. Although the origins of the multifractal features in heartbeat dynamics are not yet understood, there is evidence that they relate to the complex intrinsic neuroautonomic regulation of the heart [32,33]. Human gait, e.g., free unconstrained walking, is also a physiological process regulated by complex hierarchical feedback mechanisms involving supraspinal inputs [21]. Moreover, recent findings indicate that the scaling properties of gait fluctuations relate to neural centers on the higher supraspinal level rather than to lower motor neurons or environmental inputs [34,35]. Thus, it would be natural to hypothesize that the fluctuations in healthy unconstrained human gait exhibit similar fractal and multifractal features as heartbeat fluctuations, and that human gait dynamics may belong to the same "complexity class" as cardiac dynamics.

We employ two techniques—magnitude and sign decomposition analysis [36,37], and multifractal analysis [38,39]—to probe long-term nonlinear features, and to compare the levels of complexity in heartbeat and interstride interval fluctuations. To this end, we analyze interstride interval time series from ten young healthy men (mean age 22 years) with no history of neuromuscular disorders [40]. Subjects walked continuously for 1 h at a self-selected usual pace on level ground around a flat, obstacle-free, approximately oval, 400 m long path. The interstride interval was measured using a ground reaction force sensor—ultrathin force-sensitive switches were taped inside one shoe and data were recorded on an ambulatory recorder using a previously validated method [41]. We compare the results of our gait analysis with results we have previously obtained [32,36,42,43] from 6-h-long heartbeat interval records from 18 healthy individuals (13 female and 5 male, mean age 34 years) during daily activity (12:00 to 18:00) [40].

As described below, we systematically compare the scaling properties of the fluctuations in human gait with those in the human heartbeat using power spectral analysis, detrended fluctuation analysis (DFA), magnitude, and sign decomposition analysis, and wavelet-based multifractal analysis, and we quantify linear and nonlinear features in the data over a range of time scales.

II. METHODS

A. DFA

The DFA method was developed because conventional fluctuation analyses such as power spectral, R/S and Hurst analysis cannot be reliably used to study nonstationary data [44–48]. One advantage of the DFA method is that it allows the detection of long-range power-law correlations in noisy signals with embedded polynomial trends that can mask the true correlations in the fluctuations of a signal. The DFA method has been successfully applied to a wide range of research fields in physics [49–52], biology [53–56], and physiology [57–60].

The DFA method involves the following steps [44]:

(i) Given the original signal $s(i)$, where $i=1,\ldots,N_{\max}$ and $N_{\max}$ is the length of the signal, we first form the profile function $y(k)\equiv\sum_{i=1}^{k}[s(i)-\langle s\rangle]$, where $\langle s\rangle$ is the mean. One can consider the profile $y(k)$ as the position of a random walk in one dimension after k steps.

(ii) We divide the profile $y(k)$ into nonoverlapping segments of equal length n.

(iii) In each segment of length n, we fit $y(k)$, using a polynomial function of order ℓ which represents the polynomial *trend* in that segment. The y coordinate of the fit line in each segment is denoted by $y_n(k)$. Since we use a polynomial fit of order ℓ, we denote the algorithm as DFA-ℓ.

(iv) The profile function $y(k)$ is detrended by subtracting the local trend $y_n(k)$ in each segment of length n. In DFA-ℓ, trends of order $\ell-1$ in the original signal are eliminated. Thus, comparison of the results for different orders of DFA-ℓ allows us to estimate the type of polynomial trends in the time series $s(i)$.

(v) For a given segment of length n, the root-mean-square (rms) fluctuation for this integrated and detrended signal $s(i)$ is calculated:

$$F(n)\equiv\sqrt{\frac{1}{N_{\max}}\sum_{k=1}^{N_{\max}}[y(k)-y_n(k)]^2}. \tag{1}$$

(vi) Since we are interested in how $F(n)$ depends on the segment length, the above computation is repeated for a broad range of scales n.

A power-law relation between the average root-mean-square fluctuation function $F(n)$ and the segment length n indicates the presence of scaling:

$$F(n)\sim n^{\alpha}. \tag{2}$$

Thus, the DFA method can quantify the temporal organization of the fluctuations in a given signal $s(i)$ by a single scaling exponent α—a self-similarity parameter which represents the long-range power-law correlation properties of the signal. If $\alpha=0.5$, there is no correlation and the signal is uncorrelated (white noise); if $\alpha<0.5$, the signal is anticorrelated; if $\alpha>0.5$, the signal is correlated. The larger the value of α, the stronger the correlations in the signal.

For stationary signals with scale-invariant temporal organization, $F(n)$ is related to the Fourier power spectrum $S(f)$ and to the autocorrelation function $C(n)$. For such signals,

$$S(f)\sim f^{-\beta},\quad \text{where } [\beta=2\alpha-1] \tag{3}$$

and α is the DFA scaling exponent [Eq. (2)] [44]. Thus, signals with $1/f$ scaling in the power spectrum (i.e., $\beta=1$) are characterized by DFA exponent $\alpha=1$. If $0.5<\alpha<1$, the correlation exponent γ describes the decay of the autocorrelation function:

$$C(n)\equiv\langle s(i)s(i+n)\rangle\sim n^{-\gamma},\quad \text{where } [\gamma=2-2\alpha]. \tag{4}$$

B. Magnitude and sign decomposition method

Fluctuations in the dynamical output of physical and physiological systems can be characterized by their magnitude (absolute value) and their direction (sign). These two

quantities reflect the underlying interactions in a given system—the resulting "force" of these interactions at each moment determines the magnitude and the direction of the fluctuations. To assess the information contained in these fluctuations, the magnitude and sign decomposition method was introduced [36,37]. This method involves the following steps:

(i) Given the original signal $s(i)$ we generate the increment series, $\Delta s(i) \equiv s(i+1) - s(i)$.

(ii) We decompose the increment series into a magnitude series $|\Delta s(i)|$ and a sign series $\text{sign}[\Delta s(i)]$.

(iii) To avoid artificial trends we subtract from the magnitude and sign series their average.

(iv) We then integrate both magnitude and sign series, because of limitations in the accuracy of the DFA method for estimating the scaling exponents of anticorrelated signals ($\alpha < 0.5$).

(v) We perform a scaling analysis using second-order detrended fluctuation analysis (DFA-2) on the integrated magnitude and sign series.

(vi) To obtain the scaling exponents for the magnitude and sign series, we measure the slope of $F(n)/n$ on a log-log plot, where $F(n)$ is the root-mean-square fluctuation function obtained using DFA-2 and n is the scale.

Fluctuations following an identical $1/f$ scaling law can exhibit different types of correlations for the magnitude and the sign—e.g., a signal with anticorrelated fluctuations can exhibit positive correlations in the magnitude. Positive correlations in the magnitude series indicate that an increment with large magnitude is more likely to be followed by an increment with large magnitude. Anticorrelations in the sign series indicate that a positive increment in the original signal is more likely to be followed by a negative increment. Further, positive power-law correlations in the magnitude series indicate the presence of long-term *nonlinear* features in the original signal, and relate to the width of the multifractal spectrum [37]. In contrast, the sign series relates to the *linear* properties of the original signal [37]. The magnitude and sign decomposition method is suitable to probe nonlinear properties in short nonstationary signals, such as 1 h interstride interval time series.

C. Wavelet-based multifractal analysis

Previously, analyses of the fractal properties of physiologic fluctuations revealed that the behavior of healthy, free-running physiologic systems may often be characterized as $1/f$-like [19,23–27,29,35,41,61–72]. Monofractal signals (such as classical $1/f$ noise) are homogeneous, i.e., they have the same scaling properties throughout the entire signal [73–75]. Monofractal signals can therefore be indexed by a single exponent: the Hurst exponent H [76].

On the other hand, multifractal signals are nonlinear and inhomogeneous with local properties changing with time. Multifractal signals can be decomposed into many subsets characterized by different *local* Hurst exponents h, which quantify the local singular behavior and relate to the local scaling of the time series. Thus, multifractal signals require many exponents to fully characterize their properties [77]. The multifractal approach, a concept introduced in the context of multiaffine functions [78–81], has the potential to describe a wide class of signals more complex than those characterized by a single fractal dimension.

The singular behavior of a signal $s(t)$ at time t_0 — $|s(t) - P_n(t)| \sim |t - t_0|^{h(t_0)}$ for $t \to t_0$—is characterized by the local Hurst exponent $h(t_0)$ where $n < h(t_0) < n+1$ and $P_n(t)$ is a polynomial fit of order n. To avoid an *ad hoc* choice of the range of time scales over which the local Hurst exponent h is estimated, and to filter out possible polynomial trends in the data which can mask local singularities, we implement a wavelet-based algorithm [39]. Wavelets are designed to probe time series over a broad range of scales and have recently been successfully used in the analysis of physiological signals [82–90]. In particular, recent studies have shown that the wavelet decomposition reveals a robust self-similar hierarchical organization in heartbeat fluctuations, with bifurcations propagating from large to small scales [43,91,92]. To quantify hierarchical cascades in gait dynamics and to avoid inherent numerical instability in the estimate of the local Hurst exponent, we employ a "mean-field" approach—a concept introduced in statistical physics [1]—which allows us to probe the collective behavior of local singularities throughout an entire signal and over a broad range of time scales.

We study the multifractal properties of interstride interval time series by applying the *wavelet transform modulus maxima* (WTMM) method [38,39,93] that has been proposed as a mean-field generalized multifractal formalism for fractal signals. We first obtain the wavelet coefficient at time t_0 from the continuous wavelet transform defined as

$$W_a(t_0) \equiv a^{-1} \sum_{t=1}^{N} s(t) \psi[(t - t_0)/a], \tag{5}$$

where $s(t)$ is the analyzed time series, ψ is the analyzing wavelet function, a is the wavelet scale (i.e., time scale of the analysis), and N is the number of data points in the time series. For ψ we use the third derivative of the Gaussian, thus filtering out up to second-order polynomial trends in the data. We then choose the modulus of the wavelet coefficients at each point t in the time series for a fixed wavelet scale a.

Next, we estimate the partition function

$$Z_q(a) \equiv \sum_i |W_a(t)|^q, \tag{6}$$

where the sum is only over the maxima values of $|W_a(t)|$, and the powers q take on real values. By not summing over the entire set of wavelet transform coefficients along the time series at a given scale a but only over the wavelet transform modulus maxima, we focus on the fractal structure of the temporal organization of the singularities in the signal [93].

We repeat the procedure for different values of the wavelet scale a to estimate the scaling behavior

$$Z_q(a) \sim a^{\tau(q)}. \tag{7}$$

Analogous to what occurs in scale-free physical systems, in which phenomena controlled by the same mechanism over multiple time scales are characterized by scale-independent measures, we assume that the scale-independent measures,

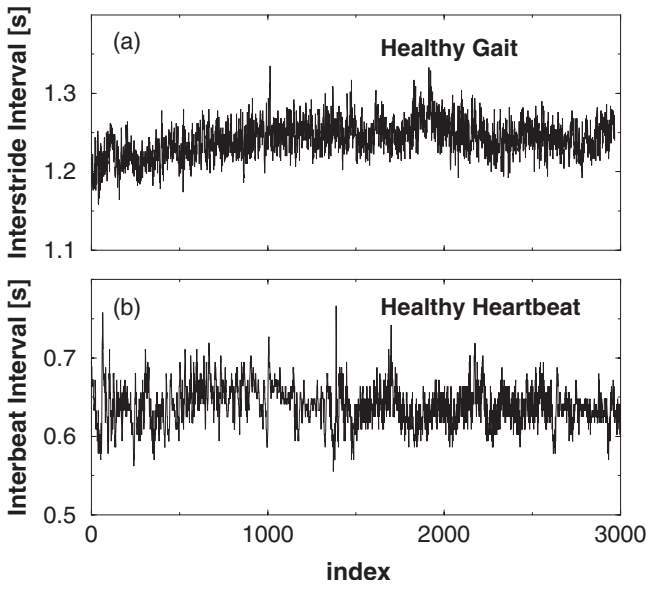

FIG. 1. Representative records of (a) interstride interval (ISI) time series from a healthy subject and (b) consecutive heartbeat (RR) intervals from a healthy subject.

$\tau(q)$, depend only on the underlying mechanism controlling the system. Thus, by studying the scaling behavior of $Z(a,q) \sim a^{\tau(q)}$ we may obtain information about the self-similar (fractal) properties of the mechanism underlying gait control.

For certain values of the powers q, the exponents $\tau(q)$ have familiar meanings. In particular, $\tau(2)$ is related to the scaling exponent of the Fourier power spectra, $S(f) \sim 1/f^{\beta}$, as $\beta = 2 + \tau(2)$ [39]. For positive q, $Z_q(a)$ reflects the scaling of the large fluctuations and strong singularities in the signal, while for negative q, $Z_q(a)$ reflects the scaling of the small fluctuations and weak singularities [74,77,94]. Thus, the scaling exponents $\tau(q)$ can reveal different aspects of the underlying dynamics.

In the framework of this wavelet-based multifractal formalism, $\tau(q)$ is the Legendre transform of the singularity spectrum $D(h)$ defined as the Hausdorff dimension of the set of points t in the signal $s(t)$ where the local Hurst exponent is h. Homogeneous monofractal signals—i.e., signals with a single local Hurst exponent h —are characterized by linear $\tau(q)$ spectrum:

$$\tau(q) = qH - 1, \tag{8}$$

where $H \equiv h = d\tau(q)/dq$ is the global Hurst exponent. On the contrary, a nonlinear $\tau(q)$ curve is the signature of nonhomogeneous signals that display multifractal properties—i.e., $h(t)$ is a varying quantity that depends upon t.

III. RESULTS

In Fig. 1 we show two example time series: (i) an interstride interval time series from a typical healthy subject during ≈ 1 h ($N = 3000$ steps) of unconstrained normal walking on a level, obstacle-free surface [Fig. 1(a)] [40]; (ii) consecutive heartbeat intervals from ≈ 1 h ($N = 3000$ beats) record of a typical healthy subject during daily activity [Fig. 1(b)] [40]. Both time series exhibit irregular fluctuations and nonstationary behavior characterized by different local trends; in fact it is difficult to differentiate between the two time series by visual inspection.

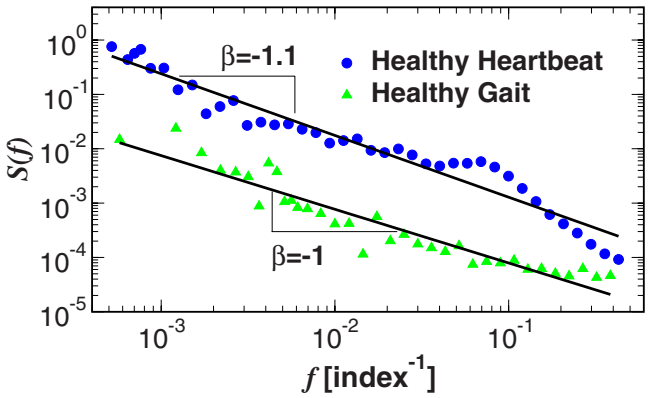

FIG. 2. (Color online) Power spectra of the gait ISI series (▲) and heartbeat RR series (●) displayed in Fig. 1, indicating a similar $1/f$-type behavior.

We first examine the two-point correlations and scale-invariant behavior of the time series shown in Fig. 1. Power spectra $S(f)$ of the gait and heartbeat time series (Fig. 2) indicate that both processes are described by a power-law relation $S(f) \sim 1/f^{\beta}$ over more than 2 decades, with exponent $\beta \approx 1$. This scaling behavior indicates self-similar (fractal) properties of the data over a broad range of time scales, suggestive of an identical level of complexity as quantified by this linear measure. We obtain similar results for the interstride interval time series from all subjects in our gait database: $\beta = 0.9 \pm 0.08$ (group mean $\pm$ std. dev.) in agreement with previous results [35].

A. DFA

Next, to quantify the degree of correlation in the interstride and heartbeat fluctuations we apply the DFA method, which also provides a linear measure: plots of the root-mean-square fluctuation function $F(n)$ vs time scale n (measured in stride or beat number) from a second-order DFA analysis (DFA-2) [44–46] indicate the presence of long-range power-law correlations in both gait and heartbeat fluctuations [Fig. 3(a)]. The scaling exponent $\alpha \approx 0.95$ for the heartbeat signal, shown in Fig. 1(b), is very close to the exponent $\alpha \approx 0.9$ for the interstride interval signal, shown in Fig. 1(a), estimated over the scaling range $6 < n < 600$, where $n_{\max} \approx N/5 = 600$ is the maximal time scale for which the DFA scaling analysis is reliable [45,46]. We obtain similar results for the remaining subjects: $\alpha = 0.87 \pm 0.03$ (group mean $\pm$ std. dev.) for the gait data (in agreement with [35]) and $\alpha = 1.01 \pm 0.06$ for the heartbeat data (in agreement with [42]). The results of both power spectral analysis and the DFA method indicate that gait and heartbeat time series have similar scale-invariant properties suggesting certain parallels in the underlying mechanisms of neural regulation.

B. Magnitude and sign decomposition method

To probe for long-term nonlinear features in the dynamics of interstride intervals we employ the magnitude and sign

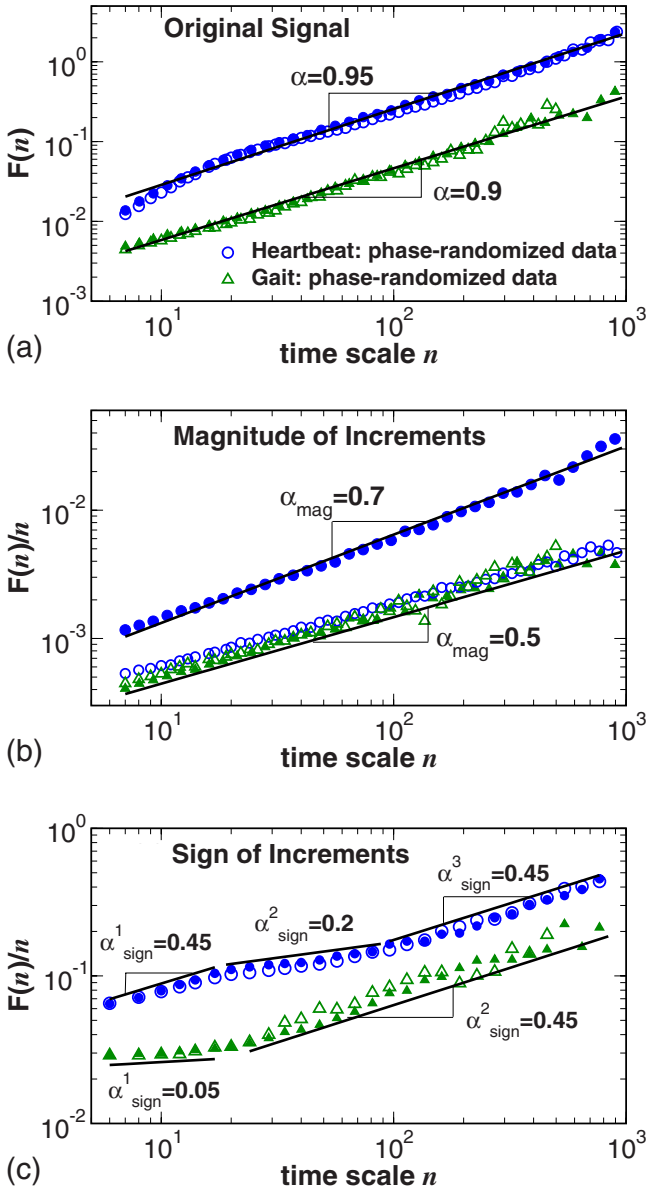

FIG. 3. (Color online) Plots of the root-mean-square fluctuation function $F(n)$ vs time scale n (measured in interstride or heartbeat number) from second-order DFA-2 analysis for (a) the gait ISI (▲) and heartbeat RR (●) time series, (b) the magnitude series, and (c) sign series of the interstride and heartbeat increments ΔISI and ΔRR. The results shown in (a), (b), and (c) are obtained for the gait and heartbeat signals displayed in Figs. 1(a) and 1(b). While both gait and cardiac dynamics exhibit similar power-law and correlations, the magnitude and sign series of interstride and heartbeat increments in (b) and (c) follow significantly different scaling relations. Open symbols (△, ○) represent the results of a Fourier phase-randomization test indicating high degree of nonlinearity ($\alpha_{\text{mag}} \approx 0.7 > 0.5$) in cardiac dynamics, in contrast to a linear behavior ($\alpha_{\text{mag}} \approx 0.5$) for gait dynamics.

decomposition analysis [36,37]. Previous studies have demonstrated that information about the nonlinear properties of heartbeat dynamics can be quantified by long-range power-law correlations in the magnitude of the increments in heartbeat intervals [36]. Further, *positive* correlations in the magnitude are associated with *nonlinear* features in the underlying dynamics. In contrast, *linear* signals are characterized by an absence of correlations (*random* behavior) in the magnitude series. To quantify the correlations in the magnitude of the interstride increments we apply the DFA-2 method to the gait data displayed in Fig. 1(a). Our results show that the magnitude series of the interstride increments exhibits close to random behavior with correlation exponent $\alpha_{\text{mag}} \approx 0.5$ [denoted by (▲) in Fig. 3(b)] suggesting linear properties of the underlying dynamics. In contrast, for the heartbeat data displayed in Fig. 1(b), we find that the magnitude series of the interbeat interval fluctuations exhibits strong positive correlations over more than two decades characterized by exponent $\alpha_{\text{mag}} \approx 0.7$ [denoted by (●) in Fig. 3(b)] suggesting nonlinear features in cardiac control. Thus, the striking difference in the magnitude correlations of gait and heartbeat dynamics (both of which are under multilevel neural control) raises the possibility that these two physiologic processes belong to different classes of complexity whereby the neural regulation of the heartbeat is inherently more nonlinear, over a range of time scales, than the neural mechanism of gait control. Our observation of a low degree of nonlinearity in the gait time series is supported by the remaining subjects in the group: over time scales $6 < n < 600$, we obtain exponent $\alpha_{\text{mag}} = 0.51 \pm 0.03$ (group mean ± std. dev.) for the gait time series, which is significantly lower than the corresponding exponent $\alpha_{\text{mag}} = 0.71 \pm 0.09$ obtained for the heartbeat data ($p = 2.7 \times 10^{-7}$, by the Student's t test). We note however, in the short-range region for time scales $6 < n < 16$ we obtain a group average exponent $\alpha_{\text{mag}} = 0.62 \pm 0.05$ for the gait data, and $\alpha_{\text{mag}} = 0.57 \pm 0.12$ for the heartbeat data (Table I), indicating a very similar (and relatively low) degree of nonlinearity in both gait and cardiac dynamics at short time scales of up to ≈15 s (with p −value=0.16 by the Student's t test). This nonlinear behavior changes significantly at intermediate and large time scales, where cardiac dynamics is characterized by a high degree of nonlinearity ($\alpha_{\text{mag}} \approx 0.8$), in contrast to gait dynamics which exhibits practically linear behavior ($\alpha_{\text{mag}} \approx 0.5$) (see Table I).

To further test for nonlinear features in the mechanisms of neural control generating heartbeat and gait dynamics we perform a Fourier phase-randomization surrogate test [95,96]. We first perform a Fourier transform of the original data. Next we eliminate the nonlinearity in the data by randomizing the Fourier phases while preserving the Fourier coefficients, and thus keeping the linear properties (power spectrum and correlation) of the original signal unchanged. An inverse Fourier transform leads to a linearized surrogate signal with identical correlations as in the original data.

The results of Fourier phase-randomization test for gait and heartbeat data are shown in Fig. 3. While the DFA scaling curves remain as expected, unchanged after the test for both gait and heartbeat signals [Fig. 3(a), open symbols], the scaling curve for the magnitude of heartbeat fluctuations changes dramatically to $\alpha \approx 0.5$, in contrast to the gait data, where the magnitude scaling curve remains practically unchanged [Fig. 3(b), open symbols]. These findings confirm our results from the magnitude analysis indicating that the multilevel neural control mechanism of gait surprisingly generates close to linear dynamics.

TABLE I. Results of the DFA analysis of the original gait ISI and heartbeat RR interval signals, and the magnitude and sign of interstride and heartbeat interval increments, ΔISI and ΔRR for 1 h gait recordings from ten healthy subjects and 6 h ECG recordings from 18 healthy subjects. We calculate the scaling exponents α over a broad range of time scales $6<n\leq 600$, as well as in three different regions: (i) the short-range regime for time scales $6<n<16$ with scaling exponent α_1, (ii) the intermediate regime for time scales $16\leq n\leq 64$ with scaling exponent α_2, (iii) and the long-range regime for time scales $64<n\leq 600$ with scaling exponent α_3. For each measure, the group average ± 1 standard deviation is presented.

Measure	Original	Magnitude	Sign
	Gait		
α	0.87 ± 0.03	0.51 ± 0.03	0.41 ± 0.05
α_1	0.71 ± 0.08	0.62 ± 0.05	0.05 ± 0.03
α_2	0.84 ± 0.06	0.53 ± 0.07	0.40 ± 0.03
α_3	0.89 ± 0.06	0.50 ± 0.08	0.48 ± 0.12
	Heartbeat		
α	1.01 ± 0.06	0.71 ± 0.09	0.35 ± 0.03
α_1	1.34 ± 0.22	0.57 ± 0.12	0.45 ± 0.13
α_2	0.97 ± 0.12	0.67 ± 0.09	0.23 ± 0.08
α_3	1.02 ± 0.10	0.80 ± 0.12	0.45 ± 0.05

Previous studies have shown that the time series composed of the sign of the consecutive increments in the original signal contain information about the underlying dynamics which is complementary and independent from the original and the magnitude series [36,37,97,98]. Our DFA scaling analysis of the sign series shows a complex and significantly different behavior for heartbeat and gait dynamics. A very strong anticorrelated behavior at small time scales with $\alpha_{\text{sign}}\approx 0.05$ is followed by a crossover to much weaker anticorrelations with $\alpha_{\text{sign}}\approx 0.45$ as shown in Fig. 3(c) for the gait data displayed in Fig. 1(a). This is in contrast to the scaling behavior of the heartbeat sign series, which exhibits weak anticorrelations ($\alpha_{\text{sign}}\approx 0.45$) at both short and long time scales with a crossover region at intermediate scales [Fig. 3(c)]. These observations are supported by the remaining subjects in the group: over time scales $6<n<16$, we obtain exponent $\alpha_{\text{sign}}=0.05\pm0.03$ (group mean $\pm$ std. dev.) for gait, which is significantly different from the corresponding exponent $\alpha_{\text{sign}}=0.45\pm0.13$ for heartbeat data ($p-$value $=10^{-9}$ by the Student's t test). At long time scales of $n>100$ both interstride and heartbeat intervals are characterized by a group average exponent $\alpha_{\text{sign}}=0.45$ with a $p-$value$=0.46$ by the Student's t test (see Table I).

Further, our analysis of the sign series from surrogate data obtained after Fourier phase randomization of the original gait and heartbeat signals indicates no change in the scaling behavior [Fig. 3(c), open symbols], suggesting that, in contrast to the magnitude series, correlations in the sign series reflect linear properties in the original data.

Our DFA, and magnitude and sign decomposition analyses show a consistent scaling behavior of gait dynamics for all 10 subjects in our database. All individual scaling curves

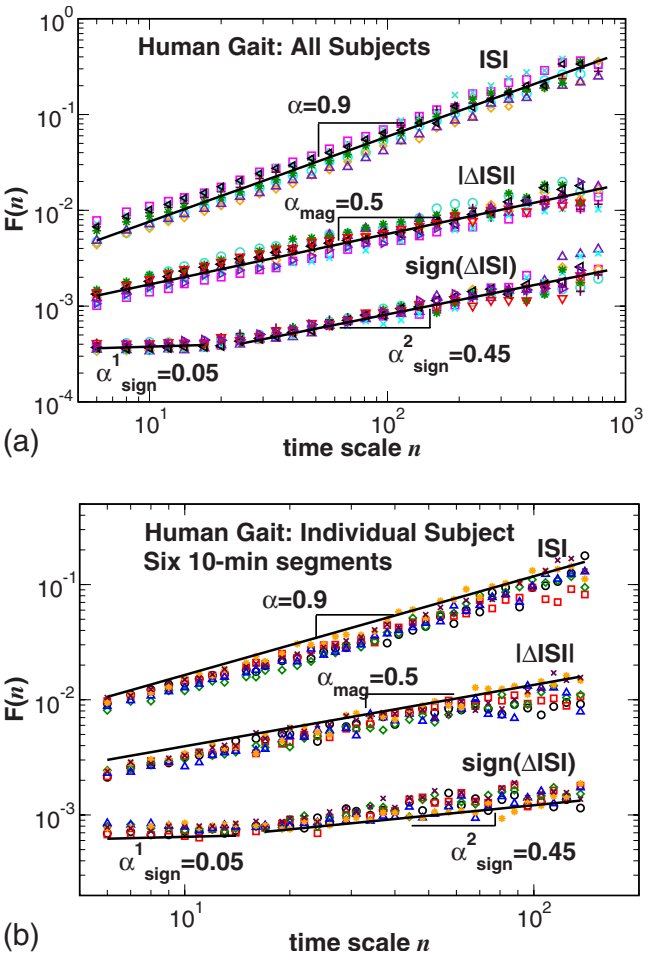

FIG. 4. (Color online) DFA-2 analysis of the gait interstride intervals (ISI) series, the magnitude series $|\Delta\text{ISI}|$ and the sign series sign(ΔISI) for (a) all ten subjects in our database and (b) six 10 min segments of a 1 h recording from one individual subject. A consistent scaling behavior is observed for all subjects as well as for different segments from individual recordings despite certain differences in the average and standard deviation of ISI among subjects and across segments.

for the interstride interval signals, magnitude and sign series practically collapse onto a single curve [Fig. 4(a)]. To further test the validity of our results for gait dynamics, and that they indeed represent the internal mechanics of gait control, and are not an artifact of external/random factors of the environment, we have segmented each 1 h gait recording into 10 min segments, and have separately analyzed each segment. While the average gait rate and standard deviation change for different segments with some subjects reporting a certain degree of fatigue or tiredness near the end of the recording, our results demonstrate a remarkable stability of the scaling results with no statistically significant change in the exponent α, α_{mag}, and α_{sign} for different segments [Fig. 4(b)].

C. Wavelet-based multifractal analysis

To further test the long-term nonlinear features in gait dynamics we study the multifractal properties of interstride

time series. We apply the WTMM method [39,93]—a "mean-field" type approach to quantify the fractal organization of singularities in the signal. We characterize the multifractal properties of a signal over a broad range of time scales by the multifractal spectrum $\tau(q)$. Gait and heartbeat time series contain densely packed, nonisolated singularities which unavoidably affect each other in the time-frequency decomposition. Therefore, rather than evaluating the distribution of the inherently unstable local singularity exponents [14,43]), we estimate the scaling of an appropriately chosen global measure: the q moments of the probability distribution of the maxima of the wavelet transform $Z_q(a)$ (using the third derivative of the Gaussian function as the analyzing wavelet).

We first examine the time series shown in Fig. 1. For the gait time series, we obtain a $\tau(q)$ spectrum which is practically a linear function of the moment q suggesting that the gait dynamics exhibit *monofractal* properties [Figs. 5(a) and 5(c)]. This is in contrast with the nonlinear $\tau(q)$ spectrum for the heartbeat signal [Figs. 5(b) and 5(c)] which is indicative of nonlinear multifractal behavior [38,39]. Further, when analyzing the remaining interstride interval recordings, we find close to linear $\tau(q)$ spectra for all subjects in the gait group [Fig. 6(a)]. Calculating the group averaged $\tau(q)$ spectra we find clear differences: multifractal behavior for the heartbeat dynamics and practically monofractal behavior for the gait dynamics [Fig. 6(b)]. Specifically, we find significant differences between the gait and heartbeat $\tau(q)$ spectra for negative values of the moment q; for positive values of q, the scaling exponents $\tau(q)$ take on similar values. This is in agreement with the similarity in power spectral and DFA scaling exponents for gait and heartbeat data, which correspond to $\tau(q=2)$ (Fig. 3). However, the heartbeat $\tau(q)$ spectrum is visibly more curved for all moments q compared with the gait $\tau(q)$ spectrum which may be approximately fit by a straight line, indicative of a low degree of nonlinearity in the interstride time series. Thus, our results show consistent differences between the nonlinear and multifractal properties of gait and heartbeat time series.

Previous studies have shown that reducing the level of physical activity under a constant routine protocol does not change the multifractal features of heartbeat dynamics, while blocking the sympathetic or parasympathetic tone of the neuroautonomic regulation of the heart dramatically changes the multifractal spectrum, thus suggesting that the observed features in cardiac dynamics arise from the intrinsic mechanisms of control [33]. Similarly, by eliminating polynomial trends in the interstride interval time series corresponding to changes in the gait pace using DFA and wavelet analyses, we find scaling features which remain invariant among individuals. Therefore, since different individuals experience different extrinsic factors, the observed lower degree of nonlinearity (as measured by the magnitude scaling exponent) and the close-to-monofractal behavior (characterized by practically linear $\tau(q)$ spectrum) appear to be a result of the intrinsic mechanisms of gait regulation. These observations suggest that while both gait and heartbeat dynamics arise from layers of neural control with multiple component interactions, and exhibit temporal organization over multiple time scales, they nonetheless belong to different complexity classes. While

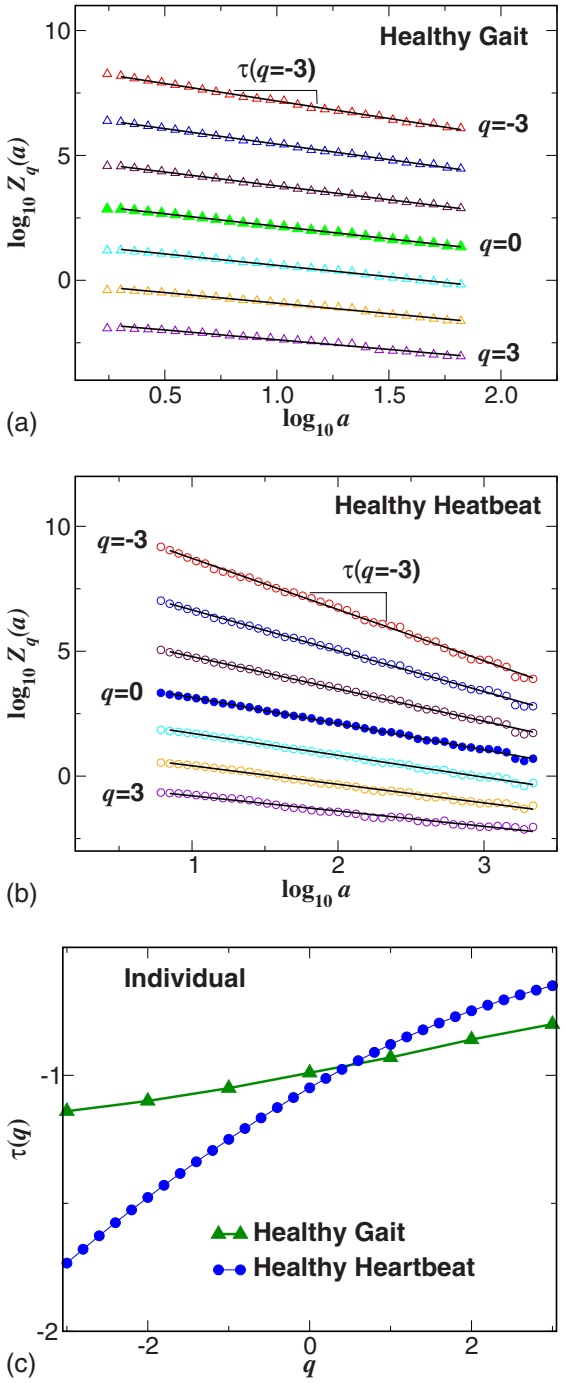

FIG. 5. (Color online) Multifractal analysis: Scaling of the partition function $Z_q(a)$ of the wavelet-transform modulus maxima obtained using the third derivative of the Gaussian as a wavelet function for (a) an individual ISI gait recording, and (b) an individual RR heartbeat recording. (c) Multifractal spectrum $\tau(q)$ for the individual records shown in (a) and (b), where τ is a scaling index associated with different moments q [Eq. (7)]. A monofractal signal corresponds to a straight line for $\tau(q)$, while for multifractal signals $\tau(q)$ is a nonlinear function of q. Thus, our results indicate multifractal/nonlinear behavior in heartbeat dynamics in contrast to monofractal/linear behavior in gait. Note that the values of $\tau(q=2)$ for both gait and heartbeat time series are very close, in agreement with our findings based on DFA-2 correlation analysis [Fig. 3(a)].

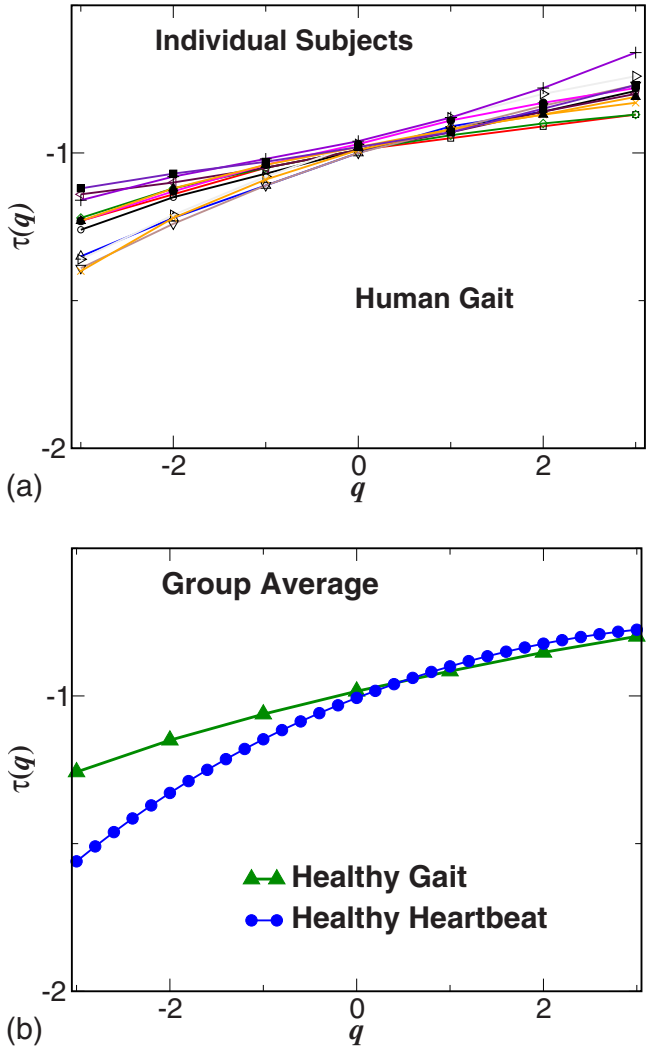

FIG. 6. (Color online) Multifractal analysis: (a) Multifractral spectra $\tau(q)$ for all ten subjects in our gait database [40] exhibit close to linear dependence on the moment q, suggesting monofractal behavior, in contrast to the nonlinear $\tau(q)$ spectra reported for heartbeat recordings [99]. (b) Group average multifractal spectra $\tau(q)$ for the gait and heartbeat subjects in our database [40]. The results show a consistent monofractal (almost linear) behavior for the gait time series, in contrast with the multifractal behavior of the heartbeat data.

both gait and heartbeat dynamics may be a result of competing inputs interacting through multiple feedback loops, differences in the nature of these interactions may be imprinted in their nonlinear and multifractal features: namely, our findings suggest that while these interactions in heartbeat dynamics are of a nonlinear character and are represented by Fourier phase correlations encoded in the magnitude scaling and the multifractal spectrum, feedback mechanisms of gait dynamics lead to decreased interactions among the Fourier phases.

D. Further validation of gait results

These findings are supported by our analysis of a second group of gait subjects. We analyze interstride intervals from an additional group of seven young healthy subjects (six male, one female, mean age 28 years) recorded using a portable accelerometer [100]. Subjects walked continuously for ≈ 1 h at a self-selected pace on an unconstrained outdoor walking track in a park environment allowing for slight changes in elevation and obstacles related to pedestrian traffic. The stride interval time series in this case were obtained from peak-to-peak intervals in the accelerometer signal output in the direction of the subjects' vertical axis. The accelerometer device we used ($9 \times 6 \times 2$ cm, weight 140 g) was developed by Sharp Co. The device, attached to subjects' back, measures the vertical and anteroposterier acceleration profile during walking. The output signals are digitized at a sampling frequency of 10^3 Hz, and are stored on a memory card. When the subjects' heel strikes the ground, a clear peak in the acceleration along the vertical axis is recorded. The positions of these peaks in time are also verified independently through matching steepest points in the anteroposterier acceleration signal output. Our analysis indicates a compatibility of the ground reaction force sensor, used for the gait recordings of the first group [40,41], with the accelerometer device used for the second group [100], as well as a strong correlation between the outputs of the two devices.

We find that for the second gait group the two-point correlation exponent $\alpha = 0.90 \pm 0.1$ (group mean $\pm$ std. dev.), as measured by the DFA-2 method in the range of time scales $6 < n < 600$ is similar to the group average exponent of the first gait group ($\alpha = 0.87 \pm 0.03$) and also to the heartbeat data ($\alpha = 1.01 \pm 0.08$). In contrast, we find again a significantly lower degree of nonlinearity, as measured by the group average magnitude exponent $\alpha_{\mathrm{mag}} = 0.57 \pm 0.04$ in the range of time scales $6 < n < 600$ and by the $\tau(q)$ spectrum, compared with heartbeat dynamics $\alpha_{\mathrm{mag}} = 0.71 \pm 0.06$ ($p = 1.3 \times 10^{-3}$, by the Student's t test). On the other hand, the group averaged value of $\alpha_{\mathrm{mag}} = 0.57 \pm 0.04$ for the second gait group is slightly higher compared to $\alpha_{\mathrm{mag}} = 0.51 \pm 0.03$ for the first gait group, and this is associated with slightly stronger curvature in the $\tau(q)$ spectrum for the second gait group. This may be attributed to the fact that the second group walked in a natural park environment where obstacles, changes in elevation and pedestrian traffic may possibly require the activation of higher neural centers of gait control.

To test to what extent our results depend on the order of polynomial detrending used in the DFA method, we have repeated our analyses using different orders DFA: DFA-1 which removes constant trends in the analyzed signal, DFA-2 which removes both constant and linear trends, and DFA-3 removing constant, linear and quadratic trends. While there is a measurable difference in the results for the scaling exponent α obtained from DFA-1 compared to DFA-2 ($\approx 3\%$ difference, with higher values for α from DFA-1), we find practically identical results for the exponent α obtained from DFA-2 and DFA-3 ($\approx 1\%$ difference in α), suggesting that removing polynomial trends of second and higher order in the recordings does not lead to significantly different scaling results (see Fig. 7). The same is also valid when wavelets with higher than third-order derivatives of the Gaussian are used for the multifractal analysis in Sec. III C.

The present results are related to a physiologically-based model of gait control where specific interactions between

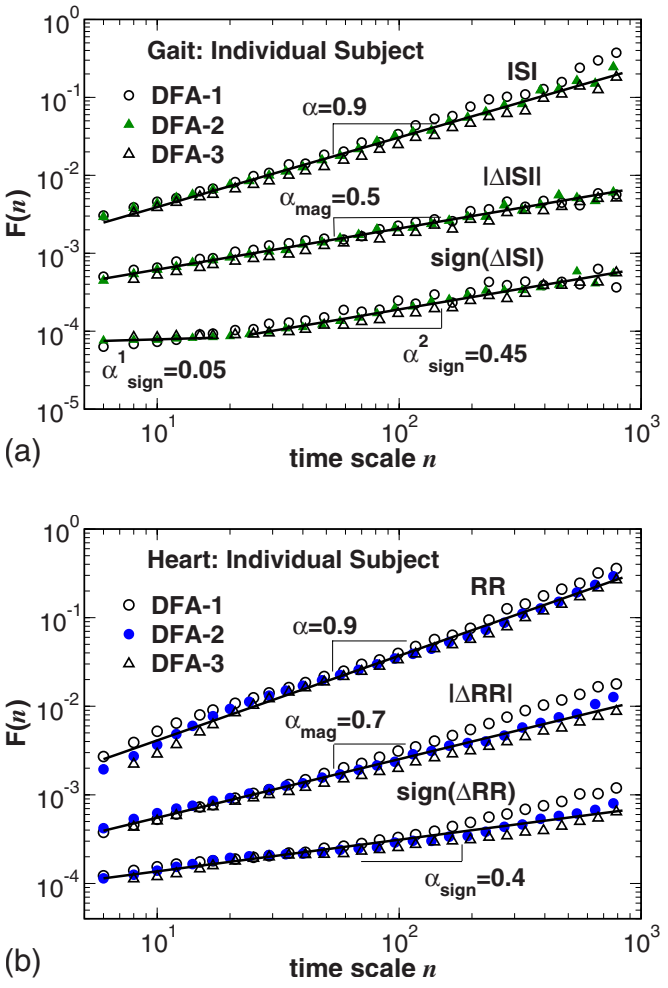

FIG. 7. (Color online) Results of DFA-l analysis with different order $l=1,2,3$ of polynomial detrending for (a) gait and (b) heartbeat data. Note that DFA-l removes trends of order up to $(l-1)$ in the time series. Considering the group average $\langle \Delta\alpha \rangle_i$ of the differences $\Delta\alpha^i_{1,2} \equiv \alpha^i(\text{DFA}-1) - \alpha^i(\text{DFA}-2)$, where i indicates different subjects, we obtain the following: for the original interstride signal $\langle \Delta\alpha_{1,2} \rangle_i = 0.03 \pm 0.03$ and $\langle \Delta\alpha_{2,3} \rangle_i = 0.007 \pm 0.009$, indicating that the results obtained from DFA-2 and DFA-3 are *not* significantly different. Thus, using higher order of polynomial detrending does not change the scaling result, i.e., compared to constant and linear trends, quadratic trends do not contribute significantly to the nonstationarity of gait. These observations remain valid also for the magnitude and sign scaling analysis as shown in (a) and (b).

neural centers are considered [12,13]. In this model a lower degree of nonlinearity (and close-to-linear monofractal $\tau(q)$ spectrum) reflects increased connectivity between neural centers, typically associated with maturation of gait dynamics in adults. The present results are also consistent with studies that used a different approach to quantify the dynamics of gait, based on estimates of the local Hurst exponents, and reported only weak multifractality in gait dynamics [14,15].

IV. SUMMARY

In summary, we find that while the fluctuations in the output of both gait and heartbeat processes are characterized by similar two-point correlation properties and $1/f$-like power spectra, they belong to different classes of complexity—human gait fluctuations exhibit practically linear $\tau(q)$ spectrum and close to monofractal properties characterized by a single scaling exponent, while heartbeat fluctuations exhibit nonlinear multifractal properties, which in physical systems have been connected with turbulence and related multiscale phenomena [32,38,43,80,81,101]. Our analyses indicate that while two systems—cardiac and locomotion, both under integrated neural control and with multicomponent feedback interactions over a range of time scales—can be characterized by long-range power-law correlations of $1/f$-type, other linear and nonlinear scaling features of their dynamics can be markedly different. This study demonstrates that different combinations of scaling behavior for the magnitude and sign of the fluctuations can lead to similar scaling behavior over a broad range of time scales in the correlations of the fluctuations in the output of these systems. Specifically, we find strong anticorrelations in the sign and close to random behavior for the magnitude of gait fluctuations at short and intermediate time scales, in contrast to weak anticorrelations in the sign and strong positive correlation for the magnitude of heartbeat interval fluctuations—suggesting that, despite certain similarities, these physiologic systems belong to different subclasses of complexity.

We note that, our observations of higher than 0.5 values for the gait magnitude exponent $\alpha_{\text{mag}} \approx 0.6$ at short time scales of up to 15 s (Table I) are in agreement with earlier reports of slightly nonlinear/multifractal behavior in gait dynamics based on estimates of the local Hölder exponents [14]. This slightly multifractal behavior at short time scales—which may result from (i) the inherent instability of nonisolated local singularities in gait fluctuations as quantified by the local Hölder exponents or (ii) may be intrinsically related to local nonlinear Fourier-phase correlations in gait dynamics—appears to be lost at time scales above 15 s, where the global scaling exponent $\alpha_{\text{mag}} \approx 0.5$ (Table I), and the multifractal spectrum $\tau(q)$ appears linear for different moments q (Fig. 5). Our observation of a transition in gait dynamics from slightly nonlinear (at short time scales) to linear/monofractal behavior (at long time scales) relates to earlier empirical and modeling studies reporting (i) a decrease in long-term gait nonlinearity, as measured by α_{mag}, with maturation from childhood to adulthood, and (ii) that this decrease in nonlinearity/multifractality with age may be related to increased connectivity (i.e., ability to operate over a broader range of frequency/time scales) among the central pattern generators responsible for gait control at different frequency modes [13].

We further note that different mechanisms may be involved in various aspects of locomotor control. For example, in contrast to gait dynamics where we observe $\alpha_{\text{mag}} \approx 0.5$ indicating linear behavior, our prior studies of forearm motion [102,103] show $\alpha_{\text{mag}} \approx 0.8$, indicating high degree of nonlinearity in wrist activity dynamics, although both gait and wrist dynamics are characterized by identical long-range power-law correlations with an exponent $\alpha \approx 0.9$ [12,13,102,103]. Thus, comparing the "mosaic" of scaling, nonlinear, and multifractal measures of gait interstride inter-

vals with similar measures of other physiologic systems is necessary for better understanding the dynamics of these systems and for further developing more adequate models of integrated neural control [104–106].

The findings reported here are of interest because they underscore the limitations of traditional two-point correlation methods in characterizing physiological and physical time series. In addition, these results suggest that feedback on multiple time scales is not sufficient to explain different types of $1/f$ scaling and scale invariance, and highlight the need for the development of new models [107–110] that could account for the scale-invariant outputs of different types of feedback systems.

ACKNOWLEDGMENTS

This work was supported by grants from Mitsubishi Chemical Co., Yokahama, Japan, NIH/National Center for Research Resources (Grants No. P41 RR13622 and AG14100) and NIH (Grant No. HL071972). We thank Yosef Ashkenazy and Ainslie Yuen for helpful discussions.

[1] H. E. Stanley, *Introduction to Phase Transitions and Critical Phenomena* (Oxford University Press, New York, 1971).
[2] P. Bak and M. Creutz, *Fractals in Science*, edited by A. Bunde and S. Havlin (Springer-Verlag, Berlin, 1994).
[3] C. Bernard, *Leçons sur les Phénoménes de la Vie Communs aux Animaux et aux Végétaus* (Baillière, Paris, 1878), Vols. 1 and 2.
[4] B. van der Pol and J. van der Mark, Philos. Mag. **6**, 763 (1928).
[5] W. B. Cannon, Physiol. Rev. **9**, 399 (1929).
[6] J. B. Johnson, Phys. Rev. **26**, 71 (1925).
[7] P. Dutta and P. M. Horn, Rev. Mod. Phys. **53**, 497 (1981).
[8] *Ninth International Symposium on Noise in Physical Systems*, edited by C. M. Van Vliet (World Scientific, Singapore, 1987).
[9] M. B. Weissman, Rev. Mod. Phys. **60**, 537 (1988).
[10] T. Musha and H. Higuchi, Jpn. J. Appl. Phys. **15**, 1271 (1976).
[11] Y. Liu, P. Gopikrishnan, P. Cizeau, M. Meyer, C.-K. Peng, and H. E. Stanley, Phys. Rev. E **60**, 1390 (1999).
[12] J. M. Hausdorff, Y. Ashkenazy, C.-K. Peng, P. Ch. Ivanov, H. E. Stanley, and A. L. Goldberger, Physica A **302**, 138 (2001).
[13] Y. Ashkenazy, J. M. Hausdorff, P. Ch. Ivanov, and H. E. Stanley, Physica A **316**, 662 (2002).
[14] N. Scafetta, L. Griffin, and B. J. West, Physica A **328**, 561 (2003).
[15] B. J. West and N. Scafetta, Phys. Rev. E **67**, 051917 (2003).
[16] M. F. Shlesinger, Ann. N. Y. Acad. Sci. **504**, 214 (1987).
[17] M. F. Shlesinger and B. J. West, *Random Fluctuations and Pattern Growth: Experiments and Models*, edited by H. E. Stanley and N. Ostrowsky (Kluwer Academic, Boston, 1988).
[18] B. J. West and M. F. Shlesinger, Int. J. Mod. Phys. B **3**, 795b (1989).
[19] J. B. Bassingthwaighte, L. S. Liebovitch, and B. J. West, *Fractal Physiology* (Oxford University Press, New York, 1994); L. S. Liebovitch and T. I. Toth, Ann. N.Y. Acad. Sci. **591**, 375 (1990).
[20] R. M. Berne and M. N. Levy, *Cardiovascular Physiology*, 6th ed. (C.V. Mosby, St. Louis, 1996).
[21] V. T. Inman, H. J. Ralston, and F. Todd, *Human Walking* (Williams and Wilkins, Baltimore, 1981).
[22] M. N. Levy, Circ. Res. **29**, 437 (1971).
[23] M. Kobayashi and T. Musha, IEEE Trans. Biomed. Eng. **BME-29**, 456 (1982).
[24] Y. Yamamoto and R. L. Hughson, J. Appl. Physiol. **71**, 1143 (1991).
[25] Y. Yamamoto and R. L. Hughson, Physica D **68**, 250 (1993).
[26] C.-K. Peng, J. Mietus, J. M. Hausdorff, S. Havlin, H. E. Stanley, and A. L. Goldberger, Phys. Rev. Lett. **70**, 1343 (1993).
[27] *Heart Rate Variability*, edited by M. Malik and A. J. Camm (Futura, Armonk, NY, 1995).
[28] M. P. Kadaba, H. K. Ramakrishnan, M. E. Wootten, J. Gainey, G. Gorton, and G. V. B. Cochran, J. Orthop. Res. **7**, 849 (1989).
[29] J. M. Hausdorff, C.-K. Peng, Z. Ladin, J. Y. Wei, and A. L. Goldberger, J. Appl. Physiol. **78**, 349 (1995).
[30] H. Yang, F. Zhao, Y. Zhuo, X. Wu, and Z. Li, Physica A **312**, 23 (2002).
[31] J. M. Hausdorff, Hum. Mov. Sci. **26**, 555 (2007).
[32] P. Ch. Ivanov, L. A. N. Amaral, A. L. Goldberger, S. Havlin, M. G. Rosenblum, Z. Struzik, and H. E. Stanley, Nature (London) **399**, 461 (1999).
[33] L. A. N. Amaral, P. Ch. Ivanov, N. Aoyagi, I. Hidaka, S. Tomono, A. L. Goldberger, H. E. Stanley, and Y. Yamamoto, Phys. Rev. Lett. **86**, 6026 (2001).
[34] J. J. Collins and I. Stewart, Biol. Cybern. **68**, 287 (1993).
[35] J. M. Hausdorff, P. L. Purdon, C.-K. Peng, Z. Ladin, J. Y. Wei, and A. L. Goldberger, J. Appl. Physiol. **80**, 1448 (1996).
[36] Y. Ashkenazy, P. Ch. Ivanov, S. Havlin, C.-K. Peng, A. L. Goldberger, and H. E. Stanley, Phys. Rev. Lett. **86**, 1900 (2001).
[37] Y. Ashkenazy, S. Havlin, P. Ch. Ivanov, C.-K. Peng, V. Schulte-Frohlinde, and H. E. Stanley, Physica A **323**, 19 (2003).
[38] J. F. Muzy, E. Bacry, and A. Arneodo, Phys. Rev. Lett. **67**, 3515 (1991).
[39] J. F. Muzy, E. Bacry, and A. Arneodo, Int. J. Bifurcat. Chaos **4**, 245 (1994).
[40] Gait Database available at http://www.physionet.org/; MIT-BIH Normal Sinus Rhythm Database available at http://www.physionet.org/physiobank/database/ecg
[41] J. M. Hausdorff, Z. Ladin, and J. Y. Wei, J. Biomech. **28**, 347 (1995).
[42] P. Ch. Ivanov, A. Bunde, L. A. N. Amaral, S. Havlin, J. Fritsch-Yelle, R. M. Baevsky, H. E. Stanley, and A. L. Goldberger, Europhys. Lett. **48**, 594 (1999).
[43] P. Ch. Ivanov, L. A. N. Amaral, A. L. Goldberger, S. Havlin, M. G. Rosenblum, H. E. Stanley, and Z. Struzik, Chaos **11**, 641 (2001).
[44] C.-K. Peng, S. V. Buldyrev, S. Havlin, M. Simons, H. E. Stan-

ley, and A. L. Goldberger, Phys. Rev. E **49**, 1685 (1994).
[45] K. Hu, P. Ch. Ivanov, Z. Chen, P. Carpena, and H. E. Stanley, Phys. Rev. E **64**, 011114 (2001).
[46] Z. Chen, P. Ch. Ivanov, K. Hu, and H. E. Stanley, Phys. Rev. E **65**, 041107 (2002).
[47] L. Xu, P. Ch. Ivanov, K. Hu, Z. Chen, A. Carbone, and H. E. Stanley, Phys. Rev. E **71**, 051101 (2005).
[48] Z. Chen, K. Hu, P. Carpena, P. Bernaola-Galvan, H. E. Stanley, and P. Ch. Ivanov, Phys. Rev. E **71**, 011104 (2005).
[49] N. Vandewalle, M. Ausloos, M. Houssa, P. W. Mertens, and M. M. Heyns, Appl. Phys. Lett. **74**, 1579 (1999).
[50] K. Ivanova and M. Ausloos, Physica A **274**, 349 (1999).
[51] A. Montanari, R. Rosso, and M. S. Taqqu, Water Resour. Res. **36**, 1249 (2000).
[52] B. D. Malamud and D. L. Turcotte, J. Stat. Plan. Infer. **80**, 173 (1999).
[53] S. V. Buldyrev, A. L. Goldberger, S. Havlin, C.-K. Peng, H. E. Stanley, and M. Simons, Biophys. J. **65**, 2673 (1993).
[54] S. M. Ossadnik, S. B. Buldyrev, A. L. Goldberger, S. Havlin, R. N. Mantegna, C.-K. Peng, M. Simons, and H. E. Stanley, Biophys. J. **67**, 64 (1994).
[55] M. S. Taqqu, V. Teverovsky, and W. Willinger, Fractals **3**, 785 (1995).
[56] S. Havlin, S. V. Buldyrev, A. L. Goldberger, R. N. Mantegna, C.-K. Peng, M. Simons, and H. E. Stanley, Fractals **3**, 269 (1995).
[57] D. T. Schmitt and P. Ch. Ivanov, Am. J. Physiol. **293**, R1923 (2007).
[58] T. H. Makikallio, J. Koistinen, L. Jordaens, M. P. Tulppo, N. Wood, B. Golosarsky, C.-K. Peng, A. L. Goldberger, and H. V. Huikuri, Am. J. Cardiol. **83**, 880 (1999).
[59] A. Bunde, S. Havlin, J. W. Kantelhardt, T. Penzel, J. H. Peter, and K. Voigt, Phys. Rev. Lett. **85**, 3736 (2000).
[60] T. T. Laitio, H. V. Huikuri, E. S. H. Kentala, T. H. Makikallio, J. R. Jalonen, H. Helenius, K. Sariola-Heinonen, S. Yli-Mayry, and H. Scheinin, Anesthesiology **93**, 69 (2000).
[61] R. I. Kitney and O. Rompelman, *The Study of Heart-Rate Variability* (Oxford University Press, London, 1980).
[62] R. I. Kitney, D. Linkens, A. C. Selman, and A. A. McDonald, Automedica **4**, 141 (1982).
[63] L. S. Liebovitch, Adv. Chem. Ser. **235**, 357 (1994).
[64] J. Kurths, A. Voss, P. Saparin, A. Witt, H. J. Kleiner, and N. Wessel, Chaos **5**, 88 (1995).
[65] A. L. Goldberger, Lancet **347**, 1312 (1996).
[66] Y. Q. Chen, M. Z. Ding, and J. A. S. Kelso, Phys. Rev. Lett. **79**, 4501 (1997).
[67] B. J. West and L. Griffin, Fractals **6**, 101 (1998).
[68] S. B. Lowen, L. S. Liebovitch, and J. A. White, Phys. Rev. E **59**, 5970 (1999).
[69] S. Havlin, S. V. Buldyrev, A. Bunde, A. L. Goldberger, P. Ch. Ivanov, C.-K. Peng, and H. E. Stanley, Physica A **273**, 46 (1999).
[70] L. Griffin, D. J. West, and B. J. West, J. Biol. Phys. **26**, 185 (2000).
[71] H. E. Stanley, L. A. N. Amaral, P. Gopikrishnan, P. Ch. Ivanov, T. H. Keitt, and V. Plerou, Physica A **281**, 60 (2000).
[72] L. A. Protsmman, H. Meeuwsen, P. Hamilton, B. J. West, and J. Wilkerson, J. Sport Exerc. Psychol. **23**, S67 (2001).
[73] *Fractals and Disordered Systems*, 2nd ed., edited by A. Bunde and S. Havlin (Springer-Verlag, Berlin, 1996).
[74] H. Takayasu, *Fractals in the Physical Sciences* (Manchester University Press, Manchester, UK, 1997).
[75] S. Stoev, V. Pipiras, and M. S. Taqqu, Signal Process. **82**, 1873 (2002).
[76] H. E. Hurst, Trans. Am. Soc. Civ. Eng. **116**, 770 (1951).
[77] J. Feder, *Fractals* (Plenum, New York, 1988).
[78] T. Vicsek and A.-L. Barabási, J. Phys. A **24**, L845 (1991).
[79] A.-L. Barabasi, P. Szepfalusy, and T. Vicsek, Physica A **178**, 17 (1991).
[80] J. Nittmann, G. Daccord, and H. E. Stanley, Nature (London) **314**, 141 (1985).
[81] C. Meneveau and K. R. Sreenivasan, Phys. Rev. Lett. **59**, 1424 (1987).
[82] C. Li and C. Zheng, *Engineering in Medicine and Biology Society.*, Proceedings of the 15th Annual International Conference of the IEEE, edited by A. Y. J. Szeto, and R. M. Rangayyan(IEEE, New York,1993), Vol. 15, p. 330.
[83] O. Meste, H. Rix, P. Caminal, and N. V. Thakor, IEEE Trans. Biomed. Eng. **41**, 625 (1994).
[84] L. Senhadji, G. Carrault, J. J. Bellanger, and G. Passariello, IEEE Eng. Med. Biol. Mag. **14**, 167 (1995).
[85] M. Karrakchou, C. V. Lambrecht, and M. Kunt, IEEE Eng. Med. Biol. Mag. **14**, 179 (1995).
[86] N. V. Thakor, X. R. Guo, Y. C. Sun, and D. F. Hanley, IEEE Trans. Biomed. Eng. **40**, 1085 (1993).
[87] D. Morlet, J. P. Couderc, P. Touboul, and P. Rubel, Int. J. Biomed. Comput. **39**, 311 (1995).
[88] D. Morlet, F. Peyrin, P. Desseigne, P. Touboul, and P. Rubel, J. Electrocardiol. **26**, 311 (1993).
[89] L. Reinhardt, M. Mäkijärvi, T. Fetsch, J. Montonen, G. Sierra, A. Martínez-Rubio, T. Katila, M. Borggrefe, and G. Breithardt, J. Am. Coll. Cardiol. **27**, 53 (1996).
[90] M. Karrakchou and M. Kunt, Ann. Biomed. Eng. **23**, 562 (1995).
[91] P. Ch. Ivanov, M. G. Rosenblum, C.-K. Peng, J. Mietus, S. Havlin, H. E. Stanley, and A. L. Goldberger, Nature (London) **383**, 323 (1996).
[92] P. Ch. Ivanov, M. G. Rosenblum, C.-K. Peng, J. Mietus, S. Havlin, H. E. Stanley, and A. L. Goldberger, Physica A **249**, 587 (1998).
[93] J. F. Muzy, E. Bacry, and A. Arneodo, Phys. Rev. E **47**, 875 (1993).
[94] T. Vicsek, *Fractal Growth Phenomena*, 2nd ed. (World Scientific, Singapore, 1993).
[95] D. Panter, *Modulation, Noise and Spectral Analysis* (McGraw-Hill, New York, 1965).
[96] J. Theiler, S. Eubank, A. Longtin, B. Galdrikian, and D. J. Garmer, Physica D **58**, 77 (1992).
[97] J. W. Kantelhardt, Y. Ashkenazy, P. Ch. Ivanov, A. Bunde, S. Havlin, T. Penzel, J. H. Peter, and H. E. Stanley, Phys. Rev. E **65**, 051908 (2002).
[98] R. Karasik, N. Sapir, Y. Ashkenazy, P. Ch. Ivanov, I. Dvir, P. Lavie, and S. Havlin, Phys. Rev. E **66**, 062902 (2002).
[99] H. E. Stanley, L. A. N. Amaral, A. L. Goldberger, S. Havlin, P. Ch. Ivanov, and C.-K. Peng, Physica A **270**, 309 (1999).
[100] N. Tanaka, S. Sonoda, Y. Muraoka, Y. Tomita, and N. Chino, Jpn. J. Rehabil. Med. **33**, 549 (1996).
[101] U. Frisch, *Turbulence* (Cambridge University Press, Cambridge, UK, 1995).
[102] K. Hu, P. Ch. Ivanov, Z. Chen, M. F. Hilton, H. E. Stanley,

and S. A. Shea, Physica A **337**, 307 (2004).
[103] P. Ch. Ivanov, K. Hu, M. F. Hilton, S. A. Shea, and H. E. Stanley, Proc. Natl. Acad. Sci. U.S.A. **104**, 20702 (2007).
[104] R. Bartsch, M. Plotnik, J. W. Kantelhardt, S. Havlin, N. Giladi, and J. M. Hausdorff, Physica A **383**, 455 (2007).
[105] K. Ohgane and K. I. Ueda, Phys. Rev. E **77**, 051915 (2008).
[106] V. B. Kokshenev, Phys. Rev. Lett. **93**, 208101 (2004).
[107] P. Ch. Ivanov, L. A. N. Amaral, A. L. Goldberger, and H. E. Stanley, Europhys. Lett. **43**, 363 (1998).
[108] D. C. Lin and R. L. Hughson, Phys. Rev. Lett. **86**, 1650 (2001).
[109] P. V. E. McClintock and A. Stefanovska, Physica A **314**, 69 (2002).
[110] R. Yulmetyev, P. Hanggi, and F. Gafarov, Phys. Rev. E **65**, 046107 (2002).

Levels of complexity in scale-invariant neural signals

By: Ivanov, PC (Ivanov, Plamen Ch.)[1,2,3,4,5]; Ma, QDY (Ma, Qianli D. Y.)[3,4,6]; Bartsch, RP (Bartsch, Ronny P.)[3,4]; Hausdorff, JM (Hausdorff, Jeffrey M.)[7,3]; Amaral, LAN (Amaral, Luis A. Nunes)[8]; Schulte-Frohlinde, V (Schulte-Frohlinde, Verena)[1,2]; Stanley, HE (Stanley, H. Eugene)[1,2]; Yoneyama, M (Yoneyama, Mitsuru)[9]

View ResearcherID and ORCID

PHYSICAL REVIEW E
Volume: 79 **Issue:** 4 **Part:** 1
Article Number: 041920
DOI: 10.1103/PhysRevE.79.041920
Published: APR 2009
Document Type: Article
View Journal Impact

Abstract

Many physical and physiological signals exhibit complex scale-invariant features characterized by 1/f scaling and long-range power-law correlations, indicating a possibly common control mechanism. Specifically, it has been suggested that dynamical processes, influenced by inputs and feedback on multiple time scales, may be sufficient to give rise to 1/f scaling and scale invariance. Two examples of physiologic signals that are the output of hierarchical multiscale physiologic systems under neural control are the human heartbeat and human gait. Here we show that while both cardiac interbeat interval and gait interstride interval time series under healthy conditions have comparable 1/f scaling, they still may belong to different complexity classes. Our analysis of the multifractal scaling exponents of the fluctuations in these two signals demonstrates that in contrast to the multifractal behavior found in healthy heartbeat dynamics, gait time series exhibit less complex, close to monofractal behavior. Further, we find strong anticorrelations in the sign and close to random behavior for the magnitude of gait fluctuations at short and intermediate time scales, in contrast to weak anticorrelations in the sign and strong positive correlation for the magnitude of heartbeat interval fluctuations-suggesting that the neural mechanisms of cardiac and gait control exhibit different linear and nonlinear features. These findings are of interest because they underscore the limitations of traditional two-point correlation methods in fully characterizing physiological and physical dynamics. In addition, these results suggest that different mechanisms of control may be responsible for varying levels of complexity observed in physiological systems under neural regulation and in physical systems that possess similar 1/f scaling.

Keywords

Author Keywords: cardiology; fluctuations; fractals; gait analysis; medical signal processing; neurophysiology; physiological models

KeyWords Plus: HEART-RATE-VARIABILITY; LONG-RANGE CORRELATIONS; NON-GAUSSIAN BEHAVIOR; TIME-SERIES; HUMAN GAIT; MULTIFRACTAL FORMALISM; WAVELET ANALYSIS; POSTINFARCTION PATIENTS; CARDIAC DYNAMICS; FRACTAL ANALYSIS

Author Information

Reprint Address: Ivanov, PC (reprint author)

+ Boston Univ, Dept Phys, 590 Commonwealth Ave, Boston, MA 02215 USA.

Addresses:

[1] Boston Univ, Dept Phys, Boston, MA 02215 USA
[2] Boston Univ, Ctr Polymer Studies, Boston, MA 02215 USA
[3] Harvard Univ, Sch Med, Boston, MA 02115 USA
[4] Brigham & Womens Hosp, Div Sleep Med, Boston, MA 02115 USA
[5] Bulgarian Acad Sci, Inst Solid State Phys, BU-1784 Sofia, Bulgaria
[6] Nanjing Univ Posts & Telecommun, Nanjing 210003, Peoples R China
[7] Tel Aviv Univ, Tel Aviv Sourasky Med Ctr, IL-69978 Tel Aviv, Israel
[8] Northwestern Univ, Dept Chem Engn, Evanston, IL 60208 USA
[9] Sci & Technol Ctr Inc, Mitsubishi Chem Grp, Yokohama, Kanagawa 2278502, Japan

E-mail Addresses: plamen@buphy.bu.edu

Funding

Funding Agency	Grant Number
Mitsubishi Chemical Co., Yokahama, Japan	
NIH/National Center for Research Resources	P41 RR13622 AG14100 HL071972

View funding text

Publisher

AMER PHYSICAL SOC, ONE PHYSICS ELLIPSE, COLLEGE PK, MD 20740-3844 USA

Categories / Classification

Research Areas: Physics

Web of Science Categories: Physics, Fluids & Plasmas; Physics, Mathematical

See more data fields

91 of 127

Cited References: 107

Showing 30 of 107 **View All in Cited References page** *(from Web of Science Core Collection)*

1. **Behavioral-independence features of complex heartbeat dynamics** **Times Cited: 186**
By: Amaral, LAN; Ivanov, PC; Aoyagi, N; et al.
PHYSICAL REVIEW LETTERS Volume: 86 Issue: 26 Pages: 6026-6029 Published: JUN 25 2001

2. **Magnitude and sign scaling in power-law correlated time series** **Times Cited: 108**
By: Ashkenazy, Y; Havlin, S; Ivanov, PC; et al.
PHYSICA A-STATISTICAL MECHANICS AND ITS APPLICATIONS Volume: 323 Pages: 19-41 Published: MAY 15 2003

3. **A stochastic model of human gait dynamics** **Times Cited: 87**
By: Ashkenazy, Y; Hausdorff, JA; Ivanov, PC; et al.
PHYSICA A-STATISTICAL MECHANICS AND ITS APPLICATIONS Volume: 316 Issue: 1-4 Pages: 662-670 Article Number: PII S0378-4371(02)01453-X Published: DEC 15 2002

4. **Magnitude and sign correlations in heartbeat fluctuations** **Times Cited: 299**
By: Ashkenazy, Y; Ivanov, PC; Havlin, S; et al.

Eur. Phys. J. B **71**, 243–250 (2009)
DOI: 10.1140/epjb/e2009-00310-5

THE EUROPEAN PHYSICAL JOURNAL B

Regular Article

Quantifying cross-correlations using local and global detrending approaches

B. Podobnik[1,2,3,a], I. Grosse[4], D. Horvatić[5], S. Ilic[6], P.Ch. Ivanov[3,7,8], and H.E. Stanley[3]

[1] Faculty of Civil Engineering, University of Rijeka, Rijeka, Croatia
[2] Zagreb School of Economics and Management, Zagreb, Croatia
[3] Center for Polymer Studies and Department of Physics, Boston University, Boston, MA 02215, USA
[4] Institute of Computer Science, Martin Luther University, Halle, Germany
[5] Physics Department, Faculty of Science, University of Zagreb, Bijenička c. 32, 10000 Zagreb, Croatia
[6] Lancaster Environment Centre, Lancaster University, Farrer Avenue, Lancaster LA1 4YQ, UK
[7] Institute of Solid State Physics, Bulgarian Academy of Sciences, Sofia 1784, Bulgaria
[8] Harvard Medical School and Division of Sleep Medicine, Brigham and Women's Hospital, Boston, MA 02115 USA

Received 18 May 2009 / Received in final form 27 July 2009
Published online 17 September 2009

Abstract. In order to quantify the long-range *cross-correlations* between two time series qualitatively, we introduce a new cross-correlations test $Q_{\rm CC}(m)$, where m is the number of degrees of freedom. If there are no cross-correlations between two time series, the cross-correlation test agrees well with the $\chi^2(m)$ distribution. If the cross-correlations test exceeds the critical value of the $\chi^2(m)$ distribution, then we say that the cross-correlations are significant. We show that if a Fourier phase-randomization procedure is carried out on a power-law cross-correlated time series, the cross-correlations test is substantially reduced compared to the case before Fourier phase randomization. We also study the effect of periodic trends on systems with power-law cross-correlations. We find that periodic trends can severely affect the quantitative analysis of long-range correlations, leading to crossovers and other spurious deviations from power laws, implying both *local* and *global* detrending approaches should be applied to properly uncover long-range power-law auto-correlations and cross-correlations in the random part of the underlying stochastic process.

PACS. 05.45.Tp Time series analysis – 05.40.-a Fluctuation phenomena, random processes, noise, and Brownian motion

There are a number of situations where different signals exhibit cross-correlations, ranging from geophysics [1] to finance [2–14] and solid-state physics [15]. Cross-correlation functions together with auto-correlation functions are commonly used to gain insight into the dynamics of natural systems. By their definitions, these techniques should be employed *only* in the presence of stationarity. However, it is an important fact that many time series of physical, biological, hydrological, and social systems are non-stationary and exhibit long-range power-law correlations [16–22]. In practice, statistical properties of these systems are difficult to study due to these nonstationarities.

For determining the scaling exponent of a long-range power-law auto-correlated time series in the presence of nonstationarities, the *detrended fluctuation analysis* (DFA) method has been developed [23] and its performance has been systematically tested for the effect of different types of trends and nonstationarities [24–27] as encountered in a wide range of different fields, such as cardiac dynamics [28], economics [29], DNA analysis [30], and meteorology [31]. The square root of the detrended variance grows with time scale n as $F_{\rm DFA}(n) \sim n^{\lambda_{DFA}}$, where λ_{DFA} is the DFA scaling exponent [23–26], where $1/2 < \lambda_{DFA} < 1$, indicates the presence of power-law auto-correlations, and $0 < \lambda_{DFA} < 1/2$ indicates the presence of long-range power-law anti-correlations.

There are many realistic situations in which one desires to quantify cross-correlations between two non-stationary time series. Examples include blood pressure and heart rate [32], air temperature and air humidity, and the temporal expression data of different genes. To quantify power-law *cross-correlations* in non-stationary time series, a new method based on detrended covariance, called detrended cross-correlations analysis (DCCA), has been recently proposed [11]. If cross-correlations decay as a power law, the corresponding detrended covariances are either always positive or always negative, and the square root of the detrended covariance grows with time scale n as

$$F_{\rm DCCA}(n) \propto n^{\lambda_{\rm DCCA}}, \qquad (1)$$

[a] e-mail: bp@phy.hr

where $\lambda_{\rm DCCA}$ is the DCCA cross-correlation exponent. If, however, the detrended covariance oscillates around zero as a function of the time scale n, there are no long-range cross-correlations.

In order to investigate power-law auto-correlations and power-law cross-correlations and effects of sinusoidal periodicity on cross-correlations, first we define a periodic two-component fractionally autoregressive integrated moving-average (ARFIMA) process [33–37], where each variable depends not only on its own past, but also on the past values of the other variable,

$$y_i = \left[W \sum_{n=1}^{\infty} a_n(\rho_1) y_{i-n} + (1-W) \sum_{n=1}^{\infty} a_n(\rho_2) y'_{i-n} \right] + A_1 \sin\left(\frac{2\pi}{T} i\right) + \eta_i, \tag{2a}$$

$$y'_i = \left[(1-W) \sum_{n=1}^{\infty} a_n(\rho_1) y_{i-n} + W \sum_{n=1}^{\infty} a_n(\rho_2) y'_{i-n} \right] + A_2 \sin\left(\frac{2\pi}{T} i\right) + \eta'_i. \tag{2b}$$

Here, η_t and η'_t denote two independent and identically distributed (*i.i.d.*) Gaussian variables with zero mean and unit variance, $a_j(\rho_m)$ are statistical weights defined by $(\rho_m) \equiv \frac{\Gamma(j-\rho_m)}{\Gamma(-\rho_m)\Gamma(1+j)}$, where $\Gamma(x)$ denotes the Gamma function, ρ_m (for $m = 1, 2$) are parameters ranging from 0 to 0.5, T is the sinusoidal period, A_1 and A_2 are two sinusoidal amplitudes, and W is a free parameter ranging from 0.5 to 1 and controlling the strength of power-law cross-correlations between y_t and y'_t. In case of $A_1 = A_2 = 0$, for $W = 1$, cross-correlations vanish, and the system of two equations decouples to two separate ARFIMA processes.

In Appendix A, for a version of the above process $y_i \equiv \sum_{j=1}^{\infty} a_j(\rho_1) y_{i-j} + \eta_i$, $y'_i \equiv \sum_{j=1}^{\infty} a_j(\rho_2) y'_{i-j} + \eta_i$ [11] where both y_i and y'_i share the *same i.i.d.* Gaussian process η_i, we analytically find that the time series $\{y_i\}$ and $\{y'_i\}$ are long-range power-law cross-correlated, where the scaling cross-correlations exponent $\lambda_{\rm DCCA}$ (Eq. (1)) is equal to the average of the Hurst exponents, $\lambda_{\rm DCCA} = \frac{H_1+H_2}{2}$, the result found numerically in reference [11], and where $H_m = 0.5 + \rho_m$ [37].

Statistical inferences based on estimation and hypothesis testing are among the most important aspects of the decision making process in science and business. Here we propose a new statistic to test the presence of cross-correlations. Suppose that $\{y_i\}$ and $\{y'_i\}$ are two discrete-time *i.i.d.* stochastic processes, where there are no cross-correlations among the time series. We may define their cross-correlation function

$$X_i = \frac{\sum_{k=i+1}^{N} y_k y'_{k-i}}{\sqrt{\sum_{k=1}^{N} y_k^2 \sum_{k=1}^{N} y_k'^2}}. \tag{3}$$

Under the assumption that $\{y_i\}$ and $\{y'_i\}$ are statistically independent, one can easily show that the X_i are uncorrelated [38]:

$$E(X_i X_{i'}) \propto \sum_{k=i+1}^{N} \sum_{k'=i'+1}^{N} E(y_k y'_{k-i} y_{k'} y'_{k'-i'}) = \sum_{k=i+1}^{N} \sum_{k'=i'+1}^{N} E(y_k y_{k'}) E(y'_{k-i} y'_{k'-i'}), \tag{4}$$

which is zero for $i \neq i'$. The expectation value of X_i is equal to zero, $E(X_i) = 0$, because there are no cross-correlations between $\{y_i\}$ and $\{y'_i\}$, and the variance is

$$V(X_i) = E(X_i^2) = \frac{\sum_{k=i+1}^{N} \sum_{k'=i+1}^{N} E(y_k y'_{k-i} y_{k'} y'_{k'-i})}{\sum_{k=1}^{N} \sum_{k'=1}^{N} E(y_k^2) E(y_{k'}'^2)} = \frac{\sum_{k=i+1}^{N} \sum_{k'=i+1}^{N} E(y_k y_{k'}) E(y'_{k-i} y'_{k'-i})}{\sigma^2 \sigma'^2 N^2}, \tag{5}$$

where we use $E(y_k y_{k'}) = \sigma^2 \delta_{k,k'}$ and $E(y'_k y'_{k'}) = \sigma'^2 \delta_{k,k'}$. Further, $V(X_i) = \frac{\sum_{k=i+1}^{N} \sum_{k'=i+1}^{N} \delta_{k,k'} \delta_{k-i,k'-i}}{N^2} = \frac{\sum_{k=i+1}^{N} \delta_{k,k}}{N^2} = \frac{N-i}{N^2}$. Thus, we find that $E(X_i^2) = \frac{N-i}{N^2}$, where $E(X_i X_{i'}) = 0$ when $i \neq i'$. The cross-correlation coefficient X_k is normally distributed for asymptotically large values of N [38], as it holds for auto-correlation function r_k [39]. Then $X_i / \sqrt{(N-i)/N^2}$ asymptotically behaves as a Gaussian distribution with zero mean and unit variance, and the sum of squares of these variables approximately follows a χ^2 distribution.

According to definition of the χ^2 distribution, we propose the cross-correlations statistic

$$Q_{\rm CC}(m) \equiv N^2 \sum_{i=1}^{m} \frac{X_i^2}{N-i}, \tag{6}$$

which is approximately $\chi^2(m)$ distributed with m degrees of freedom. The test can be used to test the null hypothesis that none of the first m cross-correlation coefficients is different from zero. The test of equation (6) is similar to the test statistic [40]

$$Q'(m) \equiv N(N+2) \sum_{i=1}^{m} \frac{X_i^2}{N-i} \tag{7}$$

proposed in analogy to the Ljung-Box (LJB) test [41] that is one of the most widely employed tests for the presence of auto-correlations. The Ljung-Box (LJB) test can be easily obtained if all cross-correlation coefficients X_k in equation (7) are replaced by auto-correlation coefficients. Clearly, for larger samples where $N(N+2) \approx N^2$, the tests of equations (6) and (7) give the same distribution.

Next we show that the test of equation (6) better approximates the $\chi^2(m)$ distribution than the test of equation (7) for small samples. In order to show that the cross-correlation test of equation (6) is applicable to real-world data where time series are commonly of small size, we test the speed of convergence of the distribution of $Q_{\rm CC}(m)$ to the $\chi^2(m)$ distribution. Thus, we first generate 10^6

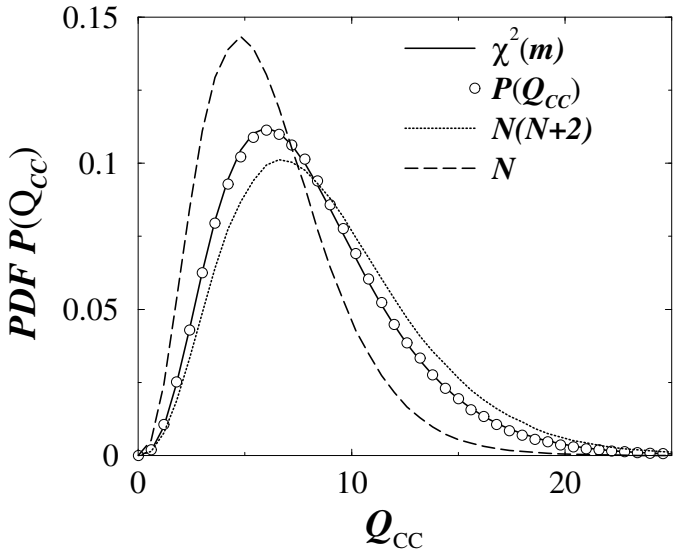

Fig. 1. Probability distribution function (pdf) $P(Q_{\rm CC})$ of $Q_{\rm CC}$ defined in equation (6) together with the $\chi^2(m)$ pdf, where m are the degrees of freedom. We also show $P(Q')$ of Q' defined in equation (7). We generate 10^6 pairs of time series $\{y_i\}$ and $\{y_i'\}$, where each time series is generated by an *i.i.d.* Gaussian process with mean zero and unit variance. Each time series is comprised of $N = 20$ data points (small time series). We choose $m = 8$, and for each pair of time series we calculate the cross-correlations X_i, where $i = 1, ..., 8$. We find a perfect match between $P(Q_{\rm CC}(m))$ and $\chi^2(m)$. In opposite, the pdf of Q' defined in equation (7) deviates from the $\chi^2(m)$ distribution. We also show the pdf of a test defined as $N\sum_i^m X_i^2$, which substantially deviates from $\chi^2(m)$.

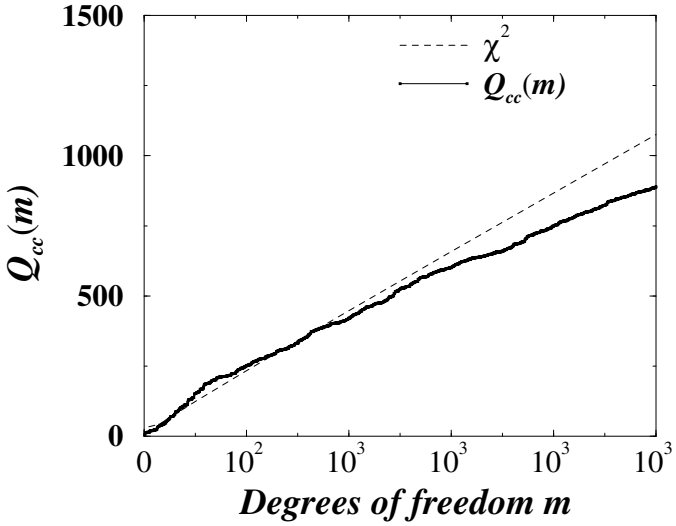

Fig. 2. Cross-correlations between the differences of logarithms of prices for IBM and General Electric (GE). We show $Q_{\rm CC}(m)$ versus the degrees of freedom m. We also show the critical values for the $\chi^2(m)$ distribution at the 5% level of significance. $Q_{\rm CC}(m)$ virtually follows the critical values for the $\chi^2(m)$ distribution that is a signal for no cross-correlations. The test of equation (7) gives practically the same result as the test of equation (6) since $N \gg 1$.

equally-sized *i.i.d.* time series $\{y_i\}$ and $\{y_i'\}$ for a small value $N = 20$ where $m = 8$. For each pair of time series, we calculate the cross-correlations X_k, where $k = 1, ..., 8$, and then the test statistic $Q_{\rm CC}(m)$. In Figure 1 we show the distribution of $P(Q_{\rm CC}(m))$ together with $\chi^2(8)$, and find a perfect agreement between these two probability distributions. We also show the distribution of the test statistic of equation (7), where for a given small sample ($N = 20$), deviation between the given distribution and $\chi^2(8)$ is obvious. Thus, when the cross-correlation test is applied in practice, we can use the critical values of the $\chi^2(m)$ distribution.

Note that the LJB test and hence the cross-correlation test of equation (6) is proposed to be applied for the *residuals* of a given model, not the original time series. However, sometimes the test is applied to the original series, e.g., return time series [42]. Accordingly, the cross-correlation test of equation (6) can be also used to measure the strength of cross-correlations in the original time series. In order to investigate cross-correlation scaling we analyze the daily adjusted closing values of the IBM and General Electric [43]. For each company's price, we calculate the time series of the differences of logarithms for successive days over the period 2 January 1962 till 1 May 2009. Then we calculate the P value of the cross-correlation test of equation (6) for different degrees of freedom m together with the critical values for the $\chi^2(m)$ distribution at the 5% level of significance. In Figure 2 we find that the cross-correlation Q_{CC} test statistic practically follows the critical values for the $\chi^2(m)$, suggesting no cross-correlations in the data.

In opposite to a common practice in statistic when a test statistic is compared with a critical value for a single value of degree of freedom m, here in the paper we plot the statistic test versus the critical value of $\chi^2(m)$ for a broad range of values of m. If for a broad range of m the test statistic of equation (6) exceeds the critical values of $\chi^2(m)$ ($Q_{\rm CC}(m) > \chi^2_{0.95}(m)$), we claim that there are not only cross-correlations, but there are long-range cross-correlations. However, the cross-correlations test of equation (6) should be used to test the presence of cross-correlations only *qualitatively*. In order to test the presence of cross-correlations *quantitatively* – to estimate the cross-correlation exponent – we suggest to employ the DCCA method of equation (1).

Next we show how the cross-correlation test of equation (6) might be useful to estimate the strength and significance of cross-correlations found in data. By using the two-component ARFIMA process of equations (2a, 2b), we generate four different pairs of time series $\{y_i\}$ and $\{y_i'\}$, where each pair is characterized by different values of ρ, while W is constant. We exclude the periodic term for now, so $A_1 = A_2 = 0$. In Figure 3 for each pair of time series we show the cross-correlation test of equation (6) (filled symbols) for different degrees of freedom m. In order to show the strength of cross-correlations, for different values of m, we also show the critical values of the $\chi^2(m)$ distribution at the 5% level of significance. We note that, for a given value of m, the deviation between the test of

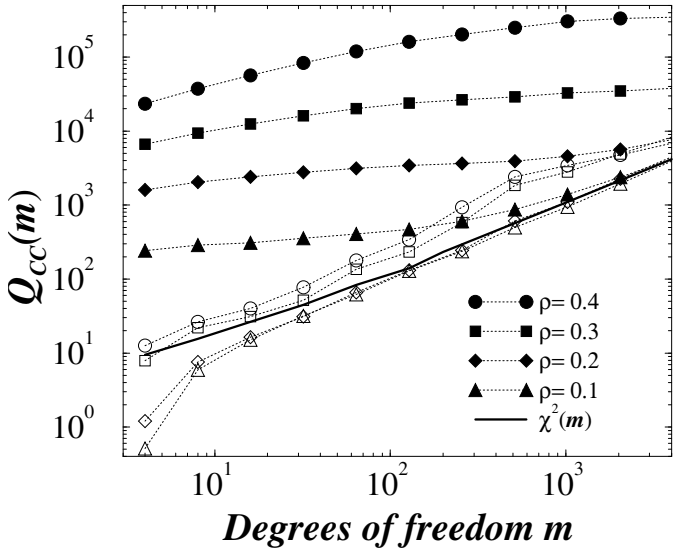

Fig. 3. $Q_{\rm CC}(m)$ for different degrees of freedom m before (filled symbols) and after (open symbols) Fourier phase-randomization of the $Q_{\rm CC}(m)$. For each of four values of ρ, the two-component ARFIMA process of equations (2a, 2b) generates the pair of time series $\{y_i\}$ and $\{y_i'\}$ where $m = 2^i$, and $i = 2, ..., 8$, and fixed $W = 0.5$. For the sinusoidal amplitude we take $A_1 = A_2 = 0$. The time series $\{y_i\}$ and $\{y_i'\}$ are $N = 5 \times 10^4$ data points each. The solid line denotes the critical values for the $\chi^2(m)$ distribution at the 5% level of significance. For each of four pairs $(\{y_i\}, \{y_i'\})$, we calculate the cross-correlations X_i, and the $Q_{\rm CC}(m)$ test statistic. The more positive is the difference between the $Q_{\rm CC}(m)$ test and the critical value of the $\chi^2(m)$ distribution, the stronger are the cross-correlations for a given m. For each value of ρ, we phase randomize the original time series $\{y_i'\}$, and obtain the surrogate time series $\{\tilde{y}_i'\}$. Then for each pair of time series $(\{y_i\}, \{\tilde{y}_i'\})$, we calculate the $Q_{\rm CC}(m)$ test statistic of equation (6). We also show the critical values for $\chi^2(m)$ distribution at the 5% level of significance. Fourier phase-randomization reduces the linear cross-correlations, since after a Fourier phase-randomization procedure (open symbols), we find that for each pair $(\{y_i\}, \{\tilde{y}_i'\})$, the cross-correlations measured by the $Q_{\rm CC}(m)$ test are substantially reduced – in fact, the cross-correlations practically vanish for time series with smaller ρ values.

equation (6) and the critical value of $\chi^2(m)$ increases with ρ, if W is kept fixed. We also note that, for each time series (specified by ρ), the test of equation (6) is larger than the critical value of $\chi^2(m)$ for a broad, but finite range of m. We propose that, if for a broad range of values of m the values of the test of equation (6) between the two time series are larger than the critical values of the $\chi^2(m)$ distribution, the cross-correlations are considered significant.

Often it is unclear to what degree the time series generated by a stochastic process exhibits linear and nonlinear correlations. Linear (nonlinear) auto-correlations are defined as those correlations which are not destroyed (are destroyed) by a Fourier phase-randomization of the original time series [28,44,45]. The Fourier phase-randomization procedure [44] works as follows: (i) perform a Fourier transform of the original time series; (ii) randomize the Fourier phases (thereby eliminating the nonlinearities of the original time series) but keep the Fourier amplitudes unchanged (thereby preserving the power spectrum and the linear properties of the original time series); and (iii) perform an inverse Fourier transform to obtain a surrogate time series.

For the four pairs of time series $\{y_i\}$ and $\{y_i'\}$ of equations (2a, 2b), in Figure 3 we show the cross-correlations test for different degrees of freedom after (open symbols) performing Fourier phase-randomization. To emphasize the impact of a phase randomization on cross-correlations we also show the critical values of $\chi^2(m)$ for different degrees of freedom. We show that after a Fourier phase-randomization (open symbols) cross-correlations are reduced [10] – for each pair of time series and for each m, the test is substantially reduced compared to the case before the Fourier phase randomization. Thus, while the Fourier phase-randomization procedure preserves linear auto-correlations [28,44], the same method substantially reduces the linear cross-correlations.

We next discuss how to quantify the scaling exponent of power-law cross-correlations between two time series, and how it relates to the DFA exponents calculated for each of two cross-correlated time series, which we generate by using the two-component process of equations (2a, 2b). Here, we assume there are no sinusoidal trends, $A_1 = A_2 = 0$. In Figures 4a, 4b, the DFA functions are given for each time series $\{y_i\}$ and $\{y_i'\}$ of 10^5 data points and $\rho_1 = 0.4$ and $\rho_2 = 0.1$. We set the cross-correlation coupling parameter to $W = 0.95$ (Fig. 4a) and $W = 0.05$ (Fig. 4b). In each figure we show that both time series $\{y_i\}$ and $\{y_i'\}$ are power-law auto-correlated, and are also power-law cross-correlated. From the definition of the process of equations (2a, 2b) it is clear that with decreasing value of W (from 1 to 0.05), each of the two processes y_i and y_i' becomes a mixture of two ARFIMA processes. Particularly, for the process y_i', the DFA correlation exponent λ_{DFA} virtually does not change with varying the parameter $W - \lambda_{DFA} \approx 0.6 = 1/2 + \rho_2$ [46]. In contrast, for the process y_i, the DFA correlation exponent λ_{DFA} gradually decreases from $\lambda_{DFA} \approx 0.9 = 1/2 + \rho_1$ (when $W = 1$, not shown) toward $\lambda_{DFA} \approx 0.6$ (when $W = 1/2$) corresponding to the y_i' process [46].

Next we focus on the DCCA cross-correlation exponent $\lambda_{\rm DCCA}$. We show in Figures 4a, 4b that, by varying the cross-correlation coupling parameter W, $\lambda_{\rm DCCA}$ follows the DFA exponent λ_{DFA} corresponding to the y_i process. By decreasing the value of W from $W = 1$ to $W = 0.5$, both the DFA correlation exponent λ_{DFA} corresponding to the y_i process and the DCCA cross-correlation exponent $\lambda_{\rm DCCA}$ gradually decrease toward $\lambda_{DFA} \approx 0.6$. Generally, for different time series of the process with parameters ρ_1 and ρ_2, where $\rho_1 > \rho_2$, we find that $\lambda_{\rm DCCA}$ is closer to the DFA exponent λ_{DFA} corresponding to the y_i process (larger ρ).

A necessary condition for power-law cross-correlations with a unique power-law exponent is that $F_{\rm DCCA}(n)$

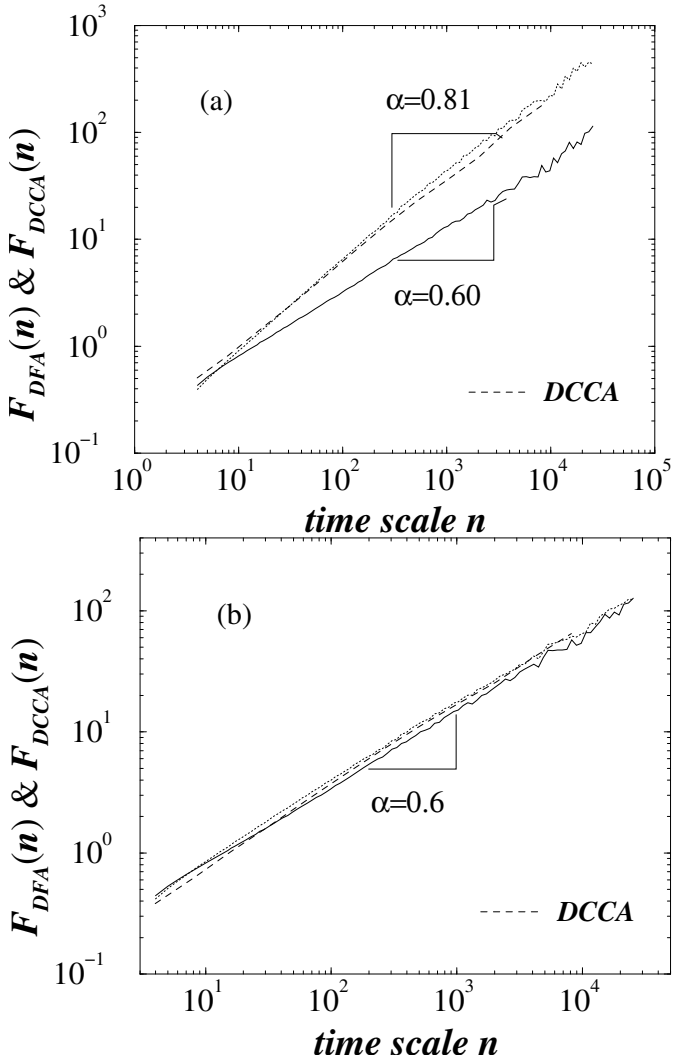

Fig. 4. DFA and DCCA scaling functions $F_{\rm DFA}(n)$ and $F_{\rm DCCA}(n)$, respectively, versus time scale n. We generate the time series $\{y_i\}$ and $\{y_i'\}$ defined by the two-component process of equations (2a, 2b) with $\rho_1 = 0.4$ and $\rho_2 = 0.1$. We exclude the sinusoidal amplitude, so $A_1 = A_2 = 0$. We show the two DFA functions, $F_{\rm DFA}(n) \propto n^{\lambda_{DFA}}$, and the DCCA function, $F_{DCCA}(n) \propto n^{\lambda_{\rm DCCA}}$, for (a) $W = 0.95$ and (b) $W = 0.5$. The closer W is to 0.5, the more the two processes y_i and y_i' become alike. $\lambda_{\rm DCCA}$ gradually decreases toward $\lambda_{DFA} \approx 0.6$. Generally, by varying W, $\lambda_{\rm DCCA}$ becomes closer to λ_{DFA} corresponding to y_i, but eventually the λ_{DFA} value corresponding to y_i tends to the λ_{DFA} value corresponding to y_i'.

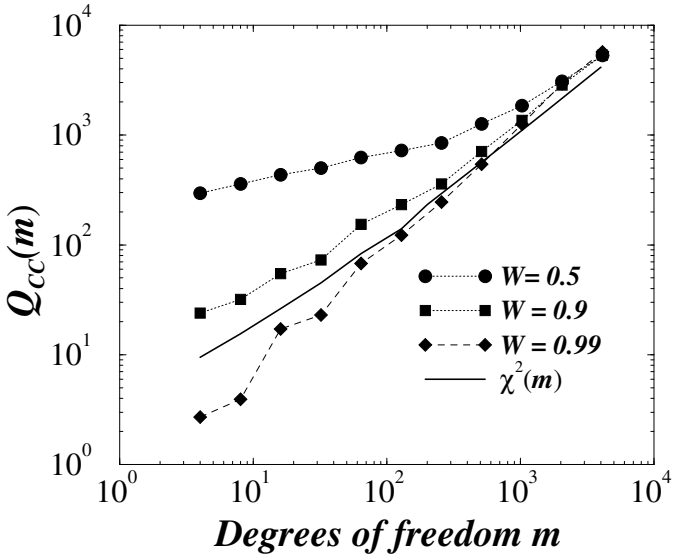

Fig. 5. $Q_{\rm CC}(m)$ versus the number of degrees of freedom m for different values of the cross-correlation coupling W. For each W, we generate one pair of time series $\{y_i\}$ and $\{y_i'\}$ defined by equations (2a, 2b). Each time series is comprised of $N = 10^4$ data points. There is no sinusoidal trend, so $A_1 = A_2 = 0$. We also show the curve of the critical values of $\chi^2(m)$ distribution at the 5% level of significance. Parameters are $\rho_1 = 0.2$ and $\rho_2 = 0.4$. For $W = 0.5$, the cross-correlations between $\{y_i\}$ and $\{y_i'\}$ are strongest and, for a wide range of m values, the curve of the test statistic of equation (6) for $W = 0.5$ is above all other curves including the curve of the critical values of $\chi^2(m)$ distribution. For values of W very close to 1, the cross-correlations between $\{y_i\}$ and $\{y_i'\}$ become very weak, below the curve of the critical values of $\chi^2(m)$ distribution.

does not change sign with increasing n, i.e. $F_{\rm DCCA}(n) = An^{\lambda_{\rm DCCA}}$ where A is constant. To this end, we find that the process of equations (2a, 2b) with $W = 0.99$ generates two particular time series $\{y_i\}$ and $\{y_i'\}$ where $F_{\rm DCCA}(n)$ versus n starts to oscillate, indicating the loss of a unique power-law dependence. Thus, even though there are cross-correlations between $\{y_i\}$ and $\{y_i'\}$, the cross-correlations are weak because the cross-correlations coupling parameter W is close to 1. For the limiting case $W = 1$, the processes y_i and y_i' are decoupled, and thus not cross-correlated, and each of two processes y_i and y_i' becomes a separate ARFIMA process controlled by parameters ρ_1 and ρ_2, respectively.

Next we analyze the cross-correlation tests between time series $\{y_i\}$ and $\{y_i'\}$, with varying W and fixed ρ parameters. We generate three pairs of time series $\{y_i\}$ and $\{y_i'\}$ with parameters $\rho_1 = 0.2$ and $\rho_2 = 0.4$, and varying W. For each pair of time series (10^4 data points each), we perform the test given in equation (6) for different degrees of freedom, m. In Figure 5, the results of the test are plotted versus m, for each pair of time series. We also show the critical values of the $\chi^2(m)$ distribution versus m at the 5% level of significance. Note that for the pairs of time series investigated with W equal to 0.5 and 0.95, the curves of the test statistic are above the curve of the critical values of the $\chi^2(m)$ distribution. Now we find that for a very small cross-correlation coupling parameter ($W = 0.99$), the values of the test of equation (6) are very close to the critical values of the $\chi^2(m)$ distribution. Generally, except for values of W very close to 1, for a broad range of m values, the difference between the value of the test of equation (6) and the corresponding critical value of the $\chi^2(m)$ distribution is *positive* ($Q_{\rm CC}(m) > \chi^2_{0.95}(m)$). If the values of the test of equation (6) calculated between two time series are smaller than the critical values of the $\chi^2(m)$ distribution, $Q_{\rm CC}(m) < \chi^2_{0.95}(m)$,

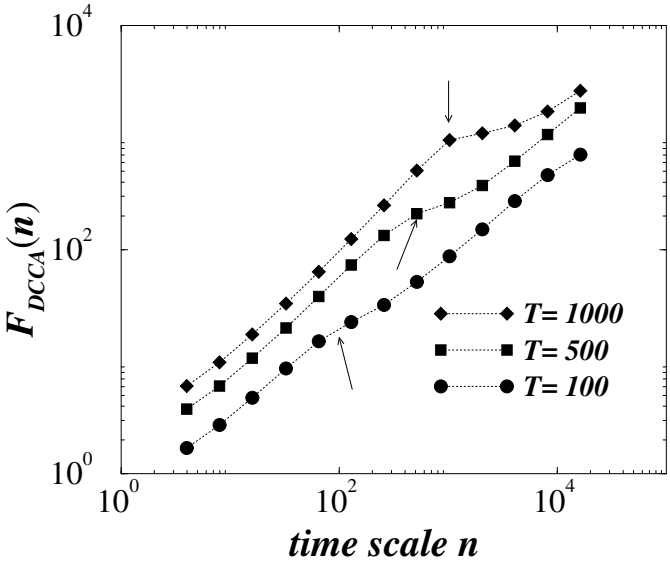

Fig. 6. Crossovers in the detrended cross-correlation analysis function $F_{\mathrm{DCCA}}(n)$, calculated for cross-correlated noise with a sinusoidal trend. The cross-correlated time series $\{y_i\}$ and $\{y_i'\}$ are generated by the periodic two-component ARFIMA process defined by equations (2a, 2b). For $\rho = 0.4$, $W = 0.5$, $A_1 = A_2 = 0.3$, and varying period T, we find a crossover in the $F_{\mathrm{DCCA}}(n)$ function that increases with T approximately as $n_{2\mathrm{CC}} \propto T$.

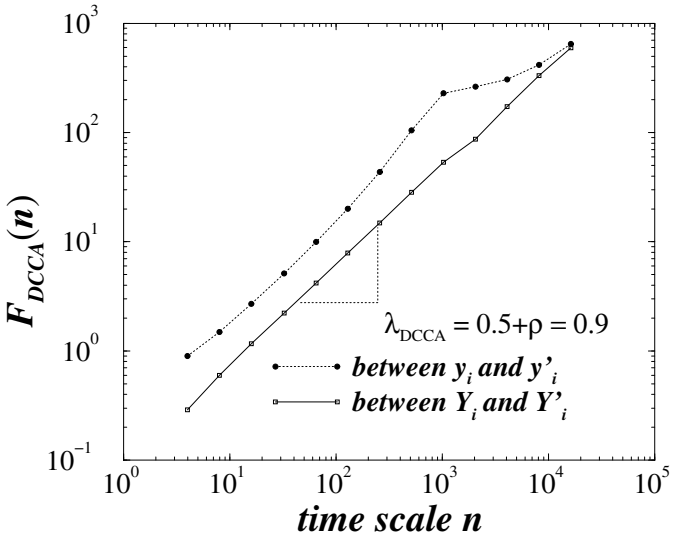

Fig. 7. DCCA function $F_{\mathrm{DCCA}}(n)$ after global and local sinusoidal detrending approaches. We generate two time series $\{y_i\}$ and $\{y_i'\}$ of the periodic two-component ARFIMA process of equations (2a, 2b) with $\rho = \rho_1 = \rho_2 = 0.4$, $W = 0.5$, $A_1 = A_2 = 0.3$, and $T_1 = T_2 = T = 10^3$. We see that $F_{\mathrm{DCCA}}(n)$ of y_i and y_i' exhibit a bump similar to that characteristic for DFA functions obtained for time series with periodic trends. After performing a global minimization of $\sum_{i=1}^{N}(y_i - A_1 \sin(2\pi/Ti + \phi_1))^2$ and $\sum_{i=1}^{N}(y_i' - A_2 \sin(2\pi/Ti + \phi_2))^2$, we find the parameters of the first harmonic (A_i, ϕ_i, T_i) in both time series $\{y_i\}$ and $\{y_i'\}$. Then, we define two new time series, $Y_i = y_i - A_1 \sin(2\pi/Ti + \phi_1)$ and $Y_i' = y_i' - A_2 \sin(2\pi/Ti + \phi_2)$. $\{Y_i\}$ and $\{Y_i'\}$ exhibit a "pure" power-law cross-correlation, with expected power-law exponent $\lambda_{\mathrm{DCCA}} = \lambda_{DFA} = 0.5 + \rho = 0.9$, since both time series are defined by the same ρ parameter.

the cross-correlations between two time series are insignificant.

Next we apply the detrended cross-correlations analysis (DCCA) to investigate cross-correlations between time series where each time series is auto-correlated and sinusoidal. In Figure 6 we present three DCCA functions $F_{\mathrm{DCCA}}(n)$ obtained for three pairs of cross-correlated time series $\{y_i\}$ and $\{y_i'\}$ with sinusoidal trends generated by the process of equations (2a, 2b), with $\rho = 0.4$, $W = 0.5$, $A_1 = A_2 = 0.3$, and varying T. We find from Figure 6 that each DCCA function $F_{\mathrm{DCCA}}(n)$ shows a crossover at time scale $n_{2\mathrm{CC}} \approx T$ similar to the findings for DFA functions [24]. We next study numerically if the relation $n_{2\mathrm{CC}} \approx T$ holds independently of the values of A, W, and ρ. We also find that the crossover bump becomes more pronounced with increasing A, but the crossover time scale $n_{2\mathrm{CC}}$ does not depend on A. We also find that the crossover time scale $n_{2\mathrm{CC}}$ virtually does not depend on ρ.

The correct interpretation of the scaling results is crucial for understanding the system that is analyzed. If the real-world time series is both correlated and periodic, periodicities should be eliminated before analyzing the correlations of the time series. First we generate two cross-correlated time series generated by the process of equations (2a, 2b) with $\rho = 0.4$ when periodicity is present in the time series. For the sake of simplicity, we set $T_1 = T_2 = T = 10^3$. We show the DCCA function $F_{\mathrm{DCCA}}(n)$ in Figure 7, and we find a crossover at scale $n_{2\mathrm{CC}} \propto T$.

Next, we investigate the influence of global detrending on DCCA results. By global fit we assume one fit for the entire time series in contrast to a local detrending approach where local fits are accomplished for windows of different sizes. To eliminate periodicities in the original time series, we globally detrend the periodicity – $\sum_{i=1}^{N}[y_i - A_1 \sin(2\pi/Ti + \phi_1)]^2$ and $\sum_{i=1}^{N}[y_i' - A_2 \sin(2\pi/Ti + \phi_2)]^2$ – and find the parameters $(A_i, \phi_i,$ and $T)$ in both time series $\{y_i\}$ and $\{y_i'\}$. Then, we define the globally detrended time series $Y_i \equiv y_i - A_1 \sin(2\pi/Ti + \phi_1)$, and $Y_i' \equiv y_i' - A_2 \sin(2\pi/Ti + \phi_2)$. We find in Figure 7 that $F_{\mathrm{DCCA}}(n)$ practically loses the bump characteristic at the crossover scale, allowing us to calculate the cross-correlations exponent λ_{DCCA}.

In this paper, we propose a new test to quantify the presence of cross-correlations. We propose that both the cross-correlation test and the detrended cross-correlations analysis (DCCA) should be used together to measure the degree of cross-correlations between different time series. We demonstrate that a good indication for the presence of cross-correlations is if the results of the statistical test of equation (6) exceeds the critical value of the $\chi^2(m)$ distribution at the given level of significance. We study long-range power-law cross-correlations between two time series, each power-law auto-correlated, in the

presence of a periodic sinusoidal trend. We show that due to the sinusoidal trend, a spurious crossover exists in the DCCA cross-correlations plots. We study the impact of a Fourier phase-randomization on the cross-correlation test and show that the cross-correlations between two cross-correlated time series practically vanish by a Fourier phase randomization.

We thank the Ministry of Science of Croatia, NIH, and NSF for financial support.

Appendix A: Analytical cross-correlations derivation

Consider two stationary time series $\{y_j\}$ and $\{y'_j\}$, denote the covariance by $\{X_j\}_{j=-\infty}^{\infty}$, and denote the cross power spectrum by $s_{YY'}(\omega)$. Due to the cross-correlation theorem, sometimes called the Wiener-Khintchine theorem, the cross covariance function and the cross power spectrum are one-to-one related by

$$s_{YY'}(\omega) = \frac{1}{2\pi} \sum_{j=-\infty}^{\infty} X_j \exp(-i\omega j). \tag{A.1}$$

A similar relationship exists for the auto-covariance function and the power spectrum for a single time series.

As an example, let us define two cross-correlated moving average MA(1) processes

$$y_i \equiv (1+\theta_1 L)\eta_i \equiv \Psi(L)\eta_i, \tag{A.2}$$

$$y'_i \equiv (1+\theta_2 L)\eta_i \equiv \tilde{\Psi}(L)\eta_i, \tag{A.3}$$

where η_i is an *(i.i.d.)* process with expectation value $E(\eta) = 0$ and variance $E(\eta^2) - E^2(\eta) = \sigma^2$, and L denotes the backward (lag) operator defined by $L\eta_i = \eta_{i-1}$, i.e., it simply relates two adjacent discrete-time coordinates i and $i-1$. Clearly, $\Psi(L)$ and $\tilde{\Psi}(L)$ are two linear polynomials in L.

For this example, one can easily calculate the only non-vanishing cross-covariances $X_0 \equiv E(y_i y'_i) = E(\eta_i^2 + \theta_1\theta_2\eta_{i-1}^2) = 1 + \theta_1\theta_2$; $X_1 \equiv E(y_i y'_{i+1}) = \theta_2\sigma^2$, and $X_{-1} \equiv E(y_i y'_{i-1}) = \theta_1\sigma^2$. By using equation (A.1) for the power spectrum of two MA(1) processes we obtain $s_{YY'}(\omega) = \frac{\sigma^2}{2\pi}[X_0 + X_1\exp(i\omega) + X_{-1}\exp(-i\omega)]$. If $\exp(i\omega)$ is replaced by the complex number z, we obtain

$$\begin{aligned} s_{YY'}(\omega) &= \frac{1}{2\pi}[X_0 + X_1 z + X_{-1} z^{-1}] \\ &= \frac{1}{2\pi}[1+\theta_2 z][1+\theta_1 z^{-1}]. \end{aligned} \tag{A.4}$$

Using equations (A.2) and (A.3) the previous equation can be expressed as [47]: $s_{YY'}(\omega) = \frac{1}{2\pi}\tilde{\Psi}(z)\Psi(z^{-1})$. This relation for finding $s_{YY'}$ generally extends to the $MA(\infty)$ processes y_i and y'_i, where e.g. $y_i = \Psi(L)\eta_i$ and $\Psi(L) = a_0 + a_1 L + a_2 L^2 + ...$

The ARFIMA process y_i can not only be represented in the AR representation, but also in the $MA(\infty)$ representation:

$$y_i = (1-L)^{-d}\eta_i = \sum_{j=0}^{\infty} \frac{\Gamma(j+\rho)}{\Gamma(\rho)\Gamma(j+1)}\eta_{i-j}, \tag{A.5}$$

where ρ need not be an integer, provided $\rho < 1/2$, where the last expression is obtained after binomial expansion, $E(\eta) = 0$, and $E(\eta^2) - E^2(\eta) = \sigma^2$.

Consider a two-component ARFIMA process $\{y_i\}$ and $\{y'_i\}$ defined $y_i \equiv \sum_{j=1}^{\infty} a_j(\rho_1) y_{i-j} + \eta_i$, $y'_i \equiv \sum_{j=1}^{\infty} a_j(\rho_2) y'_{i-j} + \eta_i$ with parameters ρ_1 and ρ_2. For the cross power spectrum we obtain:

$$\begin{aligned} s_{YY'}(\omega) &= (1-\exp(i\omega))^{-\rho_1}(1-\exp(-i\omega))^{-\rho_2} \\ &= \sum_{k=0}^{\infty}\sum_{k'=0}^{\infty} a_k(\rho_1) a_{k'}(\rho_2)\exp(i(k-k')\omega), \end{aligned} \tag{A.6}$$

where $a_k(\rho) = \Gamma(k+\rho)/[\Gamma(\rho)\Gamma(k+1)]$ as defined in equation (A.5). Taking the inverse Fourier transform of the cross power spectrum, we obtain

$$\begin{aligned} X_n &= \frac{1}{2\pi}\int_{-\pi}^{\pi} s_{XY}(\omega)\exp(i\omega n)d\omega \\ &= \frac{\sigma^2}{2\pi}\frac{1}{2\pi}\sum_{k=0}^{\infty}\sum_{k'=0}^{\infty} a_k(\rho_1)a_{k'}(\rho_2)\int_{-\pi}^{\pi}\exp(i(n+k-k')\omega)d\omega \\ &= \frac{\sigma^2}{2\pi}\sum_{k=0}^{\infty}\sum_{k'=0}^{\infty} a_k(\rho_1)a_{k'}(\rho_2)\delta(n+k-k') \\ &= \frac{\sigma^2}{2\pi}\sum_{k=0}^{\infty} a_k(\rho_1)a_{n+k}(\rho_2). \end{aligned} \tag{A.7}$$

By using Stirling's expansion we obtain $a_k(\rho) \propto k^{\rho-1}$ and thus $X_n \propto \sum_{k=0}^{\infty} k^{\rho_1-1}(n+k)^{\rho_2-1}$, which can be approximated by $X_n \propto \int_0^{\infty} dk\ k^{\rho_1-1}(n+k)^{\rho_2-1}$. By defining a new variable $k/n = t$ we obtain

$$X_n \propto n^{\rho_1+\rho_2-1}\int_0^{\infty} t^{\rho_1-1}(t+1)^{\rho_2-1}dt. \tag{A.8}$$

If long-range power-law cross-correlations exist, we obtain $X_n \propto n^{-\gamma_{CC}}$ for the asymptotic regime $n \gg 1$, i.e., by using equation (A.8) we obtain $\gamma_{CC} = 1 - \rho_1 - \rho_2$. The parameter γ_{CC} and parameter λ_{DCCA} of the covariance growth (see Eq. (1)) are related as $\lambda_{DCCA} = 1 - 0.5\ \gamma_{CC}$ [11]. Hence, we obtain the result of equation (8), $\lambda_{DCCA} = \frac{H_1+H_2}{2}$, where H_1 and H_2 are the Hurst exponents related to the processes $\{y_i\}$ and $\{y'_i\}$, respectively, and where $H_1 = 0.5 + \rho_1$ and $H_2 = 0.5 + \rho_2$ [37]. Hence, we find analytically that the time series y_i and y'_i are long-range power-law cross-correlated (besides being long-range power-law auto-correlated), where the exponent λ_{DCCA} is equal to the arithmetic mean of the two Hurst exponents H and H'.

References

1. M. Campillo, A. Paul, Science **299**, 547 (2003)
2. B. LeBaron, W.B. Arthur, R. Palmer, J. Econ. Dyn. Control **23**, 1487 (1999)
3. R.N. Mantegna, Eur. Phys. J. B **11**, 193 (1999)
4. L. Laloux et al., Phys. Rev. Lett. **83**, 1467 (1999)
5. V. Plerou et al., Phys. Rev. Lett. **83**, 1471 (1999); V. Plerou et al., Phys. Rev. E **66**, 066126 (2002)
6. L. Kullmann, J. Kertesz, K. Kaski, Phys. Rev. E **66**, 026125 (2002)
7. T. Mizunoa, H. Takayasu, M. Takayasu, Physica A **364** 336 (2006)
8. M. Tumminello, T. Aste, T. Di Matteo, R.N. Mantegna, Proceedings of the National Academy of Sciences of the United States of America (PNAS) **102**, 10421 (2005)
9. R. Coelho, S. Hutzler, P. Repetowicz, P. Richmond, Physica A **373**, 615 (2007)
10. B. Podobnik et al., Eur. Phys. J. B **56**, 47 (2007)
11. B. Podobnik, H.E. Stanley, Phys. Rev. Lett. **100**, 084102 (2008)
12. T. Conlon, H.J. Ruskin, M. Crane, Physica A **388** 705 (2009)
13. S. Arianos, A. Carbone, J. Stat. Mech. P03037 (2009)
14. P. Sieczka, J.A. Holyst, Physica A **388**, 1621 (2009)
15. P. Samuelsson et al., Phys. Rev. Lett. **91**, 157002 (2003); A. Cottet et al., Phys. Rev. Lett. **92**, 206801 (2004)
16. H.E. Hurst, Proc. Inst. of Civ. Eng. **1**, 519 (1951)
17. F. Caserta et al., Phys. Rev. Lett. **64**, 95 (1990); D.C. Hong et al., Phys. Rev. B **30**, 4083 (1984)
18. T. Vicsek, *Fractal Growth Phenomenon*, 2nd edn. (World Scientific, Singapore, 1993)
19. *Fractals in Science*, edited by A. Bunde, S. Havlin (Springer, Berlin, 1994)
20. J.B. Bassingthwaighte, L.S. Liebovitch, B.J. West, *Fractal Physiology* (Oxford U. Press, New York, 1994)
21. H. Takayasu, *Fractals in the Physical Sciences* (Manchester U. Press, Manchester, 1997)
22. D. Markovic, M. Koch, Water Resour. Res. **41**, 09420 (2005); D. Markovic, M. Koch, Geophys. Res. Lett. **32**, 17401 (2005)
23. C.-K. Peng et al., Phys. Rev. E **49**, 1685 (1994)
24. K. Hu et al., Phys. Rev. E **64**, 011114 (2001)
25. Z. Chen et al., Phys. Rev. E **65**, 041107 (2002)
26. Z. Chen et al., Phys. Rev. E **71**, 011104 (2005)
27. L. Xu et al., Phys. Rev. E **71**, 051101 (2005)
28. P.Ch. Ivanov et al., Chaos **11**, 641 (2001)
29. Y. Liu et al., Physica A **245**, 437 (1997); Y. Liu et al., Phys. Rev. E **60**, 1390 (1999); P. Cizeau, Phys. Rev. E **245**, 441 (1997); P.Ch. Ivanov et al., Phys. Rev. E **69**, 056107 (2004)
30. S. Buldyrev et al., Biophys. J. **65**, 2673 (1993); S. Buldyrev et al., Phys. Rev. E **47**, 4514 (1993)
31. K. Ivanova, M. Ausloos, Physica A **274**, 349 (1999); K. Ivanova, J. Geophys. Res. **108**, 4268 (2003)
32. Z. Chen et al., Phys. Rev. E **73**, 031915 (2006)
33. C.W.J. Granger, J. Econometrics **14**, 227 (1980)
34. C.W.J. Granger, R. Joyeux, J. Time Series Analysis **1**, 15 (1980)
35. J. Hosking, Biometrika **68**, 165 (1981)
36. B. Podobnik et al., Phys. Rev. E **71**, 025104(R) (2005)
37. B. Podobnik et al., Phys. Rev. E **72**, 026121 (2005)
38. R.H. Shumway, D.S. Stoffer, *Time Series Analysis anf Its Applications*, Springer Texts in Statistics (Springer-Verlag, New York, 2000)
39. R.L. Anderson, Annals Math. Statistics **13**, 1 (1942)
40. G.E.P. Box, G.M. Jenkins, G.C. Reinsel, *Time Series Analysis: Forecasting and Control* (Prentice Hall, New Jersey, 1994)
41. G.M. Ljung, G.E.P. Box, Biometrika **65**, 297 (1978)
42. H. Tastan, Physica A **360**, 445 (2006); K.M. Wang, T.B.N. Thi, Physica A **376**, 422 (2007); M.C. Lee, C.L. Chiu, Y.H. Lee, Physica A **377**, 199 (2007); A. Kasman, S. Kasman, Physica A **387**, 2837 (2008); C.H. Tseng, S.T. Cheng, Y.H. Wang, J.T. Peng, Physica A **387**, 3192 (2008)
43. www.yahoo.finance
44. J. Theiler et al., Physica D **58**, 77 (1992)
45. P.Ch. Ivanov et al., Nature **383**, 323 (1996)
46. B. Podobnik et al., Physica A **387**, 3954 (2008)
47. W.W.S. Wei, *Time Series Analysis Univariate and Multivariate Methods* (Addison-Wesley, Prentice Hall, 2006)

Quantifying cross-correlations using local and global detrending approaches

By: Podobnik, B (Podobnik, B.)[1,2,3,4]; Grosse, I (Grosse, I.)[5]; Horvatic, D (Horvatic, D.)[6]; Ilic, S (Ilic, S.)[7]; Ivanov, PC (Ivanov, P. Ch.)[3,4,8,9,10]; Stanley, HE (Stanley, H. E.)[3,4]

View ResearcherID and ORCID

EUROPEAN PHYSICAL JOURNAL B
Volume: 71 **Issue:** 2 **Pages:** 243-250
DOI: 10.1140/epjb/e2009-00310-5
Published: SEP 2009
Document Type: Article
View Journal Impact

Abstract

In order to quantify the long-range cross-correlations between two time series qualitatively, we introduce a new cross-correlations test Q(CC)(m), where m is the number of degrees of freedom. If there are no cross-correlations between two time series, the cross-correlation test agrees well with the X-2(m) distribution. If the cross-correlations test exceeds the critical value of the X-2 (m) distribution, then we say that the cross-correlations are significant. We show that if a Fourier phase-randomization procedure is carried out on a power-law cross-correlated time series, the cross-correlations test is substantially reduced compared to the case before Fourier phase randomization. We also study the effect of periodic trends on systems with power-law cross-correlations. We find that periodic trends can severely affect the quantitative analysis of long-range correlations, leading to crossovers and other spurious deviations from power laws, implying both local and global detrending approaches should be applied to properly uncover long-range power-law auto-correlations and cross-correlations in the random part of the underlying stochastic process.

Keywords

KeyWords Plus: TIME-SERIES; FLUCTUATION ANALYSIS; STOCK-MARKET; VOLATILITY; INDEX; DYNAMICS; BEHAVIOR; FUTURES; SIGNALS; TAIWAN

Author Information

Reprint Address: Podobnik, B (reprint author)

+ Univ Rijeka, Fac Civil Engn, Rijeka, Croatia.

Addresses:

+ [1] Univ Rijeka, Fac Civil Engn, Rijeka, Croatia
[2] Zagreb Sch Econ & Management, Zagreb, Croatia
+ [3] Boston Univ, Ctr Polymer Studies, Boston, MA 02215 USA
+ [4] Boston Univ, Dept Phys, Boston, MA 02215 USA
+ [5] Univ Halle Wittenberg, Inst Comp Sci, Halle, Germany
+ [6] Univ Zagreb, Fac Sci, Dept Phys, Zagreb 10000, Croatia
+ [7] Univ Lancaster, Lancaster Environm Ctr, Lancaster LA1 4YQ, England
+ [8] Bulgarian Acad Sci, Inst Solid State Phys, BU-1784 Sofia, Bulgaria
+ [9] Harvard Univ, Sch Med, Boston, MA 02115 USA

[10] Brigham & Womens Hosp, Div Sleep Med, Boston, MA 02115 USA

E-mail Addresses: bp@phy.hr

Suggest a correction

If you would like to improve the quality of the data in this record, please suggest a correction.

Publisher

SPRINGER, 233 SPRING ST, NEW YORK, NY 10013 USA

Journal Information

Performance Trends: Essential Science Indicators

Impact Factor: Journal Citation Reports

Categories / Classification

Research Areas: Physics

Web of Science Categories: Physics, Condensed Matter

See more data fields

Cited References: 56

Showing 30 of 56 **View All in Cited References page** *(from Web of Science Core Collection)*

1. **Distribution of the serial correlation coefficient** **Times Cited: 224**
By: Anderson, RL
ANNALS OF MATHEMATICAL STATISTICS Volume: 13 Pages: 1-13 Published: 1942

2. **Cross-correlation of long-range correlated series** **Times Cited: 82**
By: Arianos, Sergio; Carbone, Anna
JOURNAL OF STATISTICAL MECHANICS-THEORY AND EXPERIMENT Article Number: P03037 Published: MAR 2009

3. Title: [not available] **Times Cited: 328**
By: Bassingthwaighte, JB; Liebovitch, LS; West, BJ.
Fractal Physiology Published: 1994
Publisher: Oxford Univ Press, New York, NY

4. Title: [not available] **Times Cited: 2,218**
By: Box, G. E. P.; Jenkins, G. M.; Reinsel, G. C.
TIME SERIES ANAL FOR Published: 1994
Publisher: Prentice Hall, Englewood Cliffs

5. **FRACTAL LANDSCAPES AND MOLECULAR EVOLUTION - MODELING THE MYOSIN HEAVY-CHAIN GENE FAMILY** **Times Cited: 112**
By: BULDYREV, SV; GOLDBERGER, AL; HAVLIN, S; et al.
BIOPHYSICAL JOURNAL Volume: 65 Issue: 6 Pages: 2673-2679 Published: DEC 1993

6. **Fractals in science** **Times Cited: 260**
By: Bunde, A.
Fractals in Science Published: 1994
Publisher: Springer

7. **Long-range correlations in the diffuse seismic coda** **Times Cited: 647**
By: Campillo, M; Paul, A
SCIENCE Volume: 299 Issue: 5606 Pages: 547-549 Published: JAN 24 2003

Spiral wave annihilation by low-frequency planar fronts in a model of excitable media

2009 EPL 86 18005

(http://iopscience.iop.org/0295-5075/86/1/18005)

epl A Letters Journal Exploring the Frontiers of Physics

April 2009

EPL, **86** (2009) 18005 www.epljournal.org
doi: 10.1209/0295-5075/86/18005

Spiral wave annihilation by low-frequency planar fronts in a model of excitable media

Miguel A. de la Casa[1], F. Javier de la Rubia[1] and Plamen Ch. Ivanov[2,3,4(a)]

[1] *Departamento de Física Fundamental, Universidad Nacional de Educación a Distancia c/Senda del Rey 9, 28080 Madrid, Spain, EU*
[2] *Department of Sleep Medicine, Harvard Medical School and Brigham and Women's Hospital Boston, MA 02115, USA*
[3] *Center for Polymer Studies and Department of Physics, Boston University - Boston, MA 02215, USA*
[4] *Institute of Solid State Physics, Bulgarian Academy of Sciences - 1784 Sofia, Bulgaria, EU*

received 25 November 2008; accepted in final form 12 March 2009
published online 20 April 2009

PACS 87.19.Hh – Cardiac dynamics
PACS 87.85.Tu – Modeling biomedical systems
PACS 89.75.Kd – Patterns

Abstract – We perform numerical lattice simulations of an excitable medium. We show that the interaction of a spiral wave with a periodic train of planar fronts leads to annihilation of the spiral wave even when i) the period of the fronts is longer than the period of the spiral and ii) the annihilating fronts are released at a significant distance from the spiral. The observed annihilation is not due to spiral drift, and occurs well inside the lattice.

The dynamics of wave propagation in excitable media has been extensively studied in the last years [1–15] and the existence of spiral waves in this kind of system has been reported in many cases, including aggregating slime-mould cells [16], retinae [17], the Belousov-Zhabotinsky chemical oscillator [18], CO oxidation [19], and heart muscle [20,21]. Of special interest, in areas like cardiology, is the study of wavefront stability, as wave breaks generate spatio-temporal patterns that are associated with potentially fatal arrhythmias [1–3,22–32]. Therefore, it is of great interest to find out how to attenuate and annihilate spiral waves.

Here, we investigate the possibility of annihilating spiral waves by a train of periodic plain waves, which is of relevance to the dynamics in the myocardium, where fronts descending from the heart pacemaker (the sinoatrial node) interact with spiral waves. It is widely assumed that stable spiral waves cannot be eliminated by wavefronts of similar or lower frequency, since the domains of faster spiral waves grow at the expense of the slower wavefronts [31,33–37]. In this study, we consider the interaction of a stable spiral wave and planar wavefronts with frequency lower than the frequency of the spiral rotation and we show that this interaction leads to annihilation of the spiral wave over a range of physiologically meaningful parameter values.

(a) E-mail: plamen@buphy.bu.edu

It has been reported recently [38,39] that the interaction of a single spiral wave with a train of periodic planar fronts can lead, under certain circumstances, *i.e.*, when the fronts have long excitation duration, and are delivered at a specific phase relative to the rotational phase of the spiral, to the formation of complex spatio-temporal patterns characterized by the presence of periodic attenuation of the spiral wave. Since the results reported in [38,39] are based on a cellular automaton model, it is natural to raise the question of the validity of those findings for continuous models based on partial differential equations.

To perform our analysis we choose the Aliev-Panfilov model of the cardiac tissue [40]. This is a modification of the classical Fitzhugh-Nagumo model aimed at introducing the experimentally observed restitution curve, which the original model lacks [41–45]. As we will explain later, this feature is crucial for the annihilation of the spiral wave. The model equations are

$$\frac{\partial u}{\partial t} = \frac{\partial}{\partial x_i} d_{ij} \frac{\partial u}{\partial x_j} - ku(u-a)(u-1) - uv, \qquad (1)$$

$$\frac{\partial v}{\partial t} = \epsilon(u,v)\left[-v - ku(u-a-1)\right], \qquad (2)$$

where u is the transmembrane potential, v is the recovery variable (related to the conductance of the cell membrane), $\epsilon(u,v) = \epsilon_0 + \mu_1 v/(u+\mu_2)$ and the typical parameter

Fig. 1: (Color online) Evolution of the system during the first spiral rotation. The color-coding shows the gradient of variable u in eq. (1) (the transmembrane potential) from high values, in violet-blue, corresponding to excited areas, to low values, in yellow-orange, corresponding to resting areas. From left to right and top to bottom: initial condition; collision with first front, at $t = 3$; and eight other snapshots, each one after every three time units. The parameter values used are: $k = 8$, $a = 0.02$, $\epsilon_0 = 0.4$, $\mu_1 = 0.35$, $\mu_2 = 0.5$. For these parameter values, the model simulations generate a stable spiral with a period $T_{\rm sp} = 55$. The value chosen for the period of the fronts is $T = 59$.

values are $k = 8$, $a = 0.02$, $\epsilon_0 = 0.4$, $\mu_1 = 0.35$, and $\mu_2 = 0.5$. Here, k is related to the upstroke of u when the excitation occurs, a represents the excitation threshold, and $\epsilon(u, v)$ relates to the difference between the characteristic time scales of u and v. We consider a homogeneous isotropic medium with a diffusion coefficient $d_{ij} = 1$.

We use a 128×128 two-dimensional square lattice with the usual no-flux boundary conditions, by means of a standard multigrid scheme. The space and time integration steps we have used are $\delta x = 0.3$ and $\delta t = 0.1$, respectively. The model involves dimensionless variables, u, v, and t, related to the actual transmembrane potential and time by means of the formulae: $E\,(\mathrm{mV}) = 100u - 80$ (the equilibrium potential is set at $-80\,\mathrm{mV}$ and the pulse jump is $100\,\mathrm{mV}$ since the natural upper bound for u is $u = 1$) and $t(\mathrm{ms}) = 12.9t(\mathrm{t.u.})$ [40]. Assuming a propagation speed of $75\,\mathrm{cm/s}$, in agreement with the experimental results in myocardial cells of guinea pigs [13], the lattice size in our simulations corresponds to $0.6\,\mathrm{cm}$.

We generate the spiral according to a standard procedure, by propagating a planar front with one end close to the center of the lattice and the other end on the lattice boundary [46]. We wait for ≈ 15 spiral rotations until the spiral reaches a stable rotation. We next introduce planar fronts with a period T, starting from the boundary of the lattice. The fronts are introduced by setting $u = 1.0$ (the highest transmembrane potential) and $v = 0.0$ (no refractoriness) for all elements on the right boundary of the lattice; this initial condition for the fronts gives rise to long excitation durations, which plays an instrumental role to achieve spiral annihilation. We have explored periods T in the range 45–65, while the period of the spiral wave is $T_{\rm sp} = 55$ for the parameter values given above.

Once a single, stable spiral wave is generated (see fig. 1, snapshot 1) and the rotational period of the spiral stabilizes, we introduce a periodic train of planar fronts that propagate from right to left. The parameter values used for the simulation shown in fig. 1 are: $k = 8$, $a = 0.02$, $\epsilon_0 = 0.4$, $\mu_1 = 0.35$, and $\mu_2 = 0.5$. Figure 1 shows the interaction of the spiral wave and the first front of the train during the first spiral rotation. The first snapshot shows the initial condition, at $t = 0$. Then, the first front is introduced at the right-hand-side boundary of the lattice at $t = 1$ (fig. 1, snapshot 2). Every subsequent snapshot in fig. 1 is taken every 3 time units. Figure 2 shows the interaction of the spiral wave with the second and third fronts, and partially, in the last snapshot, with the fourth one. The first snapshot in fig. 2 corresponds to $t = 67$, and every following snapshot is taken after 13 time units. In agreement with the results found in [38,39], where a cellular automaton was used, we find that subsequent incoming fronts progressively invade the spiral wave domain successfully both along the advancing contour of the spiral and further away from the spiral tip, near the upper right corner of the lattice. However, in contrast with our previous analysis, it is the invasion near the lattice boundary and away from the spiral tip, and not the invasion along the spiral edge, which is successful in altering the spiral dynamics. While the invasion process is not self-evident in the figure, every subsequent front advances a little more than the previous one, in turn creating the conditions for the advance of the next one. The invasion process can also be tracked by the movement of the spiral tip which is progressively kept further and further away from the fronts. Finally, during the interaction with the fourth front (fig. 3), a second counter-rotating spiral develops and both spiral waves collide and annihilate each other. The first snapshot in fig. 3 corresponds to $t = 193$, and every following snapshot is taken after 13 time units. The remaining excited area in the upper left corner of the last but one snapshot

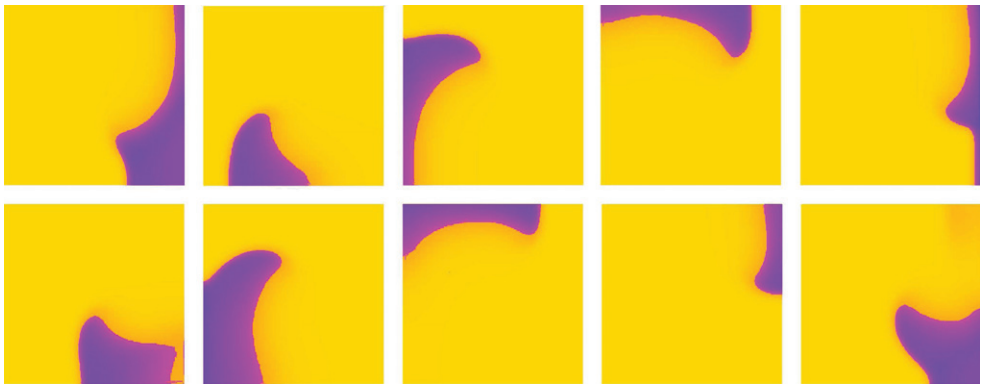

Fig. 2: (Color online) Invasion process. Color-coding and parameter values are as in fig. 1. These snapshots show how the same simulation as in fig. 1 continues. The three first fronts reach the spiral domain and progressively invade the region. The first snapshot was taken at $t = 67$ and every subsequent snapshot was taken after $\Delta t = 13$.

Fig. 3: (Color online) Spiral annihilation. Color-coding and parameter values are as in fig. 1. The fourth subsequent front invades the spiral domain deep enough to achieve the annihilation of the spiral waves. Again, the figure shows the same simulation as in figs. 1 and 2. The three first fronts reach the spiral domain and progressively invade the region. The first snapshot was taken at $t = 193$ and every subsequent snapshot was taken after $\Delta t = 9$. The last snapshot corresponds to $t = 274$. Our simulations show that, within the range of model parameters where spiral annihilation is found, releasing a single planar front at the same specific phase relative to the rotational phase of the spiral as in snapshot 6 does not lead to spiral attenuation. Thus, a train of several fronts (4–6 fronts) is needed to create the necessary preconditions leading to the spiral annihilation observed in snapshot 10. We note that the number of fronts in the train needed to annihilate the spiral does not depend on the timing of the release of the first front relative to the rotational phase of the spiral.

develops into a continuous front that does not form new spiral waves. After the last snapshot, the activity entirely disappears, and the resting state of the whole lattice is only altered by new fronts, if they are introduced. The last snapshot in fig. 3 corresponds to $t = 274$. We note that the process of spiral annihilation (shown in snapshots 6–10 in fig. 3) occurs while the spiral tip is close to the center of the lattice, and that the spiral annihilation is not due to spiral drift to the lattice boundary. Our simulations show that within the whole range of model parameters where spiral annihilation is observed, the distance between the last released front, which leads to spiral annihilation, and the spiral tip is of the order of one spiral wavelength (as shown in snapshot 6 in fig. 3 for a given choice of model parameters). Our observations of a relatively large distance between the annihilating front and the spiral are complementary to earlier studies where spiral annihilation was achieved by point stimuli released at a distance to the spiral much shorter than a wavelength [47].

In order to further survey the annihilation process, in fig. 4 we plot the total number of excited cells in the lattice as a function of time for three different values of the period of the planar fronts, two of them higher and the other one lower than the spiral period. For this purpose, we have defined a lattice element as excited when $u > 0.1$ and, simultaneously, $v < 1.0$. The curves follow a quasiperiodic behavior until the annihilation of the spiral wave occurs for the two cases of higher period than the spiral. After the annihilation the number of excited cells drops to zero, as expected.

To check the robustness of the annihilation process we have considered different parameter sets: $k = 8$, $a = 0.01$, $\epsilon_0 = 0.5$, $\mu_1 = 0.35$, $\mu_2 = 0.5$; $k = 8$, $a = 0.02$, $\epsilon_0 = 0.4$, $\mu_1 = 0.35$, $\mu_2 = 0.5$; $k = 8$, $a = 0.04$, $\epsilon_0 = 0.1$, $\mu_1 = 0.3$,

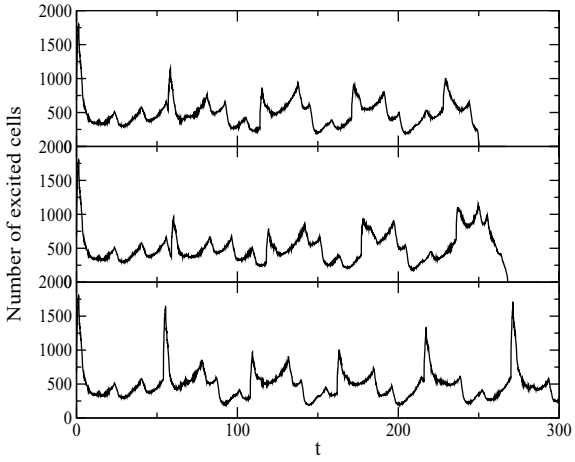

Fig. 4: Total number of excited cells in the lattice as a function of time (in dimensionless units) for three different simulation runs with, from top to bottom, $T = 57$, $T = 59$ and $T = 54$. The parameter values used are the same as in fig. 1, which implies $T_{\rm sp} = 55$. The plots clearly show that only when $T > T_{\rm sp}$ the annihilation process takes place as the number of excited cells goes to zero.

$\mu_2 = 0.4$; $k = 8$, $a = 0.08$, $\epsilon_0 = 0.07$, $\mu_1 = 0.25$, $\mu_2 = 0.35$; $k = 8$, $a = 0.10$, $\epsilon_0 = 0.05$, $\mu_1 = 0.2$, $\mu_2 = 0.3$; and $k = 8$, $a = 0.15$, $\epsilon_0 = 0.002$, $\mu_1 = 0.2$, $\mu_2 = 0.3$. The annihilation process occurs only for values of the excitation threshold parameter $a < 0.04$, and for decreasing values of a (low excitation threshold) the conditions for spiral annihilation become more favorable. Therefore, within the considered low-excitability regime (where spirals are stable), the more excitable the medium is, the easier it is to achieve spiral annihilation. We emphasize that an advantage of our model approach is that, for a broad range of parameter values, spiral annihilation is achieved even when the period of the planar fronts is longer (by 1–4 dimensionless time units or approximately 10–50 ms than the period of the spiral. We note that traditionally spiral attenuation has been achieved with periods shorter than the period of the spiral.

The long excitation duration in the fronts allows every front to leave a lasting mark of refractory area (an area that cannot be excited until the refractory time has elapsed) that outlasts the rotational period of the spiral and, therefore, affects the spiral during the next spiral rotation. The effect of this refractory area is to prevent to some extent the propagation of the spiral wave, but it is very small in the case of the first incoming front. The longer period of the fronts, compared to the rotational period of the spiral, implies that this effect is stronger with every subsequent front. The Fitzhugh-Nagumo model is unable to take into account this kind of interaction between the spiral and the fronts, since it features no significant restitution curve (all excitations have essentially the same duration); therefore, it is critical to introduce a more complex model, as in eqs. (1) and (2), where an empirically realistic restitution curve is introduced in a natural way.

We have also investigated how the front-spiral interaction depends on the relative phase between the spiral and the fronts, since it has been reported that i) the rotational phase of the spiral wave, when the first front is released, may play a critical role in the dynamics as ii) certain spatio-temporal patterns appear only for specific values of this phase [38,39]. To answer this question, we performed several tests by releasing the first front at a time T_0 after the stabilization of the period of the spiral, followed by a train of fronts with period T. We repeated the simulations for different values of T_0 and for different parameter sets. We find that the relative phase between the first released front and the spiral does not appear to play a significant role in achieving spiral annihilation in these continuous model simulations at least for the set of parameter values used in this work.

In summary, we have found that the interaction of a single, stable spiral wave with a periodic train of planar fronts, with period longer than the rotational period of the spiral and of sufficiently long excitation duration can lead, not only to spiral attenuation (as reported in [38,39]), but also to the complete annihilation of the spiral wave. After collision with as few as 4–6 fronts, the spiral domain is invaded by the fronts and the spiral is annihilated. Thus, the domain of the lower frequency planar waves expands at the expense of the spiral wave until it completely vanishes. This occurs only when the period of the fronts is slightly longer, by 1–4 time units, than the period of the spiral waves. Notably, the annihilation process is not due to spiral drift outside of the lattice boundary, and results from the front-spiral interaction which occurs well within the spatial domain of the lattice.

* * *

This work is financially supported by the Ministerio de Educación y Ciencia (Spain), Project No. FIS2005-01729.

REFERENCES

[1] Gray R. A., Jalife J., Panfilov A. V., Baxter W. T., Cabo C., Davidenko J. M. and Pertsov A. M., *Science*, **270** (1995) 1222.
[2] Witkowski F. X., Leon L. J., Penkoske P. A., Giles W. R., Spano M. L., Ditto W. L. and Winfree A. T., *Nature*, **392** (1998) 78.
[3] Hastings H.M. *et al.*, *Proc. Natl. Acad Sci. U.S.A.*, **93** (1996) 10495.
[4] Moss F., *Nature*, **391** (1998) 743.
[5] Kadar S., Wang J. C. and Showalter K., *Nature*, **391** (1998) 770.
[6] Nash M. P and Panfilov A. V., *Prog. Biophys. Mol. Biol.*, **85** (2004) 501.
[7] Steinbock O., Zykov V. and Müller S. C., *Nature*, **366** (1993) 322.
[8] Sharma V., Susil L. and Tung R., *Biophys. J.*, **88** (2005) 3038.

[9] Johnson L. R. (Editor), *Essential Medical Physiology* (Lippincott-Raven, Philadelphia) 1998.
[10] Fast V. G., Efimov I. R. and Krinsky V. I., *Phys. Lett. A*, **151** (1990) 157.
[11] Panfilov A. V. and Holden A. V., *Phys. Lett. A*, **151** (1990) 23.
[12] Zykov V. S., *Modeling of Wave Processes in Excitable Media* (Manchester University Press, Manchester) 1988.
[13] Girouard S. D., Pastore J. M., Laurita K. R., Gregory K. W. and Rosenbaum D. S., *Circulation*, **93** (1996) 603.
[14] Starobin J. M. and Starmer C. F., *Phys. Rev. E*, **54** (1996) 430.
[15] Karma A. and Fenton F., *Chaos*, **8** (1998) 20.
[16] Siegert F. and Weijer C. J., *J. Cell Sci.*, **93** (1989) 325.
[17] Gorelova N. A. and Bures J., *J. Neurobiol.*, **14** (1983) 353.
[18] Winfree A. T., *Science*, **175** (1972) 634.
[19] Jakubith S., Rotermund H. H., Engel W., von Oertzen A. and Ertl G., *Phys. Rev. Lett.*, **65** (1990) 3013.
[20] Courtemanche M. and Winfree A. T., *Int. J. Bifurcat. Chaos*, **1** (1990) 431.
[21] Davidenko J. M., Pertsov A. M., Solomonsz R. and Jalife J., *Nature*, **355** (1992) 349.
[22] Karma A., *Phys. Rev. Lett.*, **71** (1993) 1103.
[23] Bär M. and Eiswirth M., *Phys. Rev. E*, **48** (1993) R1635.
[24] Marée A. F. M. and Panfilov A. V., *Phys. Rev. Lett.*, **78** (1997) 1819.
[25] Biktashev V. N., Holden A. V., Tsyganov M. A., Brindley J. and Hill N. A., *Phys. Rev. Lett.*, **81** (1998) 2815.
[26] Bär M. and Or-Guil M., *Phys. Rev. Lett.*, **82** (1999) 1160.
[27] García-Ojalvo J. and Scimansky-Geier L., *Europhys. Lett.*, **47** (1999) 298.
[28] Winfree A. T., *The Geometry of Biological Time* (Springer-Verlag, New York) 2001.
[29] Schutze J., Steinbock O. and Muller S. C., *Nature*, **356** (1992) 45.
[30] Sawai S., Thomason P. A. and Cox E. C., *Nature*, **433** (2005) 323.
[31] Winfree A. T., *When Time Breaks Down* (Princeton University Press, Princeton) 1987.
[32] Ditto W. L., Spano M. L., In V., Neff J. and Meadows B., *Int. J. Bifurcat. Chaos*, **10** (2000) 593.
[33] Stamp A. T., Osipov G. V. and Collins J. J., *Chaos*, **12** (2002) 931.
[34] Zaikin A. N. and Zhabotinsky A. M., *Nature*, **225** (1970) 535.
[35] Aranson I., Levine H. and Tsimring L., *Phys. Rev. Lett.*, **76** (1996) 1170.
[36] Lee K. J., *Phys. Rev. Lett.*, **79** (1997) 2907.
[37] Xie F., Qu Z., Weiss J. N. and Garfinkel A., *Phys. Rev. E*, **59** (1999) 2203.
[38] de la Casa M. A., de la Rubia F. J. and Ivanov P. Ch., *Phys. Rev. E*, **75** (2007) 051923.
[39] de la Casa M. A., de la Rubia F. J. and Ivanov P. Ch., *Chaos*, **17** (2007) 015109.
[40] Aliev R. R. and Panfilov A. V., *Chaos, Solitons Fractals*, **7** (1996) 293.
[41] Sakaguchi H. and Fujimoto T., *Phys. Rev. E*, **67** (2003) 067202.
[42] Panfilov A. V., *Phys. Rev. Lett.*, **88** (2002) 118101.
[43] Aliev R. R. and Panfilov A. V., *J. Theor. Biol.*, **181** (1996) 33.
[44] ten Tussher K. H. W. J. and Panfilov A. V., *Phys. Rev. E*, **68** (2003) 062902.
[45] Panfilov A. V., *Phys. Rev. E*, **59** (1999) R6251.
[46] Biktashev V. N. and Holden A. V., *Chaos*, **8** (1998) 48.
[47] Krinsky V. I., Pertsov A. M. and Biktashev V. N., *Ann. N. Y. Acad. Sci.*, **591** (1990) 232.

Spiral wave annihilation by low-frequency planar fronts in a model of excitable media

By: de la Casa, MA (de la Casa, Miguel A.)[1]; de la Rubia, FJ (de la Rubia, F. Javier)[1]; Ivanov, PC (Ivanov, Plamen Ch.)[2,3,4,5,6]

View ResearcherID and ORCID

EPL
Volume: 86 **Issue:** 1
Article Number: 18005
DOI: 10.1209/0295-5075/86/18005
Published: APR 2009
Document Type: Article
View Journal Impact

Abstract

We perform numerical lattice simulations of an excitable medium. We show that the interaction of a spiral wave with a periodic train of planar fronts leads to annihilation of the spiral wave even when i) the period of the fronts is longer than the period of the spiral and ii) the annihilating fronts are released at a significant distance from the spiral. The observed annihilation is not due to spiral drift, and occurs well inside the lattice. Copyright (C) EPLA, 2009

Keywords

KeyWords Plus: CARDIAC TISSUE; VENTRICULAR-FIBRILLATION; DYNAMICS; EXCITATION; BREAKUP; PROPAGATION; TURBULENCE; VORTEX; ORGANIZATION; ARRHYTHMIAS

Author Information

Reprint Address: de la Casa, MA (reprint author)

+ Univ Nacl Educ Distancia, Dept Fis Fundamental, C Senda Rey 9, E-28080 Madrid, Spain.

Addresses:

+ [1] Univ Nacl Educ Distancia, Dept Fis Fundamental, E-28080 Madrid, Spain
+ [2] Brigham & Womens Hosp, Boston, MA 02115 USA
+ [3] Harvard Univ, Sch Med, Dept Sleep Med, Boston, MA 02115 USA
+ [4] Boston Univ, Dept Phys, Boston, MA 02215 USA
+ [5] Boston Univ, Ctr Polymer Studies, Boston, MA 02215 USA
+ [6] Bulgarian Acad Sci, Inst Solid State Phys, BU-1784 Sofia, Bulgaria

E-mail Addresses: plamen@buphy.bu.edu

Funding

Funding Agency	Grant Number
Ministerio de Educacion y Ciencia (Spain)	FIS2005-01729

View funding text

Publisher

EPL ASSOCIATION, EUROPEAN PHYSICAL SOCIETY, 6 RUE DES FRERES LUMIERE, MULHOUSE, 68200, FRANCE

If you would like to improve the quality of the data in this record, please suggest a correction.

Journal Information

Impact Factor: Journal Citation Reports

Categories / Classification

Research Areas: Physics

Web of Science Categories: Physics, Multidisciplinary

See more data fields

90 of 127

Cited References: 47

Showing 30 of 47 **View All in Cited References page** *(from Web of Science Core Collection)*

1. **A simple two-variable model of cardiac excitation** — **Times Cited: 332**
   By: Aliev, RR; Panfilov, AV
   CHAOS SOLITONS & FRACTALS Volume: 7 Issue: 3 Pages: 293-301 Published: MAR 1996

2. **Modeling of heart excitation patterns caused by a local inhomogeneity** — **Times Cited: 28**
   By: Aliev, RR; Panfilov, AV
   JOURNAL OF THEORETICAL BIOLOGY Volume: 181 Issue: 1 Pages: 33-40 Published: JUL 7 1996

3. **Spiral competition in three-component excitable media** — **Times Cited: 44**
   By: Aranson, I; Levine, H; Tsimring, L
   PHYSICAL REVIEW LETTERS Volume: 76 Issue: 7 Pages: 1170-1173 Published: FEB 12 1996

4. **TURBULENCE DUE TO SPIRAL BREAKUP IN A CONTINUOUS EXCITABLE MEDIUM** — **Times Cited: 255**
   By: BAR, M; EISWIRTH, M
   PHYSICAL REVIEW E Volume: 48 Issue: 3 Pages: R1635-R1637 Published: SEP 1993

5. **Alternative scenarios of spiral breakup in a reaction-diffusion model with excitable and oscillatory dynamics** — **Times Cited: 67**
   By: Bar, M; Or-Guil, M
   PHYSICAL REVIEW LETTERS Volume: 82 Issue: 6 Pages: 1160-1163 Published: FEB 8 1999

6. **Reentrant waves and their elimination in a model of mammalian ventricular tissue** — **Times Cited: 90**
   By: Biktashev, VN; Holden, AV
   CHAOS Volume: 8 Issue: 1 Pages: 48-56 Published: MAR 1998

7. **Excitation wave breaking in excitable media with linear shear flow** — **Times Cited: 31**
   By: Biktashev, VN; Holden, AV; Tsyganov, MA; et al.
   PHYSICAL REVIEW LETTERS Volume: 81 Issue: 13 Pages: 2815-2818 Published: SEP 28 1998

8. Title: [not available] — **Times Cited: 1**
   By: COURTEMANCHE M
   CHAOS Volume: 1 Pages: 431 Published: 1990

9. **STATIONARY AND DRIFTING SPIRAL WAVES OF EXCITATION IN ISOLATED CARDIAC-MUSCLE** — **Times Cited: 860**

Maternal–fetal heartbeat phase synchronization

Plamen Ch. Ivanov[a,b,1], Qianli D. Y. Ma[b], and Ronny P. Bartsch[b]

[a]Center for Polymer Studies and Department of Physics, Boston University, Boston, MA 02215; and [b]Harvard Medical School and Division of Sleep Medicine, Brigham and Women's Hospital, Boston, MA 02115

Integrated physiological systems under neural control, such as the cardiac and respiratory systems, exhibit complex dynamics with continuous noisy fluctuations even in resting "equilibrium" conditions without external perturbations (1, 2). Advances in analytic methods have made it possible to identify a surprisingly robust temporal organization embedded in physiologic fluctuations, characterized by scale-invariant (fractal), multifractal, and nonlinear features over a range of time scales (2–4). This behavior is remarkably different from the one postulated by the classical principle of homeostasis (5), and it resembles the dynamics of certain physical systems away from equilibrium (6).

Although the origins of such rich complexity in physiologic fluctuations remain poorly understood, there is growing evidence that they are related to particular mechanisms of regulation involving networks of multiple inputs and nonlinear feedback interactions (7), as various aspects of their temporal organization change with different physiological states (8, 9) and pathological conditions (2, 4, 10). This picture is further complicated by nonlinear interactions between physiologic systems, where the specific mechanism of their coupling is often masked by physiologic fluctuations, as in the case of maternal–fetal cardiac interaction.

The fetal heart rate, a primary accessible indicator of prenatal development, changes with the physiological and psychological state of the mother: fetal heart rate variability and body movement substantially decrease with hypooxygenation of maternal arterial blood (11); increased maternal stress and anxiety levels correlate with increased mean fetal heart rate (12); during the night the mean hourly fetal heart rate decreases in synchrony with the mean maternal heart rate (13). This correlated behavior in the mean heart rates suggests certain coupling between the cardiac systems of mother and fetus. However, there has been no evidence of maternal–fetal heartbeat-to-heartbeat coordination, until now. The article by Van Leeuwen et al. (14) published in this issue of PNAS does just that: applying a novel concept from physics and nonlinear dynamics to their data, they uncover a hitherto-unknown phase synchronization between the individual heartbeats of mother and fetus—a marker of coupling between their autonomous cardiac systems despite continuous noisy fluctuations in the beat-to-beat intervals.

Using multichannel magnetocardiography to simultaneously record the magnetic fields generated during each maternal and fetal heartbeat at resting supine condition, Van Leeuwen et al. (14) derive time series of consecutive heartbeat intervals, and they discover epochs of synchronization where fetal heartbeats occur at the same instantaneous phases within each consecutive maternal heartbeat cycle—the first evidence of direct coupling mediated by the maternal cardiac activity. Such

Maternal–fetal cardiac coupling may not be mediated by maternal respiration.

mother–fetus heartbeat phase synchronization at beat-to-beat time scales is rather surprising, given their autonomous central nervous systems and separate blood circulation (placental barrier). Various factors—including maternal stress and anxiety levels associated with release of glucocorticoids and corticosteroid hormones (15) (which easily pass through the placental membrane); activation of the maternal autonomous nervous system by increased levels of acetylcholine triggering excitatory actions and body movements (16); variations in catecholamine concentrations resulting in maternal vasoconstriction and consequent restriction of oxygen to the fetus (11, 12)—all suggest certain influence on the average fetal heart rate and heart rate variability, however, at time scales much larger than beat-to-beat intervals. Indeed, recent cross-correlation analyses failed to identify a beat-to-beat association between maternal and fetal heart rate (17). Then, how did Van Leeuwen et al. succeed in identifying patterns of maternal and fetal heartbeat synchronization?

They related the problem of identifying maternal–fetal heartbeat coupling to an intriguing nonlinear phenomenon called synchronization—the adjustment of rhythms of self-sustained oscillators because of their interaction (18). First described by Huygens in 1665, who observed that the oscillations of two pendulum clocks suspended from the same wooden beam coincided perfectly due to their weak interaction mediated through the beam, synchronization has since been found in various physical and biological systems—from clocks and musical instruments, to cooperative behavior of crickets and fireflies, to circadian cycles and synchronous firing of neurons (18). Notably, a very weak, often imperceptible, interaction between oscillatory systems can cause a qualitative transition: an object adjusts its rhythm in conformity with the rhythm of other objects. For two weakly coupled oscillatory systems with regular dynamics and nonidentical frequencies, synchronization results in "locking" of their frequencies f_i (i.e., $mf_1 - nf_2 = 0$, where m and n are integers) or of their respective phases ϕ_i (i.e., $m\phi_1 - n\phi_2 = const$, where $d\phi_i(t)/dt = 2\pi f_i$ and the ratios m:n correspond to different phase-synchronization patterns) (19). To identify and quantify the degree of coupling between oscillatory systems with noisy irregular or chaotic dynamics, where the amplitudes are not cross-correlated (and thus traditional cross-correlation methods do not work), a novel phase-synchronization approach has been recently developed (18, 20) and applied to several physiologic systems, including cardiorespiratory synchronization in healthy adults at rest (21) and its change across sleep stages (22); synchronous activation of cortical centers during epileptic seizures (23); and cerebral autoregulation in subjects after ischemic stroke (24). The study of Van Leeuwen et al. (14) goes further to discover phase synchronization between autonomous physiologic systems of different organisms, the maternal and fetal heart.

The specific mechanism leading to maternal–fetal heartbeat phase synchronization remains elusive, and two hypotheses for pathways mediating this

Author contributions: P.Ch.I., Q.D.Y.M, and R.P.B. wrote the paper.

The authors declare no conflict of interest.

See companion article on page 13661.

[1]To whom correspondence should be addressed. E-mail: plamen@buphy.bu.edu.

interaction are plausible: (*i*) the oscillatory rhythm of maternal respiration acts as a common driving force and influences simultaneously both maternal and fetal heart rates, leading to an apparent maternal–fetal heartbeat synchronization; (*ii*) the maternal cardiac system has a direct detuning effect on the fetal heart rhythm.

At normal breathing rates, the respiratory rhythm leads to cyclical cardiac variations where the heart rate increases during inhalation and decreases with exhalation, a phenomenon called respiratory sinus arrhythmia (RSA) (16). RSA, a noninvasive measure of parasympathetic tone reflected in high-frequency heart rate oscillations, is increasingly pronounced (i.e., larger amplitude of heart rate variation) with decreasing respiratory rates (16). Further, lower respiratory rates are associated with a higher degree (longer epochs) of cardiorespiratory phase synchronization in normal subjects (25), suggesting increased maternal cardiorespiratory synchronization. In parallel, lung tidal volume and chest and abdomen movement are larger at lower breathing frequencies, raising the possibility for increased mechanical stimulation of the uterus, and thus driving the fetal heart rate to phase-synchronize with the maternal respiration and correspondingly with the maternal heart rate. Performing measurements over a range of maternal breathing frequencies, Van Leeuwen et al. (14) show the opposite: significantly higher maternal–fetal heartbeat synchronization at higher respiratory rates, indicating that maternal–fetal cardiac coupling may not be mediated by maternal respiration.

An intriguing alternative hypothesis suggested by Van Leeuwen et al. (14) is that maternal–fetal cardiac coupling is mediated by acoustic stimuli of maternal heartbeat and vessel pulsation perceived by the fetal auditory system. These stimuli may act as an external forcing rhythm to entrain the fetal heartbeat to the beat of the mother. Indeed, experiments have demonstrated that the heartbeat of healthy subjects at rest synchronizes with periodic sequences of weak external sound pulses (19). However, this could not quite explain the findings by Van Leeuwen et al. of a higher degree of synchronization at higher respiratory rates, because both maternal and fetal mean heart rate remain practically unchanged with increased frequency of paced maternal respiration (ref. 16 and table 1 in ref. 14). A possible explanation for the increase in maternal–fetal heartbeat synchronization at higher maternal respiratory rates is the observed lower standard deviation of the maternal heartbeat increments (ref. 16 and table 1 in ref. 14), leading to a more regular maternal heartbeat at higher respiratory rates, thus generating more regular acoustic stimuli with which the fetal heartbeat can better synchronize (25). This argument is further supported by the observation that the standard deviation of the fetal heartbeat increments significantly drops at a high maternal respiratory rate when the maternal–fetal phase synchronization is most pronounced (14). Whether such an acoustic mechanism is indeed responsible for the maternal–fetal heart rate coupling remains to be further investigated, given that the gradual increase in synchronization with an increasing maternal respiratory rate is not paralleled by a simultaneous decrease in the standard deviation of the fetal heartbeat increments.

The work by Van Leeuwen et al. (14) is a significant step toward a better understanding of the complexity of maternal–fetal interaction at the integrated system level. Elucidating the mechanistic pathways underlying this interaction remains a major challenge, as these pathways involve multiple contributing factors, from the biochemical to the system level, acting through various feedback loops and over a range of time scales. Further investigations are needed to clarify the physiological significance of the maternal–fetal heart rate phase synchronization at beat-to-beat time scales, and whether mother and child benefit from this specific interaction. As the complexity in fetal heartbeat fluctuations increases with gestation age, it is conceivable that maternal–fetal cardiac coupling may also evolve with maturation. Quantifying the degree of this coupling for different gestation age may prove instrumental in deriving novel clinical markers of healthy prenatal development and pathological deviation.

ACKNOWLEDGMENTS. This work was supported by Grant P06-FQM1858 from the Spanish Junta de Andalucia.

1. Bassingthwaighte JB, Liebovitch LS, West BJ (1994) *Fractal Physiology* (Oxford Univ Press, New York).
2. Goldberger AL, et al. (2002) Fractal dynamics in physiology: Alterations with disease and aging. *Proc Natl Acad Sci USA* 99:2466–2472.
3. Suki B, et al. (1998) Life-support system benefits from noise. *Nature* 393:127–128.
4. Ivanov PCh, et al. (1999) Multifractality in human heartbeat dynamics. *Nature* 399:461–465.
5. Cannon WB (1929) Organization for physiological homeostasis. *Physiol Rev* 9:399–431.
6. Stanley HE (1971) *Introduction to Phase Transitions and Critical Phenomena* (Oxford Univ Press, New York).
7. Sugihara G, Allan W, Sobel D, Allan KD (1996) Nonlinear control of heart rate variability in human infants. *Proc Natl Acad Sci USA* 93:2608–2613.
8. Bunde A, et al. (2000) Correlated and uncorrelated regions in heart-rate fluctuations during sleep. *Phys Rev Lett* 85:3736–3739.
9. Karasik R, et al. (2002) Correlation differences in heartbeat fluctuations during rest and exercise. *Phys Rev E* 66:062902.
10. Huikuri HV, et al. (2000) Fractal correlation properties of R-R interval dynamics and mortality in patients with depressed left ventricular function after an acute myocardial infarction. *Circulation* 101:47–53.
11. Bekedam DJ, Mulder EJH, Snijders RJM, Visser GHA (1991) The effects of maternal hyperoxia on fetal breathing movements, body movements, and heart-rate variation in growth retarded fetuses. *Early Hum Dev* 27:223–232.
12. Monk C, et al. (2000) Maternal stress responses and anxiety during pregnancy: Effects on fetal heart rate. *Dev Psychobiol* 36:67–77.
13. Patrick J, Campbell K, Carmichael L, Probert C (1982) Influence of maternal heart rate and gross fetal body movements on the daily pattern of fetal heart rate near term. *Am J Obstet Gynecol* 144:533–538.
14. Van Leeuwen P, et al. (2009) Influence of paced maternal breathing on fetal–maternal heart rate coordination. *Proc Natl Acad Sci USA* 106:13661–13666.
15. Welberg LAM, Seckl JR (2001) Prenatal stress, glucocorticoids, and the programming of the brain. *J Neuroendocrinol* 13:113–128.
16. Song HS, Lehrer PM (2003) The effects of specific respiratory rates on heart rate and heart rate variability. *Appl Psychophysiol Biofeedback* 28:13–23.
17. DiPietro JA, et al. (2006) Prenatal development of intrafetal and maternal-fetal synchrony. *Behav Neurosci* 120:687–701.
18. Pikovsky AS, Rosenblum MG, Kurths J (2001) *Synchronization—A Universal Concept in Nonlinear Sciences* (Cambridge Univ Press, Cambridge, UK).
19. Anishchenko VS, Balanov AG, Janson NB, Igosheva NB, Bordyugov GV (2000) Entrainment between heart rate and weak noninvasive forcing. *Int J Bifurcat Chaos* 10:2339–2348.
20. Rosenblum MG, Pikovsky AS, Kurths J (1996) Phase synchronization of chaotic oscillators. *Phys Rev Lett* 76:1804–1807.
21. Schäfer C, Rosenblum MG, Kurths J, Abel HH (1998) Heartbeat synchronized with ventilation. *Nature* 392:239–240.
22. Bartsch RP, Kantelhardt JW, Penzel T, Havlin S (2007) Experimental evidence for phase synchronization transitions in the human cardiorespiratory system. *Phys Rev Lett* 98:054102.
23. Lehnertz K (2008) Epilepsy and nonlinear dynamics. *J Biol Phys* 34:253–266.
24. Chen Z, Hu K, Stanley HE, Novak V, Ivanov PCh (2006) Cross-correlation of instantaneous phase increments in pressure-flow fluctuations: Applications to cerebral autoregulation. *Phys Rev E* 73:031915.
25. Prokhorov MD, Ponomarenko VI, Gridnev VI, Bodrov MB, Bespyatov AB (2003) Synchronization between main rhythmic processes in the human cardiovascular system. *Phys Rev E* 68:041913.

Maternal-fetal heartbeat phase synchronization

By: Ivanov, PC (Ivanov, Plamen Ch.)[1,2,3,4] ; Ma, QDY (Ma, Qianli D. Y.)[3,4] ; Bartsch, RP (Bartsch, Ronny P.)[3,4]

View ResearcherID and ORCID

PROCEEDINGS OF THE NATIONAL ACADEMY OF SCIENCES OF THE UNITED STATES OF AMERICA
Volume: 106 **Issue:** 33 **Pages:** 13641-13642
DOI: 10.1073/pnas.0906987106
Published: AUG 18 2009
Document Type: Editorial Material
View Journal Impact

Keywords

KeyWords Plus: RATE-VARIABILITY; BODY MOVEMENTS; DYNAMICS; STRESS

Author Information

Reprint Address: Ivanov, PC (reprint author)

+ Boston Univ, Ctr Polymer Sci, Boston, MA 02215 USA.

Addresses:

+ [1] Boston Univ, Ctr Polymer Sci, Boston, MA 02215 USA

+ [2] Boston Univ, Dept Phys, Boston, MA 02215 USA

+ [3] Harvard Univ, Sch Med, Boston, MA 02115 USA

+ [4] Brigham & Womens Hosp, Div Sleep Med, Boston, MA 02115 USA

E-mail Addresses: plamen@buphy.bu.edu

Publisher

NATL ACAD SCIENCES, 2101 CONSTITUTION AVE NW, WASHINGTON, DC 20418 USA

Journal Information

Impact Factor: Journal Citation Reports

Categories / Classification

Research Areas: Science & Technology - Other Topics

Web of Science Categories: Multidisciplinary Sciences

See more data fields

Citation Network

In Web of Science Core Collection

17

Times Cited

Create Citation Alert

All Times Cited Counts

18 in All Databases

See more counts

25

Cited References

View Related Records

Most recently cited by:

Stuart, Susan A. J.
Enkinaesthesia: Proto-moral value in action-enquiry and interaction.
PHENOMENOLOGY AND THE COGNITIVE SCIENCES (2018)

Ma, Qianli D. Y.; Ji, Changjuan; Xie, Huanhuan; et al.
Transitions in physiological coupling between heartbeat and pulse across sleep stages.
PHYSIOLOGICAL MEASUREMENT (2018)

View All

Use in Web of Science

Web of Science Usage Count

0 Last 180 Days

9 Since 2013

Learn more

This record is from:
Web of Science Core Collection

View Record in Other Databases:
View **biological data** (in Biological

Abstracts)
View **medical data** (in MEDLINE®)

Suggest a correction

If you would like to improve the quality of the data in this record, please suggest a correction.

93 of 127

Cited References: 25

Showing 25 of 25 **View All in Cited References page** *(from Web of Science Core Collection)*

1. **Entrainment between heart rate and weak noninvasive forcing** **Times Cited: 48**
By: Anishchenko, VS; Balanov, AG; Janson, NB; et al.
INTERNATIONAL JOURNAL OF BIFURCATION AND CHAOS Volume: 10 Issue: 10 Pages: 2339-2348 Published: OCT 2000

2. **Experimental evidence for phase synchronization transitions in the human cardiorespiratory system** **Times Cited: 92**
By: Bartsch, Ronny; Kantelhardt, Jan W.; Penzel, Thomas; et al.
PHYSICAL REVIEW LETTERS Volume: 98 Issue: 5 Article Number: 054102 Published: FEB 2 2007

3. Title: [not available] **Times Cited: 287**
By: BASSINGTHWAIGHT.JB
FRACTAL PHYSL Published: 1994

4. **THE EFFECTS OF MATERNAL HYPEROXIA ON FETAL BREATHING MOVEMENTS, BODY MOVEMENTS AND HEART-RATE VARIATION IN GROWTH RETARDED FETUSES** **Times Cited: 29**
By: BEKEDAM, DJ; MULDER, EJH; SNIJDERS, RJM; et al.
EARLY HUMAN DEVELOPMENT Volume: 27 Issue: 3 Pages: 223-232 Published: DEC 1991

5. **Correlated and uncorrelated regions in heart-rate fluctuations during sleep** **Times Cited: 367**
By: Bunde, A; Havlin, S; Kantelhardt, JW; et al.
PHYSICAL REVIEW LETTERS Volume: 85 Issue: 17 Pages: 3736-3739 Published: OCT 23 2000

6. **Organization for physiological homeostasis** **Times Cited: 757**
By: Cannon, WB
PHYSIOLOGICAL REVIEWS Volume: 9 Issue: 3 Pages: 399-431 Published: JUL 1929

7. **Cross-correlation of instantaneous phase increments in pressure-flow fluctuations: Applications to cerebral autoregulation** **Times Cited: 35**
By: Chen, Z; Hu, K; Stanley, HE; et al.
PHYSICAL REVIEW E Volume: 73 Issue: 3 Article Number: 031915 Part: 1 Published: MAR 2006

8. **Prenatal development of intrafetal and maternal-fetal synchrony** **Times Cited: 23**
By: DiPietro, Janet A.; Caulfield, Laura E.; Irizarry, Rafael A.; et al.
BEHAVIORAL NEUROSCIENCE Volume: 120 Issue: 3 Pages: 687-701 Published: JUN 2006

9. **Fractal dynamics in physiology: Alterations with disease and aging** **Times Cited: 1,064**
By: Goldberger, AL; Amaral, LAN; Hausdorff, JM; et al.
PROCEEDINGS OF THE NATIONAL ACADEMY OF SCIENCES OF THE UNITED STATES OF AMERICA Volume: 99 Supplement: 1 Pages: 2466-2472 Published: FEB 19 2002

Effect of extreme data loss on long-range correlated and anticorrelated signals quantified by detrended fluctuation analysis

Qianli D. Y. Ma,[1,2] Ronny P. Bartsch,[1] Pedro Bernaola-Galván,[3] Mitsuru Yoneyama,[4] and Plamen Ch. Ivanov[1,3,5,*]
[1]*Harvard Medical School and Division of Sleep Medicine, Brigham and Women's Hospital, Boston, Massachusetts 02115, USA*
[2]*College of Geography and Biological Information, Nanjing University of Posts and Telecommunications, Nanjing 210003, China*
[3]*Departamento de Física Aplicada II, Universidad de Málaga, 29071 Málaga, Spain*
[4]*Mitsubishi Chemical Group, Science and Technology Research Center Inc., Yokohama 227-8502, Japan*
[5]*Center for Polymer Studies and Department of Physics, Boston University, Boston, Massachusetts 02215, USA*
(Received 19 November 2009; published 2 March 2010)

Detrended fluctuation analysis (DFA) is an improved method of classical fluctuation analysis for nonstationary signals where embedded polynomial trends mask the intrinsic correlation properties of the fluctuations. To better identify the intrinsic correlation properties of real-world signals where a large amount of data is missing or removed due to artifacts, we investigate how extreme data loss affects the scaling behavior of long-range power-law correlated and anticorrelated signals. We introduce a segmentation approach to generate surrogate signals by randomly removing data segments from stationary signals with different types of long-range correlations. The surrogate signals we generate are characterized by four parameters: (i) the DFA scaling exponent α of the original correlated signal $u(i)$, (ii) the percentage p of the data removed from $u(i)$, (iii) the average length μ of the removed (or remaining) data segments, and (iv) the functional form $P(l)$ of the distribution of the length l of the removed (or remaining) data segments. We find that the global scaling exponent of positively correlated signals remains practically unchanged even for extreme data loss of up to 90%. In contrast, the global scaling of anticorrelated signals changes to uncorrelated behavior even when a very small fraction of the data is lost. These observations are confirmed on two examples of real-world signals: human gait and commodity price fluctuations. We further systematically study the local scaling behavior of surrogate signals with missing data to reveal subtle deviations across scales. We find that for anticorrelated signals even 10% of data loss leads to significant monotonic deviations in the local scaling at large scales from the original anticorrelated to uncorrelated behavior. In contrast, positively correlated signals show no observable changes in the local scaling for up to 65% of data loss, while for larger percentage of data loss, the local scaling shows overestimated regions (with higher local exponent) at small scales, followed by underestimated regions (with lower local exponent) at large scales. Finally, we investigate how the scaling is affected by the average length, probability distribution, and percentage of the remaining data segments in comparison to the removed segments. We find that the average length μ_r of the remaining segments is the key parameter which determines the scales at which the local scaling exponent has a maximum deviation from its original value. Interestingly, the scales where the maximum deviation occurs follow a power-law relationship with μ_r. Whereas the percentage of data loss determines the extent of the deviation. The results presented in this paper are useful to correctly interpret the scaling properties obtained from signals with extreme data loss.

DOI: 10.1103/PhysRevE.81.031101 PACS number(s): 05.40.−a

I. INTRODUCTION

In real-world signals data can be missing or unavailable to a very large extent, especially in archeological, geological, and physiological recordings which often once recorded in the past cannot be generated again. Knowing the effects which data loss may have on the correlations and other dynamical properties of the output signals of a given system is instrumental in accurately quantifying and modeling the underlying mechanisms driving the dynamics of the system. Significant data loss can also be caused by failure of the data collection equipment, as well as by the removal of artifacts or noise-contaminated data segments. To correctly interpret results obtained from correlated signals with missing data, it is important to understand how the dynamical properties of such signals are affected by the degree of data loss. Here we systematically investigate how loss of data changes the scaling properties of various long-range power-law anticorrelated and positively correlated signals. Specifically, we develop a segmentation approach to generate surrogate signals by randomly removing data segments from stationary long-range power-law correlated signals and we study how the correlation properties are affected by (i) the percentage of removed data, (ii) the average length of the removed (or remaining) data segments, and (iii) the functional form of the probability distribution of the removed (remaining) segments. We utilize the detrended fluctuation analysis (DFA) to quantify the effect of extreme data loss on the scaling properties of long-range correlated signals.

Scaling (fractal) behavior was first encountered in a class of physical systems [1–3] which for a given "critical" value of their parameters, exhibit complex organization among their individual components, leading to correlated interactions over a broad range of scales. This class of complex systems are typically characterized by (i) multicomponent

*Corresponding author; plamen@buphy.bu.edu

nonlinear feedback interactions, (ii) nonequilibrium output dynamics, and (iii) high susceptibility and responsiveness to perturbations. Scaling behavior has been found in a diverse group of systems—ranging from earthquakes, to traffic jams and economic crashes, to neuronal excitations as well as the dynamics of integrated physiologic systems under neural control—and has been associated with the underlying mechanisms of regulation of these systems [4,5]. The output signals of such systems exhibit continuous fluctuations over multiple time and/or space scales [6,7], where the amplitudes and temporal/spatial organization of the fluctuations are characterized by absence of dominant scale, i.e., scale-invariant behavior. Due to the nonlinear mechanisms controlling the underlying interactions, the output signals of these systems are also typically nonstationary, which masks the intrinsic correlations. Traditional methods such as power spectrum and autocorrelation analysis [8–10] are not suitable for nonstationary signals.

DFA is a robust method suitable for detecting long-range power-law correlations embedded in nonstationary signals [11,12]. It has been successfully applied to a variety of fields where scale-invariant behavior emerges such as DNA [11,13–26], cardiac dynamics [27–46], human locomotion [5,47–49], circadian rhythm [50–53], neural receptors in biological systems [54], seismology [55,56], meteorology [57], climate temperature fluctuations [58–63], river flow and discharge [64,65], and economics [66–79]. The DFA method may also help identify different states of the same system exhibiting different scaling behavior—e.g., the DFA scaling exponent α for heart-beat intervals is significantly different for healthy and sick individuals [27,32,44] as well as for wake and sleep states [30,35,40,45,52].

Elucidating the intrinsic mechanisms of a given system requires an accurate analysis and proper interpretation of the dynamical (scaling) properties of its output signals. It is often the case that the scaling exponent quantifying the temporal (spatial) organization of the systems' dynamics across scales is not always the same, but depends on the scale of observation, leading to distinct crossovers—i.e., the value of the scaling exponent may be different for smaller compared to larger scales. Such behavior has been observed for diverse systems, for example: (i) the spontaneous motion of microbeads bound to the cytoskeleton of living cells as quantified by the mean-square displacement does not exhibit a Brownian motion but instead undergoes a transition from subdiffusive to superdiffusive behavior with time [80]; (ii) cardiac dynamics of healthy subjects during sleep are characterized by fluctuations in the heartbeat intervals exhibiting a crossover from a higher scaling exponent (stronger correlations) at small time scales (from seconds up to a minute) to a lower scaling exponent (weaker correlations) at large time scales (from minutes to hours), associated with changes in neural autonomic control during sleep [30,81]; and (iii) stock market dynamics where both absolute price returns and intertrade times exhibit a crossover from a lower scaling exponent at small time scales (up to a trading day) to much higher exponent at large time scales (from a trading day to many months), a behavior consistent for all companies on the market [69,79]. However, crossovers may also be a result of various types of nonstationarities and artifacts present in the output signals, which, if not carefully investigated, may lead to incorrect interpretation and modeling of the underlying mechanisms regulating the dynamics of a given system [44].

In previous studies, we have systematically investigated the effects of various types of nonstationarities, data preprocessing filters and data artifacts on the scaling behavior of long-range power-law correlated signals as measured by the DFA method [82–84]. In particular, we studied a type of nonstationarity which is caused by the presence of discontinuities (gaps) in the signal, i.e., how randomly removing data segments of fixed length affects the scaling properties of long-range power-law correlated signals [83]. Such discontinuities may arise from the nature of the recordings—e.g., stock exchange data are not recorded during the nights, weekends and holidays [66–73]. In these situations, discontinuities correspond to segments of fixed size.

Alternatively, discontinuities may be caused by the fact that (i) part of the data is lost due to various reasons and/or (ii) some noisy and unreliable portions of continuous recordings (e.g., measurement artifacts) are discarded prior to analysis [27–39,45,46]. In these cases, the lengths of the lost or removed data segments are random, and may follow a certain type of distribution which can often be related to the process responsible for the removal or loss of data—e.g., a data acquisition device which fails randomly with a given probability p will result in a geometric distribution $P(l)=(1-p)^l p$ with mean $\mu=1/p$, where l is the length of the data lost segments. Thus, investigating the effect of data loss is essential to determine the true correlation properties of the signal output of a given system.

To address this question, we propose a segmentation algorithm to generate surrogate signals by randomly removing data segments from long-range power-law correlated signals with a priori known scaling properties, and we investigate the effects of the percentage of the removed data, different average lengths, and different distributions of removed data segments. We compare the scaling behavior of the original signals with the scaling of the surrogate signals by systematically studying changes in the DFA scaling exponent. We utilize local scaling exponents to reveal subtle deviations and to characterize changes in the scaling behavior at different scales in signals with segment removed. We note that in our investigation we consider the effect of data loss on signals where the scaling behavior remains constant for the duration of the observations. Signals comprised of segments characterized by different scaling exponents have been considered elsewhere [83].

This paper is structured as follows: in Sec. II A, we briefly describe the DFA method. In Sec. II B we describe how to generate stationary long-range power-law correlated signals. In Sec. II C we introduce an algorithm for randomly removing data segments from these signals to test the effects of data loss on the scaling behavior. In Sec. III A, we study the effect of data loss on the global scaling of positively correlated and anticorrelated artificially generated signals with different length, and we show examples on two different sets of empirical data. In Sec. III B we compare the local scaling properties of correlated signals before and after data removal by considering the effect of several parameters of the removed segments. In Sec. III C we consider the inverse

situation—instead of focusing on the properties of the removed segments we investigate how the correlations/scaling of the signal depend on the properties of the remaining data segments. We summarize and discuss our findings in Sec. IV.

II. METHODS

A. Detrended fluctuation analysis (DFA)

The DFA is a random walk based method [11]. It is an improvement of the classical fluctuation analysis (FA) for nonstationary signals where embedded polynomial trends mask the intrinsic correlation properties in the fluctuations [11]. The performance of DFA for signals with different types of nonstationarities and artifacts has been extensively studied and compared to other methods of correlation analysis [12,82–88]. The DFA method involves the following steps [11]:

(i) A given signal $u(i)$ $(i=1,\ldots,N$, where N is the length of the signal) is integrated to obtain the random walk profile $y(k)\equiv\Sigma_{i=1}^{k}[u(i)-\langle u\rangle]$, where $\langle u\rangle$ is the mean of $u(i)$.

(ii) The integrated signal $y(k)$ is divided into boxes of equal length n.

(iii) In each box of length n we fit $y(k)$ using a polynomial function of order ℓ which represents the *trend* in that box. The y coordinate of the fit curve in each box is denoted by $y_n(k)$. When a polynomial fit of order ℓ is used, we denote the algorithm as DFA-ℓ. Note that, due to the integration procedure in step (i), DFA-ℓ removes polynomial trends of order $\ell-1$ in the original signal $u(i)$.

(iv) The integrated profile $y(k)$ is detrended by subtracting the local trend $y_n(k)$ in each box of length n

$$Y(k)\equiv y(k)-y_n(k). \tag{1}$$

(v) For a given box length n, the root-mean-square (rms) fluctuation function for this integrated and detrended signal is calculated

$$F(n)\equiv\sqrt{\frac{1}{N}\sum_{k=1}^{N}[Y(k)]^2}. \tag{2}$$

(vi) The above computation is repeated for a broad range of box lengths n (where n represents a specific space or time scale) to provide a relationship between $F(n)$ and n.

A power-law relation between the root-mean-square fluctuation function $F(n)$ and the box size n, i.e., $F(n)\sim n^{\alpha}$, indicates the presence of scaling-invariant behavior embedded in the fluctuations of the signal $u(i)$. The fluctuations can be characterized by a scaling exponent α, a self-similarity parameter which represents the long-range power-law correlation properties of the signal. If $\alpha=0.5$, there is no correlation and the signal is uncorrelated (white noise); if $\alpha<0.5$, the signal is anticorrelated; if $\alpha>0.5$, the signal is positively correlated; and $\alpha=1.5$ indicates Brownian motion (integrated white noise). For stationary signals with long-range power-law correlations, the value of the scaling exponent α is related to the exponent β characterizing the power spectrum $S(f)=f^{-\beta}$ of the signal, where $\beta=2\alpha-1$ [14]. Thus, the special case of $1/f$ noise, where $\beta=1$, observed in various physiological and biological system dynamics, corresponding to $\alpha=1$. Since the power spectrum of stationary signals is the Fourier transform of the autocorrelation function, for signals with scale-invariant long-range positive correlation and $\alpha<1$, one can find the following relationship between the autocorrelation exponent γ and the power spectrum exponent β for signals with scale-invariant long-range correlations: $\gamma=1-\beta=2-2\alpha$, where γ is defined by the autocorrelation function $C(\tau)=\tau^{-\gamma}$, and should satisfy $0<\gamma<1$ [89].

We note that for anticorrelated signals, the scaling exponent α obtained from the DFA method overestimates the true correlations at small scales n [82]. To avoid this problem, one needs first to integrate the original anticorrelated signal and then apply the DFA method. The correct scaling exponent can thus be obtained from the relation between n and $F(n)/n$ [instead of $F(n)$] [see Fig. 4(a)]. This procedure is applied for all cases of anticorrelated signals in this study. In our analysis in the following sections we apply DFA-2. The choice of DFA-2 is dictated by the fact that this order of DFA-l can accurately quantify the scaling behavior of signals with exponents in the range $0<\alpha<3$ [85], which covers practically all signals generated by real-world systems. Moreover, earlier investigations have demonstrated that DFA-2 is sufficient to accurately quantify a broad range of nonstationary signals generated by different physiologic dynamics—e.g., for heartbeat and gait dynamics the exponent α obtained from higher order DFA-l is not significantly different compared to α obtained from DFA-2 [49]. Further, deviations from scaling which appear at small scale become more pronounced in higher order DFA-l [89]. In order to provide an accurate estimate of $F(n)$, the largest box size n we use is $n=N/8$, where N is the signal length.

B. Procedure to generate stationary signals with long-range power-law correlations

We use a modified Fourier filtering technique [90] to generate stationary long-range power-law correlated signals $u(i)$ $(i=1,2,\ldots,N)$ with mean $\langle u(i)\rangle=0$ and standard deviation $\sigma=1$. The correlations of $u(i)$ are characterized by a Fourier power spectrum of a power-law form $S(f)\sim f^{-\beta}$, where f is the frequency. By manipulating the Fourier spectrum of random Gaussian-distributed sequences, we generate signal $u(i)$ with desired power-law correlations. This method consists of the following steps:

(i) first, we generate a Gaussian-distributed sequence $\eta(i)$ with mean $\langle\eta(i)\rangle=0$ and standard deviation $\sigma_\eta=1$, and we calculate its Fourier transformation $\hat{\eta}(f)$.

(ii) Next, we generate $\hat{u}(f)$ using the following transformation:

$$\hat{u}(f)=\hat{\eta}(f)\cdot f^{-\beta/2}, \tag{3}$$

where $\hat{u}(f)$ is the Fourier transform of the desired correlated signal $u(i)$ characterized by a Fourier power spectrum of the form

$$S(f)=|\hat{u}(f)|^2\sim f^{-\beta}. \tag{4}$$

(iii) We calculate the inverse Fourier transform of $\hat{u}(f)$ to obtain $u(i)$. The generated stationary signal $u(i)$ is then nor-

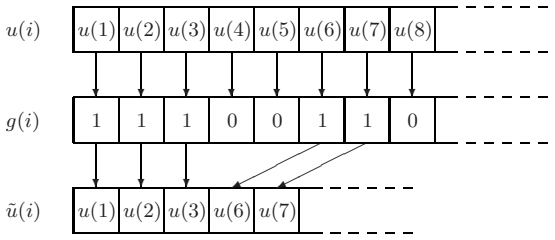

FIG. 1. Illustration of generating a surrogate signal $\tilde{u}(i)$ by removing data points from the original signal $u(i)$ according to a binary series $g(i)$. The positions i where $g(i)=0$ (or 1) correspond to the positions at which data points in $u(i)$ are removed (or preserved) to obtain $\tilde{u}(i)$.

malized to zero mean and unit standard deviation.

C. Algorithm to generate surrogate signals with randomly removed segments

We introduce a segmentation approach to generate surrogate nonstationary signals $\tilde{u}(i)$ by randomly removing data segments from a stationary correlated signal $u(i)$ and stitching together the remaining parts of $u(i)$. Such "cutting" procedure is often used in the preprocessing of data prior to analysis in order to eliminate, for example, segments of data artifacts. The proposed segmentation approach allows the simulation of empirical data series where data segments are lost or removed. The surrogate signals $\tilde{u}(i)$ are characterized by four parameters: (i) the DFA scaling exponent α of the original signal $u(i)$, (ii) the percentage p of the data removed, (iii) the average length μ of the removed data segments as well as (iv) the functional form $P(l)$ of the distribution of the length l of the removed data segments.

To generate a surrogate signal $\tilde{u}(i)$ from the original signal $u(i)$, we first construct a binary sequence $g(i)$ with the same length N as $u(i)$. In our algorithm the positions i where $g(i)=0$ will correspond to the positions at which data points in $u(i)$ are removed, while the positions where $g(i)=1$ will correspond to the positions in $u(i)$ where data points are preserved (Fig. 1).

We developed the following method to construct the binary series $g(i)$:

(i) we generate the lengths l_j $(j=1,2,\ldots,M)$ of the segments that will be removed from the original signal $u(i)$ by randomly drawing integer numbers from a given probability distribution $P(l)$ with mean value μ. Each integer number drawn from $P(l)$ represents the length of a segment removed from $u(i)$. The process continues until the summation of the lengths of all removed segments becomes equal or exceeds a predetermined amount pN of data to be removed, i.e.,

$$\sum_{j=1}^{M} l_j \geq pN, \tag{5}$$

where M is the minimal number to fulfill Eq. (5). Eventually, we will cut the size of the last segment to obtain the exact fraction pN of the lost data.

(ii) We append a "1" to each element in the series $\{l_j\}$ which will serve as a separator between two adjacent segments [see step (iv)], and results in a new series $\{[l_j,1]\}$. Note that now the summation over the series yields $pN+M$.

(iii) We append $[N-(pN+M)]$ number of elements "1" to the end of the series $\{[l_j,1]\}$ to obtain an extended series where the sum of all elements is N, equal to the length of the original series $u(i)$. This extended series is then shuffled leading to a set of M elements $[l_j,1]$ randomly scattered in a "sea" of $[N-(pN+M)]$ of elements "1" [see Eq. (6)].

(iv) Next, we replace the numbers l_j in Eq. (6) with l_j elements of zeros, to obtain a binary series $g(i)$ as shown in Eq. (7).

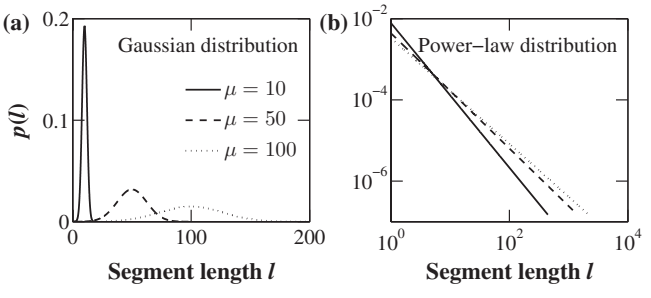

FIG. 2. Examples of theoretical probability density for (a) Gaussian distribution and (b) power-law distribution used in our simulations of different situations of data loss. The parameters for the functional form of distributions are determined by the average length μ we chose for each simulation and by specific boundary conditions, i.e., for the Gaussian distribution, we set the probability of the smallest segment length $P(l=1)=1/pN$, and for the power-law distribution we set the probability of the largest segment length $P(l=l_{\max})=1/pN$ (see text for details).

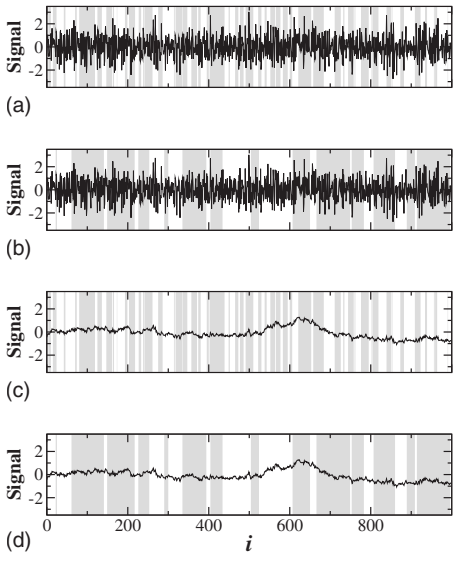

FIG. 3. Illustration of data removal from stationary correlated signals. Removed data segments (shaded regions) are randomly positioned within the original signal and their lengths l are drawn from an exponential distribution $P(l)=\frac{1}{\mu}\exp(-l/\mu)$ with average value μ. An average length $\mu=10$ is chosen for (a) the anticorrelated signal (DFA scaling exponent $\alpha=0.3$) and (b) the positively correlated signal ($\alpha=1.3$). Larger segments with $\mu=50$ are removed from (b) anticorrelated signal ($\alpha=0.3$) and (d) positively correlated signal ($\alpha=1.3$).

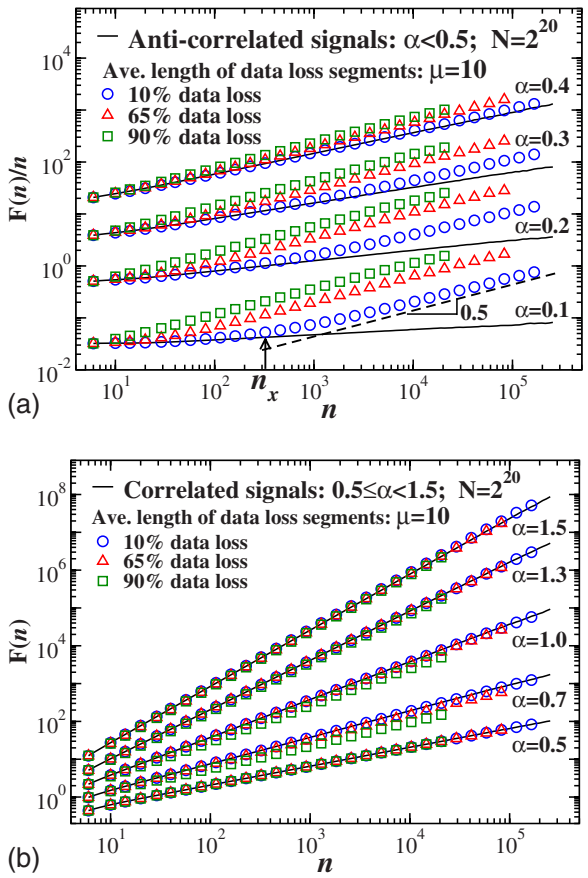

FIG. 4. (Color online) Effect of data loss on the scaling behavior of long-range correlated signals with length $N=2^{20}$ (before data removal), zero mean and unity standard deviation. The lengths of the removed segments are drawn from an exponential distribution with mean $\mu=10$. (a) Scaling behavior of anticorrelated signals (scaling exponent $\alpha<0.5$) with a data loss of 10% (blue circles), 65% (red triangles), and 90% (green squares). Note that, to obtain an accurate estimation of the DFA scaling exponent α for anticorrelated signals, we first integrate the signals and then we apply the DFA method. Thus, to obtain the correct scaling exponent for anticorrelated signals we divide $F(n)$ by n to account for the integration of the signals and next we plot $F(n)/n$ vs the scale n (see also Sec. II A and Fig. 15 in [82]). (b) Scaling behavior of positively correlated signals (scaling exponent $\alpha>0.5$) with 10%, 65%, and 90% data loss. The scaling behavior of strongly anticorrelated data is dramatically changed even when only 10% of the data are removed. A crossover at scale n_x indicates a transition (arrow), due to loss of data in the signals, from the original anticorrelated behavior with $\alpha=0.1$ to an uncorrelated behavior with $\alpha=0.5$. In contrast, for positively correlated signals, i.e., $0.5<\alpha<1.5$ only an extreme data loss of 90% leads to small deviations from the original scaling behavior. This effect becomes weaker for increasing values of α. As expected, for $\alpha=0.5$ (white noise) and $\alpha=1.5$ (Brownian noise) data removal does not affect the scaling behavior.

$$\{\ldots,1,\ [l_j,1],\quad 1,\ldots,1,\ [l_{j+1},1],\quad [l_{j+2},1],\ 1,\ldots\},\tag{6}$$

$$\{\ldots,1,\overbrace{0,\ldots,0,1},\quad 1,\ldots,1,\overbrace{0,\ldots,0,1},\quad \overbrace{0,\ldots,0,1},1,\ldots\}.\tag{7}$$

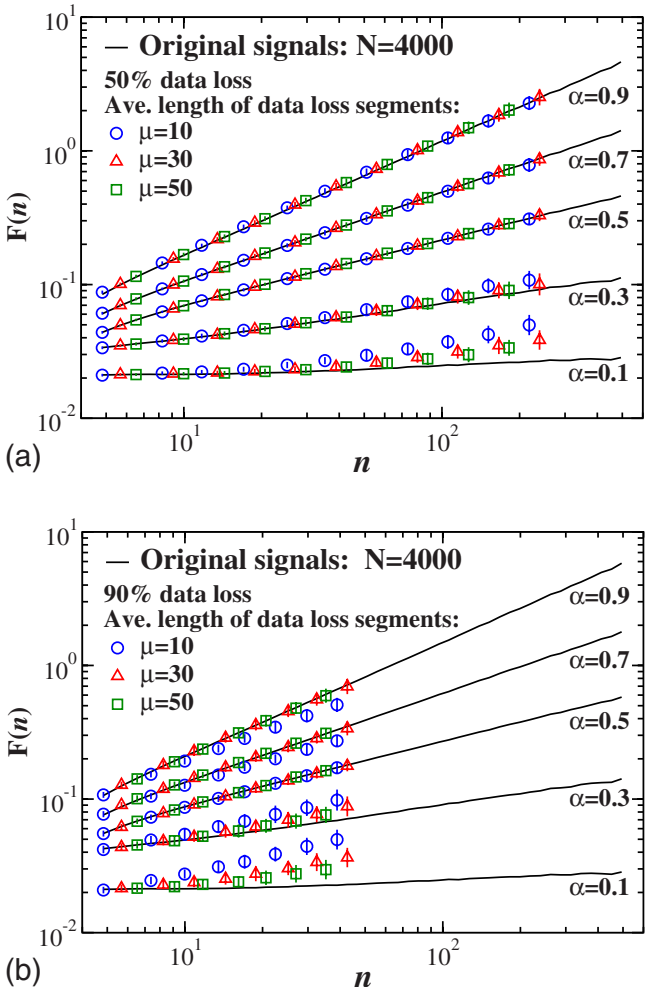

FIG. 5. (Color online) Effect of data loss on the scaling behavior of *short* signals ($N=4000$ before data removal). (a) Removing up to 50% of the data (i.e., 2000 data points remain) does not have an observable effect on the scaling behavior of positively correlated signals and leads to small deviations from the original scaling behavior in anticorrelated signals. (b) Extreme data loss of 90% (i.e., only 400 data points remain) leads to more pronounced deviations from the original scaling behavior. In general, the deviations are smaller with larger average length μ of removed segments.

Note that, in step (iii) of our algorithm, the shuffling of the extended series may lead to two or more $[l_j,1]$ elements, which represent removed data segments, to become direct neighbors [Eq. (6)]. Adding "1" to each element $\{l_j\}$ in step (ii) thus ensures that adjacent $[l_j,1]$ elements in the shuffled extended series in Eq. (6) would not allow two or more separate removed segments to be merged leading to the formation of removed segments with longer average length μ and different form of their probability distribution compared to the original choice in step (i) of the algorithm.

Finally, the surrogate signal $\tilde{u}(i)$ is obtained by simultaneously scanning the original signal $u(i)$ and the binary series $g(i)$ from Eq. (7), removing the i-th element in $u(i)$ if $g(i)\equiv 0$ and concatenating the segments of the remaining data (Fig. 1).

In this study, we consider four different functional forms of the probability distribution $P(l)$ of segment lengths l, i.e., exponential, Gaussian, δ and power-law distributions, and we use the average length μ of the removed data segments as a common parameter to compare the effect of removed data segments with different distributions. For the exponential and δ distribution, the average length μ is sufficient to determine their probability distribution functions. The Gaussian and power-law distributions require additional parameters to be clearly defined, and thus, we need to introduce boundary conditions, so that these parameters can be related to the average length μ.

The functional form of the Gaussian distribution is

$$P(l) = \frac{1}{\sqrt{2\pi\sigma^2}} \exp\left[-\frac{(l-\mu)^2}{2\sigma^2}\right], \tag{8}$$

where μ is the average and σ is the standard deviation of the segment lengths l. Since with a fixed small σ, the Gaussian distribution is not much different from a δ distribution, and with a fixed large σ, the Gaussian distribution resembles an exponential distribution, we relate σ with μ in such a way, as a boundary condition, that the smallest segment $(l=1)$ can only be obtained (statistically) once in each realization, i.e., $P(l=1) \equiv 1/pN$, where N is the length of the original signal, and p is the percentage of data loss.

The functional form of a power-law distribution is given by

$$P(l) = al^k, \quad l \in [1, l_{\max}], \tag{9}$$

with $\int_1^{l_{\max}} P(l)dl = 1$ and the average length $\mu = \int_1^{l_{\max}} lP(l)dl$. Similar to the Gaussian distribution, we set the probability of the largest segment to $P(l=l_{\max}) \equiv 1/pN$. With these three boundary conditions, we can relate the three parameters a, k, and $l_{\max}$ in Eq. (9) with the average length μ.

In Fig. 2, we show examples of Gaussian and power-law distributions with different average lengths μ based on the criteria described above. Figure 3 shows examples of our procedure of data removal. The lengths of the removed segments were chosen to be exponentially distributed with different average length.

III. RESULTS

A. Effect of data loss on global scaling

Previously, we have studied the effect of data loss on the scaling behavior of long-range correlated signals by removing data segments with fixed length [83]. We have found that data loss in anticorrelated signals substantially changes the scaling behavior even when only 1% of data are removed. In contrast, the scaling behavior of (positively) correlated signals is practically not affected even when up to 50% of the data are removed. Data loss generally causes a crossover in the scaling behavior of anticorrelated signals. At the scales larger than the crossover the anticorrelated scaling behavior is completely destroyed and resembles uncorrelated behavior. This crossover is shifted to smaller scales with increasing percentage of removed data or decreasing length of the removed segments, indicating a stronger effect on the scaling behavior.

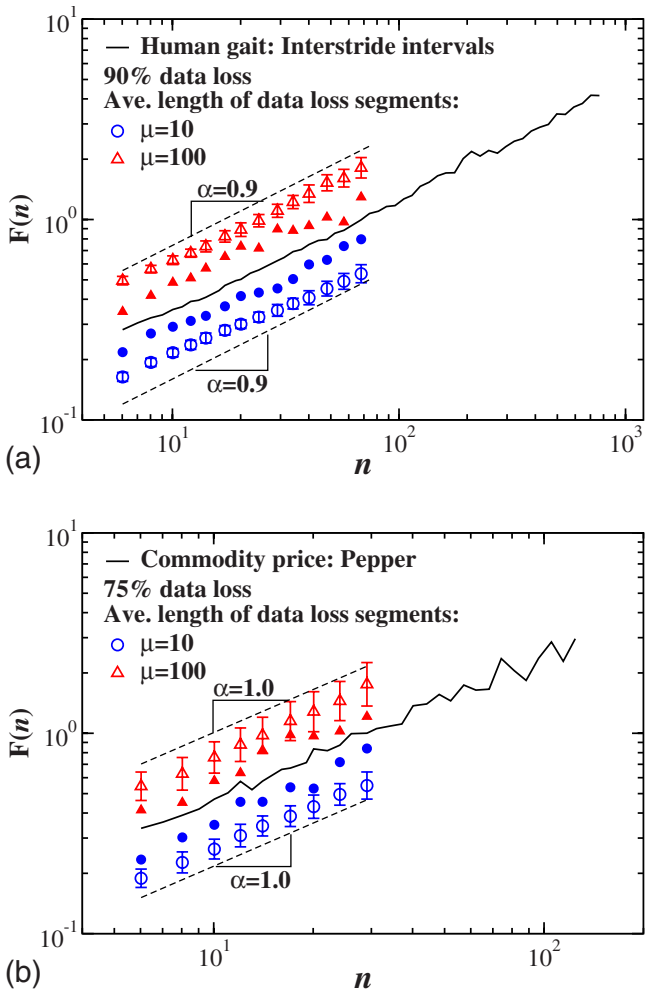

FIG. 6. (Color online) Two examples of the effect of extreme data loss: (a) interstride intervals of human gait and (b) annual prices of pepper in England in the period 1209–1914. Removing up to 90% of the gait intervals and up to 75% of the commodity data using segments of different average length μ does not significantly affect the global scaling behavior. Closed symbols represent a single realization and open symbols indicate the mean and standard deviations obtained from 100 realizations of randomly removing data segments. The lengths of the removed data segments are drawn from an exponential distribution.

In most cases, the length of data loss segments is not fixed but random and follows a certain distribution. How does the distribution of data loss segments influence the scaling behavior of correlated signals? In some cases, especially when archeological data are studied, the percentage of data loss can be extremely large (and can reach up to 95% [91]). Would the extreme data loss affect also positively correlated signals? To address these questions, in this section we study the effect of data loss caused by random removal of data segments that follow a certain distribution.

First, we consider the case in which the lengths of data loss segments are exponentially distributed. Following the approach introduced in Sec. II C, we first generate stationary correlated signals $u(i)$ with length $N=2^{20}$ and with scaling exponents α ranging from 0.1 to 1.5, and then randomly remove exponentially distributed data segments from the

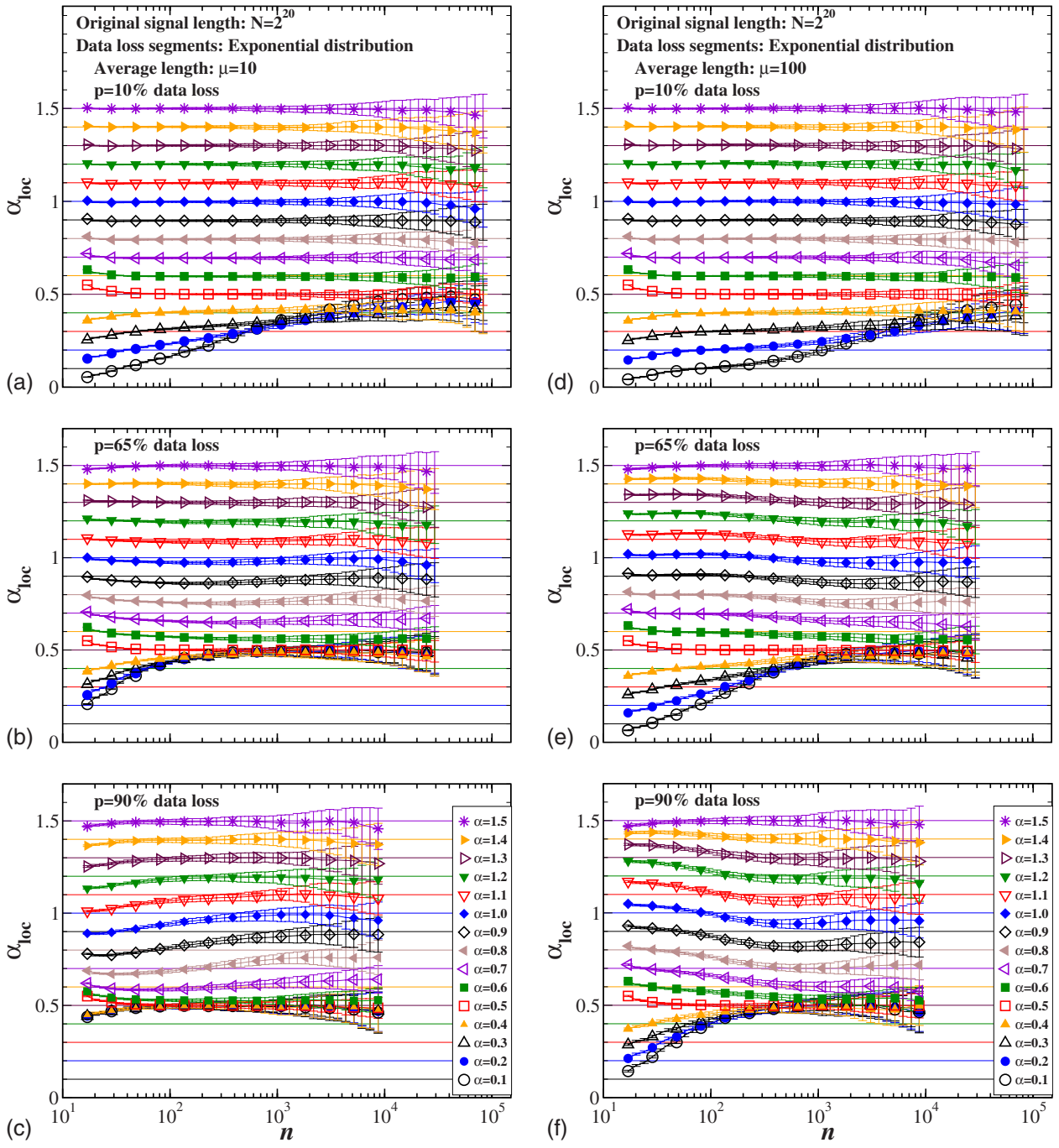

FIG. 7. (Color online) Effect of data loss on the local scaling behavior (quantified by local scaling exponent α_{loc}) of long-range power-law correlated signals. The symbols indicate average α_{loc} values obtained from 100 different realizations of surrogate signals with the same correlation exponent α and the error bars show the standard deviations. The more data are removed, the more the scaling exponent deviates from the original exponent. The data loss segments are exponentially distributed with average length $\mu=10$ [(a)–(c)] and $\mu=100$ [(d)–(f)]. For anticorrelated signals, the removal of larger segments ($\mu=100$) has less effect on the scaling behavior. For positively correlated signals, the deviations vary across scales, showing both overestimated and underestimated regions.

original signal $u(i)$ to obtain surrogate signals $\tilde{u}(i)$. As illustrated in Fig. 4, the rms fluctuation function $F(n)$ shows similar changes in the scaling behavior as observed in [83] where segments with a fixed length were removed from the original signal. (i) The scaling behavior of surrogate signals strongly depends on the scaling exponent α of the original signals. (ii) The anticorrelated signals substantially change their scaling behavior even if only 10% of the data are removed [Fig. 4(a)]. A crossover from anticorrelated to uncorrelated ($\alpha=0.5$) behavior appears at scale n_x due to data loss, i.e., at the scales larger than n_x, the anticorrelations in the original signals are completely destroyed. The crossover scale n_x is shifted to smaller scales with increasing percentage of lost data. (iii) In contrast, positively correlated signals show practically no changes for up to 65% of data loss [Fig. 4(b)]. Surprisingly, even with extreme data loss of up to 90%

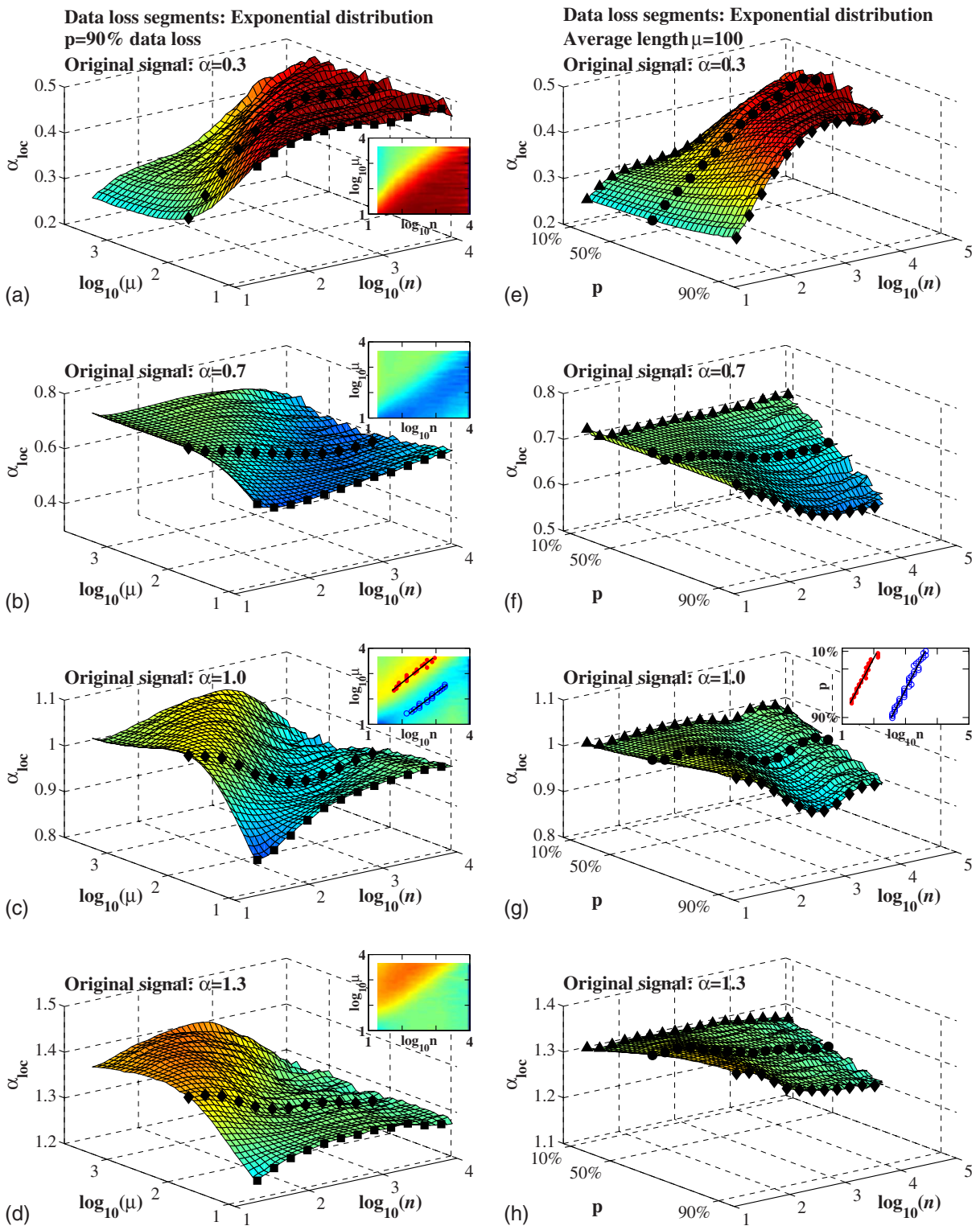

FIG. 8. (Color online) Effect of the average length μ of data loss segments (a)-(d) and effect of the percentage p of data loss (e)–(h) on the local scaling behavior in anticorrelated signals [(a), (e): $\alpha=0.3$] and positively correlated signals [(b), (f): $\alpha=0.7$; (c), (g): $\alpha=1.0$; (d), (h): $\alpha=1.3$]. For (a)–(d), $p=90\%$ of data are removed, and for (e)–(h), the average length of removed segments $\mu=100$. In all the cases, the removed segments are exponentially distributed, and the length of the original signals is $N=2^{20}$. To clearly see the power-law relation between the average length μ of removed segments and the scale n at which α_{loc} achieves the same value, the α_{loc} values are projected into the $\log_{10}\mu$-$\log_{10} n$ plane [see color-coded insets in figures (a)–(d)]. The symbols in the inset figures in (c) and (g) indicate the positions where α_{loc} values reach a maximum (red closed circle) or a minimum (blue open circle), and depict the shift of the overestimated and underestimated regions to large scales with increasing μ and decreasing p. The local scaling curves highlighted by black symbols correspond to the curves shown in Fig. 7 (rectangle: $\mu=10$, $p=90\%$; diamond: $\mu=100$, $p=90\%$; circle: $\mu=100$, $p=65\%$; triangle: $\mu=100$; $p=10\%$).

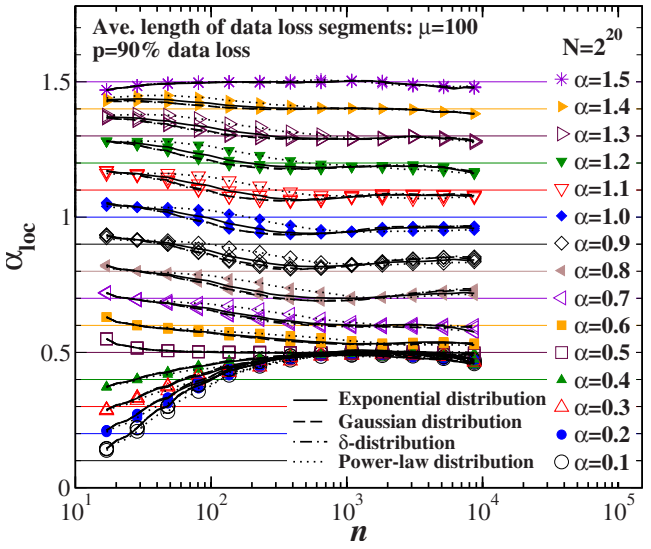

FIG. 9. (Color online) Effect of different kinds of distributions of data loss segments on the local scaling behavior. The power-law distributed data loss segments lead to higher values of α_{loc} for positively correlated signals and lower values for anticorrelated signals compared to the other distributions. There is no difference between Gaussian and δ-distributed segments which yield slightly lower α_{loc} values than exponentially distributed signals. For anticorrelated signals, exponentially, Gaussian and δ-distributed segments lead to identical α_{loc} values whereas the power-law distribution yields slightly lower local scaling exponents.

of the signal the scaling behavior is still practically preserved, exhibiting a slightly lower exponent α (waker correlations)—an effect which is less pronounced with increasing values of α [see Fig. 4(b)].

Next, we consider the case in which the length of the original signal is much shorter ($N=4000$), as illustrated in Fig. 5. We find that the scaling behavior of both anticorrelated and positively correlated signals with extreme data loss change in the same way as we observed in Fig. 4 (where $N=2^{20}$). In addition, we find (see Fig. 5) that when increasing the average length μ of the data loss segments, the scaling behavior of the surrogate signals deviates less from the original scaling behavior. Thus, removing the same percentage of the data using longer (and fewer) segments has a lesser impact on the scaling behavior of both positively correlated and anticorrelated signals compared to removing segments with smaller average length μ.

To show how missing data segments affect correlations in real-world signals, we consider two examples of complex scale-invariant dynamics: (i) human gait as a representative of integrated physiologic systems under neural control with multiple-component feedback interactions [Fig. 6(a)], and (ii) commodity price fluctuations from England across several centuries reflecting complex economic and social interactions [Fig. 6(b)]. In agreement with our tests on surrogate signals shown in Figs. 4 and 5, our analyses of real data confirm the observation that even extreme data loss of up to 90% does not significantly affect the global scaling behavior of positively correlated ($\alpha > 0.5$) signals.

B. Properties of removed data segments: Effect of data loss on local scaling

To reveal in greater detail the effect of data loss, we investigate the local scaling behavior of the $F(n)$ curves by fitting $F(n)$ locally in a window of size $w=3$ log 2. We determine the local scaling exponent α_{loc} at different scales n

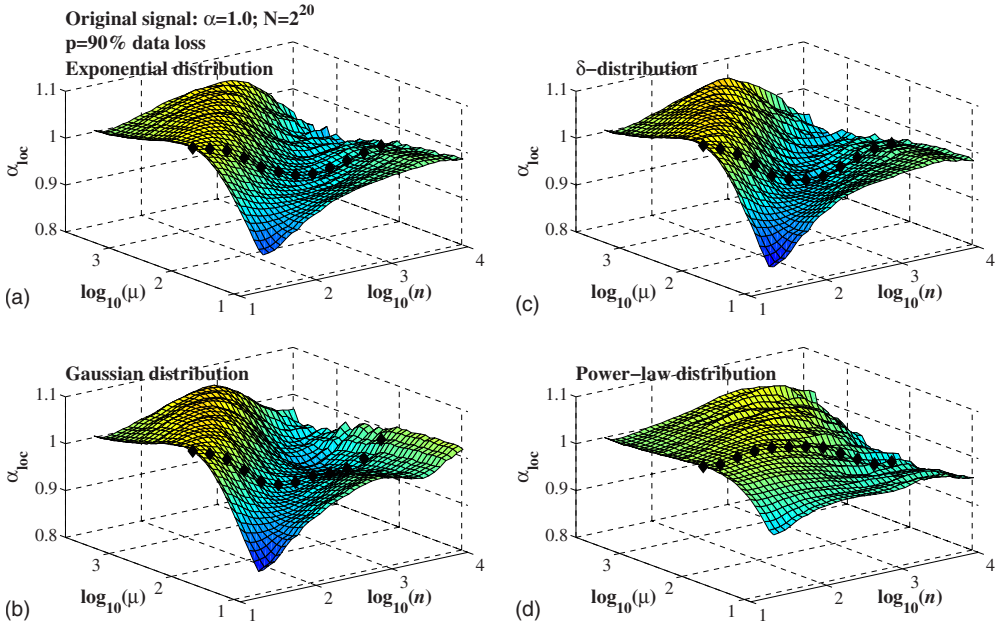

FIG. 10. (Color online) Effect of the average length μ of data loss segments on the local scaling behavior in long-range correlated signal with $\alpha=1.0$. The length of the data loss segments are (a) exponentially distributed, (b) Gaussian distributed, (c) δ distributed, and (d) power-law distributed. In all the cases, $p=90\%$ of data are removed, and the length of the original signals is $N=2^{20}$. The behavior of how α_{loc} changes with μ is similar for exponential, Gaussian and δ distribution, while the power-law distribution shows less variations. The local scaling curves highlighted by black symbols correspond to the curves shown in Fig. 9.

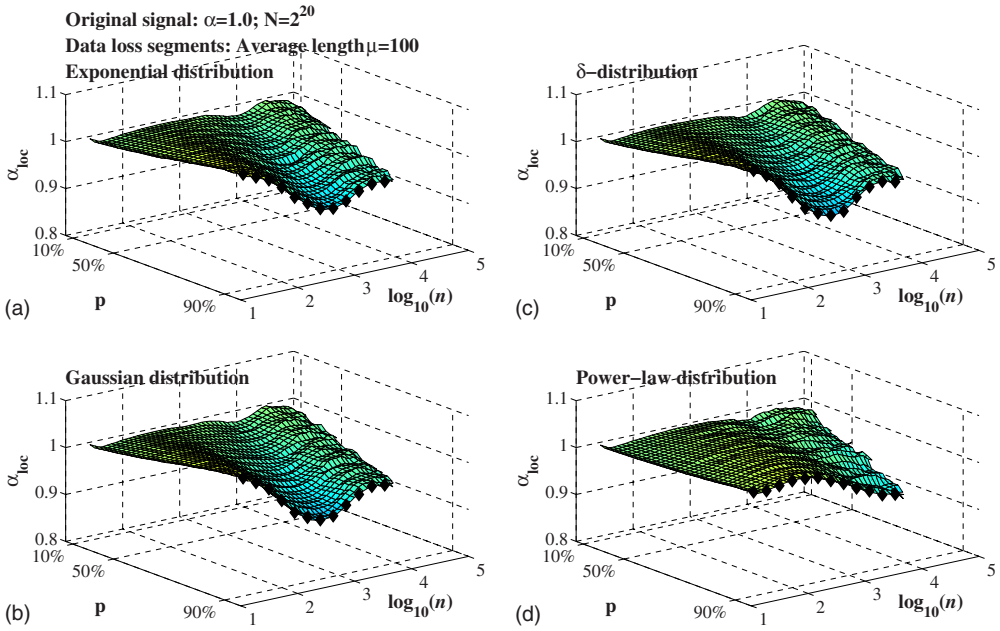

FIG. 11. (Color online) Effect of the percentage p of data loss on the local scaling behavior in long-range correlated signal with $\alpha=1.0$. The length of the data loss segments are (a) exponentially distributed, (b) Gaussian distributed, (c) δ distributed, and (d) power-law distributed. In all the cases, the average length of removed segments $\mu=100$, and the length of the original signals $N=2^{20}$. Similar to Fig. 10, the exponential, Gaussian and δ distributions show similar changes in α_{loc} with p, while the power-law distribution shows less variations. The local scaling curves highlighted by black symbols correspond to the curves shown in Fig. 9.

by moving the window w in small steps of size $\Delta=\frac{1}{4}\log 2$ starting at $n=4$.

In Fig. 7, we show α_{loc} for 10%, 65%, and 90% of data loss, and the average length of the data loss segments is $\mu=10$ (cf. Figure 4). The scaling behavior of anticorrelated signals shows systematic deviations from the original behavior: the stronger the anticorrelations, the faster is the decay of α_{loc} toward 0.5 (uncorrelated behavior). The deviations are stronger when more data were removed from the original signal. Note that when 90% of the data are removed, the correlation properties of originally anticorrelated signals are completely destroyed [Fig. 7(c)], because there are practically no consecutive data points of the original signals preserved in the surrogates when $\mu=10$ and $p=90\%$ (see Sec. III C and Eq. (10)). When increasing the average length of the removed segments from $\mu=10$ to 100 (Fig. 7), the scaling behavior of anticorrelated signals is less affected and $\alpha_{loc}=0.5$ is reached at larger scales.

For positively correlated signals ($0.5<\alpha<1.5$), the effect of data loss is more complex. The local scaling exponents show significant and systematic deviations from the original scaling behavior not observed in the rms fluctuation functions $F(n)$ in Fig. 4(b). The deviations from the original scaling behavior are more pronounced for a higher percentage of data loss and vary across scales. For small average length [$\mu=10$, Figs. 7(a)–7(c)], the local scaling exponent is underestimated at small scales and gradually recovers to the original scaling behavior at larger scales. For a larger average length of removal data segments [$\mu=100$, Figs. 7(d)–7(f)], we find overestimated regions at small scales and underestimated regions at large scales. The overestimation of the local scaling behavior is more pronounced for stronger positively correlated signals, while the underestimation is more pronounced for weaker positively correlated signals.

An interesting phenomenon seen in Fig. 7 is that for anticorrelated signals the scale at which α_{loc} reaches 0.5 (uncorrelated behavior) is shifted toward smaller scales with increasing percentage of data loss. Similarly, for positively correlated signals, the overestimated and underestimated regions are also shifted toward smaller scales, when a higher percentage of data is removed. This phenomenon occurs in both cases $\mu=10$ and 100.

To understand precisely how the two parameters—the average length μ of the data loss segments and the percentage p of data loss—influence changes in the local scaling behavior in Figs. 8(a)–8(d) we show how α_{loc} changes with the average length μ of the removed segments. For anticorrelated signals, the scale at which α_{loc} reaches 0.5 monotonically increases and shows a power-law relationship with μ [Fig. 8(a)]. For positively correlated signals, as shown in Figs. 8(b)–8(d), the overestimated regions at small scales as well as the underestimated regions at large scales are shifted to higher scales with increasing μ. This shift in the local scaling behavior also follows a power law with average length μ [Fig. 8(c), inset].

In Figs. 8(e)–8(h), we show how the percentage p of data loss influence changes in the local scaling behavior. For a fixed average length $\mu=100$, we find that the deviation from the original scaling behavior is more pronounced for higher values of p in both anticorrelated and positively correlated signals, as also observed in Fig. 7. The scaling behavior of positively correlated signals also shows overestimated regions at small scales and underestimated regions at large scales [Figs. 8(f)–8(h)], although not as clear as in Figs. 8(b)–8(d). Both regions are shifted to larger scales with de-

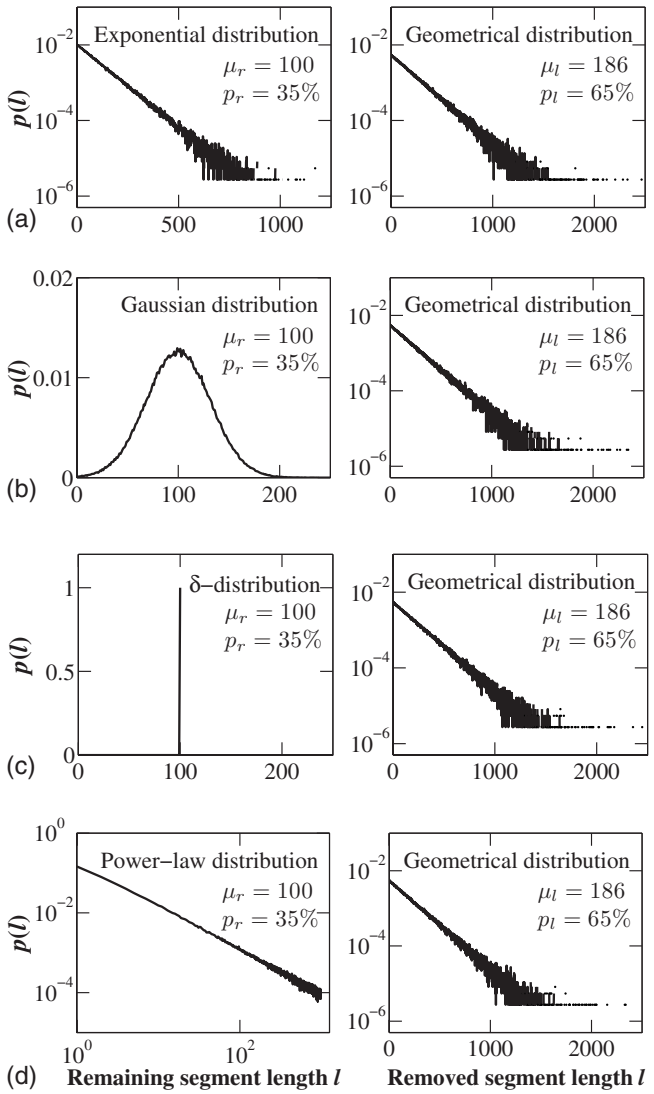

FIG. 12. The distributions of remaining data segments (left column) and corresponding distributions of data loss segments (right column). The remaining data segments follow (a) exponential, (b) power law, (c) Gaussian, and (d) δ distribution with average length μ_r=100 and 35% of data remaining. The data loss segments are always geometrically distributed independent of the distributions of remaining segments. Note that, the average lengths are practically the same as estimated from Eq. (10).

creasing percentage of data loss as illustrated in the inset in Fig. 8(g).

To understand whether different functional forms of distributions of data loss segments have different effects on the scaling behavior, we repeated the same tests with three other kinds of distributions: a Gaussian distribution, a δ distribution (i.e., segments have fixed length) and a power-law distribution. We find that all three kinds of distributions show similar deviations from the original local scaling behavior as reported above for exponentially distributed data loss segments. However, for power law distributed segments lengths, the estimated local scaling exponents are generally higher (lower) across scales for positively (anti)correlated signals [Fig. 9]. When increasing the average length μ of the removed data segments or increasing the percentage p of data loss, the power-law distribution shows less variations than the other three kinds of distributions [Figs. 10 and 11].

C. Properties of remaining data segments: Effect of data loss on local scaling

In the previous section, we tested the effect of data loss by specifying the distribution and average length of *removed* segments. In this section, we study the effect of data loss by specifying the distribution and average length of *remaining* data segments. The results obtained by focusing on the properties of remaining data segments are different from what was shown above and will lead to a better understanding of the effect of data loss on the scaling behavior of long-range correlated signals.

The approach to generate the appropriate surrogate signals with different properties of remaining data segments is similar to the one described in Sec. II C, except that now the binary series $g(i)$ are obtained according to the parameters of the remaining data segments, and the surrogate signals $\tilde{u}(i)$ are generated by removing the i-th data point in the original signal $u(i)$ if $g(i)=1$, and preserving the i-th data point if $g(i)=0$. The relation between the average length of data loss segments (μ_l) and remaining data segments (μ_r) can be derived as follows:

Let the length of the original signal be N. If p_l is the percentage of data loss, the amount of data loss is given by $N_l=p_lN$, and the amount of remaining data is given by $N_r=p_rN=(1-p_l)N$. If μ_l is the average length of the lost data segments, the number of lost segments is approximately given by $n_l \approx N_l/\mu_l$. The number of remaining data segments is approximately equal to the number of data loss segments, i.e., $n_r \approx n_l$. Hence, the average length of the remaining data segments is

$$\mu_r \approx \frac{N_r}{n_r} \approx \frac{(1-p_l)}{p_l}\mu_l. \tag{10}$$

Note that the lengths of data loss segments are always geometrically distributed due to the shuffling procedure in our segmentation approach (see Sec. II C and Fig. 12).

We find similar changes in the scaling behavior as observed in Fig. 7 where the distribution of removed segment lengths was specified. As illustrated in Fig. 13 where the lengths of remaining segments are exponentially distributed, the local scaling behavior of anticorrelated surrogate signals deviate monotonically from original behavior toward uncorrelation at larger scales. While the local scaling exponents of positively correlated surrogate signals vary across scales, showing both overestimated and underestimated regions. These regions as well as the scales at which the anticorrelated signals reach α_{loc}=0.5 are also shifted toward larger scales when the average length of remaining segments μ_r increases. However, in contrast to what was observed in Fig. 7, there is no shift to smaller scales with increasing percentage of data loss. Note that, according to Eq. (10), an average length μ_r=10 of remaining segments and a percentage p_r =10% of remaining data [as shown in Fig. 13(c)], corresponds to an average length μ_l=90 of removed segments and

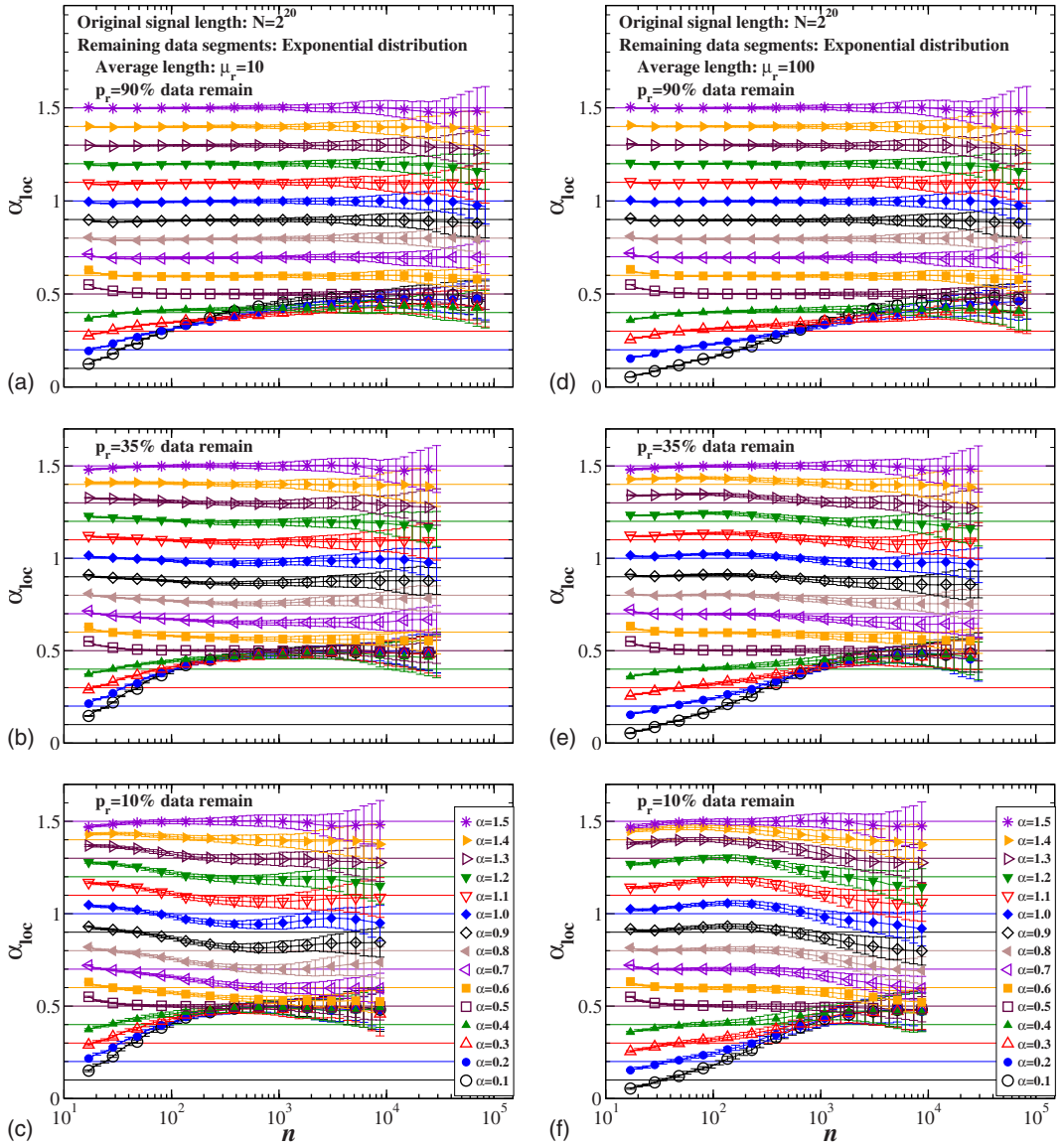

FIG. 13. (Color online) Effect of data loss on the local scaling behavior of long-range correlated signals. The lengths of the remaining data segments are exponentially distributed with average length $\mu_r=10$ [(a)–(c)] and $\mu_r=100$ [(d)–(f)]. The symbols indicate average α_{loc} values obtained from 100 different realizations of surrogate signals with the same correlation exponent α, and the error bars show the standard deviations. The more data are removed, the more the scaling exponent deviates from the original exponent. For anticorrelated signals, the removal of larger segments ($\mu_r=100$) has less effect on the scaling behavior. For positively correlated signals, the deviations vary across scales, showing both overestimated and underestimated regions.

a percentage $p_l=90\%$ of removed data. Thus the local scaling behavior observed in Fig. 13(c) is vary similar to Fig. 7(g) (where $\mu_l=100$ and $p_l=90\%$), and Fig. 13(d) ($\mu_r=100$, $p_r=90\%$, and correspondingly $\mu_l=11$, $p_l=10\%$) is similar to Fig. 7(a) ($\mu_l=10$, $p_l=10\%$).

In Figs. 14(a)–14(d), we show how the local scaling behavior changes with the average length μ_r of remaining segments. Similar to Figs. 8(a)–8(d) where the distribution of removed segments was specified, the variation in the local scaling behavior of positively correlated signals also shows overestimated regions at smaller scales followed by underestimated regions at larger scales. Both regions are shifted to larger scales, when the average length of remaining segments increases, forming a power-law relationship between the shift in the local scaling behavior and μ_r [Fig. 14(c)]. For anticorrelated signals the local scaling behavior also shows a power-law relationship between the scale at which α_{loc} reaches 0.5 and the average length μ_r. Note that, according to Eq. (10), the α_{loc} curves from $\mu_r=8$ to 455 in Figs. 14(a)–14(d) correspond to $\mu_l=72$ to 4095 in Figs. 8(a)–8(d), thus the local scaling behavior in these two regions are very similar.

With increasing percentage p_r of remaining data, the deviation from the original scaling behavior becomes smaller [Figs. 14(e)–14(h)]. However, for anticorrelated signals, the scale at which α_{loc} reaches 0.5 does not depend on the percentage of data loss [Fig. 14(e)], in contrast to Fig. 8(e) where removed data segments were studied. Similarly, the

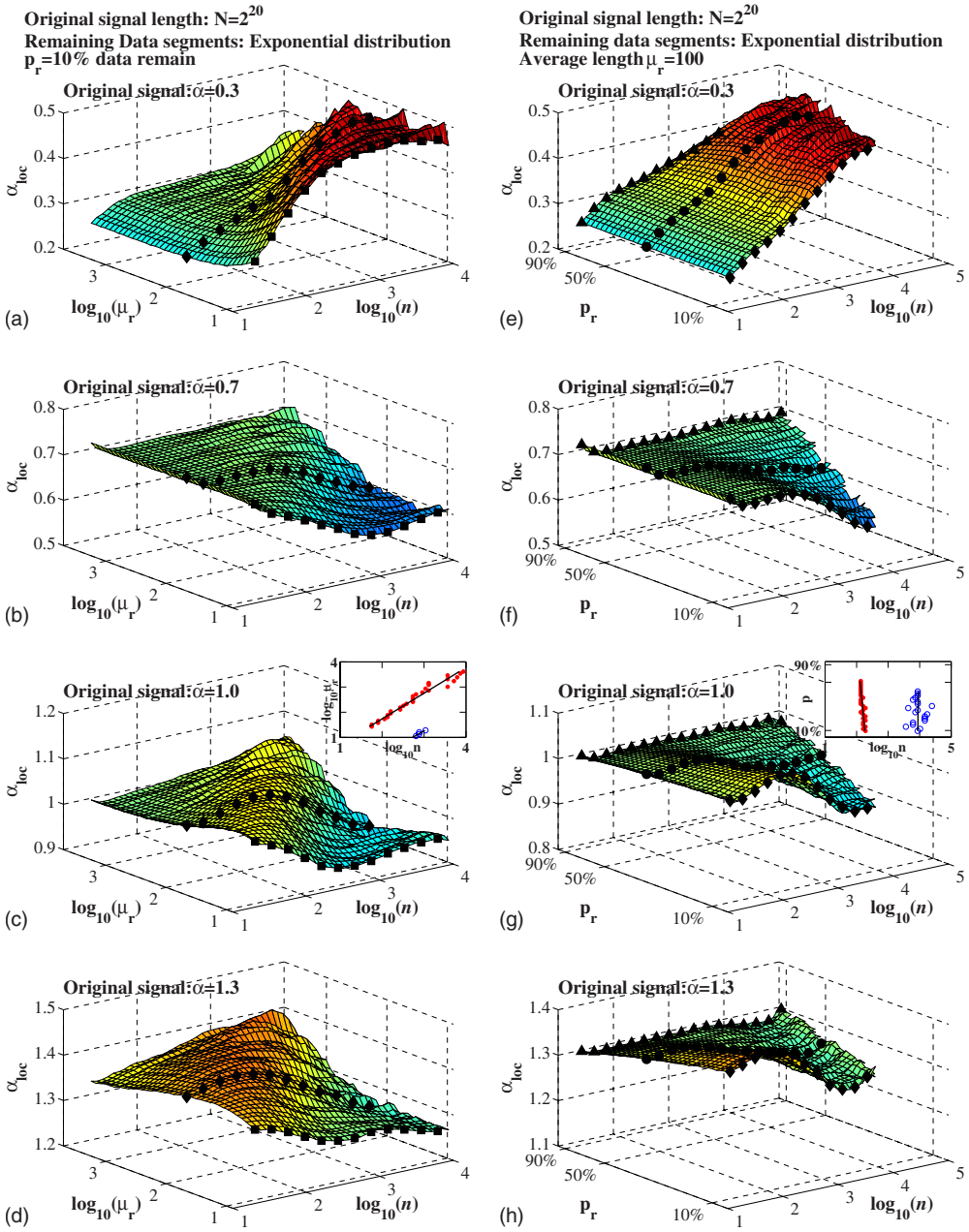

FIG. 14. (Color online) Effect of the average length μ_r of remaining data segments (a)–(d) and effect of the percentage p_r of remaining data (e)–(h) on the local scaling behavior in anticorrelated signals [(a), (e): α=0.3] and positively correlated signals [(b), (f): α=0.7; (c), (g): α=1.0; (d), (h): α=1.3]. For (a)–(d), p_r=10% of data are remained, and for (e)–(h), the average length of remaining segments μ_r=100. In all the cases, the remaining segments are exponentially distributed, and the length of the original signals $N=2^{20}$. The symbols in the inset figures in (c) and (g) indicate the positions where α_{loc} values reach a maximum (red closed circle) and a minimum (blue open circle), which show that the overestimated and underestimated regions are shifted to larger scales only with increasing μ_r and are not shifted with the percentage p_r of remaining data changes. The local scaling curves highlighted by black symbols correspond to the curves shown in Fig. 13 (rectangle: μ_r=10, p_r=10%; diamond: μ_r=100, p_r=10%; circle: μ_r=100, p_r=35%; triangle: μ_r=100; p_r=90%).

overestimated regions in positively correlated signals are also not shifted with the percentage of data loss [Figs. 14(f)–14(h), and compare to Fig. 8(f)–8(h)].

Next, we investigate how different kinds of distributions of remaining data segments influence the local scaling behavior. As illustrated in Fig. 15, the surrogate signals generated by using Gaussian or δ distribution have almost identical local scaling behavior and the most pronounced deviation from the original local scaling behavior, whereas the power-law distribution shows the smallest deviations. Note that, the local scaling exponent of surrogate signals generated by a δ-distribution jump to larger α_{loc} values at certain small scales when the scaling exponent of the original signal is 1.3, 1.4, and 1.5. This behavior is caused by the discontinuities in the surrogate signal at the transition points between remaining data segments, and since the remaining segments are of fixed length, the transition points occur periodically. If the segment length (μ=100 in Fig. 15) is an integral multiple of

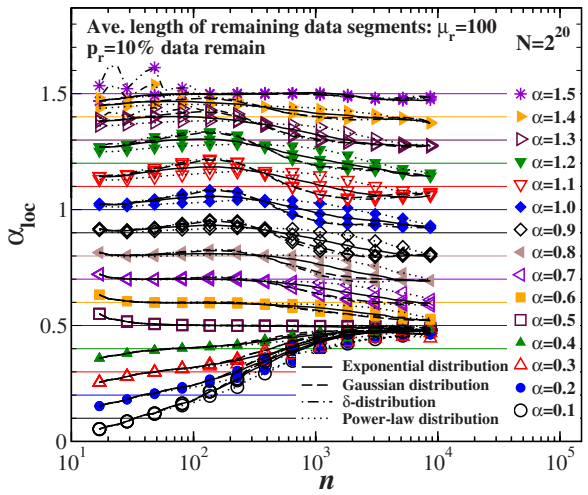

FIG. 15. (Color online) Effect of different kinds of distributions of remaining data segments on the local scaling behavior. The Gaussian and δ distributions lead to identical and most pronounced deviations from the original scaling behavior for both anticorrelated and positively correlated signals. The power-law distribution leads to lowest deviations for anticorrelated signals and a smoother behavior of α_{loc} versus μ_r, i.e., a less pronounced over and underestimation of the original scaling behavior for positively correlated signals. Interestingly, for positively correlated signals, all four kinds of distributions yield the same local scaling exponent α_{loc} at certain scale ($n \approx 300$ for $\mu_r = 100$). Note that in case of the δ-distribution, large jumps of α_{loc} values at small scales occur for original scaling exponents $\alpha = 1.3$ to 1.5 (see text for more details).

the size of the fitting boxes (scales) in the DFA algorithm (e.g., $n = 10, 20, 25, 50$), the transition points are not included in any fitting box and thus the rms fluctuation functions of the surrogate signals will be the same as in the original signals. In all other cases, the discontinuities inside the fitting box will cause larger rms fluctuation functions and lead to jumps in the local scaling exponents at certain scales $n \leq \mu_r$ as observed in Fig. 15.

In Fig. 16, we show how the local scaling curves of positively correlated signals change with the average length μ_r of remaining segments, which follow an exponential distribution [Fig. 16(a)], a Gaussian distribution [Fig. 16(b)], a δ distribution [Fig. 16(c)], and a power-law distribution [Fig. 16(d)]. The Gaussian and δ distributions lead to a similar local scaling behavior with regions of pronounced overestimation and underestimation which are shifted to larger scales for increasing values of μ_r. This shift is also observed in the case of the exponential distribution, however, the deviation from the original scaling behavior (overestimation/underestimation) is less pronounced. In contrast, the power-law distribution shows less variation in the local scaling behavior and does not lead to such distinct regions of overestimated and underestimated α_{loc} values. In addition, the local scaling curves do not show a clear dependency ("shift") with the average length of remaining segments μ_r.

The variation of the local scaling curves with the percentage p_r of remaining data for the four different distributions are presented in Fig. 17. Similar as shown in Fig. 14, the scale of most pronounced deviation from the original scaling behavior is independent of the percentage p_r of remaining data.

IV. SUMMARY AND CONCLUSION

In this paper, we studied the effect of extreme data loss on the DFA scaling behavior of long-range power-law correlated

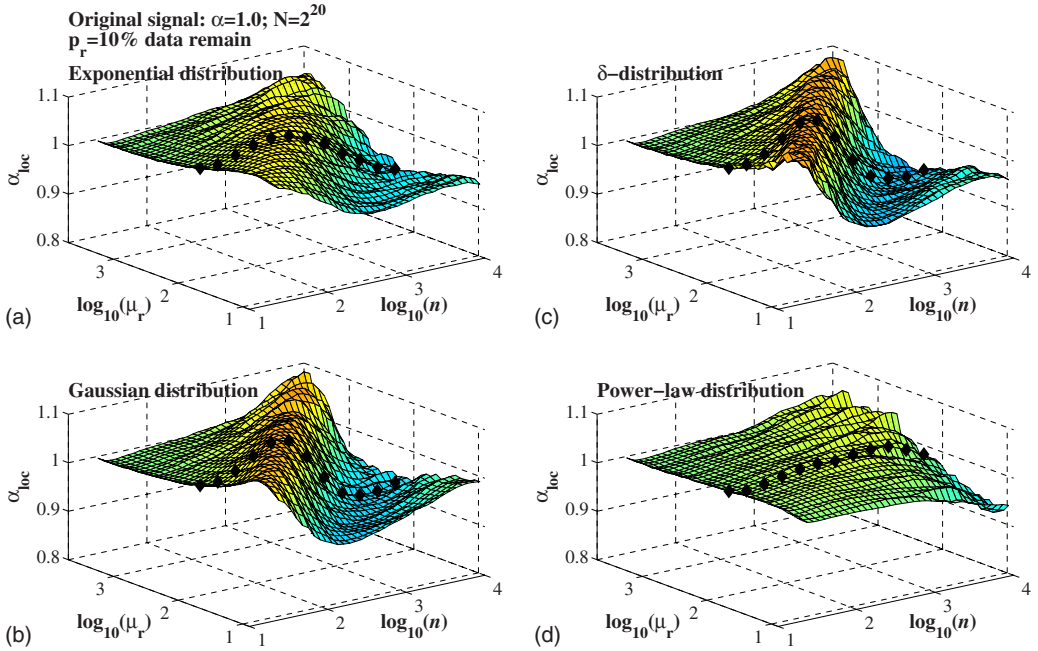

FIG. 16. (Color online) Effect of different distributions and the average length μ_r of remaining data segments on the local scaling behavior. In all the cases, $p_r = 10\%$ of data are remained, and the length of the original signals $N = 2^{20}$. The Gaussian and δ distribution lead to very similar behavior with most pronounced α_{loc} deviations and a clear shift with μ_r. In contrast, the power-law distribution shows no clear dependency of α_{loc} with μ_r. The local scaling curves highlighted by black symbols correspond to the curves shown in Fig. 15.

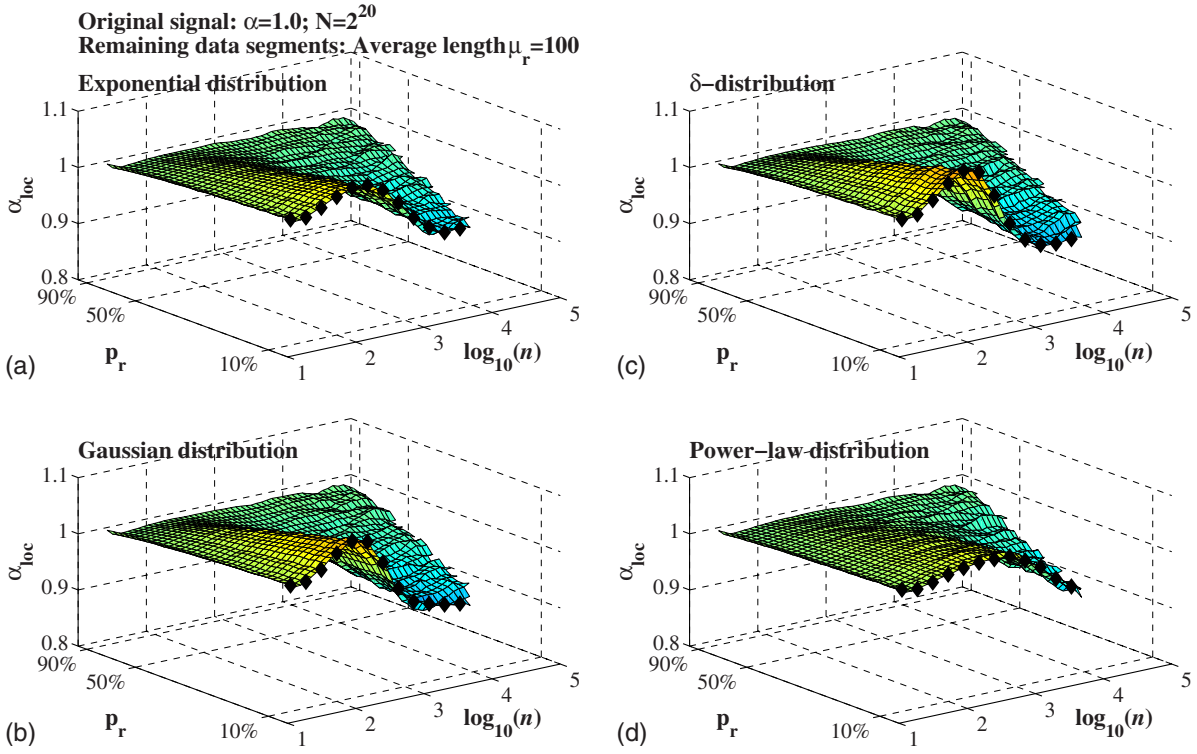

FIG. 17. (Color online) Effect of different distributions of remaining data segments and the percentage p_r of remaining data on the local scaling behavior. In all the cases, the average length of remaining segments $\mu_r=100$ and the length of the original signals $N=2^{20}$. The deviations from original scaling behavior are more pronounced for smaller percentages of remaining data. Note that the scale at which the most pronounced deviation is observed does not depend on p_r. The local scaling curves highlighted by black symbols correspond to the curves shown in Fig. 15.

signals. In order to simulate extreme data loss, often encountered in archeological and geological data, we developed a segmentation approach to generate correlated signals with randomly removed data segments. Using this approach, surrogate signals can be generated for different percentages of data loss, different average lengths and different distributions of removed/remaining data segments. We compared the difference between the DFA scaling behavior of original and surrogate signals by systematically changing the percentage of data loss and the average length of removed/remaining segments, and we also consider different functional forms of the distributions of removed/remaining segment lengths. We studied changes in the global scaling behavior as well as in the local scaling exponents to reveal subtle deviations across scales.

We find that anticorrelated signals are very sensitive to data loss. Even if only 10% of the data are removed, the scaling behavior of the surrogate signals changes dramatically, showing uncorrelated behavior at large scales. In contrast, positively correlated signals are more robust to data loss and no significant changes in the *global* scaling behavior are observed for up to 90% of data loss. However, in case of extreme data loss, we find significant and systematic deviations in the *local* scaling behavior which is overestimated at small scales and underestimated at large scales. Specifically, we find that for anticorrelated signals the scale at which the local scaling exponent α_{loc} reaches 0.5 shifts to larger scales with increasing the average length μ_l (or μ_r) of the removed (or remaining) segments, following a power-law relationship with μ_l (or μ_r). For positively correlated signals the regions of overestimation and underestimation of the local scaling exponent are also shifted to larger scales following a power law with increasing μ_l (or μ_r).

As expected, increasing the percentage of data loss leads to more pronounced deviations in the local scaling behavior. However, the variation in local scaling curves follows different rules if the properties of either removed segments or remaining segments are considered. When the average length μ_l of *removed* data segments is kept constant, for increasing percentage p_l of removed data, the deviations of both anticorrelated and positively correlated signals are shifted to smaller scales following a power law with p_l. When we focus on *remaining* data segments and keep their average length μ_r constant, the deviations become more pronounced with decreasing percentage p_r of remaining data, however, the deviations occur at the same scales.

This behavior can be explained by the relationship between removed and remaining data. In case of a fixed percentage of removed or remaining data, μ_l and μ_r are always directly proportional to each other [Eq. (10)] and therefore the deviations (and the shift of the most pronounced deviation) show a similar power-law relation with μ_l and μ_r, while fixing the average length of removed or remaining segments leads to two different scenarios: (i) fixing μ_l and changing p_l leads to changes in μ_r proportional to p_l; (ii) fixing μ_r and changing p_r leads to changes in μ_l proportional to p_r. Since

the scale of the most pronounced deviation from the original scaling behavior is shifted for scenario (i) where μ_r is changing and μ_l is fixed, but not scenario (ii) where μ_l is changing and μ_r is fixed, changes in μ_l do not contribute to the observed shift. Thus, we suggest that μ_r is the key parameter to determine the scales at which the scaling behavior is mostly influenced, whereas the percentage of data loss determines the extent of this influence.

Different distributions of the lengths of removed/remaining segments affect the local scaling behavior differently. For Gaussian and δ-distributed segment lengths, deviations are most pronounced and similar in extent, whereas power-law distributed segments show smallest deviations and a very different overall behavior when compare to exponential, Gaussian and δ-distributed segments.

In conclusion, our study shows that it is important to consider not only the percentage of data loss (removed/remaining data), but also the average length of remaining segments to identify the scales at which deviations from the original ("real") DFA scaling behavior is most pronounced. Therefore, when studying the scaling properties of signals with extreme data loss, the DFA results should be carefully interpreted to reveal the real scaling behavior.

ACKNOWLEDGMENTS

We thank the Brigham and Women's Hospital Biomedical Research Institute Fund, the Spanish Junta de Andalucia (Grant No. P06-FQM1858), Mitsubishi Chemical Corp., Japan, and the National Natural Science Foundation of China (Grant No. 60501003) for support.

[1] H. E. Stanley, Nature (London) **378**, 554 (1995).
[2] M. F. Shlesinger, Ann. N.Y. Acad. Sci. **504**, 214 (1987).
[3] L. S. Liebovitch, Adv. Chem. Ser. **235**, 357 (1994).
[4] P. Ch. Ivanov, L. A. N. Amaral, A. L. Goldberger, and H. E. Stanley, Europhys. Lett. **43**, 363 (1998).
[5] Y. Ashkenazy, J. Hausdorff, P. Ch. Ivanov, and H. E. Stanley, Physica A **316**, 662 (2002).
[6] J. B. Bassingthwaighte, L. Liebovitch, and B. J. West, *Fractal Physiology* (Oxford University Press, New York, 1994).
[7] M. Malik and A. Camm, *Heart Rate Variability* (Futura, Armonk, NY, 1995).
[8] H. E. Hurst, Trans. Am. Soc. Civ. Eng. **116**, 770 (1951).
[9] B. B. Mandelbrot and J. R. Wallis, Water Resour. Res. **5**, 321 (1969).
[10] R. L. Stratonovich, *Topics in the Theory of Random Noise* (Gordon and Breach, New York, 1981), Vol. I.
[11] C.-K. Peng, S. V. Buldyrev, S. Havlin, M. Simons, H. E. Stanley, and A. L. Goldberger, Phys. Rev. E **49**, 1685 (1994).
[12] M. Taqqu, V. Teverovsky, and W. Willinger, Fractals **3**, 785 (1995).
[13] C.-K. Peng, S. V. Buldyrev, A. L. Goldberger, S. Havlin, F. Sciortino, M. Simons, and H. E. Stanley, Nature (London) **356**, 168 (1992).
[14] C.-K. Peng, S. V. Buldyrev, A. L. Goldberger, S. Havlin, M. Simons, and H. E. Stanley, Phys. Rev. E **47**, 3730 (1993).
[15] S. V. Buldyrev, A. L. Goldberger, S. Havlin, C.-K. Peng, H. E. Stanley, and M. Simons, Biophys. J. **65**, 2673 (1993).
[16] S. M. Ossadnik, S. B. Buldyrev, A. L. Goldberger, S. Havlin, R. N. Mantegna, C.-K. Peng, M. Simons, and H. E. Stanley, Biophys. J. **67**, 64 (1994).
[17] H. E. Stanley, S. V. Buldyrev, A. L. Goldberger, S. Havlin, R. N. Mantegna, C.-K. Peng, and M. Simons, Nuovo Cimento Soc. Ital. Fis., D **16**, 1339 (1994).
[18] R. N. Mantegna, S. V. Buldyrev, A. L. Goldberger, S. Havlin, C.-K. Peng, M. Simons, and H. E. Stanley, Phys. Rev. Lett. **73**, 3169 (1994).
[19] S. Havlin, S. V. Buldyrev, A. L. Goldberger, R. N. Mantegna, S. M. Ossadnik, C.-K. Peng, M. Simon, and H. E. Stanley, Chaos, Solitons Fractals **6**, 171 (1995).
[20] C.-K. Peng, S. V. Buldyrev, A. L. Goldberger, S. Havlin, R. N. Mantegna, M. Simons, and H. E. Stanley, Physica A **221**, 180 (1995).
[21] S. Havlin, S. V. Buldyrev, A. L. Goldberger, R. N. Mantegna, C.-K. Peng, M. Simons, and H. E. Stanley, Fractals **3**, 269 (1995).
[22] R. N. Mantegna, S. V. Buldyrev, A. L. Goldberger, S. Havlin, C.-K. Peng, M. Simons, and H. E. Stanley, Phys. Rev. Lett. **76**, 1979 (1996).
[23] S. V. Buldyrev, N. V. Dokholyan, A. L. Goldberger, S. Havlin, C.-K. Peng, H. E. Stanley, and G. M. Viswanathan, Physica A **249**, 430 (1998).
[24] H. E. Stanley, S. V. Buldyrev, A. L. Goldberger, S. Havlin, C.-K. Peng, and M. Simons, Physica A **273**, 1 (1999).
[25] W. Li, P. Bernaola-Galvan, P. Carpena, and J. L. Oliver, Comput. Biol. Chem. **27**, 5 (2003).
[26] M. Hackenberg, P. Bernaola-Galvan, P. Carpena, and J. L. Oliver, J. Mol. Evol. **60**, 365 (2005).
[27] C.-K. Peng, S. Havlin, H. E. Stanley, and A. L. Goldberger, Chaos **5**, 82 (1995).
[28] K. K. L. Ho, G. B. Moody, C.-K. Peng, J. E. Mietus, M. G. Larson, D. Levy, and A. L. Goldberger, Circulation **96**, 842 (1997).
[29] M. Barbi, S. Chillemi, A. Di Garbo, R. Balocchi, C. Carpeggiani, M. Emdin, C. Michelassi, and E. Santarcangelo, Chaos, Solitons Fractals **9**, 507 (1998).
[30] P. Ch. Ivanov, A. Bunde, L. A. N. Amaral, S. Havlin, J. Fritsch-Yelle, R. M. Baevsky, H. E. Stanley, and A. L. Goldberger, Europhys. Lett. **48**, 594 (1999).
[31] S. M. Pikkujämsä, T. H. Mäkikallio, L. B. Sourander, I. J. Räihä, P. Puukka, J. Skyttä, C.-K. Peng, A. L. Goldberger, and H. V. Huikuri, Circulation **100**, 393 (1999).
[32] Y. Ashkenazy, M. Lewkowicz, J. Levitan, S. Havlin, K. Saermark, H. Moelgaard, and P. E. B. Thomsen, Fractals **7**, 85 (1999).
[33] P. A. Absil, R. Sepulchre, A. Bilge, and P. Gerard, Physica A **272**, 235 (1999).
[34] D. Toweill, K. Sonnenthal, B. Kimberly, S. Lai, and B. Goldstein, Crit. Care Med. **28**, 2051 (2000).

[35] A. Bunde, S. Havlin, J. W. Kantelhardt, T. Penzel, J.-H. Peter, and K. Voigt, Phys. Rev. Lett. **85**, 3736 (2000).
[36] T. Laitio, H. Huikuri, E. Kentala, T. Makikallio, J. Jalonen, H. Helenius, K. Sariola-Heinonen, S. Yli-Mayry, and H. Scheinin, Anesthesiology **93**, 69 (2000).
[37] Y. Ashkenazy, P. Ch. Ivanov, S. Havlin, C.-K. Peng, Y. Yamamoto, A. L. Goldberger, and H. E. Stanley, Comput. Cardiol. **27**, 139 (2000).
[38] Y. Ashkenazy, P. Ch. Ivanov, S. Havlin, C.-K. Peng, A. L. Goldberger, and H. E. Stanley, Phys. Rev. Lett. **86**, 1900 (2001).
[39] P. Ch. Ivanov, L. A. N. Amaral, A. L. Goldberger, S. Havlin, M. G. Rosenblum, H. E. Stanley, and Z. Struzik, Chaos **11**, 641 (2001).
[40] J. W. Kantelhardt, Y. Ashkenazy, P. Ch. Ivanov, A. Bunde, S. Havlin, T. Penzel, J.-H. Peter, and H. E. Stanley, Phys. Rev. E **65**, 051908 (2002).
[41] R. Karasik, N. Sapir, Y. Ashkenazy, P. Ch. Ivanov, I. Dvir, P. Lavie, and S. Havlin, Phys. Rev. E **66**, 062902 (2002).
[42] P. Ch. Ivanov, Z. Chen, K. Hu, and H. E. Stanley, Physica A **344**, 685 (2004).
[43] R. Bartsch, T. Hennig, A. Heinen, S. Heinrichs, and P. Maass, Physica A **354**, 415 (2005).
[44] D. T. Schmitt and P. Ch. Ivanov, Am. J. Physiol. Regul. Integr. Comp. Physiol. **293**, R1923 (2007).
[45] D. T. Schmitt, P. K. Stein, and P. Ch. Ivanov, IEEE Trans. Biomed. Eng. **56**, 1564 (2009).
[46] T. H. Mäkikallio, J. Koistinen, L. Jordaens, M. P. Tulppo, N. Wood, B. Golosarsky, C.-K. Peng, A. L. Goldberger, and H. V. Huikuri, Am. J. Cardiol. **83**, 880 (1999).
[47] J. M. Hausdorff, C.-K. Peng, Z. Ladin, J. Y. Wei, and A. L. Goldberger, J. Appl. Physiol. **78**, 349 (1995).
[48] R. Bartsch, M. Plotnik, J. W. Kantelhardt, S. Havlin, N. Giladi, and J. M. Hausdorff, Physica A **383**, 455 (2007).
[49] P. Ch. Ivanov, Q. D. Y. Ma, R. P. Bartsch, J. M. Hausdorff, L. A. N. Amaral, V. Schulte-Frohlinde, H. E. Stanley, and M. Yoneyama, Phys. Rev. E **79**, 041920 (2009).
[50] K. Hu, P. Ch. Ivanov, Z. Chen, M. F. Hilton, H. E. Stanley, and S. A. Shea, Physica A **337**, 307 (2004).
[51] P. Ch. Ivanov, K. Hu, M. F. Hilton, S. A. Shea, and H. E. Stanley, Proc. Natl. Acad. Sci. U.S.A. **104**, 20702 (2007).
[52] P. Ch. Ivanov, IEEE Eng. Med. Biol. Mag. **26**, 33 (2007).
[53] K. Hu, F. A. J. L. Scheer, P. Ch. Ivanov, R. M. Buijs, and S. A. Shea, Neuroscience **149**, 508 (2007).
[54] S. Bahar, J. Kantelhardt, A. Neiman, H. Rego, D. Russell, L. Wilkens, A. Bunde, and F. Moss, Europhys. Lett. **56**, 454 (2001).
[55] P. A. Varotsos, N. V. Sarlis, and E. S. Skordas, Phys. Rev. E **67**, 021109 (2003).
[56] P. A. Varotsos, N. V. Sarlis, and E. S. Skordas, Chaos **19**, 023114 (2009).
[57] K. Ivanova and M. Ausloos, Physica A **274**, 349 (1999).
[58] E. Koscielny-Bunde, A. Bunde, S. Havlin, H. E. Roman, Y. Goldreich, and H.-J. Schellnhuber, Phys. Rev. Lett. **81**, 729 (1998).
[59] E. Koscielny-Bunde, H. Roman, A. Bunde, S. Havlin, and H. Schellnhuber, Philos. Mag. B **77**, 1331 (1998).
[60] P. Talkner and R. O. Weber, Phys. Rev. E **62**, 150 (2000).
[61] A. Bunde, S. Havlin, E. Koscielny-Bunde, and H.-J. Schellnhuber, Physica A **302**, 255 (2001).
[62] R. A. Monetti, S. Havlin, and A. Bunde, Physica A **320**, 581 (2003).
[63] A. Bunde, J. F. Eichner, J. W. Kantelhardt, and S. Havlin, Phys. Rev. Lett. **94**, 048701 (2005).
[64] A. Montanari, R. Rosso, and M. S. Taqqu, Water Resour. Res. **36**, 1249 (2000).
[65] C. Matsoukas, S. Islam, and I. Rodriguez-Iturbe, J. Geophys. Res. **105**, 29165 (2000).
[66] Y. H. Liu, P. Cizeau, M. Meyer, C.-K. Peng, and H. E. Stanley, Physica A **245**, 437 (1997).
[67] N. Vandewalle and M. Ausloos, Physica A **246**, 454 (1997).
[68] N. Vandewalle and M. Ausloos, Phys. Rev. E **58**, 6832 (1998).
[69] Y. Liu, P. Gopikrishnan, P. Cizeau, M. Meyer, C.-K. Peng, and H. E. Stanley, Phys. Rev. E **60**, 1390 (1999).
[70] I. M. Janosi, B. Janecsko, and I. Kondor, Physica A **269**, 111 (1999).
[71] M. Ausloos, N. Vandewalle, P. Boveroux, A. Minguet, and K. Ivanova, Physica A **274**, 229 (1999).
[72] M. Raberto, E. Scalas, G. Cuniberti, and M. Riani, Physica A **269**, 148 (1999).
[73] N. Vandewalle, M. Ausloos, and P. Boveroux, Physica A **269**, 170 (1999).
[74] P. Grau-Carles, Physica A **287**, 396 (2000).
[75] M. Ausloos, Physica A **285**, 48 (2000).
[76] M. Ausloos and K. Ivanova, Physica A **286**, 353 (2000).
[77] M. Ausloos and K. Ivanova, Phys. Rev. E **63**, 047201 (2001).
[78] M. Ausloos and K. Ivanova, Int. J. Mod. Phys. C **12**, 169 (2001).
[79] P. Ch. Ivanov, A. Yuen, B. Podobnik, and Y. Lee, Phys. Rev. E **69**, 056107 (2004).
[80] C. Metzner, C. Raupach, D. Paranhos Zitterbart, and B. Fabry, Phys. Rev. E **76**, 021925 (2007).
[81] J. W. Kantelhardt, S. Havlin, and P. Ch. Ivanov, Europhys. Lett. **62**, 147 (2003).
[82] K. Hu, P. Ch. Ivanov, Z. Chen, P. Carpena, and H. E. Stanley, Phys. Rev. E **64**, 011114 (2001).
[83] Z. Chen, P. Ch. Ivanov, K. Hu, and H. E. Stanley, Phys. Rev. E **65**, 041107 (2002).
[84] Z. Chen, K. Hu, P. Carpena, P. Bernaola-Galvan, H. E. Stanley, and P. Ch. Ivanov, Phys. Rev. E **71**, 011104 (2005).
[85] L. Xu, P. Ch. Ivanov, K. Hu, Z. Chen, A. Carbone, and H. E. Stanley, Phys. Rev. E **71**, 051101 (2005).
[86] J. Alvarez-Ramirez, E. Rodriguez, and J. Echeverria, Physica A **354**, 199 (2005).
[87] R. Nagarajan, Physica A **363**, 226 (2006).
[88] A. Bashan, R. Bartsch, J. W. Kantelhardt, and S. Havlin, Physica A **387**, 5080 (2008).
[89] J. W. Kantelhardt, E. Koscielny-Bunde, H. H. Rego, S. Havlin, and A. Bunde, Physica A **295**, 441 (2001).
[90] H. A. Makse, S. Havlin, M. Schwartz, and H. E. Stanley, Phys. Rev. E **53**, 5445 (1996).
[91] P. Temin, Explor. Econ. Hist. **39**, 46 (2002).

Effect of extreme data loss on long-range correlated and anticorrelated signals quantified by detrended fluctuation analysis

By: Ma, QDY (Ma, Qianli D. Y.)[1,2,3]; Bartsch, RP (Bartsch, Ronny P.)[1,2]; Bernaola-Galvan, P (Bernaola-Galvan, Pedro)[4]; Yoneyama, M (Yoneyama, Mitsuru)[5]; Ivanov, PC (Ivanov, Plamen Ch.)[1,2,4,6,7]

View ResearcherID and ORCID

PHYSICAL REVIEW E
Volume: 81 **Issue:** 3 **Part:** 1
Article Number: 031101
DOI: 10.1103/PhysRevE.81.031101
Published: MAR 2010
Document Type: Article
View Journal Impact

Abstract

Detrended fluctuation analysis (DFA) is an improved method of classical fluctuation analysis for nonstationary signals where embedded polynomial trends mask the intrinsic correlation properties of the fluctuations. To better identify the intrinsic correlation properties of real-world signals where a large amount of data is missing or removed due to artifacts, we investigate how extreme data loss affects the scaling behavior of long-range power-law correlated and anticorrelated signals. We introduce a segmentation approach to generate surrogate signals by randomly removing data segments from stationary signals with different types of long-range correlations. The surrogate signals we generate are characterized by four parameters: (i) the DFA scaling exponent alpha of the original correlated signal u(i), (ii) the percentage p of the data removed from u(i), (iii) the average length mu of the removed (or remaining) data segments, and (iv) the functional form P(l) of the distribution of the length l of the removed (or remaining) data segments. We find that the global scaling exponent of positively correlated signals remains practically unchanged even for extreme data loss of up to 90%. In contrast, the global scaling of anticorrelated signals changes to uncorrelated behavior even when a very small fraction of the data is lost. These observations are confirmed on two examples of real-world signals: human gait and commodity price fluctuations. We further systematically study the local scaling behavior of surrogate signals with missing data to reveal subtle deviations across scales. We find that for anticorrelated signals even 10% of data loss leads to significant monotonic deviations in the local scaling at large scales from the original anticorrelated to uncorrelated behavior. In contrast, positively correlated signals show no observable changes in the local scaling for up to 65% of data loss, while for larger percentage of data loss, the local scaling shows overestimated regions (with higher local exponent) at small scales, followed by underestimated regions (with lower local exponent) at large scales. Finally, we investigate how the scaling is affected by the average length, probability distribution, and percentage of the remaining data segments in comparison to the removed segments. We find that the average length mu(r) of the remaining segments is the key parameter which determines the scales at which the local scaling exponent has a maximum deviation from its original value. Interestingly, the scales where the maximum deviation occurs follow a power-law relationship with mu(r). Whereas the percentage of data loss determines the extent of the deviation. The results presented in this paper are useful to correctly interpret the scaling properties obtained from signals with extreme data loss.

Keywords

KeyWords Plus: NONCODING DNA-SEQUENCES; POWER-LAW CORRELATIONS; HEARTBEAT TIME-SERIES; EUR EXCHANGE-RATES; LINGUISTIC FEATURES; STATISTICAL PHYSICS; CARDIAC DYNAMICS; TEMPERATURE-FLUCTUATIONS; NONLINEAR-ANALYSIS; INTERVAL DYNAMICS

Author Information

Reprint Address: Ivanov, PC (reprint author)

+ Harvard Univ, Sch Med, Boston, MA 02115 USA.

Addresses:

+ [1] Harvard Univ, Sch Med, Boston, MA 02115 USA
+ [2] Brigham & Womens Hosp, Div Sleep Med, Boston, MA 02115 USA
+ [3] Nanjing Univ Posts & Telecommun, Coll Geog & Biol Informat, Nanjing 210003, Peoples R China
+ [4] Univ Malaga, Dept Fis Aplicada 2, E-29071 Malaga, Spain

[5] Sci & Technology Res Ctr Inc, Mitsubishi Chem Grp, Yokohama, Kanagawa 2278502, Japan

+ [6] Boston Univ, Ctr Polymer Studies, Boston, MA 02215 USA
+ [7] Boston Univ, Dept Phys, Boston, MA 02215 USA

E-mail Addresses: plamen@buphy.bu.edu

Funding

Funding Agency	Grant Number
Brigham and Women's Hospital Biomedical Research Institute Fund	
Spanish Junta de Andalucia	P06-FQM1858
Mitsubishi Chemical Corp., Japan	
National Natural Science Foundation of China	60501003

View funding text

Publisher

AMER PHYSICAL SOC, ONE PHYSICS ELLIPSE, COLLEGE PK, MD 20740-3844 USA

Categories / Classification

Research Areas: Physics

Web of Science Categories: Physics, Fluids & Plasmas; Physics, Mathematical

See more data fields

Cited References: 91

Showing 30 of 91 **View All in Cited References page** *(from Web of Science Core Collection)*

1. **Nonlinear analysis of cardiac rhythm fluctuations using DFA method** **Times Cited: 39**
By: Absil, PA; Sepulchre, R; Bilge, A; et al.
PHYSICA A-STATISTICAL MECHANICS AND ITS APPLICATIONS Volume: 272 Issue: 1-2 Pages: 235-244 Published: OCT 1 1999

2. **Detrending fluctuation analysis based on moving average filtering** **Times Cited: 55**
By: Alvarez-Ramirez, J; Rodriguez, E; Echeverria, JC

A LETTERS JOURNAL EXPLORING THE FRONTIERS OF PHYSICS

OFFPRINT

Correlated walks down the Babylonian markets

N. E. Romero, Q. D. Y. Ma, L. S. Liebovitch, C. T. Brown and P. Ch. Ivanov

EPL, **90** (2010) 18004

A Letters Journal Exploring the Frontiers of Physics

April 2010

EPL, **90** (2010) 18004
doi: 10.1209/0295-5075/90/18004

www.epljournal.org

Correlated walks down the Babylonian markets

N. E. Romero[1(a)], Q. D. Y. Ma[2,3(a)], L. S. Liebovitch[4], C. T. Brown[5] and P. Ch. Ivanov[2,6,7(b)]

[1] *Physics Department, Florida Atlantic University - Boca Raton, FL 33431, USA*
[2] *Harvard Medical School and Division of Sleep Medicine, Brigham and Women's Hospital - Boston, MA 02115, USA*
[3] *College of Geography and Biological Information, Nanjing University of Posts and Telecommunications Nanjing 210003, China*
[4] *Center for Complex Systems and Brain Sciences, Florida Atlantic University - Boca Raton, FL 33431, USA*
[5] *Anthropology Department, Florida Atlantic University - Boca Raton, FL 33431, USA*
[6] *Center for Polymer Studies and Department of Physics, Boston University - Boston, MA 02215, USA*
[7] *Departamento de Física Aplicada II, Universidad de Málaga - 29071 Málaga, Spain, EU*

received 27 January 2010; accepted in final form 29 March 2010
published online 5 May 2010

PACS 89.65.Gh – Economics; econophysics, financial markets, business and management
PACS 02.50.-r – Probability theory, stochastic processes, and statistics
PACS 89.65.Ef – Social organizations; anthropology

Abstract – To investigate the evolution of market dynamics in different stages of historical development, we analyze commodity prices from two distinct periods —ancient Babylon, and medieval and early modern England. We find that the first-digit distributions of both Babylon and England commodity prices follow Benford's law, indicating that the data represent empirical observations typically arising from a free market. Further, we find that the normalized prices of both Babylon and England agricultural commodities are characterized by stretched exponential distributions, and exhibit persistent correlations of a power law type over long periods of up to several centuries, in contrast to contemporary markets. Our findings suggest that similar market interactions may underlie the dynamics of ancient agricultural commodity prices, and that these interactions may remain stable across centuries in two distinct historical periods.

The emergence of markets and market economics is an active area of research in archeology and economic anthropology, where a main focus is to understand how markets developed in early civilizations and what their characteristics were [1–4]. A plausible hypothesis is that markets emerge in certain societies as a result of the exchange of goods, services or information, allowing a particular distribution of resources. Buyers and sellers, as primary market participants, exert demand and supply forces responsible, among others, for driving the price of any asset. The complex interactions between numerous market agents acting through feedback at different time scales within various economic conditions and market regulation lead to highly irregular and complex dynamics of market activity [5–10]. Recent empirical investigations have demonstrated that key market observables such as price, trading volume and frequency of trading do not change in a random manner but rather exhibit surprisingly robust dynamical patterns over a wide range of time scales described by scaling laws [11–13]. To understand how these scaling laws relate to the underlying market regulatory mechanisms and interactions among market entities, most studies have focused on high-frequency recordings of modern market activity as represented by commodities, company stocks or currency foreign exchange over relatively short time periods ranging from months and years up to several decades [14–16]. However, every market is embedded in its historical, cultural and technological context, and market dynamics may evolve with changes in economic conditions, government politics and market regulations —*e.g.*, correlations in stock price fluctuations change significantly when a company is transferred from one stock market to another [17], while networks of interaction of company stocks across the entire economy exhibit stable behavior over a limited time horizon [18,19]. The evolution of market dynamics across different historical periods has not been systematically studied. Here we investigate several key aspects of the dynamics of commodity prices in two distinct historical periods corresponding to different economic conditions and development of society —ancient Mesopotamia and medieval and early modern England.

(a) These authors contributed equally to this paper.
(b) E-mail: plamen@buphy.bu.edu

We study the probability distribution and correlation properties of commodity prices from Babylon in the period of 463–72 B.C. and from England in the period of 1209–1914 A.D. These data sets represent an exceptionally long time window into the market dynamics at two important and different periods of civilization. By comparing, in an statistical framework, key measures of the market dynamics during these two periods, we can identify important similarities or dissimilarities of their respective economy in relation to empirical observations of contemporary markets.

Situated in the south region of Iraq, on the Euphrates River, Babylon was the political and cultural capital of ancient Mesopotamia. Archaeological excavations started in 1899 by Robert Koldewey have uncovered astronomical diaries, written in cuneiform on clay tablets, from the period 652 B.C. to 69 A.D. Since the tablets contain celestial observations, all information inscribed on them is dated, including records of the weather, the level of the Euphrates River, socio-political events and market quotations of six commodities: barley, dates, mustard (cascuta), cress (cardamom), sesame and wool. The commodity prices are expressed in weight quantities that could be purchased per shekel of silver, recorded three times a month. Babylon had an agriculturally based economy and its diet was primarily based on barley and dates. Mustard and cress were used as spices and sesame primarily for its oil. All six commodities were also used in official rituals of Babylonian cultic life [20]. Many clay tablets are still missing or broken. Since they were stored vertically and the prices were listed last in the monthly reports, *i.e.*, at the lower edge of each clay tablet, there is a considerable amount of data lost.

The English commodity annual price records constitute a point of reference in many historical analyses, because they represent a data set over a significantly long period. In our study, we use records from 80 agricultural and other commodities traded in England in the period 1209–1914 [21]. Prices are expressed in grams of silver per metric physical unit. To compare with Babylon data, we select six similar agricultural commodities: barley, beans, oats, peas, pepper and wheat, for which there are practically continuous annual records throughout the entire period (with relatively few missing data points mainly in the first half of the period).

Most archaeologists, epigraphers, and economic historians have inferred that the Babylonian data represent real and accurate price quotations [2,4,22]. However, there is no conclusive evidence and it is possible that the Babylon tablets record price estimates, price caps, target prices, or even astrological calculations of what prices ought to be.

Numerical records of empirical observations arising from natural or social processes often exhibit a particular probability distribution for the first significant digit of the form $\log_{10}(1+1/n)$, where $n=1,\ldots,9$ is the first digit, known as Benford's law [23,24]. Benford's law has been observed in several financial systems like stock market prices [25], census statistics [26], income tax payments, and accounting data [27]. However, numerical processes influenced by human factors such as advertised prices for consumers, assigned telephone or license plate numbers, amount of cash withdrawals, or randomly picking numbers do not follow Benford's law [26–28]. Benford's test has been utilized in identifying fraudulent reports in taxes [27], transactions of federal campaigns [29], toxic release reported by industrial plants [30], accounting audits [31] and fabricated survey answers [32]. Therefore, a distribution of the first-digits which does not follow Benford's law could indicate the presence of systematic omissions, estimations, rounding, falsification or even fabrication in the recorded data. The first-digit distribution of Babylon commodity prices could thus expose certain abnormalities, which could lead one to suspect that these prices are not a record of real empirical observations typically arising from a free market where supply and demand forces are present.

Our analysis of the first significant digits of the Babylon commodity price records indicates a good agreement with Benford's law (fig. 1a) with the coefficient of determination $R^2=0.93$. These results are comparable with our analysis of six similar agricultural commodities from medieval and early modern England, which also conform to Benford's distribution (fig. 1b) (with $R^2=0.94$). Extending our analysis to 80 different English commodities of mixed (not only agricultural) nature to significantly increase the data samples, we obtain an almost perfect fit to Benford's law (fig. 1c) (with $R^2=0.95$). These findings indicate that Babylonian market quotations exhibit properties shared by empirical observations of natural process, suggesting they represent reliable recordings of commodity prices. Further, since multiplicative process have been associated with emergence of Benford's distribution [33] and since contemporary stock market prices also follow Benford's law [25], our results in fig. 1 may indicate that processes of multiplicative nature underlie the market dynamics in distinct historical periods and economic conditions.

Next, we study the probability distributions of different agricultural commodity prices in Babylon and we compare them with the prices of similar commodities from medieval and early modern England. We find that the price distribution of each Babylonian commodity i is characterized by different average $\langle S_i(t)\rangle$ and standard deviation σ_i. However, after normalization of the prices $S_i(t)$ to $\tilde{S}_i(t)=(S_i(t)-\langle S_i(t)\rangle/\sigma_i$, where $\langle S_i(t)\rangle$ is the average recorded price of that commodity, the distributions of all Babylonian commodities fall onto a single curve. This curve is well fit by a stretched exponential function:

$$P(\tilde{S})=\int_{\tilde{S}}^{\infty} p(x)\mathrm{d}x \;\sim\; e^{-(\frac{\tilde{S}}{\tau})^{\delta}}, \qquad (1)$$

where $p(x)$ is the probability density, $\delta=1.47$ is the stretch exponent and $\tau=1.60$ is a characteristic constant (with $R^2=0.97$). Interestingly, after the same price-normalization procedure, all cumulative distributions for

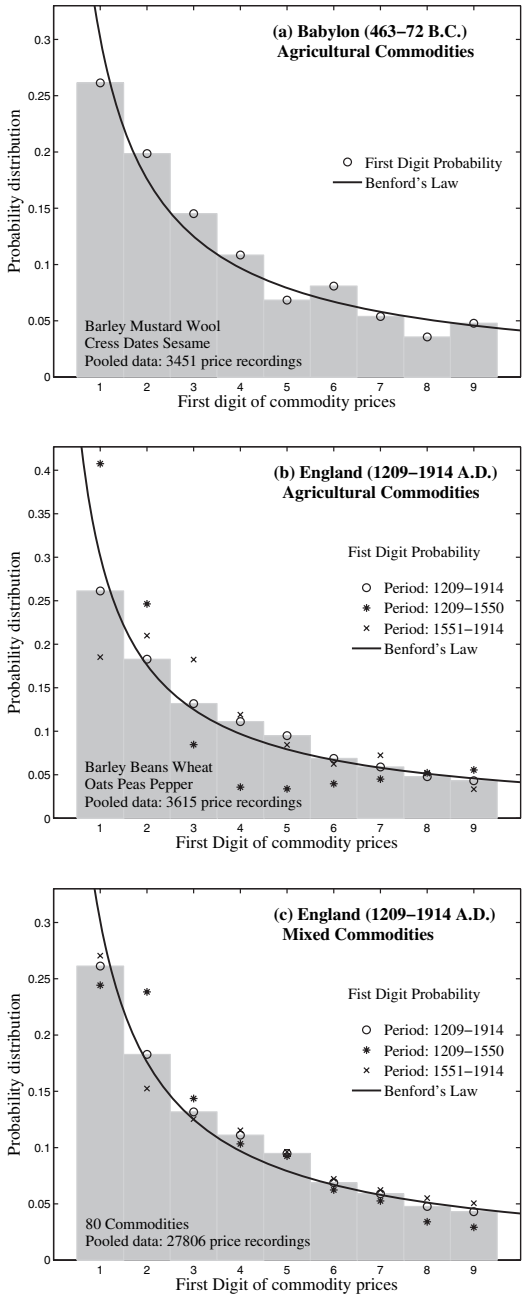

Fig. 1: First-digit distribution of the price records of (a) six agricultural commodities from Babylon, (b) six similar agricultural commodities from England and (c) 80 mixed commodities from England. All first-digit distributions are well approximated by Benford's law.

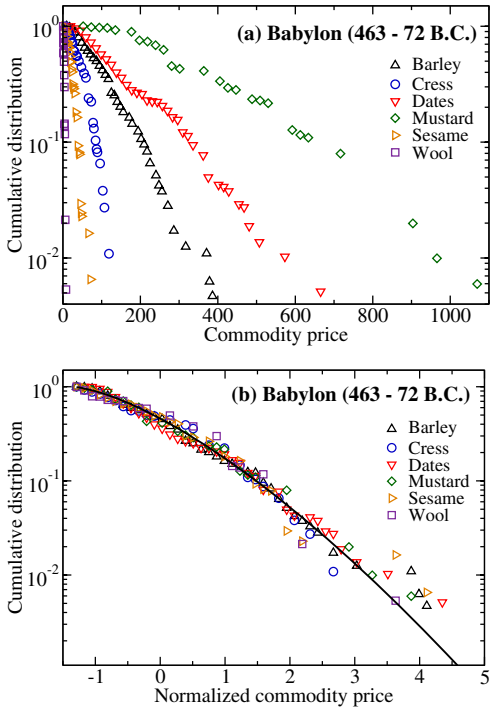

Fig. 2: (Colour on-line) Cumulative distributions of (a) agricultural commodity prices from ancient Babylon and (b) normalized prices of the same commodities as in (a). After normalization all distributions conform to a single stretched exponential curve, indicating a common functional form.

the six English commodities also fall onto a single curve following the same stretched exponential form in eq. (1) with parameters $\delta = 1.52$ and $\tau = 1.58$ (with $R^2 = 0.96$) very similar to those of the Babylonian prices. We find the same form for the probability distributions obtained for the first and the second half of the recorded period for the England data (see inset in fig. 3b), indicating time stability. Further, our analysis shows that contemporary agricultural commodity prices of wheat, barley, sugar, cocoa, coffee, tea (monthly prices for the period 1983–2009 [34]) as well as of gold (original monthly prices and prices after correction for inflation in the period 1971–2010 [35]) also exhibit a stretched exponential form for the cumulative distribution of normalized prices.

Our findings of identical functional form for the probability distribution for the agricultural commodity prices in ancient Babylon and medieval and early modern England, with very similar values for the parameters δ and τ, may suggest unexpected similarities underlying the dynamics for these two markets representing very different stages in historic and economic development. Our finding of stretched exponential distributions in fig. 2 and fig. 3 is in contrast to modern commodity and stock markets where probability distributions with power law tails have been reported [36–38], indicating a scale-invariant organization in commodity prices emerging from possibly different market organization and interactions of market participants. We note, that while most studies of contemporary markets focus on price returns, *i.e.*, the normalized forward change of the logarithm of the price at successive time's separated by a fixed time interval (*e.g.*, 1 min, 1 hour or 1 day), it is not possible to systematically define price returns for the Babylon commodities due to a large fraction of randomly lost data in the records [20,39].

Another key characteristic of market dynamics are the correlations and scaling behavior embedded in the

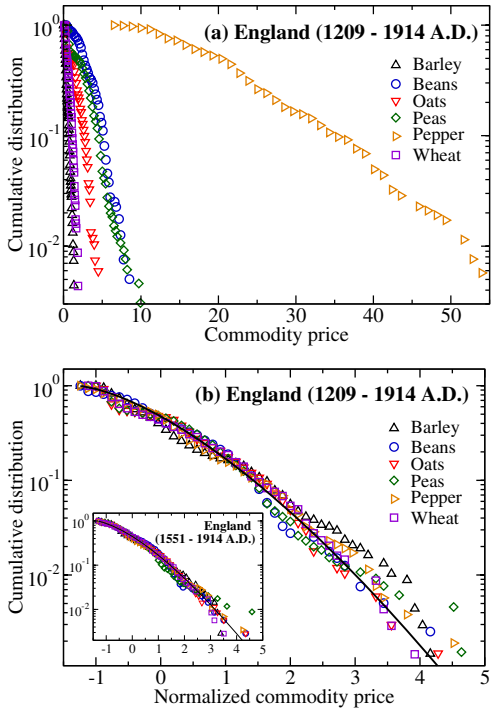

Fig. 3: (Colour on-line) Cumulative distributions of (a) agricultural commodity prices from medieval and early modern England and (b) normalized prices of the same commodities as in (a). All normalized distributions are well approximated by a stretched exponential function with parameter values similar to those for the Babylonian prices in fig. 2.

fluctuations of prices and other market observables. These characteristics reflect aspects of the temporal organization of multiple feedback interactions between many market agents, important to properly identify and model the underlying mechanisms of market regulation. To quantify the temporal structure in commodity prices in ancient Babylon and to compare it with the market dynamics of medieval and early modern England, we apply the detrended fluctuation analysis (DFA) [40]. Unlike other traditional methods such as power spectrum, autocorrelation and R/S analysis which are not well suited for nonstationary signals, the DFA method can accurately quantify correlations in the fluctuations of nonstationary signals generated by systems exhibiting nonequilibrium dynamics, with multiple degrees of freedom and nonlinear feedback interactions as observed in commodity and financial markets [6,7,9]. Moreover, recent studies of the performance of the DFA method have demonstrated that the method is robust to the presence of gaps and missing data in correlated signals [41,42].

The Babylon records contain commodity price data for the beginning, middle and end of each month. Since some of these records are missing, in our analysis we consider only monthly averaged and annually averaged prices. Applying the DFA, we calculate the root-mean-square fluctuation function $F(n)$ of the integrated and piece-wise polynomially detrended price time series for a given time window of size n (where n can be in units of months or years), and we obtain the functional dependence of $F(n)$ for varied time scale n. A power law dependence $F(n) \sim n^{\alpha}$ indicates the presence of scale-invariant (scaling) behavior, while the scaling exponent α (a self-similarity parameter) quantifies the long-term power law correlations in the data. If $\alpha = 0.5$, the signal is uncorrelated (white noise); if $\alpha < 0.5$, the signal is anti-correlated; if $\alpha > 0.5$, the signal is positively correlated. The larger the value of α, the stronger the correlations. In this study, we use the second-order DFA (DFA-2), which removes both constant and linear trends in the time series of commodity prices [43]. The choice of DFA-2 is motivated by the fact that: i) this order of DFA-l can accurately quantify the scaling behavior of signals with exponents in the range $0 < \alpha < 3$ [44], which covers practically all signals generated by real world systems; ii) earlier investigations have demonstrated that DFA-2 is sufficient to accurately quantify a broad range of nonstationary signals generated by different nonlinear dynamics —*e.g.*, for commodity and stock returns [37] and for intertrade times dynamics [45] the exponent α obtained from higher-order DFA-l is not significantly different compared to α obtained from DFA-2; and iii) deviations from scaling which appear at small scales become more pronounced in higher-order DFA-l [43].

We find that all six Babylon commodities exhibit power law correlations characterized by scaling exponent $\alpha \approx 0.7$ (fig. 4a). Moreover, the scaling exponent remains stable when changing the time scale from months to years when considering monthly and annually averaged commodity prices —$\alpha = 0.67 \pm 0.04$ (mean $\pm$ standard deviation of all six commodities) for the monthly data and $\alpha = 0.69 \pm 0.05$ for the annual data (see fig. 4a, filled and open symbols respectively). For the six agricultural English commodities (which we have selected to be similar in kind of the six Babylon commodities), we also find persistent power law correlation for their annual price fluctuations characterized by a scaling exponent $\alpha = 0.91 \pm 0.05$ over a broad range of few years to almost two hundred years (fig. 4b). Repeating our scaling analysis for the first and second half of the time period 1209–1914 A.D., we find a consistent positively correlated behavior, with an exponent $\alpha \approx 0.9$, for all six English commodities. Specifically, for the period 1209–1550 we find: barley $\alpha = 0.84$; oats $\alpha = 0.82$; peas $\alpha = 0.77$; pepper $\alpha = 0.93$; wheat $\alpha = 0.75$. For the period 1551-1914 we find: barley $\alpha = 0.92$; beans $\alpha = 0.85$; oats $\alpha = 0.95$; peas $\alpha = 0.91$; pepper $\alpha = 1.16$; wheat $\alpha = 0.82$.

Thus, our findings indicate that both ancient Babylonian and medieval English commodity prices exhibit the same kind of persistent power law correlations, suggesting common elements in the market mechanisms driving the price dynamics. Notably, our observations indicate a very different temporal organization of Babylon and medieval England price fluctuations compared to price fluctuations

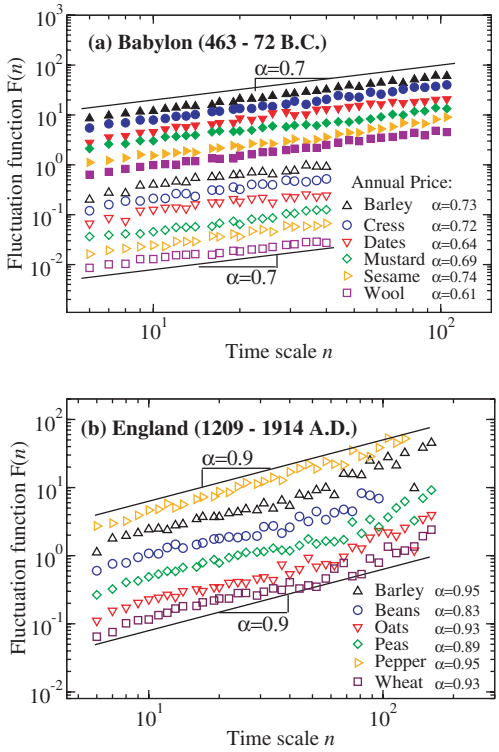

Fig. 4: (Colour on-line) Scaling analysis of (a) six agricultural commodity prices from ancient Babylon and (b) six similar agricultural commodity prices from medieval and early modern England. Open symbols in (a) represent annually averaged data and closed symbols represent monthly averaged data. Both Babylon and England data exhibit scaling behavior characterized by DFA scaling exponent $\alpha > 0.5$ indicating strong positive correlations.

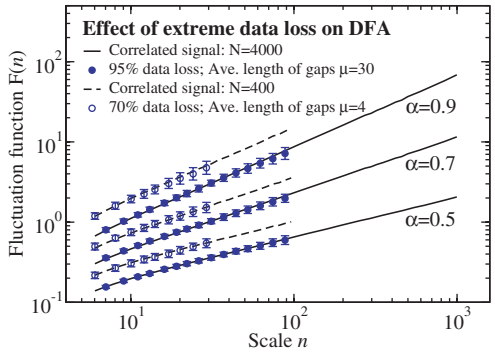

Fig. 5: (Colour on-line) Modeling the effect of extreme data loss on the scaling properties of correlated signals. Results from DFA-2 analysis for i) signals of length $N = 4000$ with different scaling exponents α and 95% of data loss where the average length of missing segments $\mu = 30$ data points (filled circles) and ii) signals of length $N = 400$ with different α and 70% of data loss where the average length of missing segments (gaps) is $\mu = 4$ data points (open circles). The missing segments in the simulations are drawn from an exponential distribution as observed in the Babylon data. Solid and dash lines indicate DFA-2 scaling before segments are removed, serving as a base line, and symbols indicate mean values of 100 different realizations with error bars showing the standard deviations. The simulations indicate that signals with long-term persistent correlations are not affected by a significant loss of data. The parameters in the simulations are chosen to represent the monthly (filled circles) and annually (open circles) averaged prices in the Babylon records.

of commodities traded on contemporary markets, where normalized price returns were found to be uncorrelated with $\alpha \approx 0.5$ for both spot and future commodity prices in contrast to the absolute price returns (volatility) where persistent long-range power law correlations were observed [37]. Indeed, our correlation analysis shows that contemporary agricultural commodity prices exhibit close to random walk behavior with $\alpha \approx 1.5$ corresponding to uncorrelated white noise behavior ($\alpha \approx 0.5$) for the price returns. Specifically, for the monthly prices in the period 1983–2009 [34] we find: wheat $\alpha = 1.38$; barley $\alpha = 1.37$; sugar $\alpha = 1.54$; cocoa $\alpha = 1.44$; coffee $\alpha = 1.50$; tea $\alpha = 1.54$. Further, for gold monthly prices in US dollars in the period 1971–2010 [35], we find $\alpha = 1.45$ for the original prices, and $\alpha = 1.54$ after correction for inflation. Our findings of strong persistent long-term correlations for the Babylon and England commodity prices (fig. 4) do not confirm earlier reports of random walk behavior for the commodities of these old markets [3].

We note, that due to significant gaps of missing data in the available Babylon commodity price records, it is not possible to perform a consistent correlation analysis for the price returns and absolute price returns. Because the missing data in the Babylon records constitute up to 70% of all annual prices and up to 95% of all monthly prices for the entire period for some of the commodities, we model the effect of extreme data loss on the scaling properties of correlated signals. We first determine the probability density function of the length of the missing gaps using the multihistogram method [46], and we find that the length of the gaps in both monthly and annually averaged data follows an exponential distribution, with mean $\mu \approx 30$ months and $\mu \approx 4$ years respectively. Considering the nature of the time series of the different Babylon commodity prices, we generate correlated signals with $\alpha > 0.5$, and we randomly remove a given percentage of the total data by cutting out segments drawn from an exponential distribution. To simulate the Babylon annual (average) prices, we generate correlated signals of length $N = 400$ data points, with DFA exponent $\alpha = 0.7$, and 70% missing data by randomly removing data segments with length drawn from an exponential distribution with mean $\mu = 4$. To simulate the monthly (average) prices of Babylon commodities, we generate correlated signals of length $N = 4000$ data points, with $\alpha = 0.7$ and 95% of missing data by randomly removing data segments from an exponential distribution with mean $\mu = 30$. Our simulations shown in fig. 5 demonstrate that even extreme loss of data does not significantly affect the scaling properties

of positively correlated signals (for details on the effect of extreme data loss see [42]). These simulations validate our findings of long-term persistent correlations in both Babylon and England commodity prices.

In summary, our findings of stretched exponential form for the probability distributions and long-term persistent correlations of a power law type for the commodity prices in both ancient Babylon and medieval and early modern England, indicate strong similarity in the dynamics of these markets despite distinct differences in historical and economic conditions and development of society, wars and governmental disruptions in these two historical periods. Since these key statistical properties do not significantly change when we consider separate segments of the recordings, such consistency may suggest that the price dynamics of agricultural arable commodities are mainly driven by natural growth, weather conditions, population distribution and growth leading to similar supply and demand market forces and interactions which remain relatively stable across centuries in these two historical periods.

* * *

PChI thanks the Spanish Junta de Andalucia (Grant No. P06-FQM1858) for support. The authors thank A. L. Slotsky and P. Temin for graciously providing their data for analysis.

REFERENCES

[1] Minc L. D., *J. Anthropol. Archaeol.*, **25** (2006) 82.
[2] Slotsky A. L., *The Bourse of Babylon: Market Quotations in the Astronomical Diaries of Babylonia* (CDL Press, Bethesda, Md.) 1997.
[3] Temin P., *Explor. Econ. Hist.*, **39** (2001) 46.
[4] Van Der Spek R. J. and Mandemakers C. A., *Bibl. Orient.*, **60** (2003) 521.
[5] Malkiel B. G., *A Random Walk down Wall Street* (Norton, New York) 1973.
[6] Mantegna R. N. and Stanley H. E., *An Introduction to Econophysics: Correlations and Complexity in Finance* (Cambridge University Press, New York) 2000.
[7] Roehner B. M., *Theory of Markets* (Springer, Berlin) 1995.
[8] Roehner B. M. and Syme T., *Pattern and Repertoire in History* (Harvard University Press, Cambridge) 2002.
[9] Bouchaud J.-P., Farmer J. D. and Lillo F., Available at SSRN: `http://ssrn.com/abstract=1266681` (2008).
[10] Giardina I. and Bouchaud J.-P., *Eur. Phys. J. B*, **31** (2003) 421.
[11] Liu Y., Gopikrishnan P., Cizeau P., Meyer M., Peng C.-K. and Stanley H. E., *Phys. Rev. E*, **60** (1999) 1390.
[12] Plerou V., Gopikrishnan P., Gabaix X. and Stanley H. E., *Quant. Finance*, **4** (2004) C11.
[13] Gabaix X., Gopikrishnan P., Plerou V. and Stanley H. E., *Nature*, **423** (2003) 267.
[14] Mandelbrot B. B., *J. Bus.*, **36** (1963) 294.
[15] Gopikrishnan P., Plerou V., Amaral L. A. N., Meyer M. and Stanley H. E., *Phys. Rev. E*, **60** (1999) 5305.
[16] Mantegna R. N. and Stanley H. E., *Nature*, **376** (1995) 394.
[17] Yuen A. and Ivanov P. Ch., arXiv:physics/0508203v1 (2005).
[18] Mantegna R. N., *Eur. Phys. J. B*, **11** (1999) 193.
[19] Bonanno G., Caldarelli G., Lillo F. and Mantegna R. N., *Phys. Rev. E*, **68** (2003) 046130.
[20] Sach A. J. and Hunger H., *Astronomical Diares and Related Texts from Babylonia,* Vols. **1**, **2**, **3** (Verlag der Osterreichischen Akademie der Wissenschaften, Vienna) 1988, 1989, 1996.
[21] Clark G., *Res. Econ. Hist.*, **22** (2004) 41.
[22] Grainger J., *J. Econ. Soc. Hist. Orient*, **42** (1999) 303.
[23] Newcomb S., *Am. J. Math.*, **4** (1881) 39.
[24] Benford F., *Proc. Am. Philos. Soc.*, **78** (1938) 551.
[25] Ley E., *Am. Stat.*, **50** (1996) 311.
[26] Hill T. P., *Am. Sci.*, **86** (1998) 358.
[27] Nigrini M. J., *J. Am. Tax. Assoc.*, **18** (1996) 72.
[28] Schindler R. M. and Kirby P. N., *J. Consum. Res.*, **24** (1997) 192.
[29] Tam Cho W. K. and Gaines B. J., *Am. Stat.*, **61** (2007) 219.
[30] de Marchi S. and Hamilton J., *J. Risk Uncertain.*, **32** (2006) 57.
[31] Durtschi C., Hillison W. and Pacini C., *J. Forensic Account.*, **5** (2004) 17.
[32] Judge G. and Schechter L., *J. Hum. Resour.*, **44** (2009) 1.
[33] Pietronero L., *Physica A*, **293** (2000) 297.
[34] World Bank, Comodity Price Data, `http://econ.worldbank.org/`.
[35] World Gold Council, Gold Research and Statistics, `http://www.research.gold.org/prices/`.
[36] Lux T., *J. Econ. Behav. Organ.*, **33** (1998) 143.
[37] Matia K., Amaral L. A. N., Goodwin S. P. and Stanley H. E., *Phys. Rev. E*, **66** (2002) 045103.
[38] Gopikrishnan P., Meyer M., Amaral L. A. N. and Stanley H. E., *Eur. Phys. J. B*, **3** (1998) 139.
[39] Van der Spek R., in *The Effect of War on the Prices of Barley and Agricultural Land in Hellenistic Babylonia*, edited by Andreau J., Briant P. and Descat R. (Entretiens d'Archeologie et d'Histoire, Saint-Benard-de-Comminges) 2000, p. 293.
[40] Peng C.-K., Buldyrev S. V., Havlin S., Simons M., Stanley H. E. and Goldberger A. L., *Phys. Rev. E*, **49** (1994) 1685.
[41] Chen Z., Ivanov P. Ch., Hu K. and Stanley H. E., *Phys. Rev. E*, **65** (2002) 041107.
[42] Ma Q. D. Y., Bartsch R. P., Bernaola-Galvn P., Yoneyama M. and Ivanov P. Ch., *Phys. Rev. E*, **81** (2010) 031101.
[43] Kantelhardt J. W., Koscielny-Bunde E., Rego H. H., Havlin S. and Bunde A., *Physica A*, **295** (2001) 441.
[44] Xu L., Ivanov P. Ch., Hu K., Chen Z., Carbone A. and Stanley H. E., *Phys. Rev. E*, **71** (2005) 051101.
[45] Ivanov P. Ch., Yuen A., Podobnik B. and Lee Y., *Phys. Rev. E*, **69** (2004) 056107.
[46] Liebovitch L., *Phys. Rev. E*, **59** (1999) 3312.

Correlated walks down the Babylonian markets

By: Romero, NE (Romero, N. E.)[1]; Ma, QDY (Ma, Q. D. Y.)[2,3,4]; Liebovitch, LS (Liebovitch, L. S.)[5]; Brown, CT (Brown, C. T.)[6]; Ivanov, PC (Ivanov, P. Ch.)[2,3,7,8,9]

View ResearcherID and ORCID

EPL
Volume: 90 **Issue:** 1
Article Number: 18004
DOI: 10.1209/0295-5075/90/18004
Published: APR 2010
Document Type: Article
View Journal Impact

Abstract

To investigate the evolution of market dynamics in different stages of historical development, we analyze commodity prices from two distinct periods-ancient Babylon, and medieval and early modern England. We find that the first-digit distributions of both Babylon and England commodity prices follow Benford's law, indicating that the data represent empirical observations typically arising from a free market. Further, we find that the normalized prices of both Babylon and England agricultural commodities are characterized by stretched exponential distributions, and exhibit persistent correlations of a power law type over long periods of up to several centuries, in contrast to contemporary markets. Our findings suggest that similar market interactions may underlie the dynamics of ancient agricultural commodity prices, and that these interactions may remain stable across centuries in two distinct historical periods. Copyright (C) EPLA, 2010

Keywords

KeyWords Plus: FLUCTUATIONS; LAW; DISTRIBUTIONS; INDEXES; DIGITS; PRICES; MODELS

Author Information

Reprint Address: Romero, NE (reprint author)

+ Florida Atlantic Univ, Dept Phys, Boca Raton, FL 33431 USA.

Addresses:

+ [1] Florida Atlantic Univ, Dept Phys, Boca Raton, FL 33431 USA
+ [2] Harvard Univ, Sch Med, Boston, MA 02115 USA
+ [3] Brigham & Womens Hosp, Div Sleep Med, Boston, MA 02115 USA
+ [4] Nanjing Univ Posts & Telecommun, Coll Geog & Biol Informat, Nanjing 210003, Peoples R China
+ [5] Florida Atlantic Univ, Ctr Complex Syst & Brain Sci, Boca Raton, FL 33431 USA
+ [6] Florida Atlantic Univ, Dept Anthropol, Boca Raton, FL 33431 USA
+ [7] Boston Univ, Ctr Polymer Studies, Boston, MA 02215 USA
+ [8] Boston Univ, Dept Phys, Boston, MA 02215 USA
+ [9] Univ Malaga, Dept Fis Aplicada 2, E-29071 Malaga, Spain

E-mail Addresses: plamen@buphy.bu.edu

If you would like to improve the quality of the data in this record, please suggest a correction.

Funding

Funding Agency	Grant Number
Spanish Junta de Andalucia	P06-FQM1858

View funding text

Publisher

EPL ASSOCIATION, EUROPEAN PHYSICAL SOCIETY, 6 RUE DES FRERES LUMIERE, MULHOUSE, 68200, FRANCE

Journal Information

Impact Factor: Journal Citation Reports

Categories / Classification

Research Areas: Physics

Web of Science Categories: Physics, Multidisciplinary

See more data fields

Cited References: 46

Showing 30 of 46 **View All in Cited References page** *(from Web of Science Core Collection)*

1. Title: [not available] **Times Cited: 516**
   By: Benford, F.
   Proc. Am. Philos. Soc. Volume: 78 Pages: 551 Published: 1938

2. **Topology of correlation-based minimal spanning trees in real and model markets** **Times Cited: 209**
   By: Bonanno, G; Caldarelli, G; Lillo, F; et al.
   PHYSICAL REVIEW E Volume: 68 Issue: 4 Article Number: 046130 Part: 2 Published: OCT 2003

3. **Effect of nonstationarities on detrended fluctuation analysis** **Times Cited: 618**
   By: Chen, Z; Ivanov, PC; Hu, K; et al.
   PHYSICAL REVIEW E Volume: 65 Issue: 4 Article Number: 041107 Part: 1 Published: APR 2002

4. Title: [not available] **Times Cited: 1**
   By: CHO WKT
   AM STAT Volume: 61 Pages: 219 Published: 2007

5. **The price history of English agriculture, 1209-1914** **Times Cited: 48**
   By: Clark, G
   RESEARCH IN ECONOMIC HISTORY, VOL 22 Book Series: Research in Economic History Series Volume: 22 Pages: 41-123 Published: 2004

6. **Assessing the accuracy of self-reported data: An evaluation of the toxics release inventory** **Times Cited: 44**
   By: de Marchi, S; Hamilton, JT
   JOURNAL OF RISK AND UNCERTAINTY Volume: 32 Issue: 1 Pages: 57-76 Published: JAN 2006

7. **The effective use of Benford's Law to assist in detecting fraud in accounting data** **Times Cited: 117**
   By: Durtschi, C.; Hillison, W.; Pacini, C.

Aging Effects on Cardiac and Respiratory Dynamics in Healthy Subjects across Sleep Stages

Aicko Y. Schumann, PhD[1,2]; Ronny P. Bartsch, PhD[3]; Thomas Penzel, PhD[4]; Plamen Ch. Ivanov, PhD[3,5]; Jan W. Kantelhardt, PhD[1]

[1]Institute of Physics, Martin-Luther-Universität Halle-Wittenberg, Halle (Saale), Germany; [2]Complexity Science Group at the Department of Physics and Astronomy, University of Calgary, Calgary, Alberta, Canada; [3]Harvard Medical School and Division of Sleep Medicine, Brigham and Women's Hospital, Boston, MA; [4]Schlafmedizinisches Zentrum der Charité Berlin, Berlin, Germany; [5]Department of Physics and Center for Polymer Studies, Boston University, Boston, MA

Study Objectives: Respiratory and heart rate variability exhibit fractal scaling behavior on certain time scales. We studied the short-term and long-term correlation properties of heartbeat and breathing-interval data from disease-free subjects focusing on the age-dependent fractal organization. We also studied differences across sleep stages and night-time wake and investigated quasi-periodic variations associated with cardiac risk.
Design: Full-night polysomnograms were recorded during 2 nights, including electrocardiogram and oronasal airflow.
Setting: Data were collected in 7 laboratories in 5 European countries.
Participants: 180 subjects without health complaints (85 males, 95 females) aged from 20 to 89 years.
Interventions: None.
Measurements and Results: Short-term correlations in heartbeat intervals measured by the detrended fluctuation analysis (DFA) exponent α_1 show characteristic age dependence with a maximum around 50-60 years disregarding the dependence on sleep and wake states. Long-term correlations measured by α_2 differ in NREM sleep when compared with REM sleep and wake, besides weak age dependence. Results for respiratory intervals are similar to those for α_2 of heartbeat intervals. Deceleration capacity (*DC*) decreases with age; it is lower during REM and deep sleep (compared with light sleep and wake).
Conclusion: The age dependence of α_1 should be considered when using this value for diagnostic purposes in post-infarction patients. Pronounced long-term correlations (larger α_2) for heartbeat and respiration during REM sleep and wake indicate an enhanced control of higher brain regions, which is absent during NREM sleep. Reduced *DC* possibly indicates an increased cardiovascular risk with aging and during REM and deep sleep.
Keywords: Sleep, aging, heart rate variability, respiration, cardiac risk, detrended fluctuation analysis, scaling, phase rectified signal averaging, deceleration capacity
Citation: Schumann AY; Bartsch RP; Penzel T; Ivanov PC; Kantelhardt JW. Aging effects on cardiac and respiratory dynamics in healthy subjects across sleep stages. *SLEEP* 2010;33(7):943-955.

IN PHYSIOLOGY, LONG-RANGE POWER-LAW CORRELATIONS HAVE BEEN STUDIED FOR MANY YEARS, E.G., IN HEARTBEAT DYNAMICS,[1,2] RESPIRATION dynamics,[3-5] brain waves,[6-8] and gait time series.[9-11] Such correlations characterize a persistent variation of the given signal on many time scales. For example, the probability of persistently larger (or smaller) values over extended periods of time is characteristically increased. Long beat-to-beat or breath-to-breath time intervals are more likely to be followed by longer intervals than by shorter ones, and vice versa.

This correlation structure of the data can be classified by fractal or multifractal scaling analysis.[12-15] Calculated scaling exponents are affected by pathologic conditions, sympathovagal balance, cardiopulmonary regulation, and circadian rhythm, paving the way towards an identification and discrimination of physiologic states, such as exercise versus rest,[16,17] wake versus sleep,[18] across circadian phases[19] or different sleep stages,[13,20,21] and for the development of diagnostic markers for diseases or physiologic risks, such as cardiac risk.[22] In particular, short-term scaling exponents were shown to be more powerful predictors of mortality than standard measures of heart-rate variability.[23]

Another parameter characterizing short-term variations of heartbeat intervals is the recently introduced deceleration capacity (*DC*) index. It is calculated by applying the phase rectified signal averaging (PRSA) technique[24] to heartbeat interval time series, and describes how quickly the heart rate decelerates. *DC* has been shown to be a powerful risk predictor of mortality in patients surviving an initial myocardial infarction,[25] as it is characteristically diminished in high-risk patients.

There have been very few studies of aging effects on these characteristic measures,[26,3,27,28] and there is a recent study comparing a group of young with a group of elderly subjects during different sleep stages.[29] However, no study has systematically examined how these scaling measures change across a wide range of age groups during different sleep stages. Heart rate variability, and in particular parasympathetic autonomic regulation, significantly decrease with aging[30-32] and with pathology. In addition, the deteriorating impact of aging on sleep quality, sleep quantity, sleep efficiency, and sleep structure is generally accepted. For reviews on sleep-related consequences of normal aging see Bliwise[33] and Espiritu[34] and references therein. Aging manifests itself in many ways, including a declined ability to initiate and maintain sleep, shorter total time of sleep, and decreased deep sleep (slow wave sleep) and REM sleep. It is accompanied by increased light sleep (stages 1 and 2), as well as a larger number and frequency of arousals, and an elevated wake duration after sleep onset.[35-37] Sleep disorders and diseases have

Submitted for publication September, 2009
Submitted in final revised form March, 2010
Accepted for publication March, 2010
Address correspondence to: Jan W. Kantelhardt, Institute of Physics, Martin-Luther-Universitaet Halle-Wittenberg, von-Seckendorff-Platz 1, 06120 Halle (Saale), Germany; Tel: +49-345-5525433; Fax: +49-345-5525446; E-mail: jan.kantelhardt@physik.uni-halle.de

been identified with an increased cardiovascular probability of morbidity and mortality in the elderly. It has been reported that nocturnal changes in respiratory function occur with age and lead to sleep apnea, hypopnea, and respiratory arousals. Besides, age-related changes in the thalamocortical regulatory mechanisms[36] and the neuroendocrine system[38] have been reported and associated with the deterioration of health and quality of sleep. Interestingly, at the age of 50 years cortisol levels suddenly rise, accompanied by a worsening of sleep fragmentation and a decline in REM sleep.[39] Here, we systematically study the effect of aging and sleep stages upon cardiovascular oscillations and correlations, as well as respiratory correlations in a large cohort and for a wide range of ages.

METHODS

Subjects and Protocol

This paper studied the data of 180 healthy subjects (85 males and 95 females) at ages from 20 to 89 years. Within the SIESTA project[37,40] 196 healthy subjects (94 males and 102 females) underwent full-night polysomnography and were monitored for 2 subsequent nights, resulting in a total of 392 polysomnographic recordings. All subjects gave informed consent, and the study was approved by the local ethics committees of all sleep laboratories involved. General exclusion criteria were a history of drug abuse or habitation (including alcohol), psychoactive medication or other drugs, e.g., β-blockers, or night-shift work. All subjects reported no symptoms of neurological, mental, medical, or cardiovascular disorders. Additional exclusion criteria for healthy subjects comprised: (1) significant medical disorders, (2) a Mini Mental State Examination (MMSE) score < 25,[41] (3) a Pittsburgh Sleep Quality Index (PSQI) global score > 5,[42] (4) a usual bedtime before 22:00 or after 00:00, (5) a Self-rating Anxiety Scale (SAS) raw score ≥ 33,[43] and (6) a Self-rating Depression Scale (SDS) raw score ≥ 35.[44] During the study the consumption of coffee, alcohol, and cigarettes was limited to each subject's habitual rate.

We excluded one 95-year-old female (the only subject above 90 years of age) and one 69-year-old male whose ECG exhibits clear signs of pacemaker interventions. We also removed 37 single-night recordings due to an apnea-hypopnea-index (AHI) ≥ 10 per hour and another 5 recordings due to missing or damaged sleep stage annotations. Altogether, this left us with 346 full-night polysomnographic recordings from 180 disease-free subjects (161 from males and 187 from females). Note that only one night was used for some subjects. The typical duration of the recordings was 7 to 8 hours. Therefore we analyzed approximately 2,500 hours of heartbeat data and the same for respiration. The data sets were binned in 7 age groups (Figure 1). For some of the calculations males and females were separated.

Measurements

Full-night polysomnographic data was obtained within the EU project SIESTA at 7 sleep laboratories located in 5 European countries.[37,40] Each recording consisted of an electroencephalogram (EEG) using at least 6 leads, a 2-lead electrooculogram (EOG), a 2-lead electromyogram (EMG, chin and leg), oronasal airflow, respiratory body movements (belts around chest and abdomen), snoring (microphone), oxygen saturation, and a single-channel electrocardiogram (ECG, modified V1 lead as typical for polysomnographic recordings). Sleep stages were identified according to the sleep scoring system of Rechtschaffen and Kales[45] by 3 trained technicians (2 independent scorers and 1 adjudicator) familiar with polysomnographic data. In this study we concentrate on ECG and oronasal airflow data. ECG was sampled at 100 Hz, 200 Hz, or 256 Hz; while airflow was sampled at 16 Hz, 20 Hz, 100 Hz, or 200 Hz, depending on the laboratory and the equipment. The detailed experimental setup has been reported elsewhere.[40]

Data Preparation

In order to study correlations and oscillations within respiratory data and heartbeat data for different sleep stages, as well as night-time wake, we split all recordings into segments corresponding to wake, light sleep (stage 1), light sleep (stage 2), deep sleep (stages 3 and 4 joined),[46] and REM sleep. Since sleep stage determination during transitions is sometimes complicated and possibly unreliable, we removed the first and last 30 s from each segment. We omitted the results of light sleep stage 1 in this paper because of insufficient statistics (see Figure 1).

Heartbeat time positions (R-peaks) were extracted from the ECG data using the semi-automatic peak detector *Raschlab* developed by the cardiology group of Klinikum Rechts der Isar, Munich Germany.[47] A beat classification (normal beat, ventricular beat, artifact) was assigned to each R-peak by the detector. Then we calculated the series of RR time intervals between each pair of consecutive heartbeats. An RR interval was excluded from our calculations if (1) the beat at the beginning or at the end of the interval was not normal, (2) the calculated interval was shorter than 330 ms or longer than 2000 ms, or (3) the interval was more than 30% shorter or more than 60% longer than the preceding interval. The purpose of the last filter was to eliminate extrasystoles and ectopic beats unnoticed by the peak detector. We discarded all sleep stage segments that contained less than 100 normal intervals or had more than 5% of the intervals excluded.

Recorded oronasal airflow data were processed by determining the times and values of the signals' maxima and minima, representing expiration and inspiration, respectively. Since noise in the data mainly consists of spikes (outliers), a simple threshold filter is sufficient. All data points exceeding a threshold of 95% of the maximum value or dropping below 95% of the (negative) minimum value within a moving time window are set to the corresponding threshold values. Data was resampled at 4 Hz before identifying maximum and minimum values. As well, we employed a classification scheme assigning to each event a measure of reliability depending on (1) the length of the identified breathing cycle, (2) the difference between cutoff threshold and extremal point, and (3) a comparison with averages over 3 preceding and 3 following breathing cycles.

All methods were applied separately for each subject and each night, taking into account all reliable segments for the same sleep stage. Preceding detrended fluctuation analysis (DFA, see below) all excluded intervals were cut and the gaps were joined. This procedure has been shown to not affect the DFA results, even if as much as 50% of the data is removed.[48] For phase-rectified signal averaging (PRSA, see below), the excluded data points were skipped in the averaging step because

a removal of data points could disturb the timing.

Detrended Fluctuation Analysis (DFA)

DFA, first introduced by Peng et al. for studying DNA sequences, has been intensely applied to studies of correlations in noisy, non-stationary time series.[49] Bunde et al. improved the method describing higher-order detrending.[13] It has been validated on surrogate (control) time series with additional correlations and trends.[50,51,48]

The method quantifies fluctuations on different time scales, s, i.e., different numbers of heartbeat or respiratory intervals. For each s the integrated (cumulated) signal, of length N, is split into non-overlapping pieces (segments) of length s. For each segment an n-th order polynomial fit is subtracted, and the remaining mean-square fluctuations are averaged. Repeating the procedure for many scales s yields the square of the fluctuation function, which scales according to a power-law with exponent α, $F^2_{DFAn} \sim s^{2\alpha}$. The exponents, α, can easily be extracted by linear fits of $\log(F_{DFAn}(s))$ versus $\log(s)$. Uncorrelated fluctuations lead to $\alpha = 1/2$, while $\alpha > 1/2$ indicates positive temporal correlations, and $\alpha < 1/2$ anti-correlations.

Fluctuation functions obtained from heartbeat data usually exhibit a crossover between 2 scaling regimes. Thus, we define 2 slopes, $\alpha_{RR,1}$ for small scales ($6 \le s \le 16$ heartbeats) and $\alpha_{RR,2}$ for larger scales ($50 \le s \le 200$ heartbeats). Since there is no clear crossover, respiration can be characterized by just one fluctuation exponent α_{RES}. Under the assumption of an average breath cycle spanning 4 heartbeats[52] we have defined an associated fitting range of $12 \le s \le 50$ breaths to allow comparison with $\alpha_{RR,2}$.

Short-term correlations quantified by $\alpha_{RR,1}$ are related to the HF-band as can be derived in a simple approximation (see footnote following acknowledgments). Scaling exponents $\alpha_{RR,2}$ and α_{RES}, on the other hand, describe long-range correlations associated with the VLF band. Thus they reflect cerebral dynamics rather than autonomic control. Hence, DFA results for large scales elucidate additional features of cardiopulmonary control and coupling.

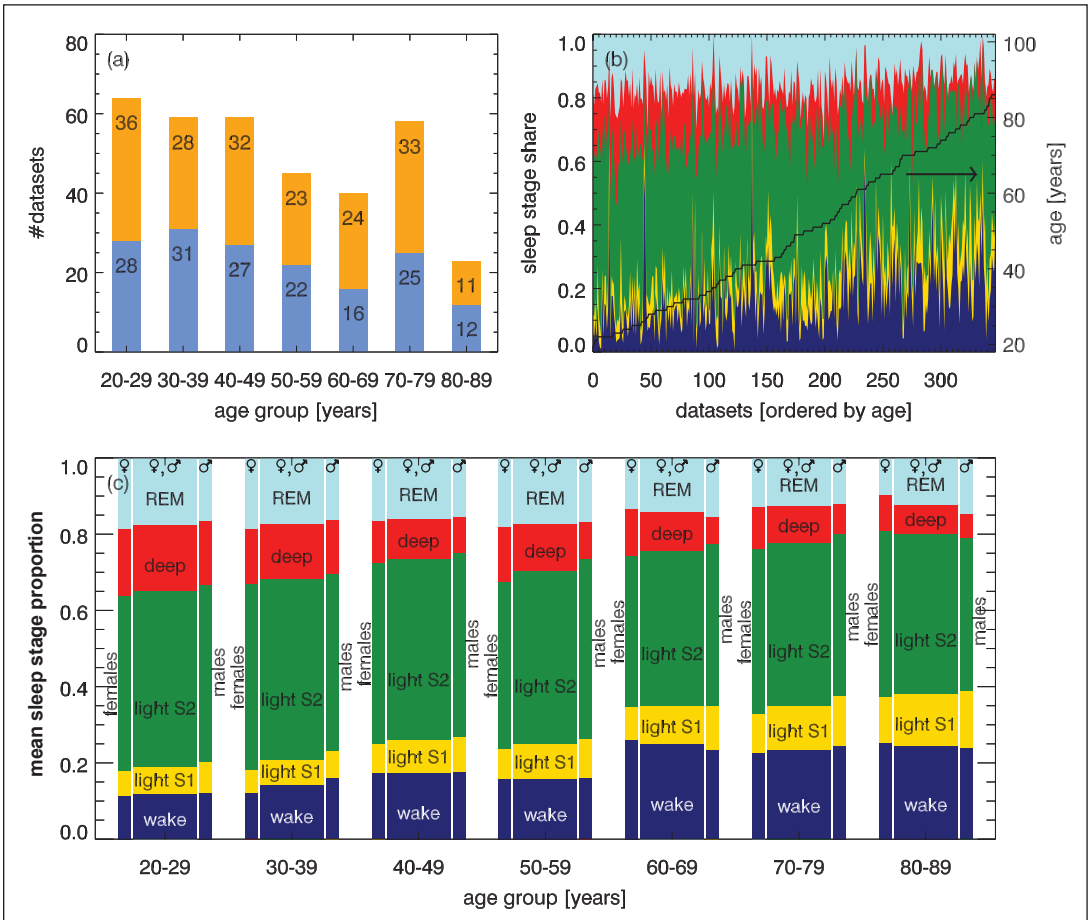

Figure 1—(a) Age and gender characteristics of the considered study cohort of disease-free humans (males blue, females orange). The total numbers of data sets (nights) are shown for each age group. (b) Proportion of sleep stages on total time in bed for all subjects sorted by age (from left to right). The colors indicate the states, from bottom to top: wake state - dark blue, light sleep stage 1 - yellow, light sleep stage 2 - green, deep sleep stages 3 and 4 - red, and REM sleep - light blue. (c) Sleep stage distribution averaged over 10 years for all subjects (large bars in the center), and separately for females (left) and males (right); colors and order as in (b).

Phase-Rectified Signal Averaging (PRSA) Method

PRSA is a powerful tool for extracting and displaying quasi-periodic oscillations in noisy, non-stationary signals.[24] It allows for the identification of complex control leading to nearly periodic oscillations despite phase resetting and noise. Focusing on particular time scales, it is complementary to the DFA procedure, which analyzes the scaling behavior by comparing variations on different time scales and characterizing the underlying noise. In addition, PRSA can be employed to study causal relationships between events, such as deceleration or acceleration of heartbeat.

The algorithm is rather simple. In the first step, anchor points are selected in the time series. In the standard form of the algorithm, anchors are defined for moderate increases in heart beat intervals, i.e., when the current heartbeat interval is longer than the preceding one, $x(t) > x(t-1)$. Here, we neglect very large changes (> 10%) in consecutive heartbeat intervals, which are most likely associated with artifacts in the data. We note that in the original version of the PRSA method[25] the limit for large changes was set to > 5% because this earlier study was designed to analyze data from post-infarction patients. Since healthy subjects have a large heart rate variability, we found that increases in consecutive heartbeat intervals between 5%

and 10% are rather common and normal. Thus, in this study we used a > 10% cutoff. In addition, we carefully removed all ventricular beats prior to the PRSA analysis.

The anchors are related to deceleration events, and thus, parasympathetic activation. Surroundings of length 2L are then defined around each anchor point, including the data from L previous points and $L - 1$ future points. Finally, all windows are aligned at the anchor positions and the PRSA curve $\bar{x}_{PRSA}(j)$ is obtained by calculating the arithmetic average over all windows separately for each point j, $j = -L,\ldots,0,\ldots, L-1$.

Taking 4 points from the center of the PRSA curve, which is equivalent to choosing $L = 2$, is sufficient to define the parameter *deceleration capacity*

$$DC = (1/4)[\bar{x}_{PRSA}(0) + \bar{x}_{PRSA}(1) - \bar{x}_{PRSA}(-1) - \bar{x}_{PRSA}(-2)]$$

DC has been shown to be a superior predictor of mortality in post-infarction patients, compared with the current gold standard, left ventricular ejection fraction (LVEF).[25]

Artifacts or outliers in the data can easily be handled by disregarding them in the selection of anchor points and in the averaging procedure. Note that a different number of data points might contribute to the PRSA averages at different locations.

Data Analysis and Statistics

For each data recording, and for each sleep stage, we calculated the values of $\alpha_{RR,1}$, $\alpha_{RR,2}$, α_{RES}, and DC, taking into account all reliable segments. In addition, we determined, for each α, the sum of squared residuals χ^2 for the linear fit in the double logarithmic plots, as well as the sum of squared deviations from the mean ($SOS = \Sigma(\log F_{DFA2}(s) - \overline{\log F_{DFA2}(s)})^2$). The coefficient of determination, $r^2 = 1 - \chi^2 / SOS$, indicates the reliability of the fits; $r^2 = 1$ for a perfect fit and $r^2 << 1$ for significant deviations from a power-law behavior in the corresponding fitting regime. The α values were considered to be reliable if (1) $F_{DFA2}(s)$ could be calculated for the whole regime and (2) $r^2 \geq 0.98$. For deceleration capacity (DC) we only considered values in the range $0 \leq DC \leq 40$ ms to be reliable. Within each age group we obtained statistical properties (mean, standard error, median, quartiles Q25 and Q75) based on reliable α and DC values only. However, we also present the distributions of the α values for unreliable fits for comparison.

RESULTS

Distribution of Sleep Stages

Figure 1a reports the study cohort with age and gender distribution. Figure 1b shows the share of the total time in bed for all states, separately for each record; and it is horizontally ordered by increasing age of the subjects. Each individual's age is indicated by the black curve, referring to the right axis. For Figure 1c, these data have been binned in age groups amounting to 10 years each. Separate results for males and females are also shown. Since effects of aging upon quantitative sleep parameters based on the SIESTA database (but without considering gender differences) were studied and reported earlier,[37] we will not discuss this in detail here.

However, in Figure 1b, it can be seen that inter-individual sleep notedly fluctuates, even within the same age class. Nevertheless, when considering group averages, total wake and total light sleep percentage obviously increase with age, while percentages of deep sleep and REM sleep decrease as shown in Figure 1c. Young females seem to have less wake and light sleep S1, but more REM sleep, when compared with males. For elderly (> 60 years) the behavior appears to be the opposite. While young males and females exhibit almost the same percentage of deep sleep, it decreases much more rapidly in males upon disease-free aging.

Correlation Properties of Heartbeat Intervals

Figure 2 shows the heartbeat fluctuation functions, $F_{DFA2}(s)$, of 3 representative subjects from different age groups: (1) young (20-39 years, lowest curves in each panel), (2) intermediate age (40-69 years, center), and (3) elderly (70-89 years, top) in a double logarithmic plot. The fitting regimes for $\alpha_{RR,1}$ (characterizing short-term correlations) and $\alpha_{RR,2}$ (characterizing long-term correlations) are indicated by gray bars. The slopes of the straight solid lines are identical with the fitted values of $\alpha_{RR,1}$ and $\alpha_{RR,2}$.

There are two important observations. First, one clearly sees the presence of long-range correlations ($\alpha_{RR,2} \approx 1 >> 1/2$) during wakefulness and REM sleep, while long-term correlations are weak or absent during light sleep and deep sleep ($\alpha_{RR,2} \approx 1/2$). This finding is consistent with earlier results.[13,21] Secondly, age differences in the scaling behavior are apparent, especially when comparing $\alpha_{RR,2}$ for young and elderly subjects during wakefulness and REM sleep, and when comparing $\alpha_{RR,1}$ for young and intermediately aged, as well as intermediately aged and elderly during all sleep stages.

To study these age dependences systematically we calculated DFA2 fluctuation functions for all data sets and fitted $\alpha_{RR,1}$ and $\alpha_{RR,2}$ in the scaling regimes shaded in Figure 2. To monitor the quality of the fits, we also calculated the coefficient of determination r^2 and disregarded fits with $r^2 < 0.98$, since the fluctuation functions are not sufficiently close to a power-law in these cases. Note that "healthy" subjects with unrecognized sleep apnea often exhibit deviations from the power scaling law, as the duration of the apneas is a characteristic time scale. This leads to a crossover in the DFA scaling function at this time scale.[28] Most data for such subjects are automatically disregarded by our $r^2 < 0.98$ criterion.

Figure 3 shows our main findings. Mean values and standard error of the means for $\alpha_{RR,1}$, $\alpha_{RR,2}$, and α_{RES} were calculated from the data of all subjects separated into 7 age groups spanning time periods of 10 years each. Results for men and women are shown separately. We have also compared the results for first and second nights (not shown) and found no systematic differences.

The corresponding distributions of individual scaling exponents for all data sets are shown in Figure 4, combining all age groups. The dark gray histograms are associated with the data included in Figure 3, while the additional light gray histogram bars include the results of non-reliable fits. One can see that the distributions are very close to Gaussian so that a Student t-test can be applied for checking the significance of differences.

Table 1 reports the numerical means and standard deviations (instead of standard errors of the means, as in Figure 3) for the 3 α parameters and the 4 states in young, intermediately aged, and

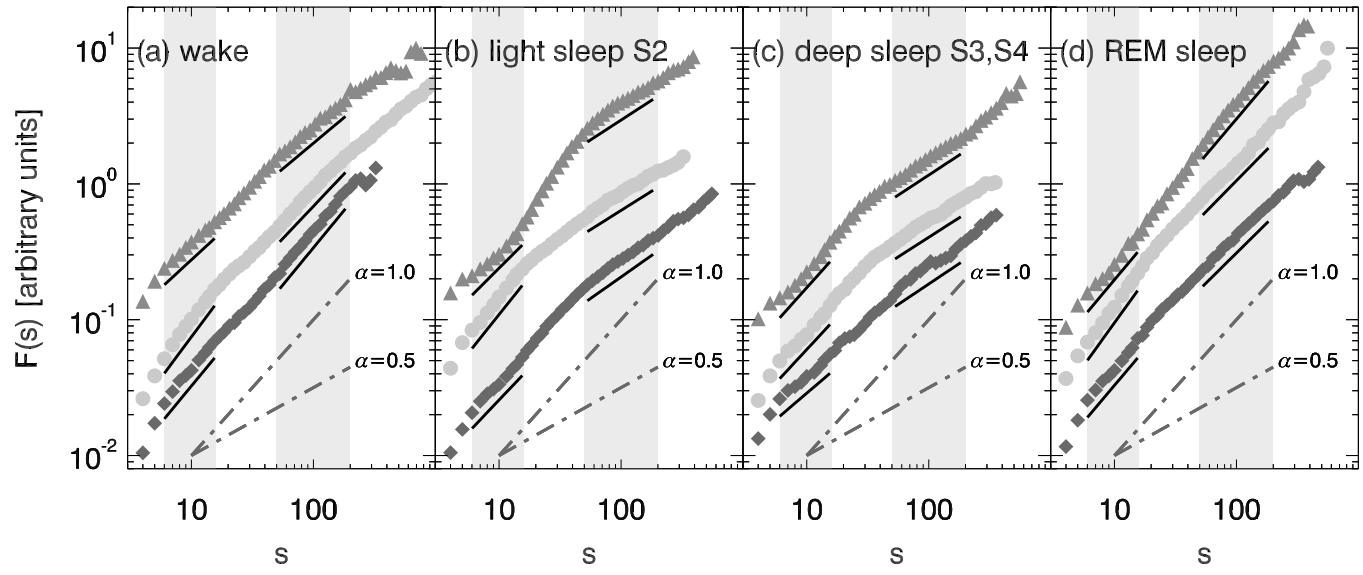

Figure 2—Examples of DFA2 heartbeat fluctuation functions for different sleep stages and representative subjects from three age groups, from bottom to top: young - dark gray diamonds, intermediate age - light gray circles, and elderly - gray triangles up. Gray shaded bars indicate the fitting regimes for $\alpha_{RR,1}$ ($6 \le s \le 16$ heartbeats) and $\alpha_{RR,2}$ ($50 \le s \le 200$ heartbeats). The slopes of the solid black lines are identical with these fitted exponents. For comparison gray dash-dotted lines indicate slopes of $\alpha = 1/2$ (uncorrelated behavior) and $\alpha = 1$ (1 / *f* noise). Fluctuation functions and fits are vertically shifted for clarity.

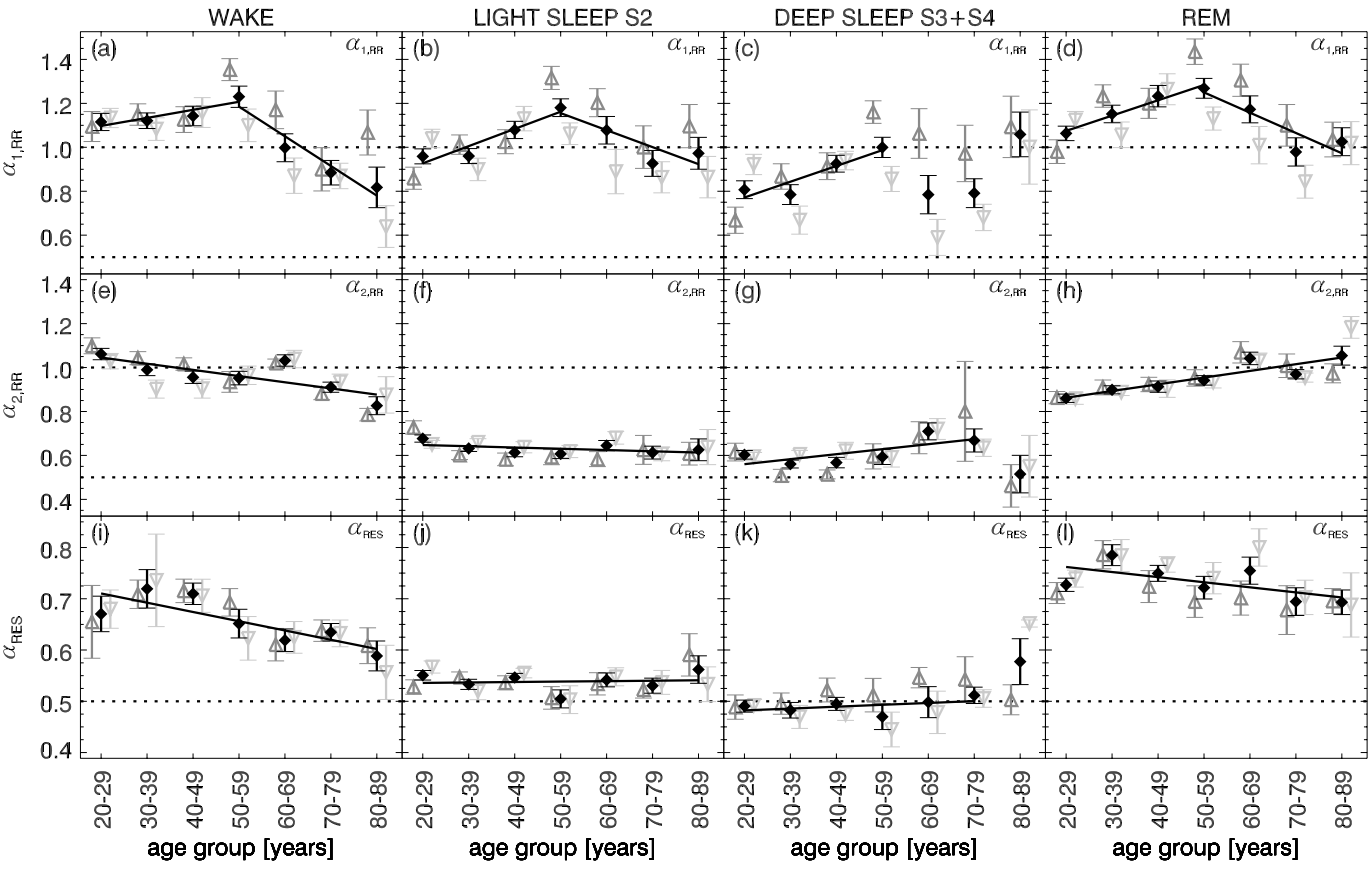

Figure 3—Age dependence of (a-d) heartbeat short-term fluctuation exponents $\alpha_{RR,1}$, (e-h) heartbeat, and (i-l) respiration long-term fluctuation exponents $\alpha_{RR,2}$ and α_{RES} for wakefulness, light sleep S2, deep sleep S3 and S4, and REM sleep. The mean values for all subjects (black diamonds), men (dark gray open triangles up), and women (light gray open triangles down) are shown with error bars representing the standard errors of the means. Black solid lines indicate linear fits to the means based on all age groups, except for $\alpha_{RR,1}$, where 2 separate fit regimes (20-59 and 50-89 years) were chosen and for deep sleep, where insufficient statistics in elderly did not allow fitting. Note that α values with $r^2 < 0.98$ or incomplete fitting regimes were disregarded. The dotted lines mark $\alpha = 1/2$ (uncorrelated behavior) and $\alpha = 1$ (1 / *f* noise).

Table 1

Measure	$\alpha_{RR,1}$	$\alpha_{RR,2}$	α_{RES}
Wake			
Young	1.12 ± 0.25†	1.02 ± 0.15†○	0.69 ± 0.16*
Middle	1.13 ± 0.33○	0.98 ± 0.15	0.66 ± 0.12
Elderly	0.87 ± 0.35†	0.89 ± 0.14‡	0.62 ± 0.10
Light sleep S2			
Young	0.96 ± 0.26	0.65 ± 0.11	0.54 ± 0.07
Middle	1.12 ± 0.29†	0.62 ± 0.13	0.53 ± 0.08
Elderly	0.95 ± 0.35‡	0.60 ± 0.14	0.54 ± 0.10
Deep sleep S3 and S4			
Young	0.80 ± 0.29	0.59 ± 0.13	0.49 ± 0.09
Middle	0.93 ± 0.29‡○	0.60 ± 0.15	0.49 ± 0.11○
Elderly	0.84 ± 0.35	0.60 ± 0.15	0.52 ± 0.07
REM sleep			
Young	1.11 ± 0.28	0.88 ± 0.13†	0.75 ± 0.11*
Middle	1.23 ± 0.33‡○	0.95 ± 0.15†	0.74 ± 0.12○
Elderly	1.00 ± 0.36†	1.00 ± 0.13	0.69 ± 0.12

Mean values and standard deviations for fluctuation exponents α during wakefulness, light sleep stage S2, deep sleep S3 and S4, and REM sleep distinguishing 3 cohort subsets: young (age 20-39), intermediately aged (age 40-69), and elderly (age 70-89). The null-hypothesis that values for a pair of cohort subsets are drawn from distributions with identical mean was checked by a 2-sided heteroscedastic Student *t*-test. Three significance levels are indicated by symbols, $P < 0.001$ (†), $P < 0.01$ (‡), and $P < 0.03$ (*). The symbols (†, ‡, *) in the line for young subjects refer to the test comparing young and elderly, the symbols in the line for intermediately (middle) aged subjects to comparing them with young, and the test in the line for elderly refers to comparing elderly with middle aged. Additionally, the symbol ○ indicates significant differences ($P < 0.03$) between males and females in the same age group.

elderly subjects. The significance of the differences between these 3 age groups is indicated in the table by different symbols that were defined according to different P-values obtained from a *t*-test.

A very interesting age dependence is observed in heartbeat correlations on short time scales, i.e., in the exponent $\alpha_{RR,1}$. We find a systematic and significant increase, in the age range from 20 to 59 years, for each sleep stage, but not during wake (where our analysis shows no significant difference between the 20-29 year and the 50-59 year group, *t*-test: $P > 0.05$). This increase is almost independent of gender (Figures 3a-d and Table 1). Above 60 years of age, a systematic and significant decrease in $\alpha_{RR,1}$ occurs with further aging, except during deep sleep, where statistics are insufficient in the elderly groups. Note that the total time spent in deep sleep is reduced in elderly subjects (Figure 1), and is usually accompanied by an increased occurrence of ectopic beats. In our analysis this results in the rejection of whole segments of data during deep sleep when dealing with elderly subjects (thus, the average $\alpha_{RR,1}$ value for the 80-89 year old group during deep sleep as shown in Figure 3c is based on only 8 $\alpha_{RR,1}$ values from 6 subjects). The general picture of a maximum in $\alpha_{RR,1}$ in the age regime of 50-60 years is, nevertheless, independent of the considered sleep stage (or wake). This is the same for both, males and females, indicating a high reliability. However, in the intermediate age group of 40-69 years, the values for females are lower than those for males, at a $P < 0.03$ significance level during wakefulness, deep sleep, and REM sleep (see Table 1). These differences might be an indication of an earlier decay in $\alpha_{RR,1}$ for females.

Besides the most interesting age dependence, our analysis showed significant differences in $\alpha_{RR,1}$ values across sleep stages for all age groups (except the 80-89 year group, where the statistics are not sufficient). These differences are comparable to the age difference within each sleep stage. Specifically, for the 20-29 year group, we find a significant difference between sleep stages, with the lowest $\alpha_{RR,1}$ values during deep sleep, higher values during light sleep and highest values during REM and wake (Figures 3a-d, $P < 0.01$ for deep sleep versus light sleep and light sleep versus wake, and $P < 0.001$ for deep sleep versus REM sleep). For the 50- to 59-year-old group, where the maximum in $\alpha_{RR,1}$ occurs, our results show a similar pattern of lowest values during deep sleep and higher values during light sleep, REM sleep, and wake (Figures 3a-d), with $P < 0.01$ for deep sleep versus light sleep; $P < 0.001$ for deep sleep versus REM sleep; and no significant differences between wake, REM sleep, and light sleep. Comparing the 20-29 year-old group with the 50-59 year-old group, we find statistically significant age related differences within each sleep stage (deep sleep $P < 0.01$, light sleep $P < 0.001$, REM sleep $P < 0.001$) but not wake ($P > 0.05$). These age differences are statistically similar to the differences across sleep stages for each of the 2 groups. These observations indicate that the effect of sleep regulation on $\alpha_{RR,1}$ in heartbeat intervals is comparable to the effect of aging.

For larger time scales $\alpha_{RR,2} \approx 0.9 > > 1/2$ indicates that there are long-term correlations in both, wake and REM sleep that are almost absent in NREM sleep (light sleep and deep sleep, $\alpha_{RR,2} \approx 0.6$). This confirms the scaling behavior observed previously in a much smaller cohort of young subjects,[13,21] as well as in a group of elderly subjects,[29] suggesting a common dependence of $\alpha_{RR,2}$ on sleep stages for all age groups. Note that data from the 2 oldest groups must be disregarded during deep sleep because of insufficient statistics (also indicated by large error bars).

Looking at the age dependence of $\alpha_{RR,2}$, we observe significant changes during REM and wake (see Figures 3e, h). During REM sleep, $\alpha_{RR,2}$ increases from $\alpha_{RR,1} = 0.86$ for young adults (aged 20-29) up to values $\alpha_{RR,2} = 1.05$ in the very elderly (aged 80-89). This increase is statistically significant for the young and middle age groups, while we find no significant difference when comparing intermediate age and elderly subjects (see Figure 3h and Table 1). For wakefulness $\alpha_{RR,2}$ decreases from $\alpha_{RR,2} = 1.06$ to $\alpha_{RR,2} = 0.83$ in the course of normal disease-free aging. This decrease is statistically significant both when comparing intermediate age and the elderly as well as young and elderly subjects, while we found no significant difference when comparing the young and the intermediate age groups (see Figure 3e and Table 1). During light sleep and deep sleep, no significant age dependence is observed in $\alpha_{RR,2}$ (see Figures 3f and g and Table 1).

Correlation Properties of Respiration

Regarding respiration we present results for inter-breath intervals obtained from maxima in the oronasal-airflow signal.

We have also checked other respiration proxies (inter-breath intervals from belt recordings and based on signal maxima or minima), but found the differences too small to warrant a separate reporting in this paper. Neglecting age dependence, one finds similar scaling behavior as for heartbeat, i.e., $\alpha_{RES} > 1/2$ for wake states and REM sleep, as well as $\alpha_{RES} \approx 1/2$ for deep sleep (Figures 3i-l and Table 1). This is consistent with earlier observations in a much smaller cohort.[4] Furthermore, it seems that weak long-term correlations are present in respiration during light sleep and absent during deep sleep (see also the histograms in Figure 4). The overall correlations are much weaker than those observed for heartbeat data. Given that the histograms are almost identical for males and females (not shown), during all studied sleep stages and wakefulness, we conclude there are hardly any gender effects. Although we note that intermediately aged females have (weakly significant) smaller and larger averages during deep sleep and REM sleep, respectively (Figures 3k-l).

Looking at the age dependence, one recognizes an opposite aging effect during REM sleep when compared with heartbeat: α_{RES} decreases with age while $\alpha_{RR,2}$ increases (Figures 3h, 3l). For wakefulness, both exponents α_{RES} and $\alpha_{RR,2}$ decrease (Figures 3e, 3i). Note, however, that the observed age dependences in α_{RES} during wake and REM are weakly significant (see Table 1). No significant age dependencies in respiratory correlations are observed during NREM sleep.

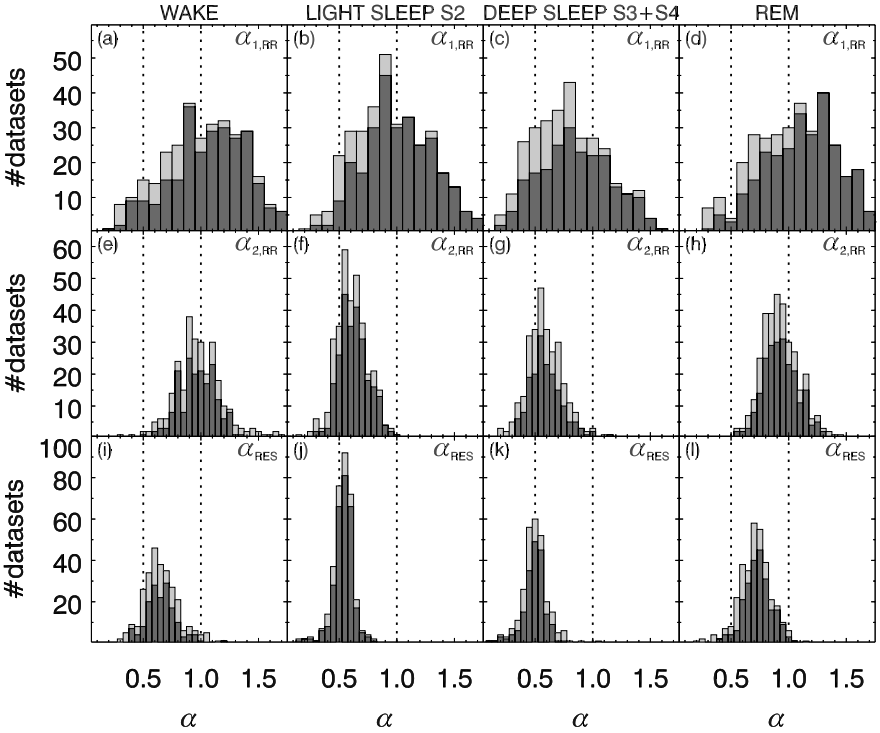

Figure 4—Histograms of (a-d) $\alpha_{RR,1}$, (e-h) $\alpha_{RR,2}$, and (i-l) α_{RES} in wake state, light sleep S2, deep sleep S3 and S4, and REM sleep. Light gray histograms show the distributions for all 348 data sets considered in this study, while the α values from fits with $r^2 < 0.98$ or incomplete fitting regimes were excluded for the dark gray histograms. Dotted lines indicate random uncorrelated behavior $\alpha = 1/2$ and strongly correlated behavior $\alpha = 1$. Note that the bins were chosen twice as wide for (a-d) compared with (e-l).

Influence of Tobacco and Alcohol on Cardiac and Respiratory Dynamics

To asses the influence of smoking on the correlation properties of cardiac and respiratory dynamics across different sleep stages and how they change with aging, we separately analyzed and compared smokers and nonsmokers. In the SIESTA database, 39 of the healthy subjects were identified as smokers and 136 as nonsmokers. There is no information available for 5 subjects in the database. For the subjects that were identified as smokers there is no information recorded in the database on the number of cigarettes per day or on the period (years) over which subjects have been actively smoking prior to the SIESTA study. We have tested whether any of the scaling exponents ($\alpha_{RR,1}$, $\alpha_{RR,2}$, α_{RES}), characterizing cardiac and respiratory dynamics for smokers, are significantly different from the values observed for non-smokers. By differentiating 3 age groups (age: 20-39 years, 40-69 years, and 70-89 years) and 4 sleep stages (wake, light sleep, deep sleep, and REM sleep), we found significant changes with smoking in 2 cases: (1) in young subjects during wake, the scaling exponent $\alpha_{RR,1}$, characterizing short-term correlations in heartbeat fluctuations, decreases when compared with nonsmokers ($P < 0.01$); and (2) in intermediately aged subjects during REM sleep, the scaling exponent α_{RES} of respiratory dynamics also decreases when compared with nonsmokers ($P < 0.03$). The number of smokers among the elderly ($n = 4$) was insufficient to assure meaningful statistics. We did not find effects of smoking upon the scaling exponent $\alpha_{RR,2}$, characterizing the long-term heartbeat correlations. The observed differences related to smoking are smaller when compared with the age-dependent and sleep-stage dependent differences presented in Figure 3 and Table 1.

Regular alcohol intake in a certain period of their life prior to the recordings was reported by 31 subjects (out of 180 subjects; no information is available on 2 subjects). Combining all age groups, we find that the short-term scaling exponent $\alpha_{RR,1}$ of heartbeat dynamics is significantly larger for the subjects with regular alcohol intake across all sleep stages – with 19% increase during wake ($P < 0.001$) when compared with subjects without a history of regular alcohol intake; 12% increase during REM sleep ($P < 0.01$), 13% increase during NREM sleep ($P < 0.01$). For the respiration scaling exponent α_{RES}, we found a 5% increase for the alcohol group during NREM sleep ($P < 0.01$). We observed no significant changes in the long-term scaling exponent $\alpha_{RR,2}$ of heartbeat dynamics. By considering separate age groups, we found a significant increase in $\alpha_{RR,1}$ during REM and in α_{RES} during NREM sleep (both with $P < 0.03$) for the group of younger subjects (age: 20-39 years) who had regular alcohol intake. For the group of intermediately aged subjects (age: 40-69 years) who had episodes of regular alcohol intake, we found a significant increase in the short-term scal-

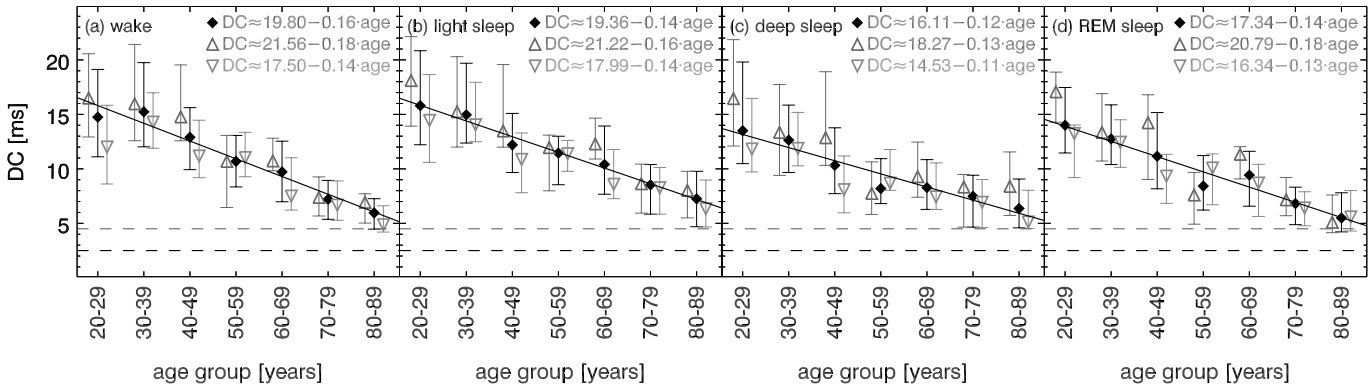

Figure 5—Deceleration capacity (*DC*) versus age for (a) wakefulness, (b) light sleep S2, (c) deep sleep S3 and S4, and (d) REM sleep for all subjects (black filled diamonds), males (dark gray open triangles up), and females (light gray open triangles down). We plotted median values and both quartiles Q25 and Q75 as lower and upper errors bars, respectively. Solid straight lines are linear fits to the medians for all subjects; the formulas of the separate fits for males and females are printed in the top right corner. Black and gray dashed lines indicate risk levels previously defined for infarction patients: high cardiac risk *DC* < 2.5 ms and low cardiac risk *DC* < 4.5 ms.

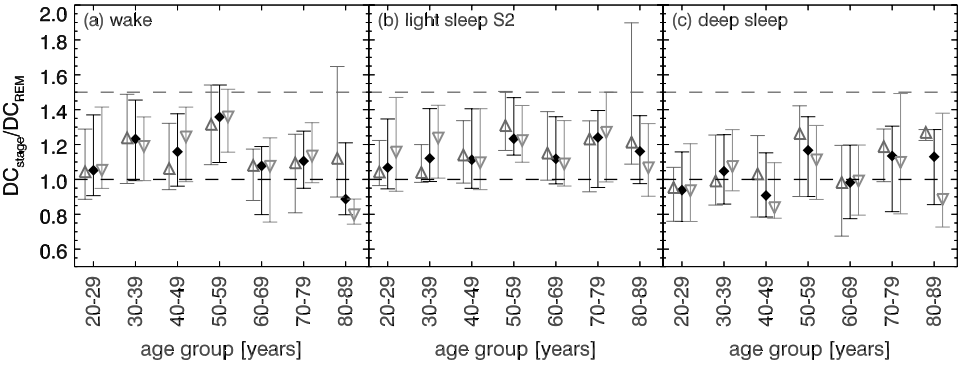

Figure 6—Age dependence of *DC* ratios: (a) DC_{wake} / DC_{REM}, (b) $DC_{light\ sleepS2} / DC_{REM}$, and (c) $DC_{deep\ sleep\ S3\&S4} / DC_{REM}$ for all subjects (black filled diamonds), males (dark gray open triangles up), and females (light gray open triangles down).

When exploring individual *DC* values we recognized for most subjects, lower values during REM sleep and deep sleep than during light sleep and wakefulness. To test this observation, Figure 6 shows the mean ratios over DC_{REM} and their standard deviations. In the case of a lower *DC* during REM sleep, the ratios are larger than 1. This is observed for young subjects during wake, and for all age groups during light sleep S2, i.e., $DC_{REM} < DC_{wake}$ and $DC_{REM} < DC_{light\ sleep}$. The results during deep sleep were inconclusive. Employing a paired *t*-test comparing all *DC*-value combinations we found highly significant differences ($P < 0.0001$) for the combinations wake vs. REM sleep, light sleep vs. REM sleep, wake vs. deep sleep, and light sleep vs. deep sleep. Marginally significant differences ($P < 0.05$) were found for wake vs. light sleep. The *DC* values during deep sleep and REM sleep were not significantly different.

ing exponent, $\alpha_{RR,1}$, of cardiac dynamics only during wake. The number of elderly subjects (age: 70-89 years) in our database who reported episodes of regular alcohol intake is insufficient for a meaningful statistical analysis.

Alcohol consumption on the day before the recordings was reported only by 30 subjects (38 night recordings). Combining all age groups, we find a slight increase (below significance level) in the exponent $\alpha_{RR,1}$ during REM and NREM sleep, and a significant increase in α_{RES} during NREM sleep.

Deceleration Capacity of the Heart

Figure 5 shows our results for the deceleration capacity of the heart (*DC* parameter) as a function of age, shown separately for the sleep stages and wake. A significant decay from younger subjects towards older subjects is obvious in all states. The slope of the decay is, however, smaller for females than for males (see different symbols and fits printed in the figure but not shown). In particular young females (age 20-29) exhibit surprisingly low *DC* values, especially during wake. If one excluded this age group from the study, the *DC* slope for males and females during wakefulness would be the same. In general, *DC* values for males and females become more similar with aging for all states.

DISCUSSION

Our study leads to the following four main observations: (1) There is a significant aging effect on the short-term correlation properties of heartbeat time series, since a maximum in $\alpha_{RR,1}$ occurs around 50-60 years of age. We also observe comparable differences across sleep stages for the young and intermediate age groups. (2) The long-term correlation properties of heartbeat and respiration data exhibit similar characteristic dependencies on sleep stages and wake: long-term correlations and effects of aging are observed only during wakefulness and REM sleep. Heartbeat correlations increase with age in REM sleep and decrease during wake, while respiratory correlations decrease with age both during REM and wake. (3) Differences between males and females of the same age are not significant for most scaling parameters in the studied cohort, except for a significantly lower average in $\alpha_{RR,1}$ for intermediately aged

females. (4) Deceleration capacity (i.e., the ability of the heart to slow down) decreases linearly with age and reduces significantly during deep sleep and REM sleep when compared with light sleep and wakefulness.

Previous studies have also analyzed the short-term and long-term correlation behavior of heartbeat and breathing intervals in healthy subjects. However, previous studies considered much less data (approx. 500 h, compared to our 2,500 h), did not distinguish sleep stages, and only compared a single group of young with a single group of elderly subjects.[26,3,27,28] Others distinguished sleep stages but did not study age dependencies and focused mainly on healthy young subjects (age ≈ 25 years).[13,20,21,4] Only one study so far has considered the effect of aging across different sleep stages based on a group of young subjects (age ≈ 33 years) and a group of elderly subjects (age ≈ 78 years).[29] Since intermediate age groups of 50-60 year-old subjects have not been studied, the pronounced maximum in short-term heartbeat correlations has not been previously observed.

Short-Term Correlation Properties of Heartbeat

While earlier studies have suggested that multi-scale complexity and fractal scaling behavior break down with healthy aging,[53,26] a recent work,[28] utilizing the same data sets as in Iyengar et al.[26] as well as a second independent database, did not find significant differences between young and elderly healthy subjects in the heartbeat scaling behavior after carefully excluding artifacts. Iyengar et al. found $\alpha_{RR,1} = 0.90$ for young (age ≈ 27 years) and $\alpha_{RR,1} = 1.12$ for elderly (age ≈ 74 years) subjects based on 40 hours of data recorded from 20 subjects during wake in a resting semi-recumbent position. Their results show the opposite trend when compared with our results of $\alpha_{RR,1} = 1.12$ for the 20-29 year-old group and $\alpha_{RR,1} = 0.88$ for the 70-79 year-old group during wake (see Figure 3a). This is perhaps due to apnea-related artifacts in the data from elderly subjects which were not taken into account in Iyengar et al.[26] but significantly alter the scaling exponent at both short and long time scales as demonstrated by Schmitt et al.[28]

However, our results for young subjects are consistent with recent studies. Penzel et al.[21] found $\alpha_{RR,1} = 1.21$ during wakefulness, 1.18 during REM sleep, 1.00 during light sleep, and 0.82 during deep sleep in a data set of 14 healthy subjects with an average age of 33 years (220 hours of data). Guzman-Vargas and Angulo-Brown[27] studied 36 hours of data from ten young and eight elderly subjects during wake using a different technique; their results correspond to $\alpha_{RR,1} \approx 1.13$ and 1.48, respectively. Clearly, the values for young subjects are consistent with ours, but the values for elderly subjects are higher than ours. We speculate that the unexpectedly large value 1.48[27] might be due to outliers among their eight elderly subjects. In addition, slightly larger α values are usually found when different states are not analyzed separately due to non-stationarities at the transitions between the states. Recently, Schmitt et al.[28] found $\alpha_{RR,1} = 1.09$ for 19 young subjects (age ≈ 26 years) and $\alpha_{RR,1} = 1.22$ for 16 elderly subjects (age ≈ 74 years) during wake in a resting semi-recumbent position. In addition they found $\alpha_{RR,1} = 1.12$ for an independent group of 29 elderly subjects (age ≈ 76 years) during sleep and $\alpha_{RR,1} = 1.09$ for the same subjects five years later (altogether ≈ 550 hours of data), reporting no significant age differences. Our results show no significant difference in $\alpha_{RR,1}$ between young (age 20-39 years) and elderly (age 70-89 years) for deep sleep, light sleep, and REM, and a significant difference only during wake (see Table 1).

As mentioned before, none of the previous studies looked at intermediate age groups and therefore the pronounced maximum in $\alpha_{RR,1}$ around 50-60 years of age, for all sleep stages as well as wakefulness, was missed. We suggest that the underlying effect of healthy aging could be an *increase* in $\alpha_{RR,1}$ as indicated by the trend present from 20 to 55 years of age (see Figure 3). If the increase continued for the next 35 years, i.e., up to 90 years of age, the values of $\alpha_{RR,1}$ would reach 1.4 or 1.5, i.e., values typical for an uncorrelated random walk. This usually does not happen, though, because another effect leads to a drop of $\alpha_{RR,1}$ for subjects of ages above 50-60 years. The drop seems to start somewhat earlier in women. A satisfying explanation of this observation would seem to require a change in the related control mechanisms which is sufficiently fundamental to affect all sleep stages and wakefulness. We speculate that this change might be related to the rise in evening cortisol levels associated with increased sleep fragmentation and a decline in REM sleep. Such a rise was reported to begin at the age of 50 years.[39] High cortisol levels have been associated with physiological stress and increased cardiac risk. We note that reduced short-term correlation exponents were shown to be better indicators than standard HRV parameters for predicting mortality in post-infarction patients.[23,22] However, we also note that the $\alpha_{RR,1}$ values for the elderly subjects are comparable to the $\alpha_{RR,1}$ values for the young subjects during all sleep stages except for wake, where $\alpha_{RR,1}$ is significantly lower in elderly (see Figures 3a-d, Table 1). We cannot exclude that the age-related drop in $\alpha_{RR,1}$ might be a reflection of a detrimental effect of this endpoint on individual survival. This means that the study of older subjects might favor individuals who had particularly favorable lower $\alpha_{RR,1}$ values throughout their entire life, whereas those with less favorable larger values had a lower probability of survival and were less likely to be included.

Regarding only the elderly subjects, there is a relevant technical point affecting the mean values of $\alpha_{RR,1}$. We observed an additional decrease in $\alpha_{RR,1}$, down to values even close to 0.5, in the oldest subjects if bad fits with coefficient of determination $r^2 < 0.98$ were not disregarded in our analysis and ectopic beats were not carefully removed (ectopic beats have the effect of random spikes in the positively correlated heartbeat interval time series that leads to a decrease in the scaling exponent on short time scales resulting in $\alpha_{RR,1} \approx 0.5$[48]). This indicates that an increasing number of ectopic beats and effects of sleep apnea (leading to deviations from the power-law scaling behavior of the fluctuation function[28]) might be partly responsible for the decrease in $\alpha_{RR,1}$ in clinically healthy, elderly subjects with possibly increased cardiac risk. We note that the coefficient of determination is usually not checked in instances where $\alpha_{RR,1}$ is used as an indicator for predicting cardiac risk and mortality in post-infarction patients.[23,22,54] In general, the aging characteristics of $\alpha_{RR,1}$ should be taken into account when using it for diagnostic purposes in post-infarction patients.

Long-Term Correlation Properties of Heartbeat and Respiration

Similar to the case for the short-term correlations in heartbeat intervals, previous studies regarding the age dependence of long-term correlation properties of heartbeat and respiration in healthy subjects have not yielded a consistent picture. Early works found significant differences between young and elderly subjects, see, e.g., $\alpha_{RR,2}$ = 0.99 versus 0.75 in Iyengar.[26] More recent studies reported no significant difference in $\alpha_{RR,2}$ between young and elderly during wake, see, e.g., $\alpha_{RR,2}$ = 1.13 versus 1.17[27] and $\alpha_{RR,2}$ = 0.76 versus 0.78.[28] The latter study also reported $\alpha_{RR,2}$ = 0.88 during sleep for elderly subjects (age ≈ 76 years) and $\alpha_{RR,2}$ = 0.97 for the same individuals five years later (P = 0.01).

For respiration during wake, Peng et al.[3] reported a gender difference, finding α_{RES} = 0.68 (0.70) versus 0.60 (0.67) for males (females) and, again, young versus elderly subjects. Although we found similar results when comparing young and elderly during wake, we did not find a significant gender difference. However, all these studies did not distinguish between physiologically different states like sleep stages, and thus, these values cannot be directly compared with ours. For both heartbeat and inter-breath intervals, we found that there is a stark contrast between the clearly long-term correlated behavior observed during wakefulness and REM sleep and the nearly uncorrelated behavior observed during NREM sleep. We also observed significant changes, with aging, during wakefulness and REM, but not during light sleep and deep sleep (see Figures 3e-l).

Most studies separating sleep stages looked at healthy young (age ≈ 25 years) subjects only.[4,13,21,55] A comparison of scaling and other characteristics of heartbeat intervals between young and elderly subjects, during different sleep stages, was presented in Schmitt et al.,[29] reporting a similar stratification pattern for both young and elderly across sleep stages. These earlier studies yielded results consistent with our findings, e.g., $\alpha_{RR,2}$ = 0.94 (wake), 0.60 (light sleep), 0.55 (deep sleep), and 0.81 (REM sleep) for a group of young (age 25 years old) subjects[21]; and $\alpha_{RR,2}$ = 0.97 (wake), 0.74 (light sleep), 0.61 (deep sleep), and 0.89 (REM sleep) for a group of 13 young (age 33 years old) subjects.[29] These results can be compared with the corresponding values $\alpha_{RR,2}$ = 1.06 (wake), 0.68 (light sleep), 0.60 (deep sleep), and 0.86 (REM sleep) for the 20-29 year-old group in this paper for heartbeat, as well as α_{RES} = 0.57 (NREM sleep) versus 0.85 (REM sleep)[4] compared with α_{RES} = 0.55 (light sleep) versus 0.73 (REM sleep) for respiration in our study. Schmitt et al.[29] also studied 24 elderly subjects (age ≈ 78 years) finding $\alpha_{RR,2}$ = 1.03 (wake), 0.63 (light sleep), 0.57 (deep sleep), and 1.02 (REM sleep), compared with $\alpha_{RR,2}$ = 0.91 (wake), 0.61 (light sleep), 0.67 (deep sleep), and 0.97 (REM sleep) in this paper for the corresponding age group of 70-79 years. This indicates a very similar stratification pattern in $\alpha_{RR,2}$ across sleep stages for elderly subjects in both studies. Moreover, this stratification pattern in $\alpha_{RR,2}$ is robust, as we observe it also for young subjects in agreement with Schmitt et al.[29] Clearly, it is not possible to find age dependencies by comparing these values with those for young subjects. Schmitt et al.[29] correctly conclude that there are no significant effects of aging observed in their data when comparing $\alpha_{RR,2}$ for young (≈ 33 years old) and elderly (≈ 78 years old) across different sleep stages. We observed a similar behavior when comparing $\alpha_{RR,2}$ for the 30-39 year-old group with the 70-79 year-old group, with P = 0.02 during REM and P > 0.02 for the other sleep stages and wake (see Figure 3). However, when we included the 20-29 year-old group and the 80-89 year-old group, we found a significant difference in $\alpha_{RR,2}$ with age during REM and wake. In contrast, we did not find an age dependence in the long-term scaling behavior of the heartbeat and breathing intervals during light sleep and deep sleep. Moreover, while we observed a significant increase with age in the strength of the long-term correlations for heartbeat intervals during REM (Figure 3h), we found the opposite trend of decreasing $\alpha_{RR,2}$ with age during wake (Figure 3e). We currently do not have a physiological explanation for the decrease in $\alpha_{RR,2}$ with age during wake, considering that $\alpha_{RR,2}$ reflects predominantly sympathetic tone, which was previously found to increase with age.

The pronounced long-term correlations, i.e., larger $\alpha_{RR,2}$ for heartbeat and α_{RES} for respiration we observe during REM sleep and wakefulness, indicate an enhanced control of higher brain regions on these autonomic functions when the brain is in a more active state. The enhanced control causing long-term correlations is obviously absent during NREM sleep, in agreement with earlier hypotheses.[4,13,55] This interpretation is strengthened by the observation of long-term correlations in the fluctuations of brain wave amplitudes and frequencies studied based on EEG data for wakefulness,[56] as well as separately for different sleep stages,[8] since the latter study revealed that long-term brain-wave correlations exist during REM sleep and wakefulness only.

Deceleration Capacity of the Heart

The decay of *DC* with age observed in this study is in full qualitative agreement with previously published results obtained from 24-h Holter-ECG recordings in 1455 post-infarction patients.[57] In that study we found DC_{all}[ms] = 12.2−0.10·age[y], DC_{males}[ms] = 12.4−0.11·age[y], $DC_{females}$[ms] = 12.2–0.07·age[y] but did not distinguish between wakefulness and sleep or sleep stages. These findings are in accordance with the general understanding that there is a loss in total vagal output with normal aging. A suppressed parasympathetic tone leads to a lower *DC* value, which is a measure of parasympathetic efficiency. A recent study revealed a significant gender difference in sympathovagal balance with higher vagal tones in females during all sleep stages.[58] Assuming *DC* is directly correlated with parasympathetic outflow, this should lead to a larger *DC* value in females than males. However, we found the opposite dependence here and in the independent study of 24-h Holter ECGs.[57] We can imagine two possible interpretations of this finding. Either the ability of the heart to decelerate quickly is not directly associated with the amplitude of parasympathetic output, or less parasympathetic output in males is more efficiently transcribed into actual deceleration than in females.

Furthermore, it is known that during REM sleep HF power, a proxy for parasympathetic tone, is diminished relative to other sleep stages and wakefulness. Concordantly, we found slightly lower *DC* values during REM sleep than during light sleep for most subjects. A lower *DC* has been associated with an increased mortality in post-infarction patients.[25,57] Increases in sympathetic output accompanied by reduced vagal activity

were related to ventricular arrhythmias that may cause sudden cardiac death.[59] Assuming these physiological conclusions are also applicable to healthy subjects, our findings suggest an increased cardiac risk during REM sleep when compared with light sleep or quiet wake. Together with the observation that most time spent in REM sleep takes place in the early morning hours the results of our analysis suggest an increase in cardiovascular risk during the morning hours. This is in agreement with earlier empirical observations based on hourly counts of sudden cardiac deaths and myocardial infarctions throughout the sleeping hours.[60]

Very few subjects had *DC* values exceeding the intermediate risk or the high risk limits (indicated by the dashed lines in Figure 5)[25] Note, however, that the risk limits have been determined for 24-h ECG recordings sampled at 128 Hz, and thus, it remains unclear whether the same limits apply to our sleep study of healthy subjects.

Limitations

In this study we concentrated on the effects of chronological age on short-term and long-term fluctuations of heartbeat and respiration. Although many risk factors and declining health have been associated with chronological age, it is a rather rough estimator for physiological age (i.e., functional age). It still remains to be explored how chronological and physiological age are correlated and to what extent chronological age is an indicator of physiological condition and function.

Another important issue is the definition of the term "healthy" especially in aged subjects. To our knowledge there is no general agreement on inclusion and/or exclusion parameters for healthy subjects. We are convinced that "healthy" should also consider biological age. During this study we realized that even supposedly healthy middle-aged and elderly subjects, without reported health complaints, show, to some extent, altered (relative to young healthy subjects) patterns in heartbeat and respiration. For instance, we found several short apnea-like episodes in data from disease-free elderly subjects. These episodes did not, however, lead to an exclusion of the subjects, because the all-night AHI index remained below 10 per hour. As well, an enhanced occurrence of ectopic beats and reduced heart rate variability is observed in several elderly subjects. Again, we have not excluded these subjects, only removed the ectopic beats from the data. However, from cardiological studies we know that some of the older subjects that were declared healthy, in full agreement with the SIESTA protocol would not be considered healthy in a more restrictive study protocol concentrating specifically on cardiac conditions. The results shown here present a retrospective analysis, and we had to accept recordings with some cardiac disturbances. Based on our experience with beat-detection and artifact removal, we suggest recording data from more ECG leads in full-night polysomnographic studies.

Summary and Outlook

In conclusion we have investigated and quantified the effects of normal aging on heartbeat-to-heartbeat and breath-to-breath variability during wakefulness, light sleep, deep sleep, and REM sleep. Our study is based on 2,500 hours of full-night recordings in a large group of 180 disease-free ("healthy") subjects ranging in age from 20 to 89 years.

We found that age significantly and systematically influences the short-term correlations of heartbeat, for all sleep stages and wakefulness. A striking maximum of the short-term correlation parameter $\alpha_{RR,1}$ occurs at around 50-60 years of age. The observed behavior is very similar for males and females. We speculate that the effect of healthy aging is an increase of $\alpha_{RR,1}$ with age that is reversed by a rise in evening cortisol levels reported to begin at the age of 50 years. Alternatively, the reduced $\alpha_{RR,1}$ could also be related to extrasystoles and ectopic beats in young and elderly subjects, respectively. Including fluctuation functions that exhibit problematic scaling behavior (often associated with sleep apnea episodes) further reduces the effective $\alpha_{RR,1}$ in elderly subjects. We believe that the aging characteristics of $\alpha_{RR,1}$ should be taken into account when using this parameter for diagnostic purposes in post-infarction patients. However, full-night data can be used without limitations, since sleep stage only weakly effects $\alpha_{RR,1}$.

Studying the auto-correlation behavior of heartbeat and respiration on longer time scales, we observed a clear difference between wakefulness and REM sleep on one hand and NREM sleep on the other. Pronounced long-term correlations occur during REM sleep and wakefulness only. They are probably related to an enhanced control of higher brain regions on these autonomic functions when the brain is in a more active state. In the case of heartbeat, we observed a slight decay of these long-term correlations with age, during wakefulness, and a slight increase during REM sleep. In the case of respiration we observed only a slight decay during both wakefulness and REM sleep.

Thus, the age dependence of heart rate and breathing rate correlations may be significantly more complex than a mere breakdown of multi-scale complexity and fractal scaling with aging.

Fluctuation characteristics have already been successfully applied to generate surrogate heartbeat data that is statistically indistinguishable from real recordings.[61] The age-related effects on short- and long-range variability discovered in this study might allow for further improvements, and ultimately lead to a more realistic model of cardiorespiratory regulation during sleep. We believe that the results should also be taken into account when developing novel scoring parameters to enhance the detection specificity for sleep related disorders.

The observed sleep-stage related changes in deceleration capacity (*DC*) can be compared with changes in long-term heartbeat correlations during different sleep stages to improve the understanding of cardiovascular regulation during sleep. In addition, the results could be applied to make ECG-based detection of sleep stages possible, instead of using more complicated brain recordings. Another possible application is the identification of anomalous autonomic regulation associated with certain disorders. We recently suggested a generalization of the PRSA method (bivariate phase rectified signal averaging = BPRSA) enabling multivariate studies of quasi-periodicities.[62] For example, one can separately analyze the behavior of heartbeat intervals at the phases of inspiration and expiration, or tackle the question how increases or decreases in heartbeat intervals affect respiratory rhythms and/or blood pressure. We are planning to apply BPRSA to heartbeat and respiration to further study cardiorespiratory control mechanisms during sleep and investigate respiratory gating.[63]

ACKNOWLEDGMENTS

We thank Prof. Dorffner and the SIESTA group for providing the data for this study. We also thank the European Community (project DAPHNet, grant FP6 IST 018474-2), the Deutsche Forschungsgemeinschaft (project KA 1676/3-2 and PE 628/3), the Brigham and Women's Hospital Biomedical Research Institute Fund, and the Office of Naval Research (ONR grant 000141010078) for support.

FOOTNOTE FROM PAGE 945

A scale correction depending on the detrending-order has to be applied,[50] since observed crossovers are larger than real ones: DFA2 $s_{real} \approx s_{observed} / 2.5$. A considered scaling range [6,16] heartbeats hence transforms to a real scaling range of [2.4,6.4] heartbeats corresponding to the frequency band [0.156,0.417] Hz under the simplified assumption of an average heartbeat interval of 1s. The HF band is usually associated with [0.15,0.4] Hz.

DISCLOSURE STATEMENT

This was not an industry supported study. Dr. Penzel has received research support from Actelion, Resmed, Respironics, Sanofi, and Weinmann; is shareholder of The Siestagroup and of the CRO Advanced Sleep Research; and has received travel support from Respironics, Weinmann, and Hoffrichter.

REFERENCES

1. Kobayashi M, Musha T. 1/f fluctuation of heartbeat period. IEEE Trans Biomed Eng 1982;29:456-7.
2. Saul JP, Albrecht P, Berger RD, Cohen JR. Analysis of long term heart rate variability: methods 1/f scaling and implications. Comput Cardiol 1988;14:419-22.
3. Peng CK, Mietus JE, Liu YH, et al. Quantifying fractal dynamics of human respiration: Age and gender effects. Ann Biomed Eng 2002;30:683-92.
4. Rostig S, Kantelhardt JW, Penzel T, et al. Nonrandom variability of respiration during sleep in healthy humans. Sleep 2005;28:411-7.
5. Frey U, Brodbeck T, Majumdar A, et al. Risk of severe asthma episodes predicted from fluctuation analysis of airway function. Nature 2005;438:667-70.
6. Linkenkaer-Hansen K, Nikouline VV, Palva JM, Ilmoniemi RJ. Long-range temporal correlations and scaling behavior in human brain oscillations. J Neurosci 2001;21:1370-7.
7. Shen Y, Olbrich E, Achermann P, Meier PF. Dimensional complexity and spectral properties of the human sleep EEG. Clin Neurophysiol 2003;114:199-209.
8. Gans F, Schumann AY, Kantelhardt JW, Penzel T, Fietze I. Cross-modulated amplitudes and frequencies characterize interacting components in complex systems. Phys Rev Lett 2009;102:098701.
9. Hausdorff JM, Purdon PL, Peng CK, Ladin Z, Wei JY, Goldberger AL. Fractal dynamics of human gait: Stability of long-range correlations in stride interval fluctuations. J Appl Physiol 1996;80:1448-57.
10. Bartsch R, Plotnik M, Kantelhardt JW, Havlin S, Giladi N, Hausdorff JM. Fluctuation and synchronization of gait intervals and gait force profiles distinguish stages of Parkinson's disease. Physica A 2007;383:455-65.
11. Ivanov PC, Ma QD, Bartsch RP, et al. Levels of complexity in scale-invariant neural signals. Phys Rev E 2009;79:041920.
12. Peng CK, Havlin S, Stanley HE, Goldberger AL. Quantification of scaling exponents and crossover phenomena in nonstationary heartbeat time series. Chaos 1995;5:82-7.
13. Bunde A, Havlin S, Kantelhardt JW, Penzel T, Peter JH, Voigt K. Correlated and uncorrelated regions in heart-rate fluctuations during sleep. Phys Rev Lett 2000;85:3736-9.
14. Ivanov PC, Amaral LA, Goldberger AL, et al. Multifractality in human heartbeat dynamics. Nature 1999;399:461-5.
15. Ivanov PC, Amaral LA, Goldberger AL, et al. From 1/f noise to multifractal cascades in heartbeat dynamics. Chaos 2001;11:641-52.
16. Karasik R, Sapir N, Ashkenazy Y, et al. Correlation differences in heartbeat fluctuations during rest and exercise. Phys Rev E 2002;66:062902.
17. Martinis M, Knežević A, Krstačić G, Vargović E. Changes in the Hurst exponent of heartbeat intervals during physical activity. Phys Rev E 2004;70:012903.
18. Ivanov PC. Sleep-wake differences in scaling behavior of the human heartbeat: Analysis of terrestrial and long-term space flight data. Europhys Lett 1999;44:594-600.
19. Ivanov PC. Scale-invariant aspects of cardiac dynamics - Observing sleep stages and circadian phases. IEEE Eng Med Biol 2007;26:33-7.
20. Kantelhardt JW, Ashkenazy Y, Ivanov PC, et al. Characterization of sleep stages by correlations in the magnitude and sign of heartbeat increments. Phys Rev E 2002;65:051908.
21. Penzel T, Kantelhardt JW, L. Grote, Peter J-H, Bunde A. Comparison of detrended fluctuation analysis and spectral analysis for heart rate variability in sleep and sleep apnea. IEEE Trans Biomed Eng 2003;50:1143-51.
22. Huikuri HV, Mäkikallio TH, Peng CK, Goldberger AL, Hintze U, Moller M. Fractal correlation properties of rr interval dynamics and mortality in patients with depressed left ventricular function after an acute myocardial infarction. Circulation 2000;101:47-53.
23. Mäkikallio TH, Hoiber S, Kober L, et al. Fractal analysis of heart rate dynamics as a predictor of mortality in patients with depressed left ventricular function after acute myocardial infarction. Trace investigators. trandolapril cardiac evaluation. Am J Cardiol 1999;83:836-9.
24. Bauer A, Kantelhardt JW, Bunde A, et al. Phase-rectified signal averaging detects quasiperiodicities in non-stationary data. Physica A 2006;64:423-34.
25. Bauer A, Kantelhardt JW, Barthel P, et al. Deceleration capacity of heart rate as a predictor of mortality after myocardial infarction. Lancet 2006;367:1674.
26. Iyengar N, Peng CK, Morin R, Goldberger AL, Lipsitz LA. Age-related alterations in the fractal scaling of cardiac interbeat interval dynamics. Am J Physiol Regul Integr Comp Physiol 1996;271:R1078-84.
27. Guzman-Vargas L, Angulo-Brown F. Simple model of the aging effect in heart interbeat time series. Phys Rev E 2003;67:052901.
28. Schmitt DT, Ivanov PC. Fractal scale-invariant and nonlinear properties of cardiac dynamics remain stable with advanced age: a new mechanistic picture of cardiac control in healthy elderly. Am J Physiol Regul Integr Comp Physiol 2007;293:R1923-37.
29. Schmitt DT, Stein PK, Ivanov PC. Stratification pattern of static and scale-invariant dynamic measures of heartbeat fluctuations across sleep stages in young and elderly. IEEE Trans Biomed Eng 2009;56:1564-73.
30. O'Brian IA, O'Hare P, Corrall RJ. Heart rate variability in healthy subjects: effect of age and the derivation of normal ranges for tests of autonomic function. Br Heart J 1986;55:348-54.
31. Tsuji H, Venditti FJ, Manders ES, et al. Reduced heart rate variability and mortality risk in an elderly cohort. The Framingham heart study. Circulation 1994;90:878-83.
32. Umetani K, Singer DH, McCraty R, Atkinson M. Twenty-four hour time domain heart rate variability and heart rate: Relations to age and gender over nine decades. JACC 1998;31:593-601.
33. Bliwise DL. Sleep in normal aging and dementia. Sleep 1993;16:40-81.
34. Espiritu JR. Aging-related sleep changes. Clin Geriatr Med 2008;24:1-14.
35. Webb WB. Sleep in older persons: sleep structures of 50- to 60-year-old men and women. J Gerontol 1982;37:581-6.
36. Landolt HP, Borbely AA. Age-dependent changes in sleep EEG topography. Clin Neurophysiol 2001;112:369-77.
37. Danker-Hopfe H, Schäfer M, Dorn H, et al. Percentile reference charts for selected sleep parameters for 20-80-year old healthy subjects from the SIESTA database. Somnologie 2005;9:3-14.
38. Kern W, Dodt C, Born J, et al. Changes in the cortisol and growth hormone secretion during nocturnal sleep in the course of aging. J Gerontol A Biol Sci Med Sci 1996;51:M3-9.
39. Van Cauter E, Leproult R, Plat L. Age-related changes in slow wave sleep and rem sleep and relationship with growth hormone and cortisol levels in healthy men. JAMA 2000;284:861-8.
40. Klosch G, Kemp B, Penzel T, et al. The SIESTA project polygraphic and clinical database. IEEE Eng Med Biol 2001;20:51-7.
41. Folstein MF, Folstein SE, McHugh PR. Mini mental state: A practical method for grading the cognitive state of patients for the clinician. J Psychiatr Res 1975;12:189-98.

42. Buysse DJ, Reynolds CH, Monks TH, Berman S, Kupfer DJ. The Pittsburgh Sleep Quality Index: a new instrument for psychiatric practice and research. Psychiatry Res 1998;28:193-213.
43. Zung WW. Rating instrument for anxiety disorders. Psychosomatics 1971;12:371-9.
44. Zung WW, Richards CB, Short MJ. Self-rating depression scale in an outpatient clinic – further validation of SDS. Arch Gen Psychiatry 1965;13:508.
45. Rechtschaffen A, Kales A. A manual of of standardized terminology, techniques, and scoring system for sleep stages of human subjects. US Public Health Service, US Government Printing Office 1968.
46. Iber C, Ancoli-Israel S, Chesson AL Jr, Quan SF. The AASM manual for the scoring of sleep and associated events. rules, terminology and technical specifications. Westchester, IL: American Academy of Sleep Medicine, 2007.
47. R. Schneider. Opensource toolbox for handling cardiologic data, available on the internet, www.librasch.org.
48. Chen Z, Ivanov PC, Hu K, Stanley HE. Effect of nonstationarities on detrended fluctuation analysis. Phys Rev E 2002;65:041107.
49. Peng CK, Buldyrev SV, Havlin S, Simons M, Stanley HE, Goldberger AL. Mosaic organization of DNA nucleotides. Phys Rev E 1994;49:1685-9.
50. Kantelhardt JW, Koscielny-Bunde E, Rego HH, Havlin S, Bunde A. Detecting long-range correlations with detrended fluctuation analysis. Physica A 2001;295:441-54.
51. Hu K, Ivanov PC, Chen Z, Carpena P, Stanley HE. Effect of trends on detrended fluctuation analysis. Phys Rev E 2001;64:011114.
52. Bartsch R, Kantelhardt JW, Penzel T, Havlin S. Experimental evidence for phase synchronization transitions in the human cardiorespiratory system. Phys Rev Lett 2007;98:054102.
53. Lipsitz LA, Goldberger AL. Loss of complexity and aging – potential applications of fractals and chaos theory to senescence. JAMA 1992;267:1806-9.
54. Jokinen V, Tapanainen JM, Seppänen T, Huikuri HV. Temporal changes and prognostic significance of measures of heart rate dynamics after acute myocardial infarction in the beta-blocking era. Am J Cardiol 2003;92:907-12.
55. Kantelhardt JW, Penzel T, Rostig S, Becker HF, Havlin S, Bunde A. Breathing during rem and non-rem sleep: correlated versus uncorrelated behaviour. Physica A 2003;319:447-57.
56. Nikulin VV, Brismar T. Long-range temporal correlations in alpha and beta oscillations: effect of arousal level and test-retest reliability. Clin Neurophysiol 2004;115:1896-1908.
57. Kantelhardt JW, Bauer A, Schumann AY, et al. Phase-rectified signal averaging for the detection of quasi-periodicities and the prediction of cardiovascular risk. Chaos 2007;17:015112.
58. Valladares EM, Eljammal SM, S. Motivala S, Ehlers CL, Irwin MR. Sex differences in cardiac sympathovagal balance and vagal tone during nocturnal sleep. Sleep Med 2008;9:310-6.
59. Verrier RL, Josephson ME. Impact of sleep on arrhythmogenesis. Circ Arrhythmia Electrophysiol 2009; 2:450-9.
60. Lavery CE, Mittleman MA, Cohen MC, Muller JE, Verrier RL. Nonuniform nighttime distribution of acute cardiac events - a possible effect of sleep states. Circulation 1997;96:3321-7.
61. Kantelhardt JW, Havlin S, Ivanov PC. Modeling transient correlations in heartbeat dynamics during sleep. Europhys Lett 2003;62:147-53.
62. Schumann AY, Kantelhardt JW, Bauer A, Schmidt G. Bivariate phase rectified signal averaging. Physica A 2008;387:5091-5100.
63. Eckberg DL. The human respiratory gate. J. Physiol 2003;548:339-52.

Aging Effects on Cardiac and Respiratory Dynamics in Healthy Subjects across Sleep Stages

By: Schumann, AY (Schumann, Aicko Y.)[1,2]; Bartsch, RP (Bartsch, Ronny P.)[3,4]; Penzel, T (Penzel, Thomas)[5]; Ivanov, PC (Ivanov, Plamen Ch.)[3,4,6,7]; Kantelhardt, JW (Kantelhardt, Jan W.)[1]

View ResearcherID and ORCID

SLEEP
Volume: 33 **Issue:** 7 **Pages:** 943-955
DOI: 10.1093/sleep/33.7.943
Published: JUL 1 2010
Document Type: Article
View Journal Impact

Abstract

Study Objectives: Respiratory and heart rate variability exhibit fractal scaling behavior on certain time scales. We studied the short-term and long-term correlation properties of heartbeat and breathing-interval data from disease-free subjects focusing on the age-dependent fractal organization. We also studied differences across sleep stages and night-time wake and investigated quasi-periodic variations associated with cardiac risk.

Design: Full-night polysomnograms were recorded during 2 nights, including electrocardiogram and oronasal airflow.

Setting: Data were collected in 7 laboratories in 5 European countries.

Participants: 180 subjects without health complaints (85 males, 95 females) aged from 20 to 89 years.

Interventions: None.

Measurements and Results: Short-term correlations in heartbeat intervals measured by the detrended fluctuation analysis (DFA) exponent alpha(1) show characteristic age dependence with a maximum around 50-60 years disregarding the dependence on sleep and wake states. Long-term correlations measured by alpha(2) differ in NREM sleep when compared with REM sleep and wake, besides weak age dependence. Results for respiratory intervals are similar to those for alpha(2) of heartbeat intervals. Deceleration capacity (DC) decreases with age; it is lower during REM and deep sleep (compared with light sleep and wake).

Conclusion: The age dependence of alpha(1) should be considered when using this value for diagnostic purposes in post-infarction patients. Pronounced long-term correlations (larger alpha(2)) for heartbeat and respiration during REM sleep and wake indicate an enhanced control of higher brain regions, which is absent during NREM sleep. Reduced DC possibly indicates an increased cardiovascular risk with aging and during REM and deep sleep.

Keywords

Author Keywords: Sleep; aging; heart rate variability; respiration; cardiac risk; detrended fluctuation analysis; scaling; phase rectified signal averaging; deceleration capacity

KeyWords Plus: HEART-RATE-VARIABILITY; ACUTE MYOCARDIAL-INFARCTION; DETRENDED FLUCTUATION ANALYSIS; RANGE TEMPORAL CORRELATIONS; LEFT-VENTRICULAR FUNCTION; SCALING BEHAVIOR; FRACTAL DYNAMICS; NOCTURNAL SLEEP; GROWTH-HORMONE; REM-SLEEP

Author Information

Reprint Address: Kantelhardt, JW (reprint author)

Univ Halle Wittenberg, Inst Phys, Von Seckendorff Pl 1, D-06120 Halle, Saale, Germany.

Addresses:

[1] Univ Halle Wittenberg, Inst Phys, D-06120 Halle, Saale, Germany

[2] Univ Calgary, Dept Phys & Astron, Complex Sci Grp, Calgary, AB T2N 1N4, Canada

[3] Harvard Univ, Sch Med, Boston, MA USA

[4] Brigham & Womens Hosp, Div Sleep Med, Boston, MA 02115 USA

[5] Charite, Schlafmed Zentrum, Berlin, Germany

[6] Boston Univ, Dept Phys, Boston, MA 02215 USA

[7] Boston Univ, Ctr Polymer Studies, Boston, MA 02215 USA

E-mail Addresses: jan.kantelhardt@physik.uni-halle.de

Funding

Funding Agency	Grant Number
European Community	FP6 IST 018474-2
Deutsche Forschungsgemeinschaft	KA 1676/3-2 PE 628/3
Brigham and Women's Hospital Biomedical Research Institute	
Office of Naval Research (ONR)	000141010078

View funding text

Publisher

AMER ACAD SLEEP MEDICINE, ONE WESTBROOK CORPORATE CTR, STE 920, WESTCHESTER, IL 60154 USA

Journal Information

Impact Factor: Journal Citation Reports

Categories / Classification

Research Areas: Neurosciences & Neurology

Web of Science Categories: Clinical Neurology; Neurosciences

See more data fields

99 of 127

Cited References: 63

Showing 30 of 63 **View All in Cited References page** *(from Web of Science Core Collection)*

1. **Fluctuation and synchronization of gait intervals and gait force profiles distinguish stages of Parkinson's disease** **Times Cited: 41**

   By: Bartsch, Ronny; Plotnik, Meir; Kantelhardt, Jan W.; et al.

   PHYSICA A-STATISTICAL MECHANICS AND ITS APPLICATIONS Volume: 383 Issue: 2 Pages: 455-465 Published: SEP 15 2007